7.0 SENSITIVITY ANALYSES

This chapter summarizes the results of four multiple-day sensitivity simulations with the UAM-IV and CALGRID-IV models using the 5-7 September, 1984 and 16-17 September, 1984 episodes. The results are summarized in Tables 7-1 through 7-8 which appear at the end of the chapter.

7.1 Objectives

Current ARB guidelines for evaluating photochemical models (ARB, 1992) recommend a general set of sensitivity simulations that involve "global" or across-the-board changes in major model inputs. The objective of these simulations is to examine the model's response to these major inputs in light of previous sensitivity results obtained with the same or similar models in comparable settings. Unusual model response alerts one to the need for more detailed investigations to determine the cause, whether it be flaws in the model or its inputs, or whether it represents a realistic situation previously not encountered. The specific sensitivity experiments performed in this study are as follows:

> Zero emissions;

> Zero initial conditions;

> Zero boundary conditions; and

> Zero surface deposition.

These simulations were carried out by making simple changes to the model input files. The experimental results, presented next, are summarized using the following statistical measures: sensitivity ratio, average and peak change in hourly ozone concentrations from the base case, normalized signed deviation, and normalized absolute deviation. These measures were defined previously in Chapter 5. The base case simulations results are used as the basis for comparing the four sensitivity experiments. Only the ozone results are presented here. While simulation results are tabulated for all five modeling days, we focus on the last day(s) of each episode.

Tables 7-1 through 7-4 present the peak station concentrations for the UAM-IV and CALGRID-IV sensitivity runs for both episodes. Tables 7-5 through 7-8 list sensitivity ratio, normalized signed deviation, and normalized absolute deviation results from the models for the two episodes.

7.2 Zero Emissions

Zeroing all emissions in the UAM-IV reduces the average of the station peak ozone values on the 6th and 7th by 1.8 pphm and 2.7 pphm, respectively. In the 17th, the reduction in the average of all peak values is 2.3 pphm. For CALGRID-IV, the reductions are 1.4 pphm, 1.3 pphm, and 1.7 pphm, respectively.

Another useful metric is the absolute deviation, presented in Tables 7-5 through 7-8. (This measure includes all simulation hours for which the base case value equals or exceeds 4 pphm). The UAM-IV's absolute deviations for the 6th, 7th, and 17th are 30%, 30%, and 35%. For CALGRID-IV, these deviations are 25%, 22%, and 25%. Thus, both models are moderately sensitive to emissions conditions on each episode and the UAM-IV is slightly more sensitive than CALGRID-IV.

7.3 Zero Initial Conditions

For both episodes, the importance of initial conditions diminishes rapidly with time in both the UAM-IV and CALGRID-IV simulations. By the 6th, for example, the peak ozone concentrations at nearly all monitoring stations simulated by both models are unaffected by zeroing the initial field. The absolute deviations for both models on the 6th, 7th, and 17th are within 1 to 2% of the base case values. The signed deviations are even smaller. Thus, both models exhibit essentially the same insensitivity to initial conditions after the first simulation day.

7.4 Zero Boundary Conditions

Boundary conditions play a dominant role in producing peak ozone concentrations on all modeling days examined in this study. On the 7th, for example, the average peak ozone concentration in the zero boundary conditions experiment with UAM-IV is 2.1 pphm compared with the base case value of 10.8. CALGRID-IV produced an average of 1.1 pphm compared with the base case value of 9.5. On the 6th and 7th, boundary conditions represent nearly 80% to 85% of the peak ozone concentrations from UAM-IV based on the average of the station peak one-hour values. For CALGRID-IV, boundary conditions constitute 83% to 89% of the total base case ozone for these two days. A similar, though less dramatic role is played by boundary conditions on 17 September. They constitute approximately 74% and 81% of the average of the station peak one-hour values.

For the UAM-IV, the absolute deviations for the 6th, 7th, and 17th are 93%, 91%, and 88%. For CALGRID-IV, these deviations are 96%, 96%, and 95%. Thus, both models are strongly sensitive to boundary conditions on each episode. CALGRID-IV is only slightly more sensitive than the UAM-IV.

7.5 Zero Surface Deposition

For both episodes, surface deposition is relatively unimportant in both the UAM-IV and CALGRID-IV simulations. Peak ozone concentrations tend to increase very slightly (at most a few tenths of a pphm) with both models. Some differences between the two models are seen in the hourly ozone results. For example, while the absolute deviations for UAM-IV on the 6th, 7th, and 17th are 12%, 15%, and 12%, for CALGRID-IV the values are 1% for all three days. Thus, both models exhibit essentially the same sensitivity to surface deposition when measured by the average of the station daily peak ozone values. In contrast, the UAM-IV's hourly ozone estimates are noticeably more sensitivity to deposition that CALGRID-IV's.

For the two episodes studied, we may summarize as follows. To first order, boundary conditions and emissions play the dominant roles in station peak and hourly ozone concentrations, with boundary conditions being by far the most influential. For both episodes, surface dry deposition has little influence on peak ozone levels but for hourly values, the UAM-IV appears to be somewhat more sensitive than CALGRID-IV. Emissions appear to produce an ozone contribution somewhat smaller than that of naturally occurring background levels. Overall, both models exhibit similar sensitivities to across-the-board input changes.

Table 7-1. Peak Ozone Concentrations for Four UAM-IV Sensitivity Simulations of the 5-7 September, 1984 Episode. (Concentrations in pphm).

(a) 5 September, 1984

Monitoring Station	Base Case Peak O_3	Zero Emiss	Zero ICs	Zero BCs	Zero Depos
ELRO	6.3	5.5	5.3	1.3	6.4
SIMI	11.5	11.3	11.0	3.3	11.5
VENT	6.4	5.9	5.0	1.9	6.4
SBAR	8.3	5.9	7.6	1.9	8.5
CASI	10.7	6.3	9.9	3.2	11.0
PIRU	11.9	10.0	11.6	2.5	12.1
OJAI	7.0	5.8	6.1	2.7	7.3
OAKS	8.5	8.8	7.9	1.8	8.6
ELCP	7.0	5.5	6.6	1.8	7.2
GOLA	6.9	5.7	6.5	1.4	7.2
VBGH	3.7	3.7	3.7	0.4	3.7
VBGW	3.8	3.8	3.8	0.8	3.8
SYNZ	7.9	5.5	7.4	2.3	8.1
LOMH	5.5	5.2	5.7	1.4	5.6
MOLI	6.8	5.5	6.5	2.0	7.1
GAVI	6.3	5.6	6.3	2.3	6.5
AVG	7.4	6.3	6.9	1.9	7.6

Table 7-1. Continued.

(b) 6 September, 1984

Monitoring Station	Base Case Peak O_3	Zero Emiss	Zero ICs	Zero BCs	Zero Depos
ELRO	7.1	5.8	7.1	0.9	7.2
SIMI	23.1	19.0	23.1	2.5	23.7
VENT	6.5	6.0	6.5	0.9	6.6
SBAR	8.7	5.4	8.7	1.6	8.9
CASI	7.5	5.8	7.4	1.2	7.8
PIRU	14.6	9.5	14.5	3.6	15.0
OJAI	11.0	6.2	10.8	2.1	11.6
OAKS	17.9	17.7	17.9	2.6	17.8
ELCP	6.8	6.1	6.8	1.0	6.9
GOLA	8.5	6.3	8.5	1.4	8.7
VBGH	5.0	4.9	5.0	0.1	5.0
VBGW	4.9	4.9	4.9	0.0	4.9
SYNZ	8.0	6.3	8.0	1.8	8.2
LOMH	6.9	6.5	6.9	1.0	7.1
MOLI	8.1	6.3	8.1	0.7	8.2
GAVI	7.0	6.0	7.0	1.4	7.2
AVG	9.5	7.7	9.5	1.4	9.7

Table 7-1. Concluded.

(c) 7 September, 1984

Monitoring Station	Base Case Peak O_3	Zero Emiss	Zero ICs	Zero BCs	Zero Depos
ELRO	7.9	7.0	7.9	1.1	8.2
SIMI	20.4	19.3	20.4	2.9	20.7
VENT	9.1	5.6	9.1	2.0	9.3
SBAR	12.9	5.4	12.8	2.9	13.5
CASI	9.0	5.7	9.0	1.5	9.7
PIRU	16.3	16.0	16.3	3.3	16.1
OJAI	12.0	5.7	12.0	3.7	12.5
OAKS	16.9	16.4	16.9	1.4	17.2
ELCP	11.1	5.9	11.1	2.5	11.4
GOLA	12.9	5.2	12.9	2.8	13.4
VBGH	6.3	6.4	6.3	0.3	6.4
VBGW	6.7	6.7	6.7	0.4	6.8
SYNZ	8.1	6.2	8.1	2.6	8.3
LOMH	6.8	6.3	6.8	1.5	6.9
MOLI	9.0	6.1	9.0	2.4	9.9
GAVI	7.8	6.2	7.8	2.2	8.7
AVG	10.8	8.1	10.8	2.1	11.2

Table 7-2. Peak Ozone Concentrations for Four CALGRID-IV Sensitivity Simulations of the 5-7 September, 1984 Episode. (Concentrations in pphm).

(a) 5 September, 1984

Monitoring Station	Base Case Peak O_3	Zero Emiss	Zero ICs	Zero BCs	Zero Depos
ELRO	4.0	4.2	3.8	1.0	4.0
SIMI	14.7	13.6	14.1	3.5	14.7
VENT	4.7	4.1	4.4	1.6	4.7
SBAR	6.6	5.1	6.1	1.6	6.6
CASI	7.3	5.6	6.8	1.9	7.3
PIRU	13.7	12.3	12.6	4.3	13.7
OJAI	8.7	6.0	8.3	3.2	8.7
OAKS	10.5	9.0	10.3	1.3	10.5
ELCP	5.4	5.1	4.7	1.4	5.4
GOLA	6.0	5.0	5.2	1.3	6.0
VBGH	5.5	4.8	5.4	1.3	5.5
VBGW	4.8	4.5	4.8	1.3	4.8
SYNZ	14.3	13.1	14.4	2.6	15.1
LOMH	6.4	5.4	6.3	1.4	6.3
MOLI	7.2	7.0	7.2	0.9	7.2
GAVI	8.2	7.5	8.2	1.2	8.2
AVG	8.0	7.0	7.7	1.9	8.0

Table 7-2. Continued.

(b) 6 September, 1984

Monitoring Station	Base Case Peak O_3	Zero Emiss	Zero ICs	Zero BCs	Zero Depos
ELRO	6.4	4.7	6.4	0.6	6.4
SIMI	20.7	19.2	20.8	1.4	20.8
VENT	5.7	4.9	5.8	0.8	5.8
SBAR	8.9	6.4	9.0	1.5	9.0
CASI	8.1	5.6	8.1	0.8	8.0
PIRU	17.3	14.0	17.4	3.1	17.4
OJAI	9.3	5.2	9.4	0.9	9.4
OAKS	18.1	17.4	18.1	1.0	18.1
ELCP	6.0	5.7	6.0	0.8	6.0
GOLA	7.2	5.4	7.2	1.3	7.2
VBGH	6.7	5.9	6.7	0.6	6.8
VBGW	6.2	5.9	6.1	0.4	6.2
SYNZ	10.0	8.8	10.2	2.1	10.0
LOMH	7.2	6.7	7.2	1.2	7.2
MOLI	6.2	5.2	6.2	0.7	6.3
GAVI	8.5	8.2	8.5	1.3	8.6
AVG	9.5	8.1	9.6	1.2	9.6

Table 7-2. Concluded.

(c) 7 September, 1984

Monitoring Station	Base Case Peak O_3	Zero Emiss	Zero ICs	Zero BCs	Zero Depos
ELRO	6.0	5.9	6.0	0.3	6.0
SIMI	18.9	18.3	18.9	1.3	19.0
VENT	6.8	5.3	6.8	0.7	6.8
SBAR	9.4	6.4	9.4	1.2	9.3
CASI	7.5	5.8	7.5	0.7	7.5
PIRU	20.1	19.3	20.1	2.7	20.1
OJAI	9.4	6.0	9.5	0.9	9.5
OAKS	17.5	17.3	17.5	0.7	17.5
ELCP	6.3	5.6	6.3	0.6	6.3
GOLA	8.6	5.7	8.6	1.1	8.6
VBGH	6.0	5.4	6.0	0.7	6.0
VBGW	5.5	5.2	5.6	0.6	5.6
SYNZ	9.8	8.4	9.8	2.3	9.7
LOMH	6.5	6.0	6.5	0.9	6.5
MOLI	7.0	5.7	7.0	0.7	7.1
GAVI	8.3	7.0	8.3	0.8	8.1
AVG	9.6	8.3	9.6	1.1	9.6

Table 7-3. Peak Ozone Concentrations for Four UAM-IV Sensitivity Simulations of the 16-17 September, 1984 Episode. (Concentrations in pphm).

(a) 16 September, 1984

Monitoring Station	Base Case Peak O_3	Zero Emiss	Zero ICs	Zero BCs	Zero Depos
ELRO	8.3	6.1	7.0	2.4	8.4
SIMI	9.2	7.6	7.3	4.4	9.1
VENT	7.6	6.0	6.6	2.0	7.7
SBAR	7.8	6.1	7.2	2.2	7.9
CASI	7.8	6.2	6.9	2.6	7.9
PIRU	12.0	7.8	8.4	7.8	11.9
OJAI	8.3	7.6	7.1	3.8	8.0
OAKS	7.3	5.9	6.7	2.0	7.4
ELCP	7.5	5.6	6.8	1.9	7.6
GOLA	7.7	5.8	7.2	2.0	7.8
VBGH	5.5	5.2	5.4	3.0	5.5
VBGW	5.0	5.0	5.0	2.3	5.0
SYNZ	7.9	4.9	6.4	5.7	8.2
LOMH	6.2	5.5	6.3	3.3	6.4
MOLI	6.7	5.1	6.0	2.8	6.8
GAVI	5.6	4.8	4.8	2.7	5.8
AVG	7.5	6.0	6.6	3.2	7.6

Table 7-3. Concluded.

(b) 17 September, 1984

Monitoring Station	Base Case Peak O_3	Zero Emiss	Zero ICs	Zero BCs	Zero Depos
ELRO	6.5	4.8	6.5	1.0	6.6
SIMI	10.2	4.9	10.2	3.7	10.9
VENT	6.4	4.5	6.3	1.9	6.5
SBAR	7.4	4.8	7.4	1.5	7.8
CASI	8.3	4.9	8.2	2.0	8.5
PIRU	8.5	5.0	8.5	3.6	9.1
OJAI	11.5	4.9	11.5	4.0	11.9
OAKS	7.3	5.1	7.3	2.0	7.4
ELCP	6.8	5.1	6.8	1.8	7.1
GOLA	7.8	4.9	7.8	1.7	8.2
VBGH	5.4	5.2	5.4	0.6	5.4
VBGW	5.1	5.1	5.1	0.6	5.1
SYNZ	7.1	5.2	7.1	2.9	7.3
LOMH	5.8	5.4	5.8	0.8	5.9
MOLI	6.0	5.2	6.0	1.7	6.5
GAVI	6.0	5.4	6.0	1.3	6.1
AVG	7.3	5.0	7.2	1.9	7.5

Table 7-4. Peak Ozone Concentrations for Four CALGRID-IV Sensitivity Simulations of the 16-17 September, 1984 Episode. (Concentrations in pphm).

(a) 16 September, 1984

Monitoring Station	Base Case Peak O_3	Zero Emiss	Zero ICs	Zero BCs	Zero Depos
ELRO	5.0	4.0	4.4	1.1	5.0
SIMI	8.9	5.2	8.4	3.3	8.9
VENT	4.8	3.9	4.2	1.7	4.7
SBAR	6.1	4.9	4.8	3.0	6.0
CASI	7.2	4.7	6.4	2.7	7.1
PIRU	10.0	4.8	9.1	4.9	10.0
OJAI	7.8	6.0	6.7	3.1	7.8
OAKS	6.6	5.0	6.3	1.8	6.6
ELCP	5.2	4.5	4.1	2.9	5.1
GOLA	5.6	4.6	4.5	3.0	5.6
VBGH	5.9	5.0	5.9	3.5	5.9
VBGW	5.8	5.2	5.8	3.1	5.8
SYNZ	6.0	4.6	5.1	4.4	6.0
LOMH	5.5	4.7	5.4	2.9	5.4
MOLI	4.9	4.2	4.1	2.6	4.9
GAVI	5.3	5.2	5.1	2.6	5.1
AVG	6.3	4.8	5.6	2.9	6.3

Table 7-4. Continued.

(b) 17 September, 1984

Monitoring Station	Base Case Peak O_3	Zero Emiss	Zero ICs	Zero BCs	Zero Depos
ELRO	5.0	4.5	5.1	0.8	5.0
SIMI	8.8	5.0	8.8	2.9	8.8
VENT	6.1	5.0	6.2	0.7	6.3
SBAR	8.0	5.1	8.0	1.3	8.0
CASI	6.9	5.5	6.9	0.8	6.9
PIRU	9.4	5.0	9.4	2.7	9.4
OJAI	10.0	5.5	10.0	1.5	10.1
OAKS	7.8	5.2	7.8	1.6	7.8
ELCP	6.1	5.1	6.1	0.8	6.1
GOLA	7.2	4.8	7.2	0.9	7.1
VBGH	5.4	5.0	5.4	0.8	5.4
VBGW	5.4	5.2	5.4	0.6	5.4
SYNZ	7.6	6.3	7.7	2.7	7.6
LOMH	5.7	5.2	5.7	1.0	5.7
MOLI	6.1	6.2	6.1	1.1	5.9
GAVI	6.7	6.2	6.7	1.2	6.6
AVG	7.0	5.3	7.0	1.3	7.0

Table 7-5. UAM-IV Ozone Model Sensitivity Results for Four Simulations of the 5-7 September, 1984 Episode. (Concentrations in pphm).

(a) 5 September, 1984 (Cutoff = 1 pphm)

Sensitivity Attribute	Zero Emiss	Zero ICs	Zero BCs	Zero Depos
Peak base case concentration	11.9 (Piru)	11.9 (Piru)	11.9 (Piru)	11.9 (Piru)
Peak sensitivity case concentration	11.3 (Simi)	11.6 (Piru)	3.4 (Simi)	12.1 (Piru)
Sensitivity ratio	0.945	0.975	0.286	1.017
Peak change from base case (paired)	-17.4%	-2.2%	-85.6%	1.3%
Peak change from base case (unpaired)	3.6%	9.5%	-49.1%	13.0%
Average peak change from base case (unpaired)	15.1%	6.5%	76.6%	2.2%
Normalized signed deviation (%)	7.6%	-14.9%	-77.4%	4.4%
Normalized absolute deviation (%)	20.9%	15.3%	77.5%	4.5%

Table 7-5. Continued.

(b) 6 September, 1984 (Cutoff = 1 pphm)

Sensitivity Attribute	Zero Emiss	Zero ICs	Zero BCs	Zero Depos
Peak base case concentration	23.1 (Simi)	23.1 (Simi)	23.1 (Simi)	23.1 (Simi)
Peak sensitivity case concentration	19.0 (Simi)	23.1 (Simi)	3.6 (Piru)	23.7 (Simi)
Sensitivity ratio	0.823	1.000	0.156	1.026
Peak change from base case (paired)	-17.9%	-0.2%	-91.8%	2.6%
Peak change from base case (unpaired)	2.7%		-79.7%	23.3%
Average peak change from base case (unpaired)	18.0%	19.7%	85.6%	2.2%
Normalized signed deviation (%)	14.6%	-1.1%	-93.0%	11.8%
Normalized absolute deviation (%)	29.7%	1.7%	93.0%	11.9%

Table 7-5. Concluded.

(c) 7 September, 1984 (Cutoff = 1 pphm)

Sensitivity Attribute	Zero Emiss	Zero ICs	Zero BCs	Zero Depos
Peak base case concentration	20.4 (Simi)	20.4 (Simi)	20.4 (Simi)	20.4 (Simi)
Peak sensitivity case concentration	19.3 (Simi)	20.4 (Simi)	3.7 (Ojai)	20.7 (Simi)
Sensitivity ratio	0.946	1.000	0.183	1.015
Peak change from base case (paired)	-5.4%	-0.2%	-92.7%	0.5%
Peak change from base case (unpaired)	3.8%	7.8%	-66.3%	9.7%
Average peak change from base case (unpaired)	25.8%	0.3%	80.4%	3.9%
Normalized signed deviation (%)	9.1%	-0.0%	-91.0%	15.1%
Normalized absolute deviation (%)	29.7%	0.6%	91.0%	15.1%

Table 7-6. CALGRID-IV Ozone Model Sensitivity Results for Four Simulations of the 5-7 September, 1984 Episode. (Concentrations in pphm).

(a) 5 September, 1984 (Cutoff = 1 pphm)

Sensitivity Attribute	Zero Emiss	Zero ICs	Zero BCs	Zero Depos
Peak base case concentration	14.7 (Simi)	14.7 (Simi)	14.7 (Simi)	14.7 (Simi)
Peak sensitivity case concentration	13.6 (Simi)	14.4 (SYnz)	4.3 (Piru)	15.1 (SYnz)
Sensitivity ratio	0.925	0.978	0.293	1.027
Peak change from base case (paired)	-12.7%	-4.0%	-77.1%	-0.2%
Peak change from base case (unpaired)	23.2%	43.7%	-18.1%	52.7%
Average peak change from base case (unpaired)	12.6%	4.9%	80.7%	0.7%
Normalized signed deviation (%)	7.4%	-20.4%	-73.5%	0.0%
Normalized absolute deviation (%)	20.5%	20.8%	73.7%	1.0%

Table 7-6. Continued.

(b) 6 September, 1984 (Cutoff = 1 pphm)

Sensitivity Attribute	Zero Emiss	Zero ICs	Zero BCs	Zero Depos
Peak base case concentration	20.7 (Simi)	20.7 (Simi)	20.7 (Simi)	20.7 (Simi)
Peak sensitivity case concentration	19.2 (Simi)	20.8 (Simi)	3.1 (Piru)	20.8 (Simi)
Sensitivity ratio	0.928	1.005	0.150	1.005
Peak change from base case (paired)	-7.0%	0.4%	-93.1%	0.2%
Peak change from base case (unpaired)	20.1%	21.8%	-69.5%	21.2%
Average peak change from base case (unpaired)	18.1%	0.6%	87.6%	0.6%
Normalized signed deviation (%)	12.9%	0.1%	-95.7%	-0.1%
Normalized absolute deviation (%)	25.3%	0.9%	95.7%	0.9%

Table 7-6. Concluded.

(c) 7 September, 1984 (Cutoff = 1 pphm)

Sensitivity Attribute	Zero Emiss	Zero ICs	Zero BCs	Zero Depos
Peak base case concentration	20.1 (Piru)	20.1 (Piru)	20.1 (Piru)	20.1 (Piru)
Peak sensitivity case concentration	19.3 (Piru)	20.1 (Piru)	2.7% (Piru)	20.1 (Piru)
Sensitivity ratio	0.960	1.000	0.134	1.000
Peak change from base case (paired)	-3.7%	-0.0%	-92.1%	0.1%
Peak change from base case (unpaired)	40.7%	43.8%	-77.9%	43.7%
Average peak change from base case (unpaired)	15.4%	0.4%	89.3%	0.6%
Normalized signed deviation (%)	10.3%	-0.1%	-96.4%	-0.0%
Normalized absolute deviation (%)	21.7%	0.7%	96.4%	0.8%

Table 7-7. UAM-IV Ozone Model Sensitivity Results for Four Simulations of the 16-17 September, 1984 Episode. (Concentrations in pphm).

(a) 16 September, 1984 (Cutoff = 1 pphm)

Sensitivity Attribute	Zero Emiss	Zero ICs	Zero BCs	Zero Depos
Peak base case concentration	12.0 (Piru)	12.0 (Piru)	12.0 (Piru)	12.0 (Piru)
Peak sensitivity case concentration	7.8 (Piru)	8.4 (Piru)	7.8 (Piru)	11.9 (Piru)
Sensitivity ratio	0.650	0.700	0.650	0.992
Peak change from base case (paired)	-34.9%	-30.3%	-34.6%	-1.1%
Peak change from base case (unpaired)	-23.7%	-15.8%	-30.5%	3.4%
Average peak change from base case (unpaired)	20.0%	12.1%	60.7%	1.8%
Normalized signed deviation (%)	10.4%	-29.7%	-59.5%	4.0%
Normalized absolute deviation (%)	24.7%	29.8%	59.7%	4.2%

Table 7-7. Concluded.

(b) 17 September, 1984 (Cutoff = 1 pphm)

Sensitivity Attribute	Zero Emiss	Zero ICs	Zero BCs	Zero Depos
Peak base case concentration	11.5 (Ojai)	11.5 (Ojai)	11.5 (Ojai)	11.5 (Ojai)
Peak sensitivity case concentration	5.4 (Lomh)	11.5 (Ojai)	4.1 (Ojai)	11.9 (Ojai)
Sensitivity ratio	0.470	1.000	0.357	1.035
Peak change from base case (paired)	-60.9%	-0.4%	-73.7%	3.5%
Peak change from base case (unpaired)	-46.6%	7.9%	-58.1%	10.3%
Average peak change from base case (unpaired)	28.1%	0.4%	74.9%	3.1%
Normalized signed deviation (%)	13.4%	-1.5%	-87.7%	12.1%
Normalized absolute deviation (%)	34.6%	1.9%	87.7%	12.1%

Table 7-8. CALGRID-IV Ozone Model Sensitivity Results for Four Simulations of the 16-17 September, 1984 Episode. (Concentrations in pphm).

(a) 16 September, 1984 (Cutoff = 1 pphm)

Sensitivity Attribute	Zero Emiss	Zero ICs	Zero BCs	Zero Depos
Peak base case concentration	10.0 (Piru)	10.0 (Piru)	10.0 (Piru)	10.0 (Piru)
Peak sensitivity case concentration	6.0 (Ojai)	9.1 (Piru)	4.9 (Piru)	10.0 (Piru)
Sensitivity ratio	0.600	0.910	0.490	1.000
Peak change from base case (paired)	-53.3%	-8.6%	-53.7%	-0.3%
Peak change from base case (unpaired)	6.6%	24.6%	-43.4%	27.6%
Average peak change from base case (unpaired)	22.4%	11.8%	59.5%	0.9%
Normalized signed deviation (%)	3.1%	-33.1%	-56.7%	-0.1%
Normalized absolute deviation (%)	20.5%	33.1%	56.8%	1.0%

Table 7-8. Concluded.

(b) 17 September, 1984 (Cutoff = 1 pphm)

Sensitivity Attribute	Zero Emiss	Zero ICs	Zero BCs	Zero Depos
Peak base case concentration	10.0 (Ojai)	10.0 (Ojai)	10.0 (Ojai)	10.0 (Ojai)
Peak sensitivity case concentration	6.3 (SYnz)	10.0 (Ojai)	2.9 (Simi)	10.1 (Ojai)
Sensitivity ratio	0.630	1.000	0.290	1.010
Peak change from base case (paired)	-45.6%	0.1%	-85.2%	0.7%
Peak change from base case (unpaired)	21.1%	79.7%	-6.9%	80.7%
Average peak change from base case (unpaired)	23.5%	0.5%	82.6%	0.8%
Normalized signed deviation (%)	10.2%	-0.1%	-94.5%	-0.1%
Normalized absolute deviation (%)	25.3%	0.9%	94.5%	0.9%

8.0 DIAGNOSTIC ANALYSES

Ideally, several diagnostic simulations with UAM-IV and CALGRID-IV models should be carried out to explore the underlying causes for the differences between their results for the two September base cases. For example, the in both episodes, CALGRID-IV produces higher ozone levels in the northeastern portion of the model domain. Also, the region north of Santa Ynez is a CALGRID-IV ozone "hot spot". Exploratory simulations focusing on precursor and ozone transport into these regions would be helpful in clarifying why CALGRID-IV produces these features yet the UAM-IV does not. As another example, CALGRID-IV tends to estimate peak ozone earlier in the day compared with the UAM-IV. Presumably, this is the result of advective and dispersive processes since the emissions and chemistry processes are essentially the same. Exploration of this feature of the simulations would also be valuable. Unfortunately, the scope of this evaluation did not allow thorough investigation of these and other intriguing facets of the model.

This chapter summarizes the results of three photochemically reactive model simulations aimed at complimenting the results obtained in the comparative evaluation (chapter 6) and the sensitivity study (chapter 7). These simulations provide additional insight into the influence on CALGRID-IV's ozone estimates arising from specific input changes, grid structure options, and the relative contribution of various processes active in ozone formation, transport and dissipation. The results of these simulations are given in Tables 8-1 through 8-4 (appearing at the end of the chapter).

Appendix A contains an analysis carried out by Systems Applications, Int in which the CALGRID-IV model was run in the inert mode to ascertain the relative contribution of initial conditions, boundary conditions, emissions, etc. to model estimates for both episode periods.

8.2 Reactive CALGRID-IV Diagnostic Simulations

Three CALGRID-IV model runs were performed for both September episodes. Tables 8-1 through 8-4 present the results of these simulations. The structure of these runs, their intended purpose, and a description of the model results is discussed below.

8.2.1 Short Time Step

In the CALGRID-IV base case, the integration time step was 20 minutes. We reduced this time step to 6 minutes to assess whether a shorter integration step would produce improved ozone results.

Reducing the integration time step has little effect on the base case ozone results for the episodes studied here. From Tables 8-1 and 8-3, typical changes in the maximum ozone at the monitoring stations are in the fractions of a pphm range. No systematic

trend is observed in the results. From Tables 8-2 and 8-3, the biases and gross errors are largely unchanged. Curiously, the peak base case ozone concentration on the 17th (10.0 at Ojai) is reduced to 9.5 pphm. The ozone time series plots of the base case and this diagnostic run for Ojai show the latter's hourly ozone levels in the mid-morning to early-afternoon hours to be only slightly lower than those for the base case. No great significance is attached to this result, however.

8.2.2 Option C Grid Structure

As defined by Scire et al., (1989) CALGRID Option C allows for an arbitrary, fixed vertical system of user-specified layers. Layer 1 is fixed at 20 meters as in all CALGRID configurations. Option C results in layers which are fixed in time and space. For this diagnostic run, we set the following heights for the four grid layers:

>	Layer 1	20 m
>	Layer 2	250 m
>	Layer 3	500 m
>	Layer 4	1000 m

The motivation for making this run was to explore the influence of variable Layer 2 cell thickness (which occurs in the base case Option B specification) on ozone concentrations. By removing variable cell heights through the use of Option C and then comparing Option B and C results, we are able to examine the influence of CALGRID-IV cell height variations (in time and space) on hourly ozone levels.

In this experiment, peak ozone levels are reduced from the base case. More specifically, the average of the station peak ozone concentrations on the 6th, 7th, and 17th were reduced from the base case values by 0.5 pphm, 0.4 pphm, and 0.4 pphm, respectively (see Tables 8-1 and 8-2). However, the effect on the daily maximum ozone concentration varies depending upon the day. For example, on the 6th, a higher peak ozone value is simulated at Simi (23.0 pphm) compared with the base case (20.7 pphm). On the 7th, the magnitude of the base case peak (20.1 pphm at Simi) is unchanged but the station where the peak is simulated changes to Piru. Finally, on the 17th, the ozone peak is reduced from 10.0 pphm at Ojai to 9.4 at Piru.

The fixed layer model produces somewhat lower gross errors compared with the base case for all five simulation days (Tables 8-2 and 8-4), yet the magnitudes of the biases tend to increase very slightly.

Examination of the ozone time series for both episodes reveals one very interesting feature. With the exception of the Santa Ynez station, the Option C grid specification produces very little change from the base case ozone concentrations at the monitors. However, at Santa Ynez, the base case ozone peak is significantly "trimmed"

using Option C as seen in Figure 8-1. This is particularly the case for the 5-7 September episode.

8.3 18 Level Model

CALGRID Option C was again used for the 18 level model diagnostic run. For this experiment, we set the following heights for the 18 grid layers:

>	Layer 1	20 m
>	Layer 2	40 m
>	Layer 3	60 m
>	Layer 4	80 m
>	Layer 5	100 m
>	Layer 6	150 m
>	Layer 7	200 m
>	Layer 8	250 m
>	Layer 9	300 m
>	Layer 10	350 m
>	Layer 11	400 m
>	Layer 12	450 m
>	Layer 13	500 m
>	Layer 14	600 m
>	Layer 15	700 m
>	Layer 16	800 m
>	Layer 17	900 m
>	Layer 18	1000 m

The motivation for this run was to explore the influence on ozone concentrations of much finer vertical resolution.

Running CALGRID-IV with 18 vertical layers systematically produces lower average peak ozone levels for both episodes except for 16 September (Tables 8-1 and 8-3). For the daily maximum ozone concentrations (Tables 8-2 and 8-4), the peak at Simi on the 16th (20.7 pphm) is lowered to 19.9 pphm while the next day the Simi base case peak (20.1 pphm) is increased in this experiment to 23.2 pphm. On the 17th, the Ojai base case peak (10.0 pphm) is lowered to a maxima of 9.2 pphm, occurring at Simi. On the 6th, 7th, and 17th, the overall bias and error statistics are degraded somewhat from the base cases.

The most noteworthy changes to the ozone time series produced by this diagnostic experiment occur for the 5-7 September episode. Figure 8-2 presents ozone time series at the Santa Ynez, Gaviota, Thousand Oaks, and Piru stations. At Santa Ynez, the ozone time series is even more significantly reduced than in the 4 layer Option C experiment previously discussed. The truncation, most evident on the 5th, occurs on

all three days. At this location, the 18 level model does far better in estimating the daily average ozone at Santa Ynez yet the timing the peaks is off by several hours. Ozone time series at Gaviota and Piru also show significant reduction of the peak daily values; generally better agreement with the daily maximum is achieved. Finally, at all four stations, the 18 level model results exhibit rapid reduction of ozone levels (to near-zero) after 1200 whereas the observed values remain fairly high throughout the afternoon period.

Table 8-1. Peak Ozone Concentrations for Three CALGRID-IV Diagnostic Simulations for the 5-7 September, 1984 Episode. (Concentrations in pphm).

(a) 5 September, 1984

Monitoring Station	CALGRID-IV Base Case	CALGRID-IV Short Time Step	CALGRID-IV Option C 4 Level Grid	CALGRID-IV 18 Vertical Levels
ELRO	4.0	3.8	5.1	4.4
SIMI	14.7	14.8	13.8	9.2
SBAR	6.6	6.3	6.3	6.5
CASI	7.3	7.0	8.3	7.4
PIRU	13.7	13.6	12.7	6.3
OJAI	8.7	8.4	8.4	7.8
OAKS	10.5	10.6	10.0	7.6
ELCP	5.4	5.4	4.9	5.3
GOLA	6.0	5.8	5.8	5.7
VBGH	5.5	5.8	5.2	5.1
VBGW	4.8	4.9	4.8	4.6
SYNZ	14.3	14.5	5.8	5.9
LOMH	6.4	6.1	5.2	5.2
GAVI	8.2	7.2	5.8	5.5
AVG	8.3	8.2	7.3	6.2

Table 8-1. Continued.

(b) 6 September, 1984

Monitoring Station	CALGRID-IV Base Case	CALGRID-IV Short Time Step	CALGRID-IV Option C 4 Level Grid	CALGRID-IV 18 Vertical Levels
ELRO	6.4	6.3	6.7	5.6
SIMI	20.7	20.9	23.0	19.9
SBAR	8.9	8.6	7.6	7.7
CASI	8.1	8.0	8.1	7.0
PIRU	17.3	17.3	16.8	15.6
OJAI	9.3	9.2	10.0	8.0
OAKS	18.1	17.8	17.4	16.2
ELCP	6.0	5.9	6.0	6.1
GOLA	7.2	7.2	6.8	6.7
VBGH	6.7	7.0	6.1	6.0
VBGW	6.2	6.4	5.8	5.7
SYNZ	10.0	9.8	5.7	5.6
LOMH	7.2	7.7	5.9	6.0
GAVI	8.5	8.0	7.1	7.7
AVG	10.0	10.0	9.5	8.8

Table 8-1. Concluded.

(c) 7 September, 1984

Monitoring Station	CALGRID-IV Base Case	CALGRID-IV Short Time Step	CALGRID-IV Option C 4 Level Grid	CALGRID-IV 18 Vertical Levels
ELRO	6.0	6.0	6.8	5.0
SIMI	18.9	18.9	20.0	23.2
SBAR	9.4	9.1	7.8	8.6
CASI	7.5	7.2	8.4	8.2
PIRU	20.1	20.0	20.1	14.1
OJAI	9.4	9.0	9.7	8.6
OAKS	17.5	17.5	17.0	16.8
ELCP	6.3	6.6	6.2	6.2
GOLA	8.6	8.2	7.7	8.3
VBGH	6.0	6.0	6.0	5.9
VBGW	5.5	5.5	5.7	5.6
SYNZ	9.8	9.5	6.7	6.4
LOMH	6.5	6.7	5.7	5.6
GAVI	8.3	7.9	6.4	6.8
AVG	10.0	9.9	9.6	9.2

Table 8-2. CALGRID-IV Ozone Statistics for Three Diagnostic Simulations of the 5-7 September, 1984 Episode. (Concentrations in pphm).

(a) 5 September, 1984 (Cutoff = 4 pphm)

Performance Attribute	CALGRID-IV Base Case	CALGRID Short Time Step	CALGRID-IV Option C 4 Level Grid	CALGRID-IV 18 Vertical Levels
Maximum Modeled concentration at a station	14.7 (Simi)	14.8 (Simi)	13.8 (Simi)	9.2 (Simi)
Maximum observed concentration at a station	10.0 (Casitas)	10.0 (Casitas)	10.0 (Casitas)	10.0 (Casitas)
Ratio of maximum estimated to observed concentration	1.470	1.480	1.380	0.920
Accuracy of peak estimation (paired)	-39%	-41%	-23%	-29%
Accuracy of peak estimation (unpaired)	121%	133%	49%	14%
Mean normalized deviation (bias)	-0.037	-0.062	-0.049	-0.260
Mean absolute normalized deviation (gross error)	0.410	0.415	0.361	0.405

Table 8-2. Continued.

(b) 6 September, 1984 (Cutoff = 4 pphm)

Performance Attribute	CALGRID-IV Base Case	CALGRID Short Time Step	CALGRID-IV Opt[illegible] C 4 L[illegible] Grid	CALGRID-IV 18 Vertical Levels
Maximum Modeled concentration at a station	20.7 (Simi)	20.8 (Simi)	23.0 (Simi)	19.9 (Simi)
Maximum observed concentration at a station	17.0 (Simi)	17.0 (Simi)	17.0 (Simi)	17.0 (Simi)
Ratio of maximum estimated to observed concentration	1.176	1.224	1.353	1.171
Accuracy of peak estimation (paired)	-29%	-25%	-23%	-30%
Accuracy of peak estimation (unpaired)	48%	60%	45%	25%
Mean normalized deviation (bias)	-0.116	-0.133	-0.123	-0.280
Mean absolute normalized deviation (gross error)	0.364	0.367	0.331	0.413

Table 8-2. Concluded.

(c) 7 September, 1984 (Cutoff = 4 pphm)

Performance Attribute	CALGRID-IV Base Case	CALGRID Short Time Step	CALGRID-IV Option C 4 Level Grid	CALGRID-IV 18 Vertical Levels
Maximum Modeled concentration at a station	20.1 (Simi)	20.0 (Piru)	20.1 (Piru)	23.2 (Simi)
Maximum observed concentration at a station	18.0 (Casitas)	18.0 (Casitas)	18.0 (Casitas)	18.0 (Casitas)
Ratio of maximum estimated to observed concentration	1.117	1.111	1.117	1.2899
Accuracy of peak estimation (paired)	-72%	-72%	-72%	-100%
Accuracy of peak estimation (unpaired)	60%	80%	27%	71%
Mean normalized deviation (bias)	-0.041	-0.051	-0.054	-0.310
Mean absolute normalized deviation (gross error)	0.340	0.351	0.317	0.479

Table 8-3. Peak Ozone Concentrations for Three CALGRID-IV Diagnostic Simulations for the 16-17 September, 1984 Episode. (Concentrations in pphm).

(a) 16 September, 1984

Monitoring Station	CALGRID-IV Base Case	CALGRID-IV Short Time Step	CALGRID-IV Option C 4 Level Grid	CALGRID-IV 18 Vertical Levels
ELRO	5.0	4.7	5.6	6.1
SIMI	8.9	8.8	8.7	9.1
VENT	4.8	4.7	5.0	5.5
SBAR	6.1	5.8	6.2	6.2
CASI	7.2	6.7	6.8	6.6
PIRU	10.0	9.9	9.8	9.9
OJAI	7.8	7.5	8.7	8.5
OAKS	6.6	6.6	6.6	6.5
ELCP	5.2	5.0	4.9	5.5
GOLA	5.6	5.5	6.2	6.3
VBGH	5.9	5.9	5.8	5.7
VBGW	5.8	5.7	5.6	5.8
SYNZ	6.1	6.0	6.5	6.6
LOMH	5.5	5.6	4.9	5.5
GAVI	5.3	5.1	4.6	5.1
AVG	6.4	6.2	6.4	6.6

Table 8-3. Concluded.

(b) 17 September, 1984

Monitoring Station	CALGRID-IV Base Case	CALGRID-IV Short Time Step	CALGRID-IV Option C 4 Level Grid	CALGRID-IV 18 Vertical Levels
ELRO	5.0	4.7	6.2	5.8
SIMI	8.8	9.1	9.2	9.2
VENT	6.1	6.4	6.2	6.4
SBAR	8.0	7.9	7.3	7.6
CASI	7.0	6.5	7.0	7.2
PIRU	9.4	9.5	9.4	8.5
OJAI	10.0	9.5	8.2	8.1
OAKS	7.8	7.6	7.1	6.5
ELCP	6.1	5.9	6.3	6.7
GOLA	7.2	6.8	6.9	7.0
VBGH	5.4	5.5	5.4	5.3
VBGW	5.4	5.3	5.6	5.7
SYNZ	7.7	7.7	6.0	6.1
LOMH	5.7	5.7	5.1	5.5
GAVI	6.6	6.3	5.1	5.6
AVG	7.1	7.0	6.7	6.7

Table 8-4. CALGRID-IV Ozone Statistics for Three Diagnostic Simulations of the 16-17 September, 1984 Episode. (Concentrations in pphm).

(a) 16 September, 1984 (Cutoff = 4 pphm)

Performance Attribute	CALGRID-IV Base Case	CALGRID Short Time Step	CALGRID-IV Option C 4 Level Grid	CALGRID-IV 18 Vertical Levels
Maximum Modeled concentration at a station	10.0 (Piru)	9.9 (Piru)	9.8 (Piru)	9.9 (Piru)
Maximum observed concentration at a station	11.0 (Simi)	11.0 (Simi)	11.0 (Simi)	11.0 (Simi)
Ratio of maximum estimated to observed concentration	0.909	0.900	0.891	0.900
Accuracy of peak estimation (paired)	-28%	-20%	-29%	-32%
Accuracy of peak estimation (unpaired)	17%	24%	-6%	-3%
Mean normalized deviation (bias)	-0.030	-0.051	0.006	0.023
Mean absolute normalized deviation (gross error)	0.213	0.215	0.177	0.202

Table 8-4. Concluded.

(b) 17 September, 1984 (Cutoff = 4 pphm)

Performance Attribute	CALGRID-IV Base Case	CALGRID Short Time Step	CALGRID-IV Option C 4 Level Grid	CALGRID-IV 18 Vertical Levels
Maximum Modeled concentration at a station	10.0 (Ojai)	9.5 (Ojai)	9.4 (Piru)	9.2 (Simi)
Maximum observed concentration at a station	14.0 (Casitas)	14.0 (Casitas)	14.0 (Casitas)	14.0 (Casitas)
Ratio of maximum estimated to observed concentration	0.714	0.679	0.671	0.657
Accuracy of peak estimation (paired)	-51%	-54%	-55%	-50%
Accuracy of peak estimation (unpaired)	28%	31%	-22%	-29%
Mean normalized deviation (bias)	-0.163	-0.186	-0.177	-0.199
Mean absolute normalized deviation (gross error)	0.274	0.286	0.236	0.276

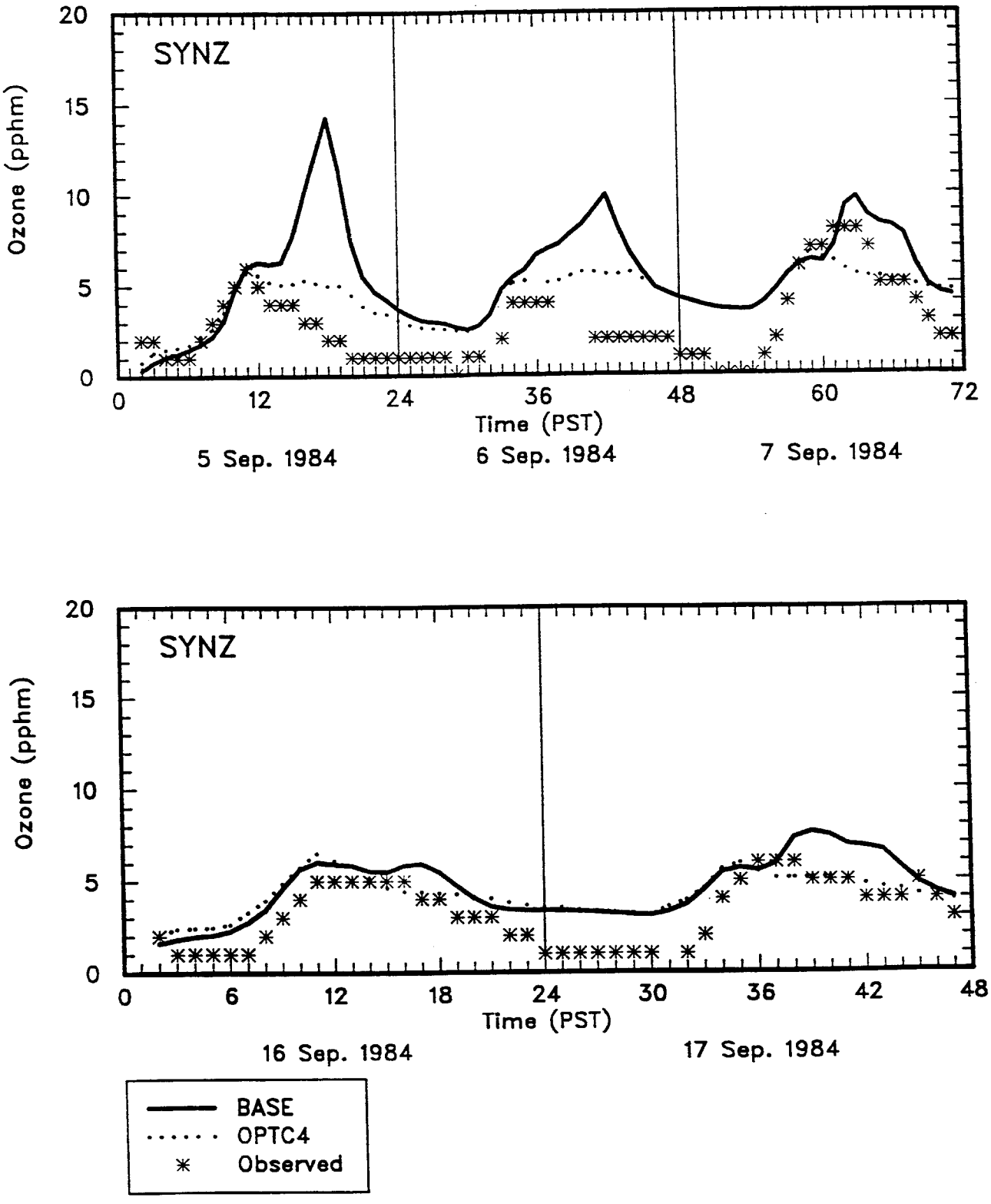

Figure 8-1. Ozone Time Series At Santa Ynez Comparing the Effects of Option B (Base Case) and Option C Grid Specifications for the 5-7 September and 16-17 September, 1984 Episodes.

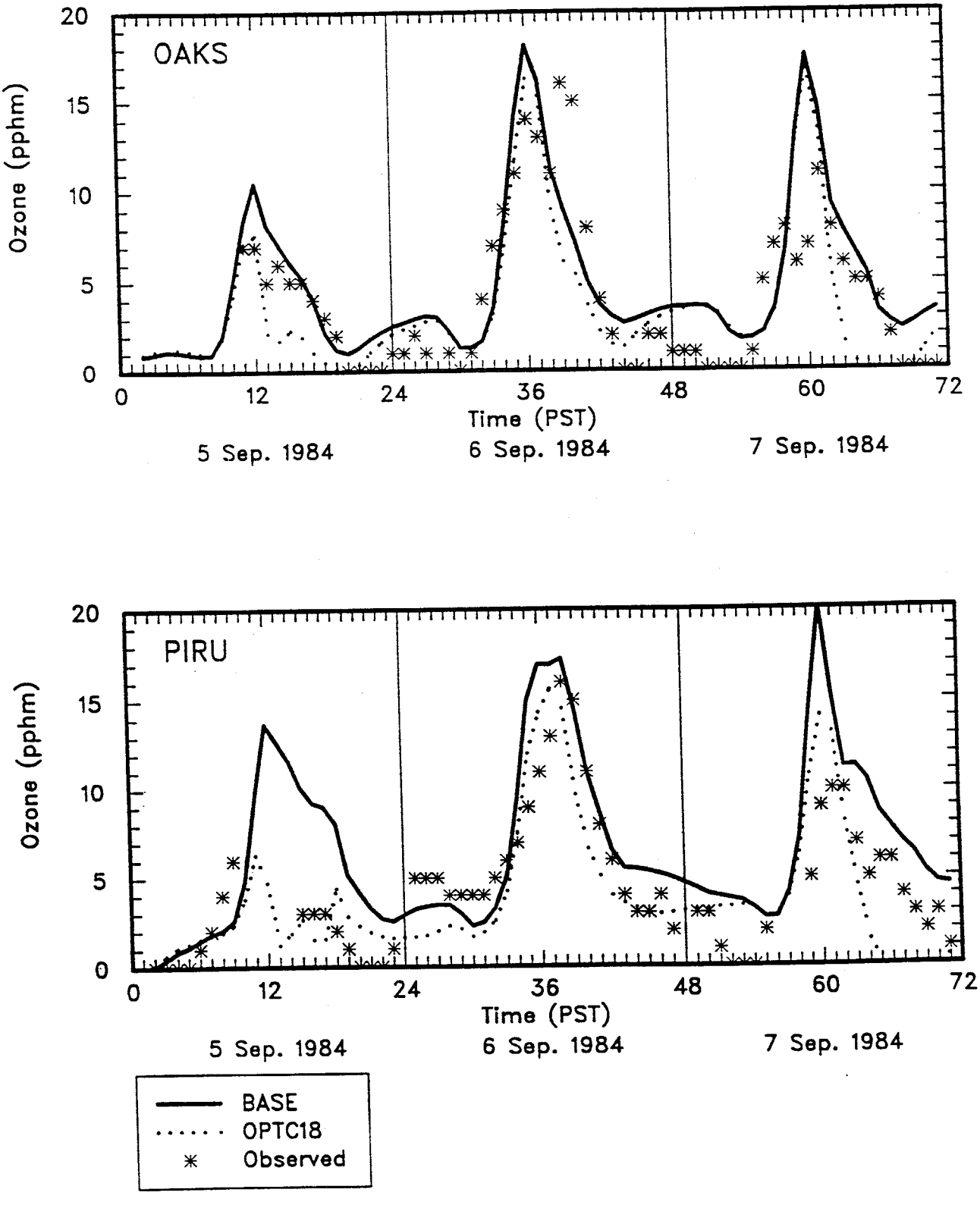

Figure 8-2. Concluded.

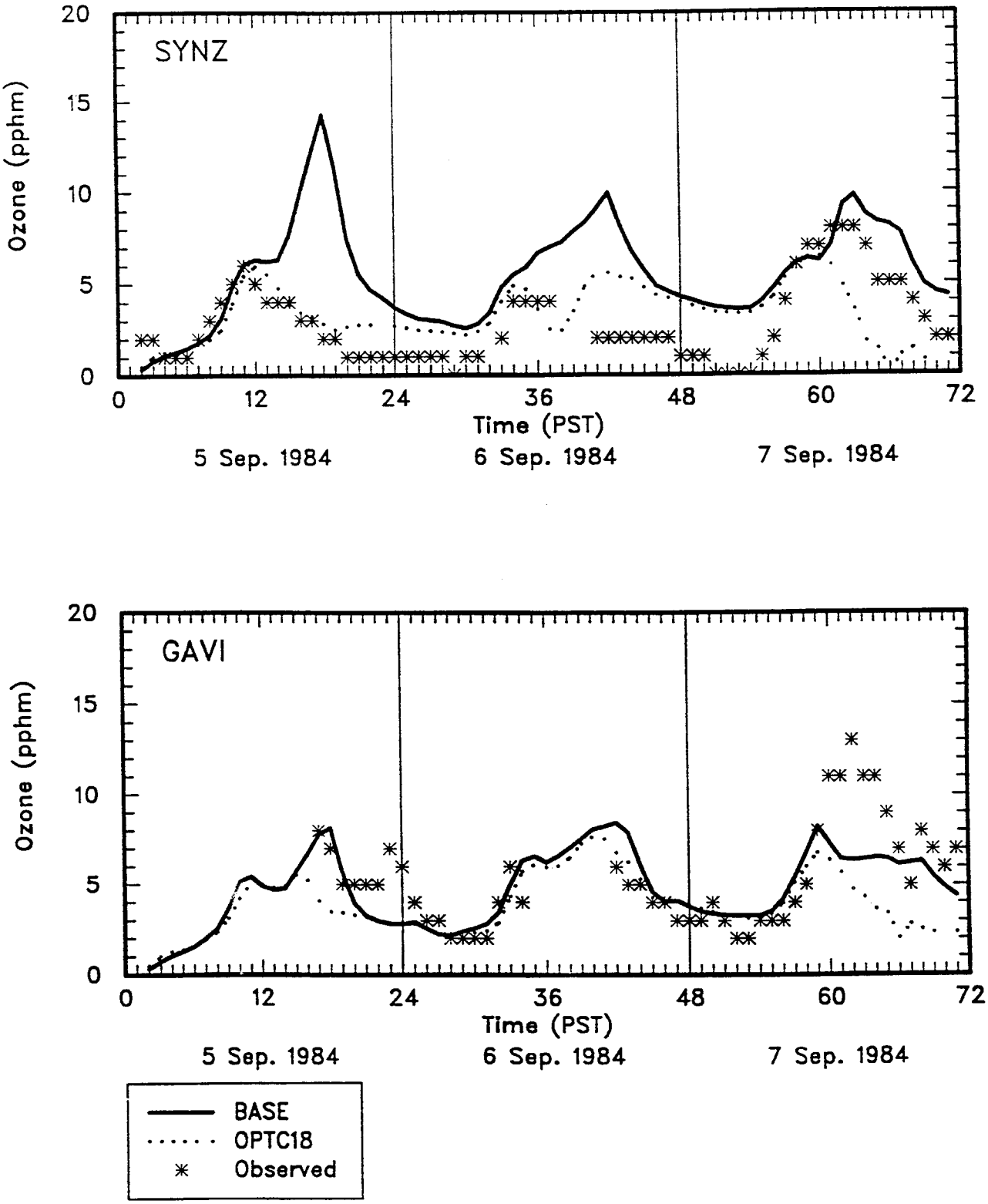

Figure 8-2. Ozone Time Series Comparing the Effects of Option B (Base Case) and Option C (18 Level Grid) Specifications for the 5-7 September, 1984 Episode.

9.0 SUMMARY AND RECOMMENDATIONS

9.1 Summary

9.1.1 Model Evaluation Results

5-7 September, 1984 Base Case

We summarize the comparative model evaluation results for this base case as follows:

> UAM-IV and CALGRID-IV significantly underestimated the maximum measured hourly NO concentrations. For example, on the 6th, the maximum observed NO was 19 pphm at Simi. CALGRID-IV produced a peak of 2.1 pphm at Simi while UAM-IV gave 2.8 pphm.

> In general, the UAM-IV produced NO peaks approximately 30% higher than CALGRID-IV.

> Both models underestimate NO_2 concentration although the UAM-IV peak estimates of NO_2 were nearly 50% larger than those for CALGRID-IV.

> For all three days, the UAM-IV's estimates of the average station peak ozone value was slightly better than those for CALGRID-IV.

> CALGRID-IV underestimates hourly NO_2 concentrations by -55% to -70% compared to -40% to -49% for the UAM-IV.

> Both model's give gross errors in the 60% to 70% percent range with the UAM-IV's average discrepancy being slightly less. Both model's estimates of the peak one-hour NO_2 concentrations are only about 1/2 of the observed values for the three days.

> On the 7th, the two models produce similar peaks on the extreme west and east ends of the basin, but in the central region, from Gaviota to El Rio (a total of eight stations), the CALGRID-IV ozone maxima are systematically lower than the UAM-IV's. UAM-IV's estimates of peak ozone are uniformly better than CALGRID-IV's on the 7th at those stations with maxima exceeding 6 pphm.

> During the early morning hours of the 7th, CALGRID-IV exhibits greater ozone underestimation than UAM-IV. Mid-day, CALGRID-IV overestimates ozone (positive bias) by a greater amount that UAM-IV. From early afternoon on, both models bias estimates goes from positive to negative;

late in evening, both model's tend to underestimate ozone. CALGRID-IV's underestimation is more pronounced that UAM-IV's.

> On the 7th, both models underestimate ozone concentrations (above 9 pphm) but this bias is nearly double for CALGRID-IV compared with the UAM-IV.

> On the 7th, the UAM-IV's ozone gross errors are approximately 50% to 60% less than CALGRID-IV's particularly during the early morning hours and during the afternoon high-ozone period.

> For both models on the 7th, all but one maximum ozone estimate-observation pairs fall within a factor of 2 agreement.

> For the 6th and 7th, CALGRID-IV hourly means are slightly less than those for the UAM-IV and the peak values for CALGRID-IV occur 1 to 2 hours earlier that those for the UAM-IV.

> Both models systematically overestimate ozone in the western basin; CALGRID-IV's overestimation is slightly larger than that for the UAM-IV.

> Mid-basin, both models poorly replicate the observed ozone peaks at Casitas on the 6th and 7th and CALGRID-IV produces maximum ozone levels several hours earlier on the 7th compared with UAM-IV. At Ojai, better agreement in the estimated and observed time series is obtained, with the UAM-IV producing better agreement with the elevated afternoon ozone levels than CALGRID-IV, especially on the 7th.

> In the eastern basin (e.g., Thousand Oaks, Piru, and Simi), both models reproduce the general buildup of ozone levels from the 5th to the 6th but neither adequately captures the reduction in peak ozone that occurred at these monitors on the 7th. At Thousand Oaks and Piru, both models simulate the peak value to within 2 pphm at about the correct time. CALGRID-IV ozone estimates at Piru are systematically higher than the UAM-IV values for most of the daylight period. At Piru and Simi on the 7th, both models significantly overestimate the peak observed values of 10 pphm and 13 pphm, respectively.

> The UAM-IV simulates an east-west band of high surface ozone on the 7th, beginning offshore Goleta and extending inland to Piru. This feature is absent in the CALGRID-IV simulation. Aloft, an elevated ozone cloud is simulated in the northeastern portion of the domain by both models. The cloud, defined by the 20 pphm contour, is approximately 250 meters above ground and extends up to the top of the computational domain. Both

models produce similar results in the vertical distribution of this cloud and in the magnitude of the peak concentrations aloft.

> Maximum daily ozone residual plots (constructed by subtracting the peak gridded CALGRID-IV ozone estimates from the UAM-IV peak estimates and contouring the residuals) indicate that the UAM-IV simulates as much as 7.5 pphm more ozone than CALGRID-IV over the Santa Barbara channel region on the 7th. CALGRID-IV estimates as much as 4.6 pphm more ozone than UAM-IV north of Santa Ynez.

16-17 September, 1984 Base Case

The comparative model evaluation results for the second episode may be summarized as follows:

> UAM-IV and CALGRID-IV both significantly underestimated the maximum hourly NO concentrations during the 16-17 September, 1984 episode. For example, on the 17th, the maximum observed NO was 11 pphm at the Simi and Santa Barbara monitors. CALGRID-IV produced a peak of 1.8 pphm at Santa Barbara while UAM-IV gave 5.3 pphm at Ventura. In general, the UAM-IV produced NO peaks approximately double those for CALGRID-IV during this episode.

> Both models underestimate NO_2 concentrations; the UAM-IV NO_2 peaks are in better agreement with observations than those from CALGRID-IV.

> UAM-IV and CALGRID-IV underestimated the average station peak ozone value of 9.3 pphm on the 17th by -22% and -24%, respectively.

> CALGRID-IV underestimates hourly NO_2 concentrations by -40% to -69% while the bias in UAM-IV estimates ranges between -22% to -49%. Both model's give gross errors in the 50% to 70% percent range with the UAM's average discrepancy being slightly less.

> The systematic bias in CALGRID-IV and UAM-IV hourly ozone estimates on the 17th are -16% and -14%, respectively. Gross errors for both models are approximately the same (27% and 29%, respectively).

> UAM-IV's estimate of the maximum measured ozone concentration during the 16-17 September episode (14.0 pphm at Casitas) is 11.6 pphm (at Ojai). CALGRID-IV produced a maximum of 10.0 pphm at Ojai.

> On the 16th, CALGRID-IV systematically produces lower ozone peaks at the monitoring stations compared with the UAM-IV, whereas on the 17th,

both models produce approximately similar peaks at the various stations. The temporally-unpaired peak ozone estimates for the UAM-IV tend to be better across nearly all of the monitoring stations compared with CALGRID-IV.

> During the early morning through mid-day hours, the UAM-IV underestimates ozone levels substantially more than does CALGRID-IV. In the afternoon of the 17th, however, the UAM-IV bias is very close to zero while CALGRID-IV underestimates by 10 to 20%. After sunset, the underestimation problem with both models increases again.

> On the 17th, both models produce nearly identical negative bias-concentration plots for ozone levels above 4 pphm. From 8 to 13 pphm, the bias is nearly constant for both models at approximately -30%.

> CALGRID-IV and UAM-IV errors have similar patterns on the 17th after approximately 1200. However, from midnight to noon on the 17th, the UAM-IV exhibits substantially larger error than CALGRID-IV. After 1200, the UAM-IV's errors are less than CALGRID-IV's but, because of the large UAM-IV errors before noon, the overall gross error for UAM-IV in the 17th (29%) exceeds that for CALGRID-IV (27%).

> Above 5 pphm on the 16th, the UAM-IV's ozone gross errors are systematically smaller than CALGRID-IV's while on the 17th the error-concentration plots are roughly comparable.

> Both models exhibit the tendency to underestimate as ozone concentration levels increase.

> For both models on the 17th, all maximum ozone estimate-observation pairs fall within a factor of 2 agreement.

> Neither model reproduces the variability in hourly ozone concentrations particularly well, especially during midday.

> On the western end of the basin, both models replicate well the diurnal trends in the hourly ozone measurements.

> At the El Capitan, Goleta, and Santa Barbara monitors, both models fail to capture the buildup to the peak mid-afternoon ozone concentrations. In particular, at Goleta and Santa Barbara, the models underestimate the peak values by 4-5 pphm. The extent of the underestimation in this subregion is roughly twice as great for the 17th as for the 6th and 7th.

> Mid-basin, both models poorly replicate the ozone peak at Casitas (14 pphm) that was the highest observation during this episode. As with the earlier episode, better agreement in the estimated and observed time series is obtained at Ojai, with the UAM-IV producing slightly better correspondence with the peak (11.6 pphm) than CALGRID-IV (10.0 pphm).

> In the eastern basin (e.g., Thousand Oaks, Piru, and Simi), neither model reproduces well the general buildup of ozone levels from the 16th to the 17th. At Thousand Oaks and Simi, both models significantly underestimate (i.e., by 3-4 pphm) the magnitude of the broad ozone peaks that lasted for as much as 4-5 hours after noon. CALGRID-IV produce ozone maxima a few hours earlier than UAM-IV. Both models slightly underestimate the 10 pphm peak at Piru on the 17th.

> For both models the region of high ozone during on the 16th-17th appears as a cloud, aligned along a northwest-south east axis for the UAM-IV and along a southwest-northeast axis for CALGRID-IV.

> On the 17th, the UAM-IV simulates as much as 5.5 pphm more ozone than CALGRID-IV in the region just west of Piru. CALGRID-IV estimates 4 to 6 pphm or more ground level ozone than UAM-IV in two areas: north of Piru and north of Santa Ynez. The largest difference between the two models over the full domain is 5.5 pphm near Piru.

> For both September, 1984 modeling episodes, CALGRID-IV consistently produces higher ozone levels relative to the UAM-IV in the northeastern portion of the domain.

9.1.2 Sensitivity Analysis Results

Four sensitivity runs were carried out with the two models for both episodes. These runs involved reducing to zero the: (a) emissions inventory, (b) initial conditions, (c) boundary conditions, and (e) surface dry deposition. The results of these runs indicated that:

> Zeroing all emissions in the UAM-IV reduces the average of the station peak ozone values on the 6th and 7th by 1.8 pphm and 2.7 pphm, respectively. In the 17th, the reduction in the average of all peak values is 2.3 pphm. For CALGRID-IV, the reductions are 1.4 pphm, 1.3 pphm, and 1.7 pphm, respectively.

> Both models are moderately sensitive to emissions conditions on each episode and the UAM-IV is slightly more sensitive than CALGRID-IV.

> The importance of initial conditions diminishes rapidly with time in both the UAM-IV and CALGRID-IV simulations.

> Both models exhibit essentially the same insensitivity to initial conditions after the first simulation day.

> Boundary conditions play a dominant role in producing peak ozone concentrations on all modeling days examined in this study.

> On the 6th and 7th, boundary conditions represent nearly 80% to 85% of the peak ozone concentrations from UAM-IV based on the average of the station peak one-hour values. For CALGRID-IV, boundary conditions constitute 83% to 89% of the total base case ozone for these two days. A similar, though less dramatic role is played by boundary conditions on 17 September. They constitute approximately 74% and 81% of the average of the station peak one-hour values.

> Both models are strongly sensitive to boundary conditions on each episode. CALGRID-IV is only slightly more sensitive than the UAM-IV.

> Surface deposition is relatively unimportant in both the UAM-IV and CALGRID-IV simulations.

> Both models exhibit essentially the same sensitivity to surface deposition when measured by the average of the station daily peak ozone values; however, the UAM-IV's hourly ozone estimates are noticeably more sensitivity to deposition that CALGRID-IV's.

9.1.3 Diagnostic Experiments

Three diagnostic model simulations were made with the CALGRID-IV model for the two September episodes. These runs involved: (a) reducing the integration time step from 20 minutes to 6 minutes, (b) use of a temporally-invariant vertical grid structure, and (c) use of an 18-level vertical grid structure. The results of these runs are summarized as follows:

> Reducing the integration time step has little effect on the base case ozone results for the episodes studied. Typical changes in the maximum ozone at the monitoring stations are in the fractions of a pphm range. No systematic trend is observed in the results.

> Fixing the four grid levels at 20 m, 250 m, 500 m, and 1000 m reduced the average of the station peak ozone concentrations on the 6th, 7th, and 17th from the base case values by 0.5 pphm, 0.4 pphm, and 0.4 pphm,

respectively. On the 6th, a higher peak ozone value is simulated at Simi (23.0 pphm) compared with the base case (20.7 pphm). On the 7th, the magnitude of the base case peak (20.1 pphm at Simi) is unchanged but the station where the peak is simulated changes to Piru. On the 17th, the ozone peak is reduced from 10.0 pphm at Ojai to 9.4 at Piru. The fixed layer model produces somewhat lower gross errors compared with the base case, yet the magnitudes of the biases tend to increase very slightly.

> Running CALGRID-IV with 18 vertical layers systematically produces lower average peak ozone levels for both episodes except for 16 September. The overall bias and error statistics are degraded somewhat from the base cases.

> The 18 level model produces a significant reduction (relative to the base case) in the midday ozone levels at the Santa Ynez, Gaviota, Thousand Oaks, and Piru stations. The results exhibit rapid reduction of ozone levels (to near-zero) after 1200 whereas the observed values remain fairly high throughout the afternoon period.

9.1.4 Ease of Use of the UAM-IV and CALGRID-IV Models

The user interface to the UAM-IV and CALGRID-IV models are very different. The UAM-IV model provides an extensive preprocessor network to assist in preparing inputs but is strict as to what files are necessary in order to run the model. The CALGRID-IV model does not include preprocessors to help prepare model inputs but is more flexible in which files are necessary to run the model.

CALGRID-IV provides options of how the initial, boundary, and region top concentration files can be specified. The files can either be gridded time dependent binary files or formatted files which provide less detail but are easier to modify. Having these options is very useful. For the base case simulations the detailed binary files were used, just as in UAM-IV. However, for sensitivity tests, formatted files were prepared without using other programs and the model runs were performed with less operator time.

The CALGRID-IV model appears to have been designed using the assumption that the CALMET model would be used to prepare meteorological inputs. The format of the CALMET.DAT meteorological file is fairly complex. If methods or models other than Calmet are used to prepare the meteorological data, a fairly complicated processor must be written to put the file into the CALMET.DAT format. The UAM-IV method of storing different meteorological fields in different files makes using the UAM-IV model with a variety of meteorological models much simpler.

9.1.5 Computing Requirements

As with nearly all Eulerian photochemical models, the computing requirements of both of these models are fairly extensive. The simulations of both models were performed on the an IBM RS/6000 model 530 workstation with 64 Mbytes of memory. Run times for both models for both episodes are presented in Table 9.1. Both models were compiled with optimization but no "hand-tuning" was performed.

TABLE 9.1 CPU TIME REQUIREMENTS FOR THE CALGRID-IV AND UAM-IV MODELS IN THE SCCAB ON AN IBM RS/6000 MODEL 530 WORKSTATION.

MODEL CODE	5-7 Sept, 1984	16-17 Sept, 1984
UAM-IV	8 Hours	4 Hours
CALGRID-IV	6 Hours	4 Hours

Early in the project we attempted to run CALGRID-IV on the SUN SPARCstation 1 with 24 Mbytes of memory. The code would compile with no problems but seemed to hang when we tried to run it. We postulated this was caused by a memory limitation on the SPARCstation. This problem was never resolved because the RS/6000 was able to run the model with no problems.

9.1.6 Synthesis of Results

Based on the collection of statistical measures and graphical tools applied to the base case model results for both episodes, the UAM-IV has performed somewhat better than CALGRID-IV in simulating hourly NO, NO_2, and ozone concentrations for the two September episodes. Moreover, the sensitivity simulation results indicate that the two models respond similarly to gross changes in major inputs. In particular, boundary conditions and emissions play the dominant roles in station peak and hourly ozone concentrations, with boundary conditions being by far the most influential. Surface dry deposition has little influence on peak ozone levels but for hourly values, the UAM-IV appears to be somewhat more sensitive than CALGRID-IV. Emissions appear to produce an ozone contribution somewhat smaller than that of naturally occurring background levels.

These findings do not confirm superiority of the UAM-IV over CALGRID-IV as an ozone assessment tool, however. First, the September episode modeling files were tailored to the specific requirements and limitations of the UAM system. These data bases are therefore not optimal for fully testing CALGRID-IV's capabilities. Second, the

time and resource constraints of this study only allowed for an "operational" evaluation of the two models. It has not been possible to explore the modeling results more fully to reveal the causes for the various differences seen in the performance results. Diagnostic analyses of the model differences is needed to clarify whether the differences stem from model flaws in UAM-IV, CALGRID-IV or both, or are instead the result of data base limitations. Finally, a comparative evaluation of the two models using two episodes in one air basin is insufficient to draw firm conclusions regarding which is the better overall model. Both models should be exercised with episodes drawn from other regions possessing higher quality data bases (e.g., SCAQS, SARMAP, LMOS).

Two important model applications issues are raised by the results of this evaluation. The first issue concerns bias in model ozone estimates. The second involves the very high sensitivity of ozone concentrations to uncertain boundary conditions. These issues are addressed briefly.

Bias in Estimation

Bias refers to the inaccurate (as opposed to imprecise) estimation of pollutant concentrations. A minor degree of bias is tolerable; a larger degree testifies to significant flaws or weaknesses in the model or input data. Obviously, the risk of developing a flawed control strategy through the use of a flawed model is considerable. This specter hangs over virtually all past UAM model applications, largely because of the high probability that VOC emissions estimates were too low, perhaps by 50-70%. If underestimation of VOC emissions pervades past efforts and, yet, the average discrepancy between estimation and observation is only 25-40%, then compensation internal to the model must exist. Compensation can be introduced, for example, by underestimating mixing depth, underestimating wind speed, or overestimating boundary conditions.

It is essential that an effort be made to reduce substantive bias to insignificance using appropriate and justifiable procedures. Acceptable practice involves adhering to the "scientific method" -- identifying the existence of the bias, carrying out diagnostic analyses to determine its possible causes, making appropriate corrections to the model or input, repeating the simulations, examining the results and determining their acceptability, and repeating the process until satisfactory results are obtained.

Although biases may be reduced, it is difficult to eliminate them entirely. Thus, correction must often be made for residual bias. One procedure recommended by EPA (EPA, 1991) involves scaling the observed peak concentration by the ratio of predicted peak concentration for a control strategy to the predicted peak concentration for the base case. Although this procedure is convenient, it is not scientifically well-founded; moreover, it may not be correct or accurate.

Of principal concern is the current practice nationwide of accepting a model for application despite the fact that it is found to be deficient (e.g., biased). Another issue involves the estimation of concentrations that result from emissions reductions in the presence of residual bias. Questions that regulatory agencies involved in ozone attainment planning in California should address include:

> How should current ozone modeling practice be modified to minimize both the existence of bias and the risk of inaccurate estimation that attends its presence? Also, under what circumstances should a model be deemed acceptable?

> What procedures should be adopted to compensate for the presence of residual bias?

To date, efforts to reduce or eliminate bias through application of the scientific method have mainly focused on the quality of estimated ozone concentrations. In some studies, serious attention has also been given to estimated NO and NO_2 concentrations; occasionally, predicted and observed VOC concentrations have been compared.

As a practical matter, substantive (in contrast to residual) bias in estimated ozone concentrations often remains despite attempts to improve accuracy. In cases in which NO_X and VOC concentrations have been examined, significant bias virtually always exists. The UAM is nevertheless usually applied in subsequent control strategy assessment. In fact, unless performance is quite inadequate, application of the model in the presence of bias is routinely accepted. (In cases in which bias has been significantly reduced through diagnostic analysis and model improvement, compensation for residual bias is made through use of the ratio adjustment described earlier.)

Recommended efforts to remove bias in the UAM-IV and CALGRID-IV model results are presented in Section 9.2.

Treating the Transport Problem at the Boundaries of the SCCAB Model Domain

Pollutants "enter" the UAM-IV or CALGRID-IV simulations in the SCCAB through initial conditions, injection of emissions, and inflow at the upwind and aloft boundaries. For many air basins, after one to two days of simulation, the influence of the initial conditions generally becomes quite low; emissions contributions often dominate at this stage. However, as we have seen in the sensitivity experiments, boundary conditions to the UAM-IV and CALGRID-IV are critical inputs. They represent a continuous emissions source at the upwind boundary, injecting pollutants at a rate that is well above 50-75% of the emissions rate within the model domain.

Boundary conditions can either be measured in the field or generated using a model of coarser scale and covering a larger domain. Inflow at the boundaries of the

SCCAB substantially contribute to atmospheric loading of pollutants in the basin under the following conditions:

> The intensity of emissions (number of sources, emissions rates) upwind is high.

> Pollutants from the study area recirculate, leaving the region to return later.

> Pollutants are either held or transported aloft into the area of interest and later mixed down to the surface.

> Vertical motions are significant and the top of the modeling region is limited in height.

> Biogenic sources of VOCs upwind are intense.

> Anthropogenic emissions are reduced significantly, thereby increasing the ratio of boundary conditions to emissions.

Implied from the UAM-IV and CALGRID-IV sensitivity results, the accuracy of the boundary conditions greatly influences the overall accuracy of concentration estimates derived from the models and, thus, the overall value of the simulations. Furthermore, boundary conditions for the September 1984 episodes in the SCCAB will become even more important at the reduced emissions levels associated with control strategy simulations in Ventura and Santa Barbara counties.

Although monitored concentrations are more accurate in prescribing boundary conditions, they represent local, rather than grid-averaged conditions, and they portray air quality at only a few fixed locations along the boundary, generally at the ground. In contrast, boundary conditions generated through regional-scale modeling describe air quality all along the boundary, both at the surface and aloft. Even so, they are usually uncertain because the data bases supporting the larger-scale modeling are frequently sparse. In general, regional modeling is much more attractive than monitoring for establishing boundary conditions when emissions are reduced. The regional model can be used to estimate the urban-scale boundary conditions at varying emissions levels; observations can only be subjectively adjusted to account for emissions reductions. Given the differing attributes of modeled and monitored boundary conditions and the significant limitations that attend the use of both, guidance is urgently needed regarding the best method of estimating boundary conditions when they significantly contribute to pollutant loading in the region of interest.

Current practice in boundary conditions estimation involves one or more of the following:

> Making considered, but partially subjective, judgments: Estimates are often taken to be constant throughout the day or for a defined portion of the day along a given main spatial segment.

> Making judgments heavily influenced by the relatively few data sources available; in some cases, these may not represent the conditions of interest sufficiently well.

> Performing sensitivity runs to determine the influence on air quality estimates of boundary conditions relative to that of initial conditions or emissions rates. [Note that for cases in which sensitivities are high (e.g., say, a change in peak ozone of 20-30% or more), the effects of variations (i.e., uncertainties) should be reported.]

> Using variable-grid regional-scale models (e.g., Chang et al., 1989). This method is generally preferred to nesting, which is less efficient because it requires communication back and forth between grids of differing scale. When employing variable grid structures, grid patterns of the same scale must be of simple overall geometry (i.e., regular rectangular patterns).

> In areas where boundary conditions are not well determined but may be significant, expanding modeling regions upwind to locate the boundary in an area of reduced concentrations. In this way, their influence (and thus the impact of their uncertainty) is reduced. Even then, the impact of boundary conditions aloft remains the same; it is not current practice to increase the height of the modeling region to gain a similar effect.

Recommended efforts to improve the reliability of the crucial boundary conditions for the September, 1984 episodes in either the UAM-IV and CALGRID-IV models are outlined in the next section.

9.2 Recommendations

Our recommendations are presented in four categories.

9.2.1 Continue the Evaluation Process of the CALGRID-IV Model

Given the generally similar model evaluation results found in this study, the evaluation of the CALGRID-IV model should continue. Three specific investigations are recommended:

> Diagnostic efforts should be undertaken to provide explanations for the different surface and aloft ozone patterns generated by UAM-IV and CALGRID-IV for both episodes. This analysis, if carried out, may reveal potential flaws in either the UAM-IV, in CALGRID-IV, in both models, or perhaps inherent weaknesses in the September, 1984 data bases.

> The comparative evaluation of the UAM-IV and CALGRID-IV models should extended to other urban areas. Alpine Geophysics is performing such an effort with the 23-25 June, 1987 and 26-28 August, 1987 SCAQS data bases in the South Coast Air Basin. Similar exercises should be considered for the SARMAP and LMOS episodes.

> Model inputs to future CALGRID-IV performance evaluations should be constructed directly, rather than "mapping" UAM-IV input data bases onto the CALGRID-IV structure. This will provide a more reliable test of those formulation and implementation features of CALGRID-IV that are closer to the current state-of-science than the UAM-IV's.

9.2.2 Upgrade the Photochemical Models

Below we summarize the needed improvements to the UAM-IV in order to bring it closer to the state-of-science in urban-scale photochemical modeling. If the UAM-IV is to be used in California for designing multi-billion dollar emissions control programs, it is prudent that many of these upgrades be implemented. CALGRID-IV, by design, is much closer to this elusive target, but there are still some areas (e.g., inclusion of prognostic meteorological modeling, upgrading the CBM-IV chemistry) where refinements can be made. Specific recommendations for improving the UAM-IV ar as follows:

<u>Model Code Refinement</u>

> Elimination of the mixing height concept, supplying instead vertical turbulent mixing fields calculated from an appropriate prognostic meteorological model.

> Rewriting the UAM-IV code and preprocessor programs to take advantage of modern vector and parallel computers.

> Updating the code to allow (1) nested or variable grid systems, (2) automatic structuring of the vertical grid mesh, (3) the use of coarse-scale regional models to derive boundary conditions for base case performance evaluation and future-year control strategy testing.

Chemistry

> Reevaluation of the excessively large activation energy used for the PAN-forming reaction $NO_2 + C_2O_3 > PAN$ in light of recent laboratory measurements (the activation energy of this reaction is essentially zero).

> Updating the ozone-olefin chemistry (correct overproduction of radicals and associated acceleration of ozone formation).

> Updating the chemical rate data base to include the pressure dependencies of the reactions.

> Verifying the validity of the treatment of nitrogen trioxide (NO_3) and dinitrogen pentoxide (N_2O_5) at night.

> Reevaluating the CBM-IV (following a rigorous evaluation protocol) using the new actinic flux files and much larger data sets from smog chamber experiments used to evaluate other state-of-science mechanisms (RADM and SAPRC).

> Strengthening the CBM-IV documentation to include (1) delineation of estimated parameters from known parameters, (2) identification of the species or cases for which good performance is a result of parameter optimization, (3) the disclosure of the portions of the mechanism that are not well tested, (4) the derivation of the condensed paraffin (PAR) chemistry, (5) a discussion of the scope of the mechanism.

> Redesigning and updating the UAM-IV's radiation preprocessing program that calculates photolysis rates from basic data (i.e., from solar actinic fluxes, absorption cross sections, and quantum yields), and documenting the solar actinic fluxes upon which the default photolytic rates are based.

Meteorology

> Promoting and extending the use of prognostic mesoscale meteorological models using four-dimensional data assimilation or "objective combination" of observations where appropriate.

> Updating the treatment of atmospheric pressure and specific humidity as three-dimensional, time-dependent variables.

> Updating the UAM-IV to receive, as input, fully three-dimensional hourly average temperature fields that are consistent with those used in determining the windfields and mixing heights (or turbulent exchange coefficients).

> Updating the plume rise and plume dispersion treatment using modern methods for plume rise through multiple layers and the plume descent phase (subsequent to initial rise).

> Updating the procedures for calculating vertical turbulent dispersion coefficients with algorithms based on recent advances in boundary layer theory, numerical modeling, and observational studies.

> Evaluating the procedures that "map" three-dimensional windfields, produced by meteorological models, onto the UAM-IV grid mesh.

Emissions

> Treating emissions modeling as a formal process (including thorough performance and sensitivity-uncertainty testing). The development of the Emissions Modeling System (EMS) in the SARMAP program will contribute significantly to this endeavor.

> Improving the emissions forecasting process by incorporating planning at the local and regional levels.

> Improving the transportation and mobile source emissions modeling used to develop motor vehicle emissions estimates.

> Improving biogenic emissions estimation procedures via use of (1) remote sensing data, (2) greater specificity in leaf biomass factors, collection of emissions factor data for a larger set of species, (3) incorporation of site-specific meteorological variables, (4) extension of the canopy modeling concepts.

Numerical Methods

> Replacing the Smolarkiewicz horizontal advection scheme in UAM-IV with a state-of-science method.

> Replacing the fully implicit scheme used in the UAM-IV to calculate the vertical turbulent exchange terms with a hybrid numerical method to account for diurnal variations in stability.

9.2.3 Implement Procedures to Reduce Bias in Photochemical Models

Both models exhibit a tendency to underestimate ozone concentration levels. While this finding is not surprising given previous experience in urban-scale ozone

modeling, it poses a practical problem for decision-makers who will use the UAM-IV with the September, 1984 data bases for ozone attainment planning in the South Central Coast Air Basin. How important is this bias and how should it be dealt with in the process of emission control strategy design and evaluation?

Efforts to remove bias in the UAM-IV and CALGRID-IV model results for the September episodes should be mounted along several lines, e.g., improving model formulation and, perhaps more importantly, improving model inputs. More specifically, we recommend:

> Developing and applying emissions models (e.g., the EMS), improving emissions representations, and evaluating the performance of emissions models. Improvement in representation of emissions will require a significant commitment to applied research, an investment that, if made, should have a high payoff. Methods for evaluating model performance are urgently needed. A few worthwhile ideas have been proffered; however, additional ideas must be developed.

> Testing of individual modules (chemistry, meteorology, deposition) to the extent feasible. The SCAQS and especially the SARMAP data bases offer higher resolution data bases than that available in the present study.

> Acquiring and using comprehensive data bases that permit adequate preparation of inputs and "stressful" testing of performance. Model adaptation, testing, and application should be a fully integrated process, whenever possible, comprising well-planned monitoring, model evaluation and application, and data analysis activities.

> Eschewing too-ready acceptance of a potentially flawed model. Stringent process-oriented performance evaluation guidelines should be developed, and modelers should be required to apply them.

9.2.4 Treat the Transport Problem at the Boundaries of the SCCAB Model Domain

To account for and to characterize better the influence of boundary conditions in simulation studies in the SCCAB (and other California air basins), the air quality technical community should pursue the following activities:

> Expand modeling regions, where feasible, sufficiently far upwind to include major source areas and thus diminish the magnitude and importance of upwind determinations.

> Expand modeling regions, where feasible, to greater distances aloft, thereby diminishing the frequency of occurrence of intrusions of polluted air and the concentrations of entering pollutants (note that what were previously boundary conditions aloft are now pollutants contained within the modeling region and followed in the simulation).

> Adopt the use of a coarser-scale model applied to a much larger, more encompassing geographical area to generate boundary conditions through simulation.

> Focus study efforts on regions, rather than urban areas, where principal cities lie within one-half to one day's transport distance of each other.

> Carry out supporting data collection programs, portions of which will be devoted to careful and detailed monitoring of boundaries likely to experience incoming pollutant fluxes that will substantively influence concentration estimates.

> Develop new methods for estimating boundary conditions that rely on the use of both measurements and simulations, capitalizing on the advantages of each.

REFERENCES

ARB, 1992. "Technical Guidance Document: Photochemical Modeling," prepared by the Modeling Support Section, Technical Support Division, California Air Resources Board, Sacramento CA.

Bass A.M., L.C. Glasgow, C. Miller, J.P. Jesson, and D.L. Fiken, 1980, "Temperature Dependent Absorption Cross-Sections for Formaldehyde (CH_2O): The Effect of Formaldehyde on Stratospheric Chlorine Chemistry," Planet. Space Sci., Vol. 28, pp. 675-679.

Businger, J. L., 1982. "Equations and Concepts. In Atmospheric Turbulence and Air Pollution Modeling, (edited by Nieuwstadt, F. T. M. and van Dop H.,) pp. 1-36. D. Reidel, Dordrecht.

Carter, W.P.L., 1988. "Documentation of a Gas-Phase Photochemical Mechanism for Use in Airshed Modeling", Final Report on Contract No. A5-122-32 for the California Air Resources Board, Sacramento, CA.

Carter, W.P.L., 1990. "A Detailed Mechanism for the Gas-Phase Atmospheric Reactions of Organic Compounds," Atmos. Environ., Vol. 24A, pp. 481-518.

Dabberdt, W. F., 1984. "Preliminary Summary of the 1984 South Central Coast Cooperative Aerometric Monitoring Program (SCCCAMP) Exploratory Study", Report by SRI International, Menlo Park, prepared for the Western Oil and Gas Association.

Dabberdt, W. F., and W. Viezee, 1987. "South Central Coast Cooperative Aerometric Monitoring Program (SCCCAMP)", Bulletin of the American Meteorological Society, Vol. 68, pp. 1098-1110.

EPA, 1991. "Guidance for Regulatory Application of the Urban Airshed Model (UAM), "Office of Air Quality Planning and Standards, U.S. Environmental Protection Agency, Research Triangle Park, N.C.

Gery, M. W., G. Z. Whitten, and J. P. Killus, 1988. "Development and Testing of the CBM-IV for Urban and Regional Modeling", EPA/600/3-88/012, U.S. Environmental Protection Agency, Research Triangle Park, NC.

Godowitch, J. M., R. T. Tang, and J. S. Newsom, 1992. "Development of an Improved Urban Airshed Modeling System", 85th Annual Meeting of the Air and Waste Management Association, 21-26 June, Kansas City, MO.

Goodin, W. R., G. J. McRae, and J. H. Seinfeld, 1980. "An Objective Analysis Technique for Constructing Three-Dimensional Urban-Scale Wind Fields", Journal of Applied Meteorology, Vol. 19, pp. 96-106.

Holtslag, A. A. M., and A. P. van Ulden, 1983. "A Simple Scheme for Daytime Estimates of the Surface Fluxes From Routine Weather Data", Journal of Climate and Applied Meteorology, Vol. 22, pp. 517-529.

Holtslag, A. A. M., and Nieuwstadt, F. T. M., 1986. "Scaling the Atmospheric Boundary Layer", Boundary Layer Meteorology, Vol. 36, pp. 201-209.

Killus, J. P., et al., 1977. "Continued Research in Mesoscale Air Pollution Simulation Modeling: Volume V--Refinements in Numerical Analysis, Transport, Chemistry, and Pollutant Removal," EPA Contract No. 68-02-2216, Systems Applications, Inc., San Rafael CA.

Kumar, N., A. G. Russell, and G. J. McRae, 1992. "A Project to Add the Carbon-Bond 4 Chemistry to the California Air Resources Board Airshed Model (CALGRID)", prepared for the California Air Resources Board, Sacramento, CA.

Lamb, R. G., et al., 1977. "Continued Research in Mesoscale Air Pollution Simulation Modeling -- Volume II: Modeling of Microscale Phenomena," EPA-600/4-76-016c, Systems Applications, Inc., San Rafael CA.

Marchuk, G. I., 1975. Methods of Numerical Mathematics, Springer, New York.

Moortgat, G. K., W. Klippel, K. H. Mobus, W. Seiler, and P. Warneck, 1980. "Laboratory Measurement of Photolytic Parameters for Formaldehyde," FAA-EE-80-47, Office of Environment and Energy, Federal Aviation Administration, Washington DC.

Morris, R. E., T. C. Myers, and J. L. Haney, 1990. "User's Guide for the Urban Airshed Model. Volume I. User's Manual for UAM(CB-IV)", Report by Systems Applications, Inc., No. SYSAPP-90/018a, Prepared for U.S. Environmental Protection Agency, Office of Air Quality Planning and Standards, Research Triangle Park, NC.

Myers, T. C., 1990. "Modeling of the South Central Coast Air Basin with the Carbon-Bond IV Version of the Urban Airshed Model", prepared for Region IX, U.S. Environmental Protection Agency, prepared by Systems Applications, Int., San Rafael, CA. SYSAPP-90/117.

Odman, M. T., et al., 1992. "An Investigation of Error Propagation in the California Air Resources Board Air Quality Model", Final Report the the California Air Resources Board.

Peterson, J. T., and E. C. Flowers, 1976. "Urban-Rural Solar Radiation and Aerosol Measurements in St. Louis and Los Angeles," unpublished manuscript.

Reynolds, S. D., T. W. Tesche, and D. R. Souten, 1985. "Overall Study Protocol for the South Central Coast Cooperative Aerometric Monitoring Program", Final Report to the Western Oil and Gas Association, by Systems Applications, Inc., San Rafael, CA.

Smagorinsky, J., 1963. "General Circulation Experiments with the Primitive Equaitons: 1. The Basic Experiment", Monthly Weather Review, Vol. 91, pp. 99-164.

Smolarkiewicz, P. K., 1983. "A Simple Positive Definite Advection Scheme with Small Implicit Diffusion", Monthly Weather Review, Vol. III, pg. 479.

Stauffer, D. R., and N.L. Seaman, 1990. "Use of Four Dimensional Data Assimilation in a Limited-Area Mesoscale Model", Monthly Weather Review, vol. 118, pp. 1250-1277.

Scire, J. S., R. J. Yamartino, G. R. Carmichael, and Y.S. Chang, 1989. "CALGRID: A Mesoscale Photochemical Model. Volume II: User's Guide", report to the California Air Resources Board, prepared by Sigma Research Corporation, Westford, Mass.

Tennekes, H., 1982. "Similarity Relations, Scaling Laws, and Spectral Dynamics", in Atmospheric Turbulence and Air Pollution Modeling, (Nieuwstadt, F. T. M. and van Dop, H.), pg 37-68. D. Reidel, Dordrecht.

Tesche, T. W., 1991. "Evaluating Procedures for Using Numerical Meteorological Models as Input to Photochemical Models", 7th Joint Conference on Applications of Air Pollution Meteorology, American Meteorological Society, 13-18 January, New Orleans, LA.

Tesche, T. W., 1992. "SARMAP Model Evaluation Protocol", prepared for the Valley Air Pollution Study Agency, prepared by Alpine Geophysics, Crested Butte, CO (AG-90/TS21).

Tesche, T. W., and D. E. McNally, 1991. "Photochemical Modeling of Two 1984 SCCCAMP Ozone Episodes," J. Appl. Meteor., Vol. 30, No.5, pp. 745-763.

Tesche, T. W., C. Seigneur, B. Oliver, and J. L. Haney, 1984. "Modeling Ozone Control Strategies in Los Angeles", Journal of Environmental Engineering, Vol. 110, No. 1, pp. 208-225.

Tesche, T. W., C. Daly, B. D. Miller, and S. D. Reynolds, 1985. "Analysis of the Data Collected in the 1984 SCCCAMP Field Program", SYSAPP-85/029, Final Program Report to the South Central Coast Cooperative Aerometric Monitoring Program, Systems Applications, Inc., San Rafael, CA.

Tesche, T. W., D. E. McNally, and W. R. Oliver, 1988a. "Airshed Model Simulation of the 6-7 September 1984 Ozone Episode in Support of the Santa Barbara Air Quality Attainment Plan," prepared for the Santa Barbara County Air Pollution Control District, Radian Corporation, Sacramento CA.

Tesche, T. W., J. G. Wilkinson, D. E. McNally, R. Kapahi, and W. R. Oliver, 1988b. "Photochemical Modeling of Two SCCCAMP 1984 Oxidant Episodes, II: Modeling Procedures and Evaluation Results," prepared for the U.S. Environmental Protection Agency, Region IX, Radian Corporation, Sacramento CA.

Tesche, T. W., P. Georgopoulos, J. H. Seinfeld, P. M. Roth, F. Lurmann, and G. Cass, 1990a. "Improvement of Procedures for Evaluating Photochemical Models," Contract No. A832-103, prepared for the California Air Resources Board, Sacramento, CA.

Tesche, T. W., P. M. Roth, S. D. Reynolds, and F. W. Lurmann, 1992. "Scientific Assessment of the Urban Airshed Model (UAM-IV)", report to the American Petroleum Institute, prepared by Alpine Geophysics, Crested Butte, CO (AG-90/TS16).

van Ulden, A. P., and A. A. M. Holtslag, 1985. "Estimation of Atmospheric Boundary Layer Parameters for Diffusion Applications", Journal of Climate and Applied Meteorology, Vol. 24, pp. 1196-1207.

Wehner, J. F., and R. H. Wilhelm, 1956. "Boundary Conditions of Flow Reactor," Chem. Eng. Sci., Vol. 6, p. 89.

Wilczak, J. M., and M. S. Phillips, 1986. "An Indirect Estimation of Convective Boundary Layer Structure for Use in Pollution Dispersion Models", Journal of Climate and Applied Meteorology, Vol. 25, pp. 1069-1624.

Wyngaard, J. C., 1985. "Structure of the Planetary Boundary Layer and Implications for Its Modeling", Journal of Climate and Applied Meteorology, Vol. 24, pp. 1111-1130.

Wyngaard, J. C., 1988. "Structure of the PBL". In Lectures on Air Pollution Meteorology, pp. 9-62, American Meteorological Society, Boston, Mass.

Yamartino, R. J., J. S. Scire, S. R. Hanna, G. R. Carmichael, and Y. S. Chang, 1989. "CALGRID: A Mesoscale Photochemical Grid Model," Model Formulation Document, A049-1, prepared for the California Air Resources Board, Sigma Research Corporation and the Department of Chemical Engineering, University of Iowa, Iowa City, Iowa.

Yamartino, R. J., J. S. Scire, and S. R. Hanna, 1991. "Formulation of the CALGRID Photochemical Oxidant Grid Model," Seventh Joint Conference on Applications of Air Pollution Meteorology, American Meteorological Society, New Orleans LA, 14-18 January.

Final Report

EVALUATION OF THE UAM-IV AND CALGRID-IV PHOTOCHEMICAL MODELS WITH TWO SANTA BARBARA-VENTURA OZONE EPISODES

Appendices: Inert Tracer Simulation Results

October 26, 1992

Prepared for

Dr. Kit Wagner
California Air Resources Board
Technical Support Division
P.O. Box 2815
Sacramento, California 95812

ARB Agreement No. A974-212
Alpine Geophysics Subcontractor Agreement No. AG-90/TS14/SO1

Prepared by

R. E. Morris
B. Shi

Systems Applications International
101 Lucas Valley Road
San Rafael, California 94903
415/507-7100

Contents

Appendix A

DISCUSSION OF WEIGHTED-TRACER SIMULATION RESULTS

Appendix A

DISCUSSION OF WEIGHTED-TRACER SIMULATION RESULTS

INTRODUCTION

Photochemical grid model calculations are influenced by the initial concentrations, boundary conditions, emissions, and meteorological inputs. The usual use of a photochemical grid model is to estimate the effects of alternative emission control strategies on ozone and other pollutant concentrations. Ideally, one would like the model estimates to be primarily influenced by the emission inputs. In some regions, such as the northeastern U.S., ozone concentrations are highly influenced by transported pollutants from upwind regions and, thus, the model estimates are always going to be heavily influenced by boundary conditions. However, over the last decade there has been a move toward minimizing the influences of initial concentrations and boundary conditions. The duration of simulations have been extended and the first one or two days of the simulation are categorized as initialization days whose primary purpose are to wash out the initial concentrations. Larger modeling domains are also currently in use to reduce the effects of the boundary conditions on the model calculations in the center portion of the modeling domain. Current regulatory guidance for photochemical grid model applications (e.g., EPA, 1991; CARB, 1992) include recommendations that modelers should estimate how highly the calculations are influenced by initial and boundary conditions.

One methodology for assessing the influences of initial concentrations, boundary conditions, and emissions on model calculations is through the use of sensitivity or diagnostic simulations as recommended by Tesche and co-workers (1990) in which the values for initial concentrations, boundary conditions, and emissions are separately set to

zero. These types of simulations are not only useful for determining the influence of these model inputs for a current or future year base case simulation, but such diagnostic simulations can also be utilized to determine the definition of some of the modeling inputs. For example, the optimal simulation initialization time could be determined by exercising the model with and without initial concentrations for several different start times and then selecting a start time such that: (1) the initial concentrations do not significantly influence the ozone concentrations during the period of interest; and (2) the length of the simulation is minimized to reduce computer costs. However, performing many photochemical grid model simulations, like those just described, to determine the optimal simulation start time requires extensive computer time.

For the Urban Airshed Model (UAM-IV), software has been developed so that it could be exercised in a "weighted-tracer" simulation mode in which the model is run without chemistry using inert tracers to estimate the relative contributions of emissions, initial concentrations, and boundary conditions to the total inert mass loading in the region. Because the weighted-tracer simulations are run without any chemistry, and chemistry tends to consume approximately 85 percent of the computation time in a photochemical grid model, the weighted-tracer simulations run approximately 6-8 times faster than a full chemistry simulation. In the weighted-tracer simulations, total NO_x, total reactive organic gases (ROG), and total "potential ozone" (i.e., a measure of ROG that takes into account of the reactivities of the ROG compounds through maximum incremental reactivity factors, Carter, 1991) are partitioned into "area emissions" (including biogenics), "point emissions", "initial concentrations", and "boundary conditions" (separately for each lateral boundary and aloft). The mass flux inputs of each of the weighted tracer species is based on the actual mass fluxes prescribed in the UAM-IV inputs. The utility of using the weighted-tracer simulation for analyzing the relative effects of initial and boundary conditions and emissions on model calculations has been demonstrated in the EPA Five Cities UAM Study (Morris et al., 1990a,b).

The UAM weighted-tracer software has been extended to the nested-grid version of the UAM-V and utilized in the preliminary UAM-V simulations performed for the Lake

Michigan Ozone Study (LMOS) (Morris et al., 1992). In this study we have further extended the weighted-tracer software to be used with the CALGRID model. The following sections discuss the development of the weighted-tracer software for the CALGRID followed by a comparison of weighted-tracer simulations using the UAM-IV and CALGRID for 6-7 September and 16-17 September 1984. Finally, the UAM-IV and CALGRID weighted-tracer simulations are compared with the full photochemical sensitivity simulations.

DEVELOPMENT OF WEIGHTED-TRACER SOFTWARE FOR CALGRID

The UAM-IV weighted-tracer simulation software was adapted for the CALGRID model. This software converts the CALGRID area source emission files (AREM.DAT), point source emission files (PTEMCYC.DAT, PTEMARB.DAT, and PTEMMOB.DAT), initial concentration file (ICON.DAT), lateral boundary condition files (BCON.DAT), and top boundary condition file (TCON.DAT) into the inert NO_x, reactive hydrocarbons (RHC), and "potential ozone " (PO3) species used in the weighted-tracer simulation. Initially, the goal was to not modify the CALGRID code and instead specify no chemical transformation in the chemical mechanism files (LMPBE221.MOD and CALBE221.RXP) and no deposition in the deposition velocity input file (VD.DAT). However, after several attempts at trying to implement the weighted-tracer software without modifying the CALGRID code it became apparent that much of the code is hard-wired for photochemical simulations. Thus, instead two minor modifications were made to the CALGRID so that weighted-tracer simulations could be performed: (1) the statement "lchem=.true." on line 239 of subroutine opslpt.f was commented out; and (2) a command "read(io5,(7x,l10)) lchem" was added to subroutine readcf.f such that the variable "lchem" is now defined on line 4 of the CALGRID run specification file. Thus, full photochemical or inert (including weighted-tracer) CALGRID simulations can now be performed by specifying the variable lchem as either true or false in line 4 of the CALGRID input file.

To perform weighted-tracer simulations the CALGRID or UAM-IV model inputs must first be processed by the weighted-tracer preprocessor ALLTRAC which creates new input files of several different "colored" tracers that represent the different boundary conditions, initial concentrations, and emission inputs for three species: NO_x (defined as NO_2+NO), reactive hydrocarbon (RHC, carbon weighted CB-IV species), and potential ozone (PO3, use of Carter Maximum Incremental Reactivity (MIR) factors to obtain a measure of the reactivity of the RHC).

COMPARISON OF CALGRID AND UAM-IV WEIGHTED-TRACER SIMULATIONS

The CALGRID and UAM-IV were both exercised in the weighted-tracer mode using input files generated by processing the 5-7 September and 16-17 September 1984 base case modeling input data bases. The CALGRID inputs for these base cases were derived from the historical UAM-IV base case input files in a manner to try as match the inputs for the two models as closely as possible. However, because of the different vertical layer structures in the two models, the model inputs could not be matched exactly.

A postprocessor was used to process the output from the weighted-tracer simulations to display the percent contribution of boundary conditions (lateral boundaries and aloft), initial concentrations, area source emissions, and point source emissions to the total NO_x, RHC, or potential ozone (PO3) inert tracer. The weighted-tracer results are then displayed in spatial plots to analyze the spatial and temporal progression of the influences of initial concentrations, boundary conditions, and emissions to the total inert tracer. The weighted-tracer simulations contain much more information than will be displayed here (e.g., separate characterization of the contributions of boundary conditions from the north, south, east, and west lateral boundaries as well as the boundary aloft), however, the display of the simulation into the gross contributions of initial concentrations, boundary conditions, area source, and point source represents a synthesis of the results into a manageable amount of output.

Appendix B displays the weighted-tracer simulation results in the surface layer every 12 hours (at 1100 and 2300) for the CALGRID and UAM-IV 5-7 September, 1984 base case inputs. Similar plots for the 16-17 September, 1985 CALGRID and UAM-V simulations are contained in Appendix C. The following paragraphs discuss the weighted-tracer results for these two episodes.

1100 September 5, 1984

At 1100 on 5 September (9 hours after the beginning of the simulation) the influence of the NO_x boundary tracer is already present in the CALGRID and UAM-IV simulations; the UAM-IV exhibiting a higher influence than the CALGRID in the western portion and the CALGRID showing a higher influence in the eastern portion of the domain. Both the CALGRID and UAM-IV are heavily influenced by the inert RHC boundary condition tracer at this time; the CALGRID showing a higher influence (80-100 percent) of the inert RHC boundary tracer over water (results for the potential ozone are very similar to the RHC and are not shown). The UAM-IV displays a higher influence of initial concentration NO_x and RHC tracer than the CALGRID. The CALGRID and UAM-IV exhibit different influences of point and area source emissions; the CALGRID NO_x tracer in the Santa Barbara channel is dominated by the point and area source emissions whereas the UAM-IV shows very small (< 20 percent) influence of point source NO_x emissions and, except for a small strip south of Point Conception, the influence of area source NO_x is also very small (< 20 percent). Onshore the CALGRID and UAM-IV exhibit similar influences of point and area source RHC and NO_x tracers.

2300 September 5, 1984

By 2300 on 5 September (21 hours after the beginning of the simulation), the influence of the NO_x boundary tracer has increased in the UAM-IV but decreased in the CALGRID. However, in both the CALGRID and UAM-IV, the inert RHC tracer concentrations are

dominated (80-100 percent) by boundary conditions, except near the urban areas of Ventura and Santa Barbara. For both the CALGRID and UAM-IV, the influence of initial NO_x and RHC concentrations are very small at this time, with the CALGRID exhibiting almost no influence in the surface concentrations. Again the CALGRID and UAM-IV are exhibiting different relative influences of point and area source NO_x emissions in the Santa Barbara channel; the CALGRID inert point source NO_x is dominating the total NO_x tracer. The area source emissions RHC tracer exhibits a high influence just offshore of Santa Barbara in the UAM-IV simulations, presumably due to the presence of downslope winds pushing the urban emissions slightly offshore. The CALGRID area source RHC tracer has a smaller influence than the UAM-IV on the total RHC tracer and its influence is more rooted to the urban areas.

1100 September 6, 1984

By 1100 on 6 September (33 hours into the simulation), the influence of the boundary condition NO_x tracer in the CALGRID simulation is almost identical to that seen 24 hours previously (1100 on 5 September). The UAM-IV is also exhibiting similar characteristics of boundary NO_x tracer at 1100 on 5 and 6 September, although there is a higher influence of the boundary NO_x at 1100 on 6 September. However, both the CALGRID and UAM-IV inert RHC tracer concentrations are dominated (80-100 percent) by boundary conditions across most of the modeling domain. The exceptions are over Santa Barbara and the Ventura plain where the urban emissions lessen the RHC boundary contribution to 20-40 percent. After 33 hours of simulation, the initial concentrations (RHC and NO_x) do not significantly contribute to the inert mass loadings in the modeling domain.

The effects of the CALGRID and UAM-V NO_x emission tracers at 1100 on 6 September are exhibiting a similar curious behavior as on 5 September. The CALGRID point source NO_x tracer concentration is dominating (60-100 percent) the total NO_x tracer concentration in the center of the Santa Barbara channel. On the other hand, at this time

the UAM-IV is exhibiting a lower influence (0-60 percent) of the point source NO_x tracer in this region. This region is where a shipping lane exists whose emissions are specified in the point source emission file. The area and point source emission files (Appendix E) confirm that there is a large amount of point source NO_x emissions coming from the shipping traffic, as well as some additional point source NO_x emissions from oil drilling operations. This difference between the two models in the influence of the shipping NO_x emissions in the surface layer is most probably due to differences in the model formulations. The CALGRID has a 20 m surface layer in which the shipping NO_x emissions, which typically have fairly low plume rise, are injected. It also appears that the CALGRID has fairly low mixing between layers 1 and 2 over water. The UAM-IV, on the other hand, has two vertical layers below the diffusion break, which is typically 100-200 m agl over water. Thus layer 1 of the UAM-IV is over 2 times thicker than layer 1 of the CALGRID. Furthermore, the UAM-IV also probably has more vigorous mixing over water than the CALGRID, further diluting the shipping NO_x emissions below the entire DIFFBREAK and, hence, resulting in a lower influence of point source NO_x emissions in the surface layer.

A similar curious difference between the influence of CALGRID and UAM-IV inert area source NO_x concentrations is seen off of Point Conception in the channel. Again this difference between the two models was also seen on 5 September, 1984. The CALGRID area source NO_x tracer dominates (80-100 percent) the total NO_x tracer in a large blob located between San Miguel Island and Point Conception, whereas, the UAM-IV is exhibiting a much lower influence (0-60 percent) of the area source NO_x tracer in this region. Area source NO_x emissions in this area, as well as further north just west of Point Arguello, are due primarily to the presence of three grid cells with large area source NO_x, presumably due to oil drilling operations (see Appendix E). Again the differences in the influence of the platform area source NO_x emissions between the CALGRID and UAM-IV is most probably due to lower dilution in the CALGRID due to the lower surface layer and less vigorous mixing. More similarities between the CALGRID and UAM . source RHC tracer are seen at 1100 on 6 September where the high influence of RHC area source emissions is rooted to the major urban areas around

Santa Barbara and in the Ventura plain.

2300 September 6, 1984

The CALGRID and UAM-IV results for the weighted-tracer simulation at 2300 on 6 September are very similar to those seen at 2300 on 5 September and 1100 on 6 September and all the discussion for those times also pertain to 2300 on 6 September.

1100 and 2300 on 7 September

The results of the weighted-tracer simulations on 7 September are very similar to those seen on 6 September with the following exceptions. Area source NO_x emissions seem to dominate the total NO_x tracer more at 1100 on 7 September. In the UAM-IV, the regions of high influence of area source RHC emissions appears offshore of Santa Barbara and Ventura on 7 September rather than rooted to the urban areas as seen on September 5th and 6th. This effect is more pronounced at 1100 than 2300 on 7 September. Presumably this is due to differences in meteorology on 7 September.

September 16-17, 1984

Appendix C displays the percent contributions of initial concentrations, boundary conditions, and emissions to the total surface NO_x and RHC tracer concentrations for the 16-17 September, 1984 CALGRID and UAM-IV base case modeling inputs. The results for 16-17 September are, qualitatively, very similar to those seen for the 5-7 September, 1984 episode. The high influence of the point source NO_x (shipping) emissions to the total tracer concentration in the Santa Barbara channel appears to be greater and more widespread in the 16-17 September episode resulting in a lowering of the influence of area source NO_x (platform operations) in the channel. Boundary conditions again appear

to be the principle source of domain wide RHC tracer concentrations.

Summary of the Weighted-Tracer Simulations

Although there are many similarities between the CALGRID and UAM-IV weighted-tracer simulations for 5-7 and 16-17 September, 1984, there are also several major differences in the sources of the surface layer tracer concentrations. Many of the differences between the two model calculations can be traced to their different vertical layer structures: the CALGRID layer 1 is always 20 m deep whereas the UAM-IV layer 1 is half the mixing height; and that the CALGRID most likely has a lower mixing rate in the lower atmosphere over water. The major findings from the weighted-tracer simulations are as follows:

In both the CALGRID and UAM-IV the RHC surface tracer concentrations are dominated (80-100 percent) by boundary conditions over most of the region. The exceptions are over the city of Santa Barbara and the Ventura plain where the local emissions limit the influence of the boundary RHC to as low as approximately 20 percent. NO_x boundary conditions also have some influence in the peripheral portions of the region with the UAM-IV indicating a higher influence of NO_x boundary conditions to the total surface NO_x tracer than CALGRID.

Initial concentrations (RHC and NO_x) do not contribute significantly to the surface tracer concentrations by the second day of the simulations.

In the CALGRID, NO_x emissions dominate the NO_x surface tracer concentrations in the Santa Barbara channel; point source NO_x emissions from shipping traffic dominate in the region between the San Miguel, Santa Rosa, and Santa Cruz Islands to the coast of Santa Barbara county and NO_x emissions from platform operations dominate in the region from San Miguel Island up to just west of Point

Arguello.

Area source RHC emissions only have high influence on the surface RHC tracer in the immediate vicinity of the urban areas of Santa Barbara and communities on the Ventura Plain.

COMPARISON OF WEIGHTED-TRACER AND PHOTOCHEMICAL SIMULATIONS

Although weighted-tracer simulations have been used in the past to help define and diagnose the influences of various components of modeling inputs, the comparison of weighted-tracer results to photochemical grid model calculations has not been performed in a systematic fashion. For the first time in this study we have weighted-tracer simulation results, which provide estimates of the relative contribution of initial concentration, boundary conditions, and emissions to the total NO_x and RHC tracers, and full photochemistry sensitivity simulations with zero initial conditions, boundary conditions, and emissions. It should be noted that the zero initial concentrations and zero boundary conditions sensitivity simulations may provide misleading results because the conditions are unrealistic. The complete removal of boundary conditions, for example, may so perturb the chemical equilibrium of the system such that ozone concentrations are drastically altered from the base case. A more realistic sensitivity test would be to utilize clean tropospheric background concentrations for the initial and boundary condition sensitivity tests.

In this section we compare the relative influences of initial concentrations, boundary conditions, and emissions to ozone concentration calculated in the CALGRID and UAM-IV sensitivity tests with each other and with the results from the weighted-tracer simulations. The relative influence of the initial, boundary, and emission inputs to the total ozone concentrations is obtained by taking the ratio of the ozone increment obtained by subtracting the ozone concentration predicted at a site for the base case simulation

from the result from the sensitivity simulation divided by the sum of the three increments. Note that the sum of the ozone increments will usually not equal the base case ozone concentration estimate. However, this approach allows for the relative comparison on a percentage basis of the influences of the three major model inputs to the total ozone concentration.

Appendix D displays plots of the relative contribution of initial concentrations, boundary conditions, and emissions to the CALGRID and UAM-IV estimated ozone concentration at several sites on the last day of the two simulations (7 and 17 September, 1984). Appendix D also compares the results from the photochemical sensitivity simulations with those from the weighted-tracer simulations. Several features immediately become apparent when examining the results given in Appendix D:

The inert RHC and PO3 tracers provide a much better representation than the NO_x tracer of the photochemical model sensitivity simulation estimates on the relative influences of initial concentrations, boundary conditions, and emissions to the estimated ozone concentrations.

By the last day of the two episodes, the initial concentrations do not have any influences on ozone concentrations in the photochemical simulations; the inert RHC, PO3, and NO_x concentrations in the weighted-tracer simulations also show no influence.

The CALGRID model estimates that almost all inert NO_x tracer is due to emissions, whereas, the UAM-IV also has a fairly large boundary condition component, especially at those sites close to the boundary away from the high density urban regions.

The following paragraphs discuss the results from the weighted-tracer simulations and photochemical model sensitivity simulations by site.

Santa Ynez

The Santa Ynez ozone monitor is located in the northwestern portion of the modeling domain within approximately 5 grid cells of the northern boundary. Similar results are seen in the photochemical model simulations on both September 7 and 17. On both days the CALGRID model estimates that approximately 20 percent of the ozone is due to emissions with the other 80 percent due to boundary conditions. Whereas, the UAM-IV estimate that 25-30 percent of the ozone concentration is due to emissions with the rest due to boundary conditions. For both the CALGRID and UAM-IV, the RHC and potential ozone (PO3) tracer matches the photochemical model sensitivity simulation results quite well on 7 and 17 September (within about 5 percent). However, it is curious that the relative reactivity of the RHC tracer for emissions and boundary conditions is different for the CALGRID and UAM-IV; the CALGRID emissions are more and the UAM-IV emissions are less reactive than the boundary conditions. The main differences at Santa Ynez between the CALGRID and UAM-IV simulations is in the inert NO_x tracer; the CALGRID calculates that all of the NO_x tracer is due to emissions whereas the UAM-IV estimates that 40 percent of the inert NO_x tracer is due to boundary conditions.

Goleta

The Goleta site is located on the coast near the center of the modeling domain. Again the results for the CALGRID photochemical and weighted-tracer simulations are quire similar on 7 and 17 September with the inert RHC tracer tracking the photochemical model ozone estimates quite well; both estimating that 20-30 percent of the ozone at this site is due to emissions with the rest due to boundary conditions. The CALGRID PO3 tracer does not track the ozone estimates as well as the RHC tracer. However, the UAM-IV calculations exhibit different behavior on 7 and 17 September and the RHC tracer does not respond the same as the photochemical model simulations. On 7 September the UAM-IV calculates that the contribution of emissions to photochemical

ozone, RHC tracer, and PO3 tracer are approximately 45, 60, and 55 percent, respectively. Similar numbers for 17 September are approximately 30, 50, and 30 percent. The UAM-IV PO3 tracer appears to track the ozone results better than the RHC tracer at Goleta.

Santa Barbara

Although the Santa Barbara site is located just east of Goleta, the behavior of the two models is slightly different. The CALGRID photochemical calculations are quite similar at the two sites but due to higher urban density in this region the influence of the RHC emissions is greater in Santa Barbara (50 percent) than Goleta (20-30 percent). The UAM-IV is exhibiting similar behavior between the two sites on 7 September, but on 17 September the contribution of emissions to the total ozone is greater at Goleta (42 percent) than Santa Barbara (35 percent). At the Santa Barbara site, the PO3 tracer tracks the photochemical ozone results best for CALGRID while none of the tracers replicate the photochemical results for UAM-IV.

Casitas

The Casitas monitor is located on the coast at the mouth of the Ojai valley between Santa Barbara and Ventura. The RHC and PO3 generally do a good job in replicating the relative influences of emissions and boundary conditions on ozone. However, again the tracer concentration are not as good an estimate for determining the influences of emissions and boundary conditions on ozone concentrations in the UAM-IV as compared to CALGRID. On 7 September, the UAM-IV estimates that emissions contribute approximately 30 percent to the daily maximum ozone concentration at Casitas but the RHC and PO3 tracers indicate that they should contribute about 50 percent. On 17 September the UAM-IV estimates that emissions contribute about 35 percent to the daily maximum ozone but the RHC tracer estimates emissions contribute almost 70 percent and

the PO3 tracer estimates emissions contribute around 55 percent. Both the UAM-IV and CALGRID tracer simulations indicate that RHC emissions are less reactive, on a MIR scale, than boundary conditions.

Ojai

Results at Ojai are similar to those seen at the other sites; the UAM-IV is estimating a larger contribution of emissions to the daily maximum ozone concentration (40-50 percent) than the CALGRID (30-35 percent) and, in most cases, the RHC tracer mimics the relative contribution of emissions and boundary conditions to the total ozone fairly well. The exception to this is for the UAM-IV on 17 September where the UAM-IV estimates that emissions contribute 80 percent of the RHC tracer, whereas the actual emissions contribution to ozone is less than 50 percent.

Ventura

At the Ventura site the contribution of emissions to the total ozone, RHC tracer, and PO3 tracer ranges from approximately 20 to 45 percent for the two models and days. The PO3 tracer appears to track the ozone results the best.

Piru, Simi Valley, and Thousand Oaks

The last three sites are all located in eastern Ventura County near the east boundary. On 7 September the boundary conditions dominate the CALGRID and UAM-IV estimated ozone, RHC tracer, and PO3 tracer concentrations. Emissions always contribute less than 25 percent and usually less than 10 percent to the ozone, RHC tracer, or PO3 tracer for these three sites and the two models on 7 September. However, on 17 September the emissions contribution to the total ozone is much greater ranging from 35 to 45 percent

for the CALGRID and UAM-IV. The PO3 tracer appears to do a better job in tracking the ozone results than the RHC tracer.

SUMMARY AND RECOMMENDATIONS

A comparison of the weighted-tracer simulations with the results from the photochemical sensitivity tests is encouraging in that the RHC and potential ozone (PO3) tracer estimates, usually, act as fairly good surrogates in estimating the relative contributions of initial concentrations, boundary conditions, and emissions to photochemical ozone production. However, the NO_x tracer does not appear to respond in a similar fashion to the photochemical ozone calculations from the sensitivity simulations. Furthermore, although the RHC and PO3 generally give a fairly good qualitative estimate on the relative contribution of initial concentrations, boundary conditions, and emissions to ozone concentrations, there are substantial quantitative differences between the RHC and PO3 estimates and those obtained from the zero sensitivity simulations. However, it is unclear how accurately the zero sensitivity simulations represent the relative contributions of initial concentrations, boundary conditions, and emissions to the total ozone concentrations. As noted previously, use of zero initial or boundary conditions is not a realistic situation and it would be interesting to perform similar sensitivity tests with tropospheric background concentrations.

The weighted-tracer simulations also helped to emphasize the differences in the formulations of the CALGRID and UAM-IV and how these differences affect the model calculations. Although one of the objectives of this study was to run the CALGRID and UAM-IV with "identical" sets of inputs, because of the differences in model formulations this could not be accomplished. The weighted-tracer simulations have identified areas where the differences in model formulation are causing the two models to see different model inputs. Most notably, the CALGRID constant 20 m surface layer and vertical diffusion over water appear to be two major differences that may explain some of the differences in the CALGRID and UAM-IV photochemical calculations.

Finally, this project did not have the resources to perform an in depth analysis of the photochemical and weighted-tracer simulations. Further analysis would provide additional insights into the utility of the CALGRID model and the use of weighted-tracer simulations. However, the results to date are promising, the CALGRID model appears to be behaving in a manner similar to the UAM-IV and the weighted-tracer simulations, in most instances, respond in a similar fashion as the photochemical sensitivity simulations.

References

ARB. 1992. "Technical Guidance Document: Photochemical Modeling." California Air Resources Board.

EPA. 1991. "Guideline for Regulatory Application of the Urban Airshed Model." U.S. Environmental Protection Agency (EPA-450/4-91-013).

Morris, R. E., and T. C. Myers. 1990. "User's Guide for the Urban Airshed Model -- Volume I: User's Manual for UAM(CB-IV)". U.S. Environmental Protection Agency, RTP, North Carolina (EPA-450/4-90-007a).

Morris, R. E., T. C. Myers, E. L. Carr, and M. C. Causley. 1990a. "Urban Airshed Model of Five Cities -- Demonstration of the Low-Cost Application of the Model to the City of Atlanta and the Dallas-Fort Worth Metroplex Region." U.S. Environmental Protection Agency (EPA-450/4-90-006B).

Morris, R. E., T. C. Myers, M. C. Causley, L. A. Gardner, and E. L. Carr. 1990c. "Urban Airshed Model Study of Five Cities -- Low-Cost Application of the Model to Atlanta and Evaluation of the Effects of Biogenic Emissions on Emission Control Strategies." U.S. Environmental Protection Agency (EPA-450/4-90-006D).

Morris, R. E., C. A. Emery, T. C. Myers, R. C. Kessler, B. Shi, M. A. Yocke. 1992. "Preliminary Photochemical Modeling of the Lake Michigan Region Using the Nested-Grid Urban Airshed Model (UAM-V)." Systems Applications International, San Rafael, California (SYSAPP-92/055).

Tesche, T. W., P. Georgopoulos, J. H. Seinfeld, G. Cass, F. L. Lurmann, and P. M. Roth. 1990. "Improvement of Procedures for Evaluating Photochemical Models." Radian Corporation (90-264-069-05-02).

Appendix B

CALGRID AND UAM-IV WEIGHTED-TRACER SIMULATION RESULTS FOR 5-7 SEPTEMBER 1984

CALGRID–IV

BNDRY NOX CONTRIBUTION AT: 1100 September 5 LEVEL 1

MAXIMUM CONTRIBUTION IN CELL (52,5) = 99.66 (%)

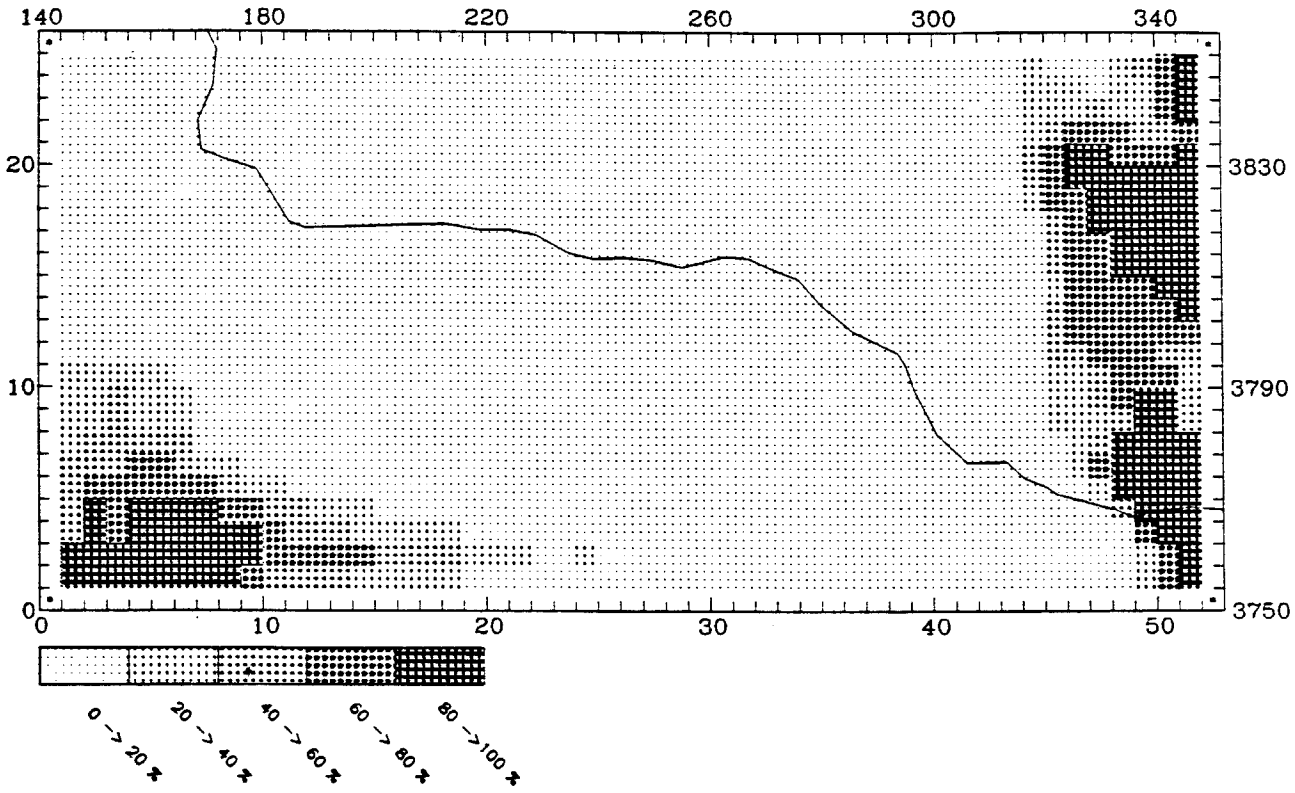

UAM–IV

BNDRY NOX CONTRIBUTION AT: 1100 September 5 LEVEL 1

MAXIMUM CONTRIBUTION IN CELL (2,9) = 100.00 (%)

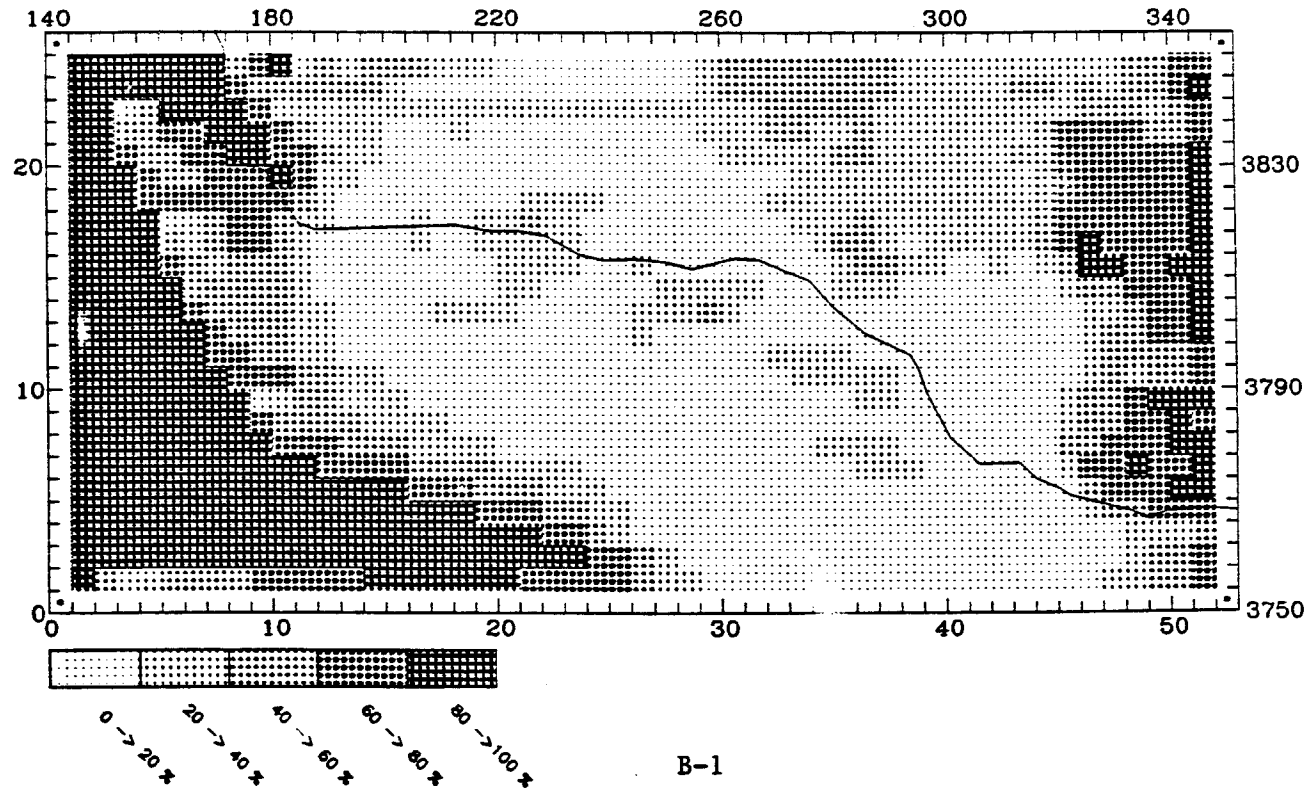

CALGRID–IV

BNDRY RHC CONTRIBUTION AT: 1100 September 5 LEVEL 1

MAXIMUM CONTRIBUTION IN CELL (2,6) = 100.00 (%)

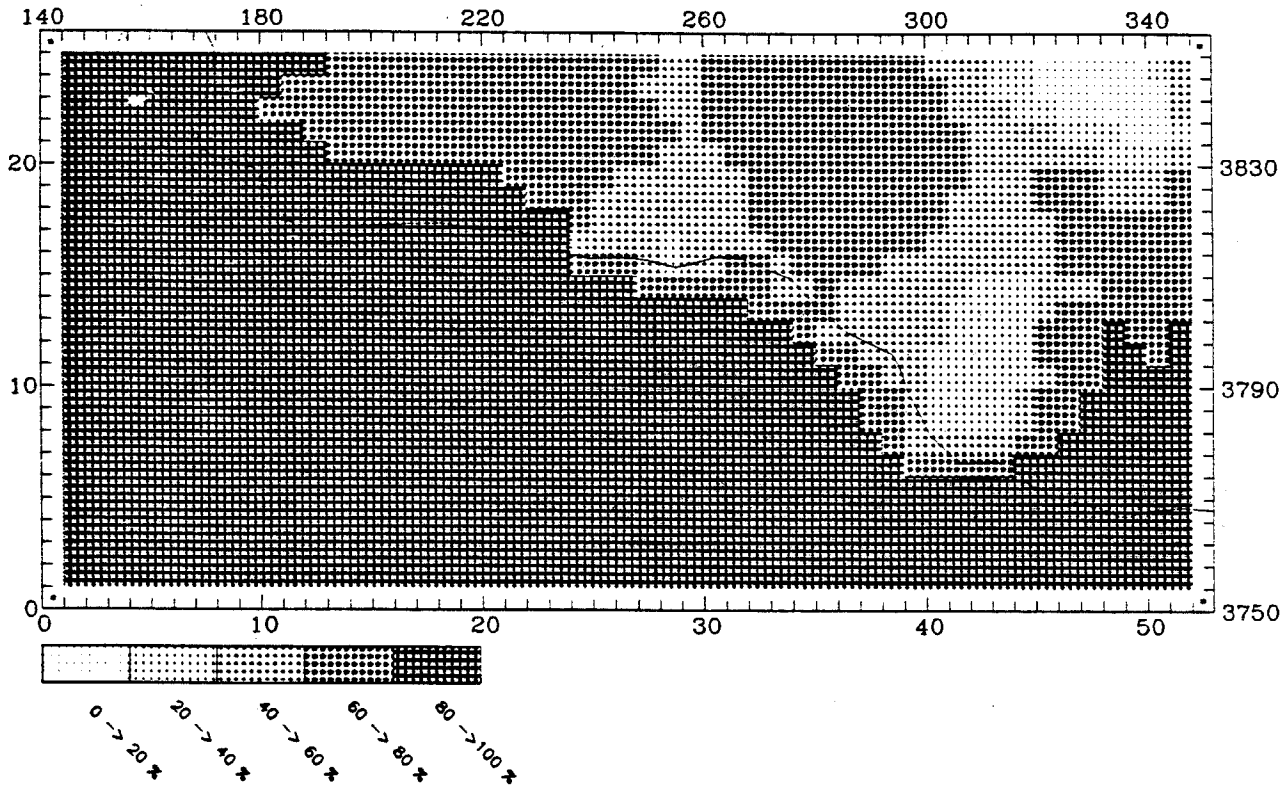

UAM–IV

BNDRY RHC CONTRIBUTION AT: 1100 September 5 LEVEL 1

MAXIMUM CONTRIBUTION IN CELL (2,9) = 100.00 (%)

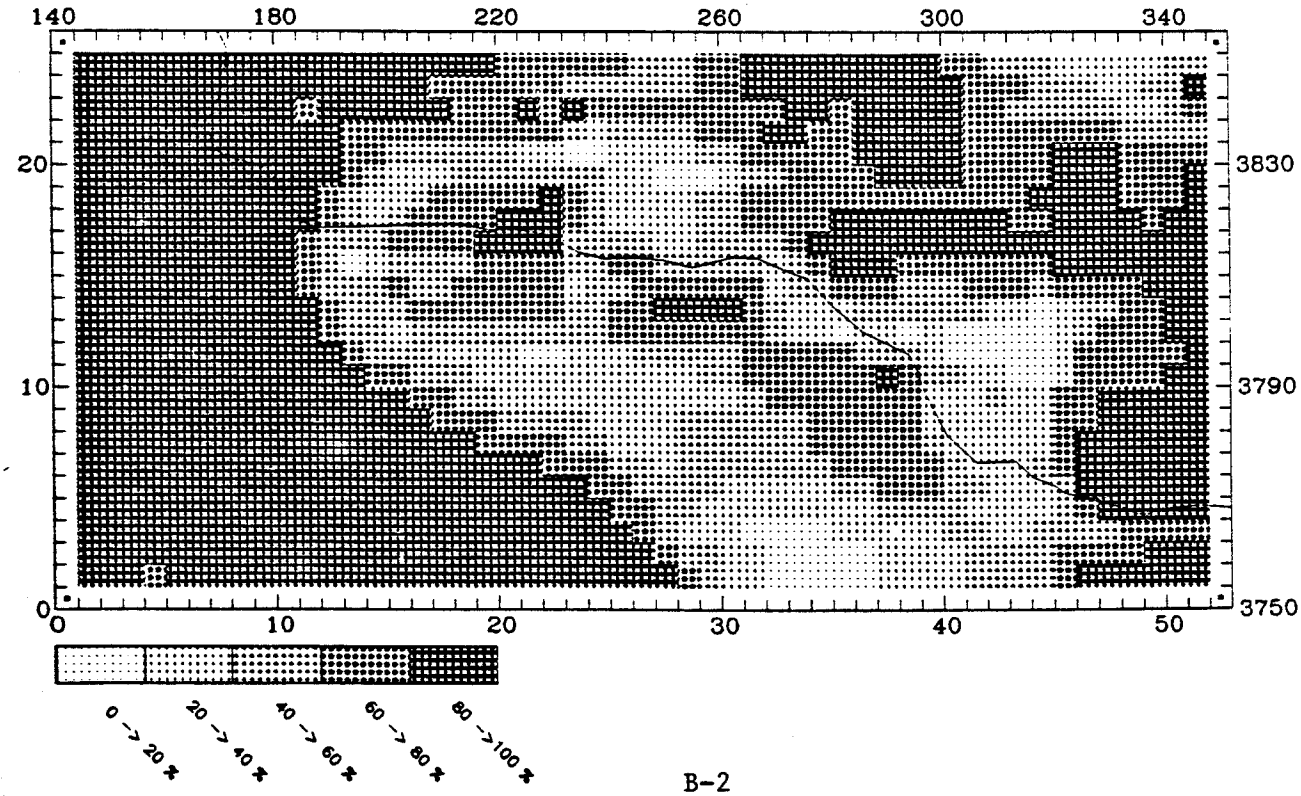

CALGRID–IV

INTNOX CONTRIBUTION AT: 1100 September 5 LEVEL 1

MAXIMUM CONTRIBUTION IN CELL (49,25) = 5.41 (%)

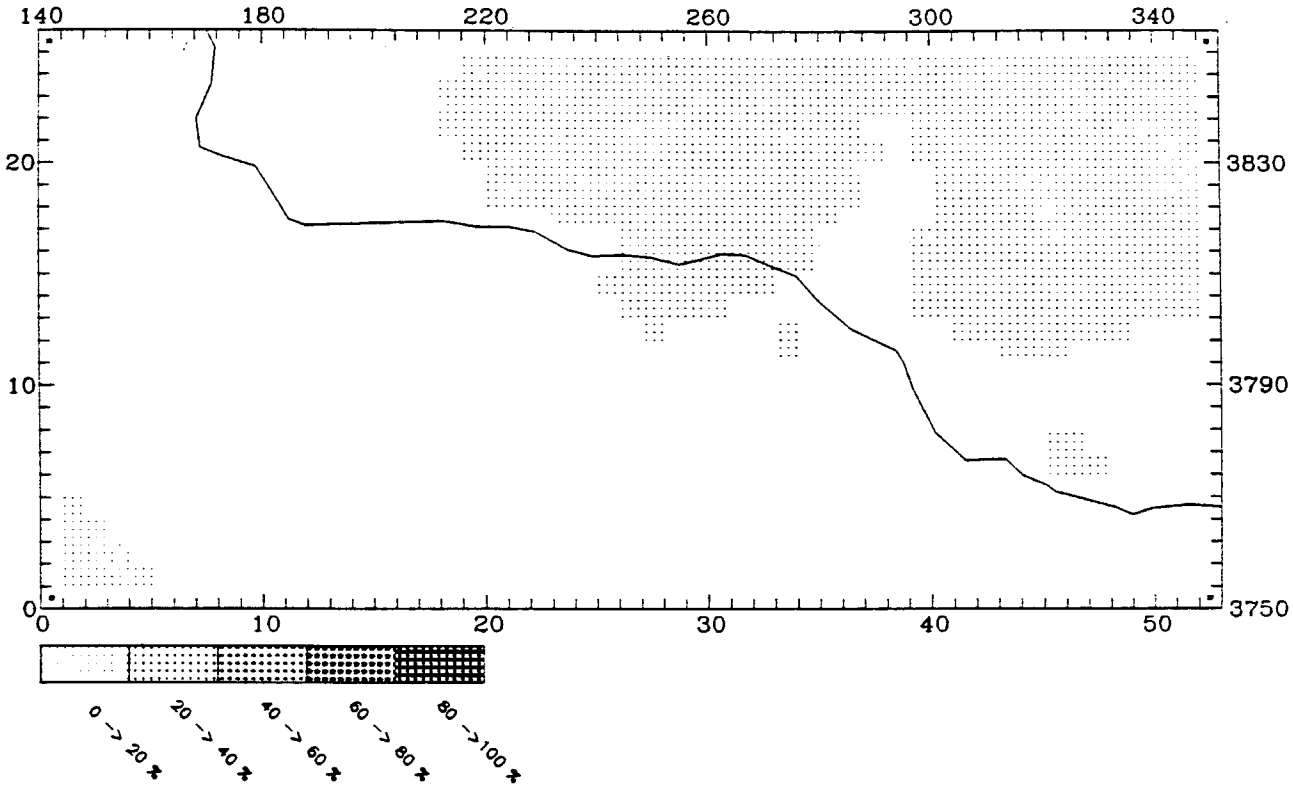

UAM–IV

INTNOX CONTRIBUTION AT: 1100 September 5 LEVEL 1

MAXIMUM CONTRIBUTION IN CELL (37,2) = 97.61 (%)

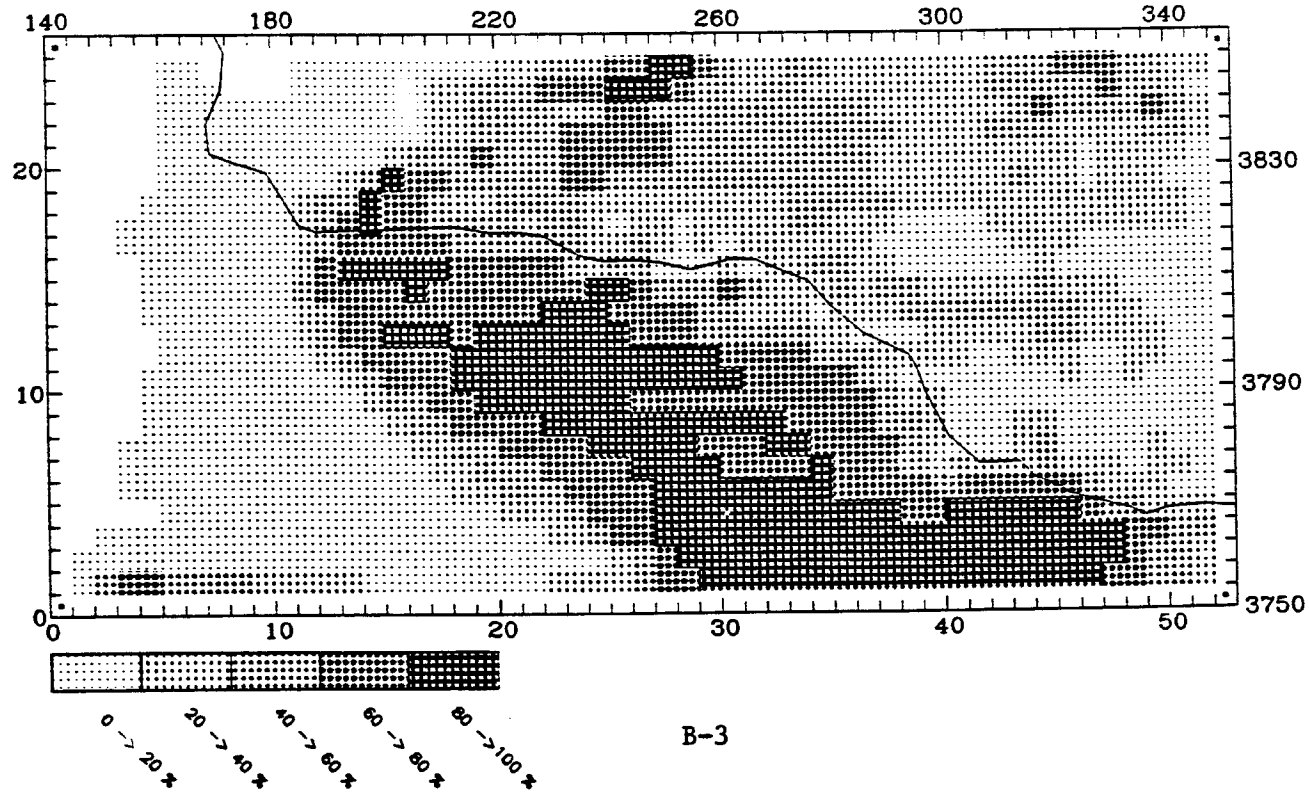

CALGRID–IV

INTHC CONTRIBUTION AT: 1100 September 5 LEVEL 1

MAXIMUM CONTRIBUTION IN CELL (49,24) = 83.74 (%)

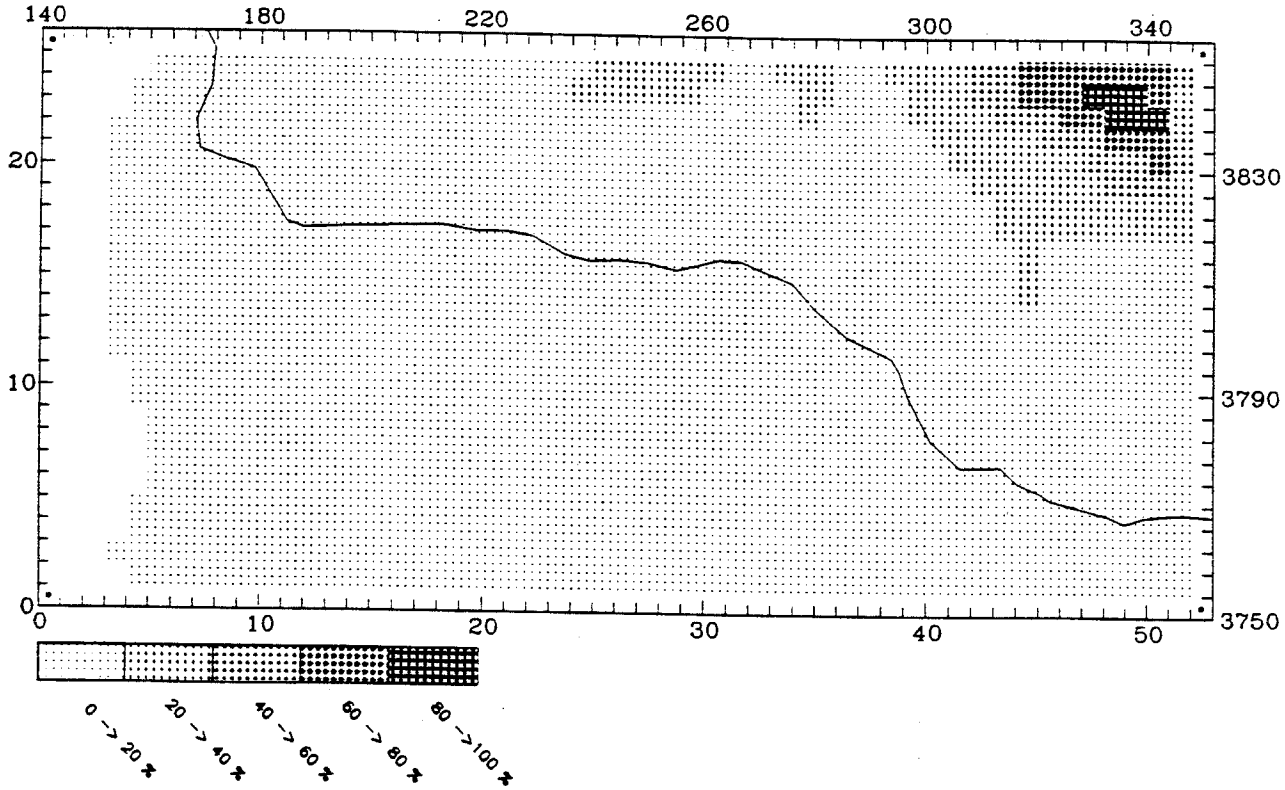

UAM–IV

INTHC CONTRIBUTION AT: 1100 September 5 LEVEL 1

MAXIMUM CONTRIBUTION IN CELL (36,2) = 89.73 (%)

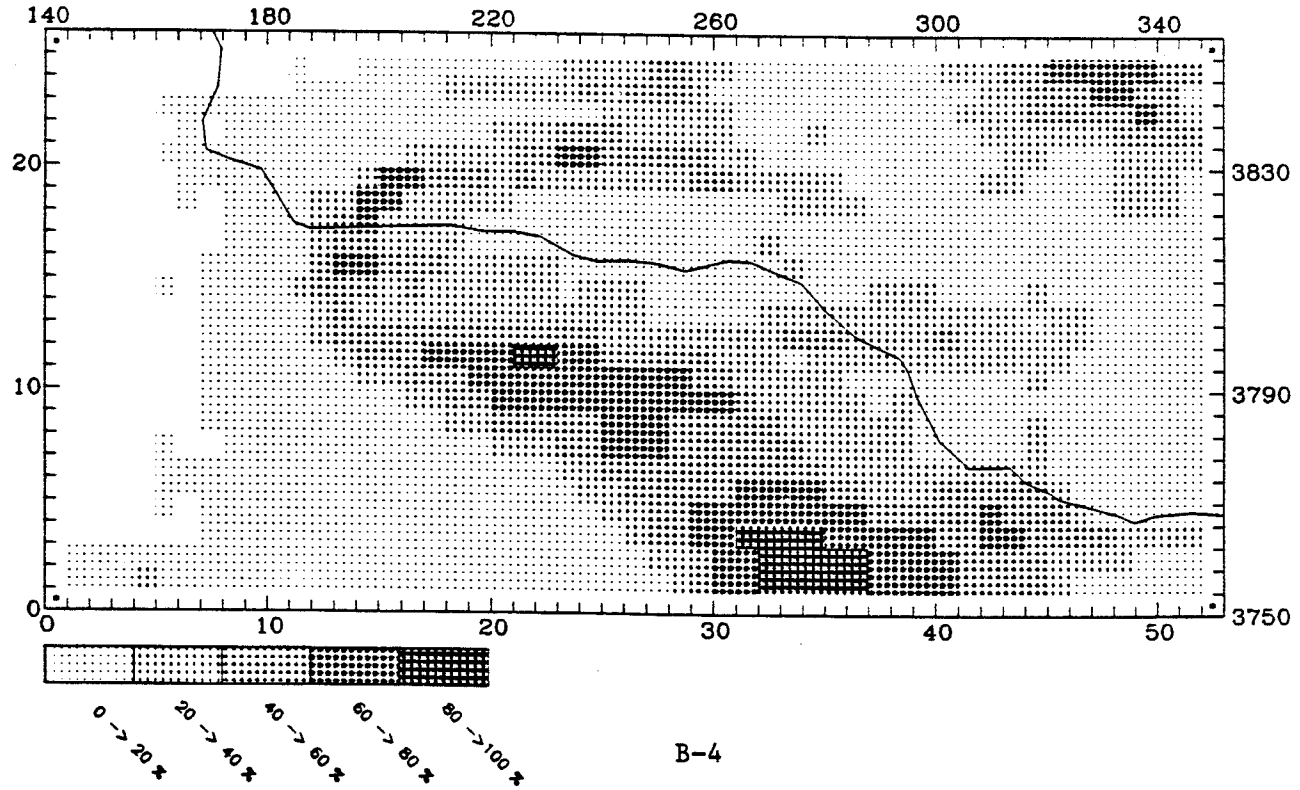

CALGRID–IV

PTARBNOX CONTRIBUTION AT: 1100 September 5 LEVEL 1

MAXIMUM CONTRIBUTION IN CELL (45,2) = 99.90 (%)

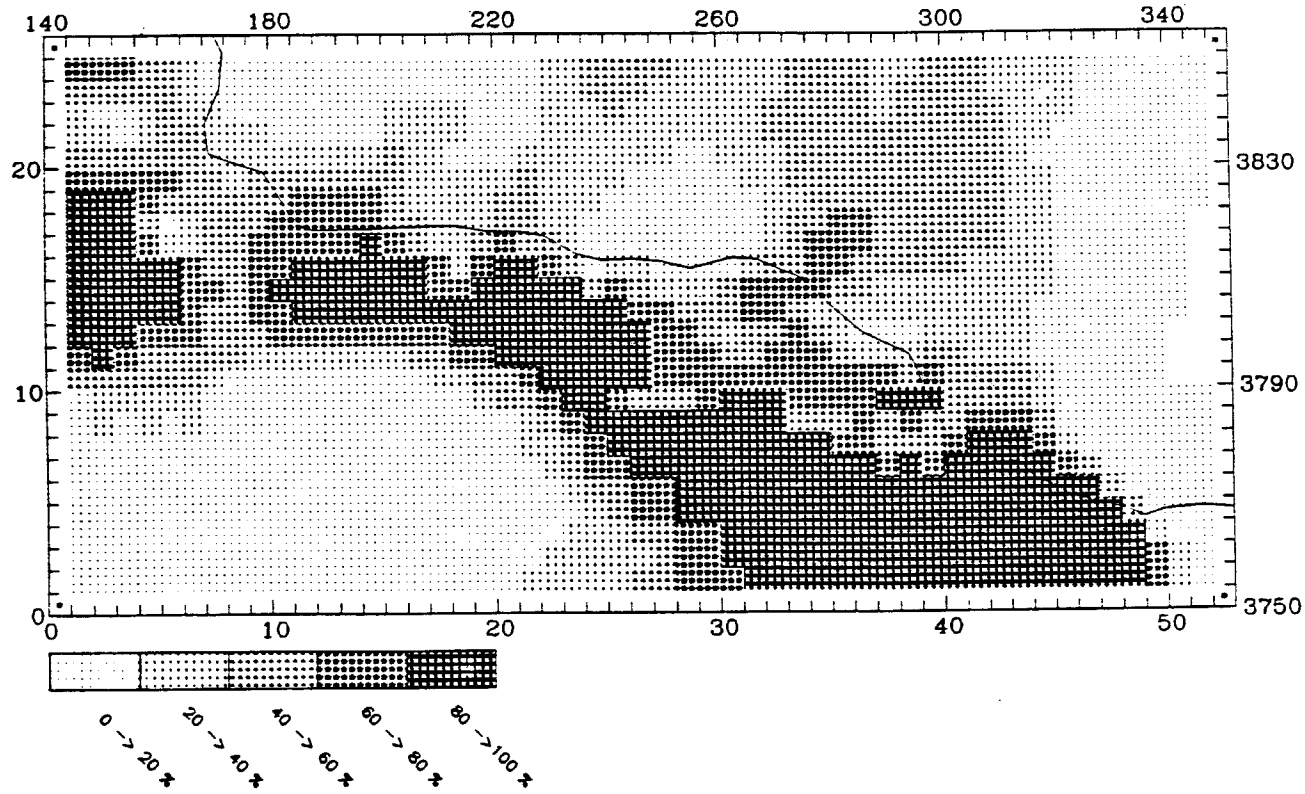

UAM–IV

PTNOX CONTRIBUTION AT: 1100 September 5 LEVEL 1

MAXIMUM CONTRIBUTION IN CELL (32,14) = 37.79 (%)

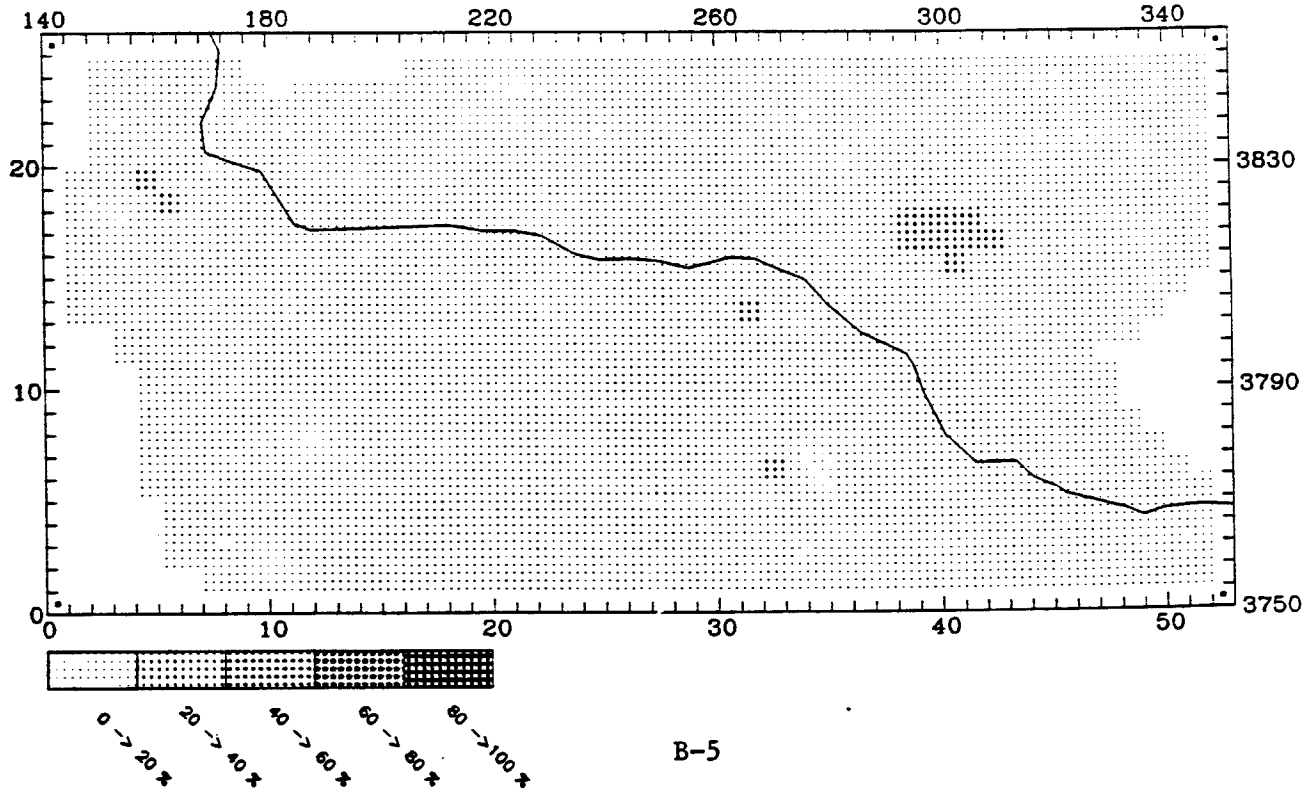

CALGRID–IV

PTARBHC CONTRIBUTION AT: 1100 September 5 LEVEL 1

MAXIMUM CONTRIBUTION IN CELL (33,7) = 3.98 (%)

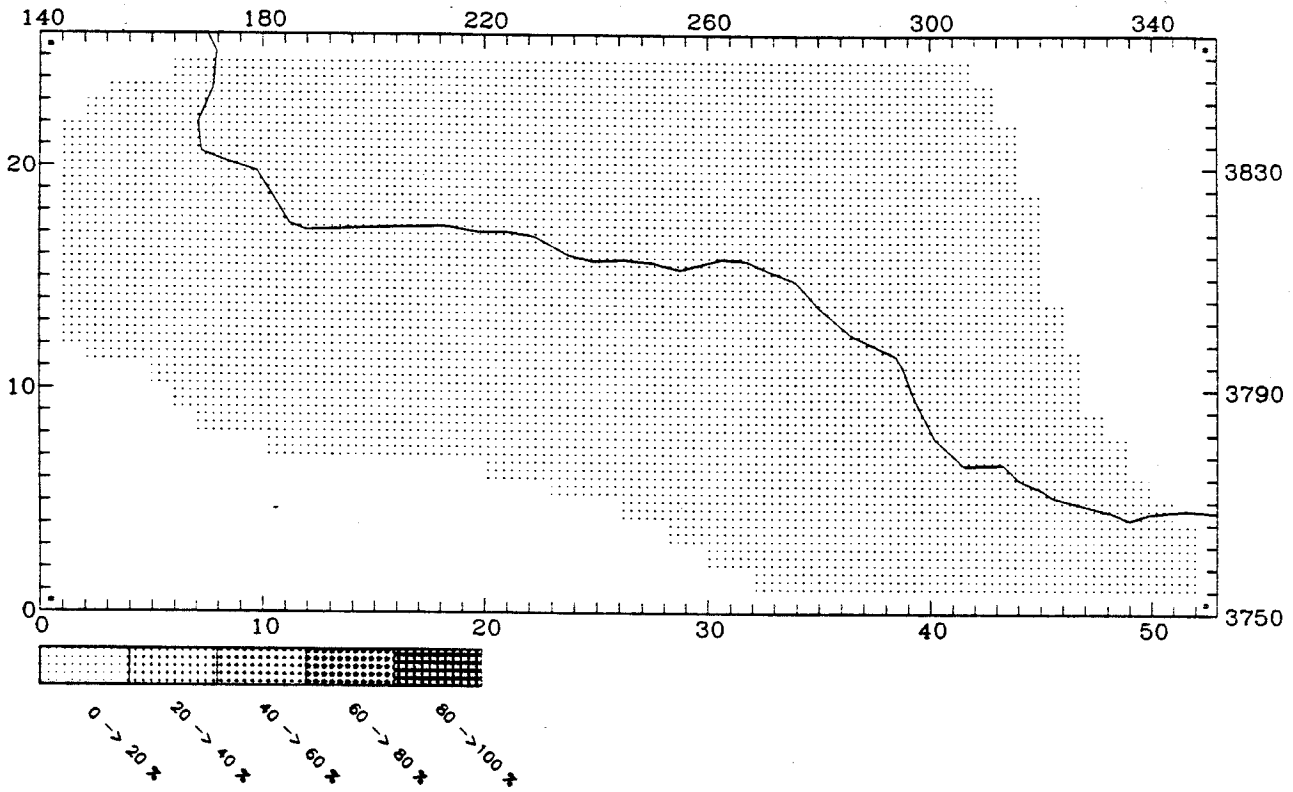

UAM–IV

PTHC CONTRIBUTION AT: 1100 September 5 LEVEL 1

MAXIMUM CONTRIBUTION IN CELL (33,7) = 1.54 (%)

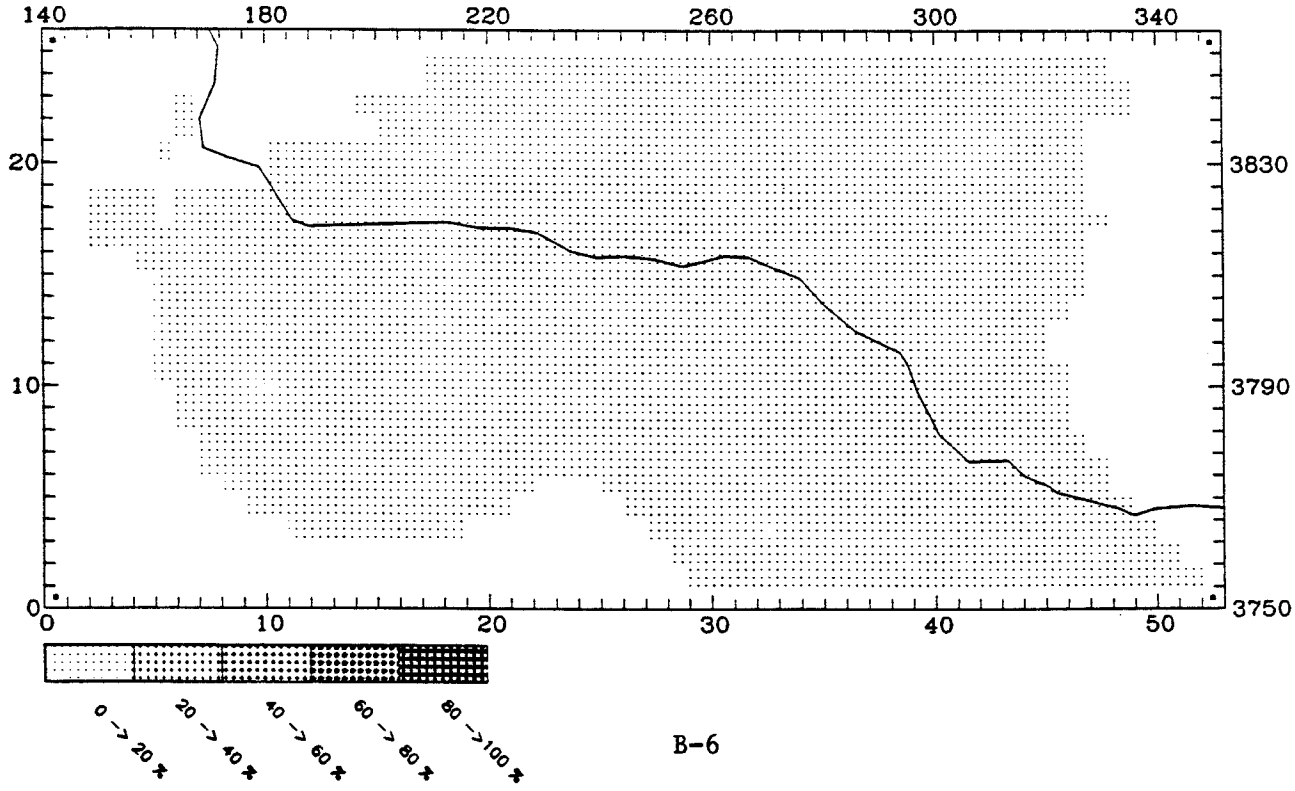

CALGRID–IV

ANOX CONTRIBUTION AT: 1100 September 5 LEVEL 1

MAXIMUM CONTRIBUTION IN CELL (10,10) = 98.80 (%)

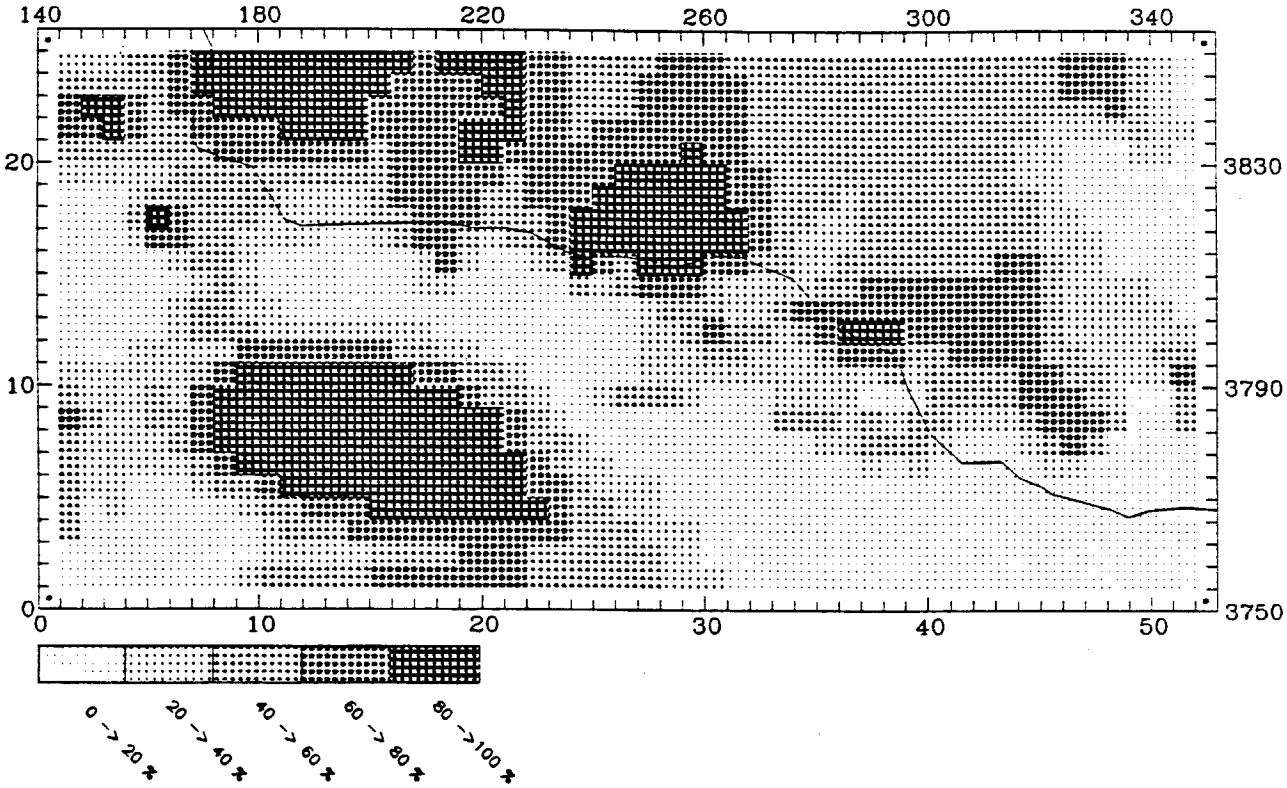

UAM–IV

NOX CONTRIBUTION AT: 1100 September 5 LEVEL 1

MAXIMUM CONTRIBUTION IN CELL (44,11) = 89.09 (%)

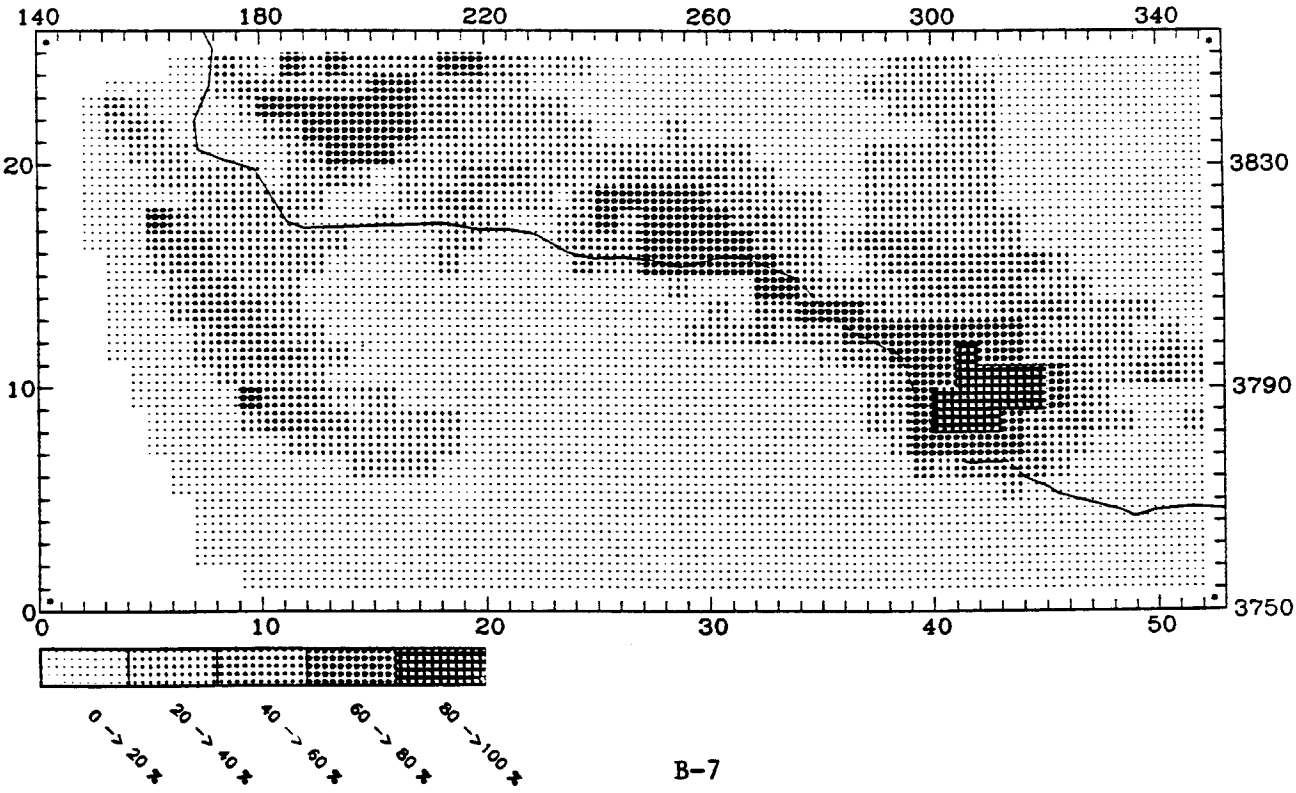

CALGRID–IV

ATHC CONTRIBUTION AT: 1100 September 5 LEVEL 1

MAXIMUM CONTRIBUTION IN CELL (42,12) = 72.93 (%)

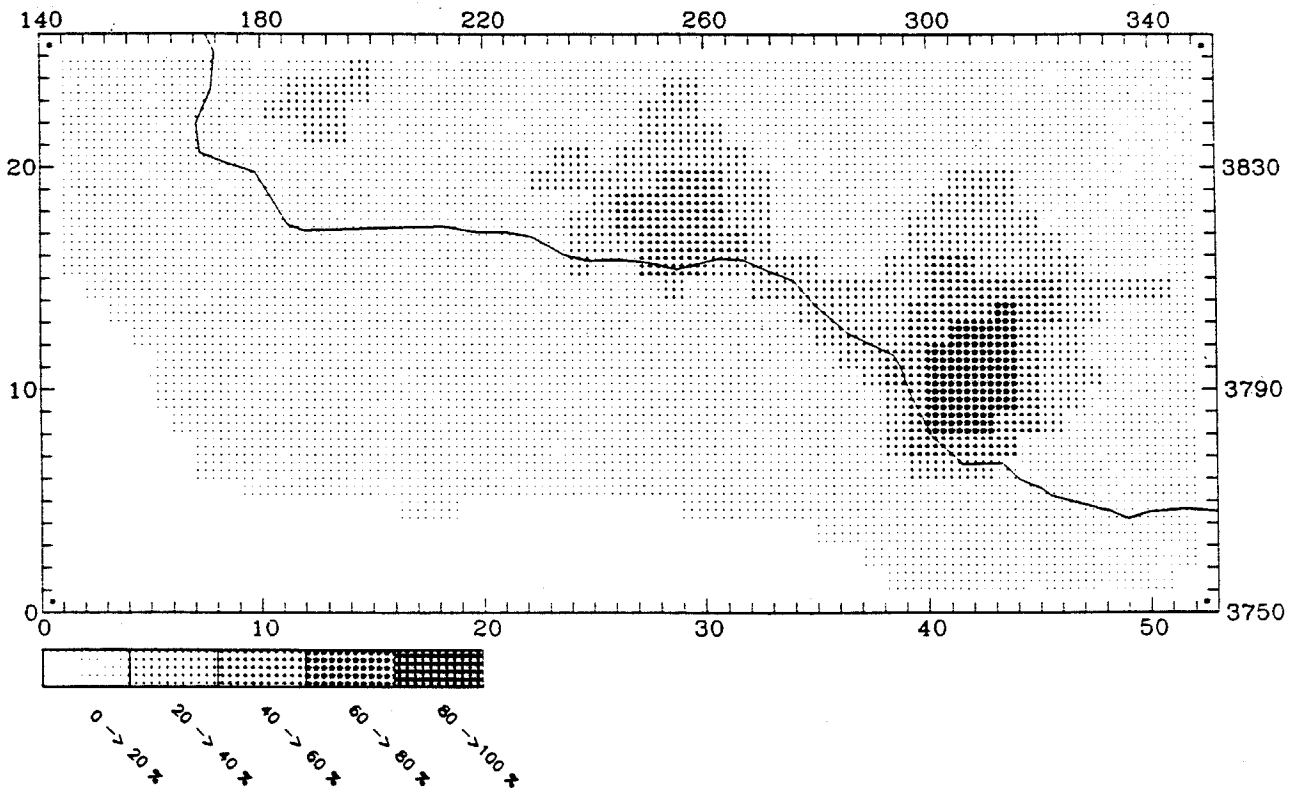

UAM–IV

RHC CONTRIBUTION AT: 1100 September 5 LEVEL 1

MAXIMUM CONTRIBUTION IN CELL (44,11) = 74.98 (%)

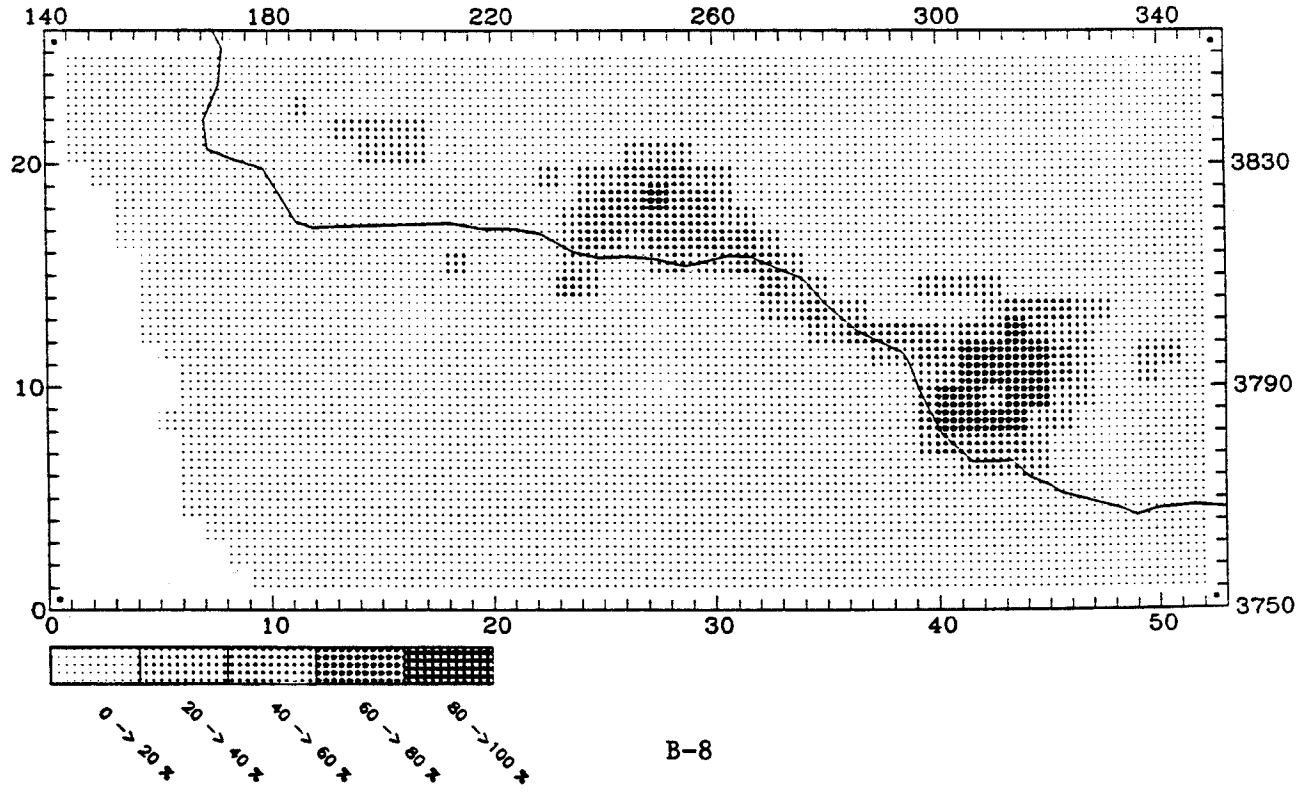

CALGRID–IV

BNDRY NOX CONTRIBUTION AT: 2300 September 5 LEVEL 1

MAXIMUM CONTRIBUTION IN CELL (7,2) = 92.58 (%)

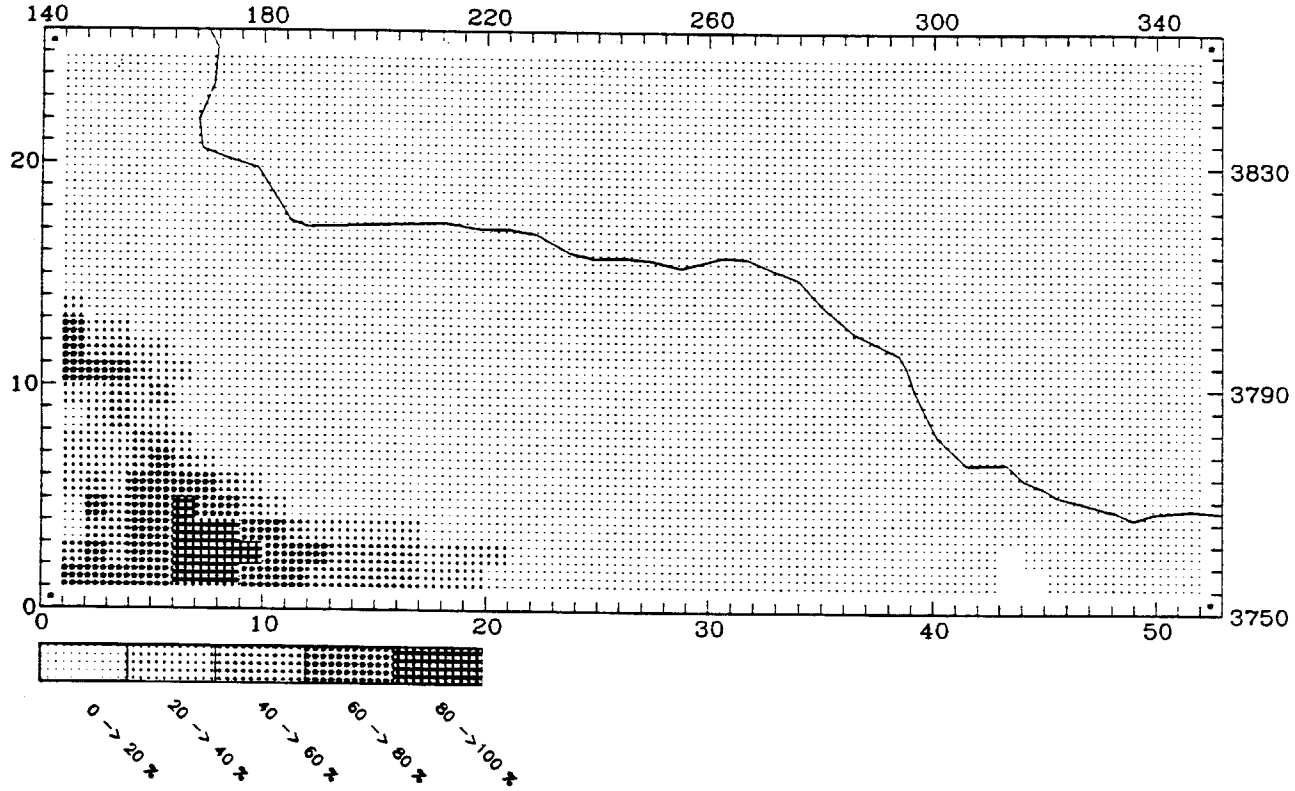

UAM–IV

BNDRY NOX CONTRIBUTION AT: 2300 September 5 LEVEL 1

MAXIMUM CONTRIBUTION IN CELL (2,8) = 100.00 (%)

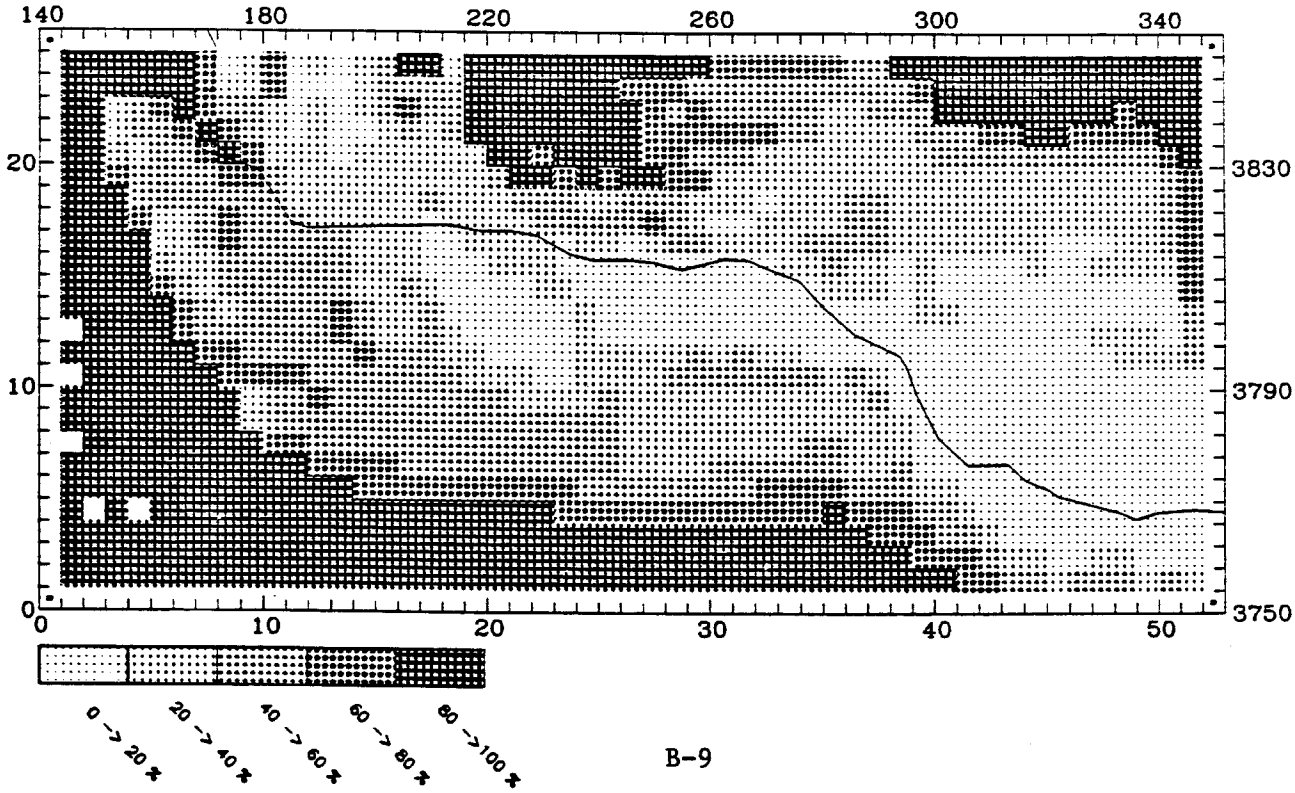

CALGRID–IV

BNDRY RHC CONTRIBUTION AT: 2300 September 5 LEVEL 1

MAXIMUM CONTRIBUTION IN CELL (2,3) = 100.00 (%)

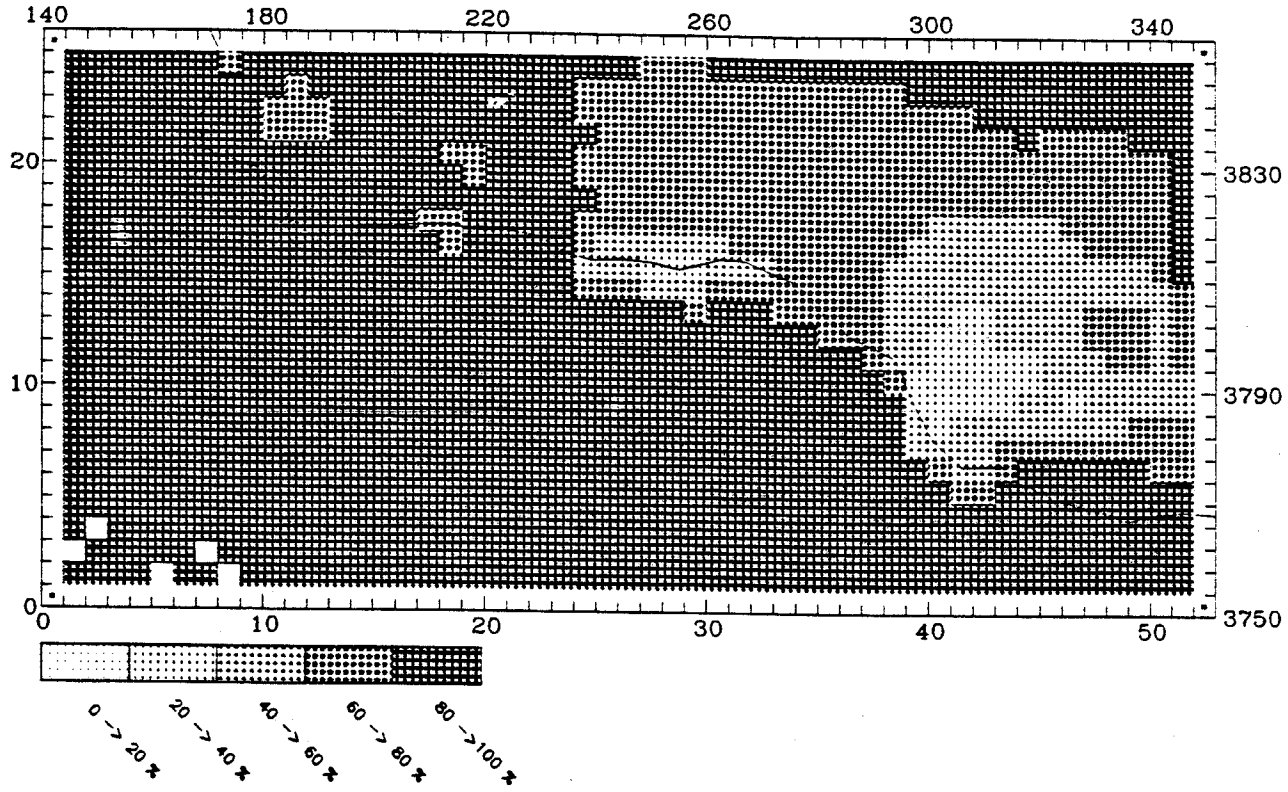

UAM–IV

BNDRY RHC CONTRIBUTION AT: 2300 September 5 LEVEL 1

MAXIMUM CONTRIBUTION IN CELL (2,8) = 100.00 (%)

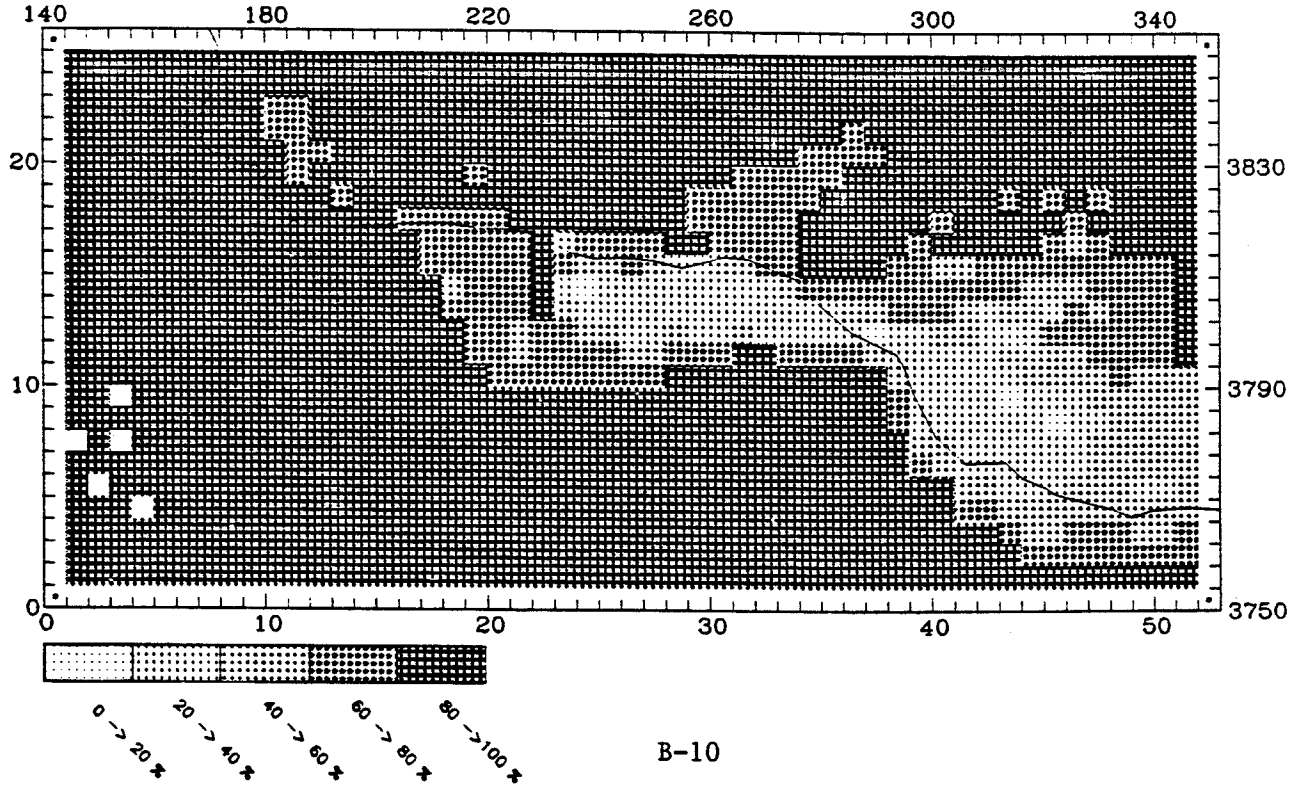

INTNOX CONTRIBUTION AT: 2300 September 5 LEVEL 1

MAXIMUM CONTRIBUTION IN CELL (2,2) = 0.04 (%)

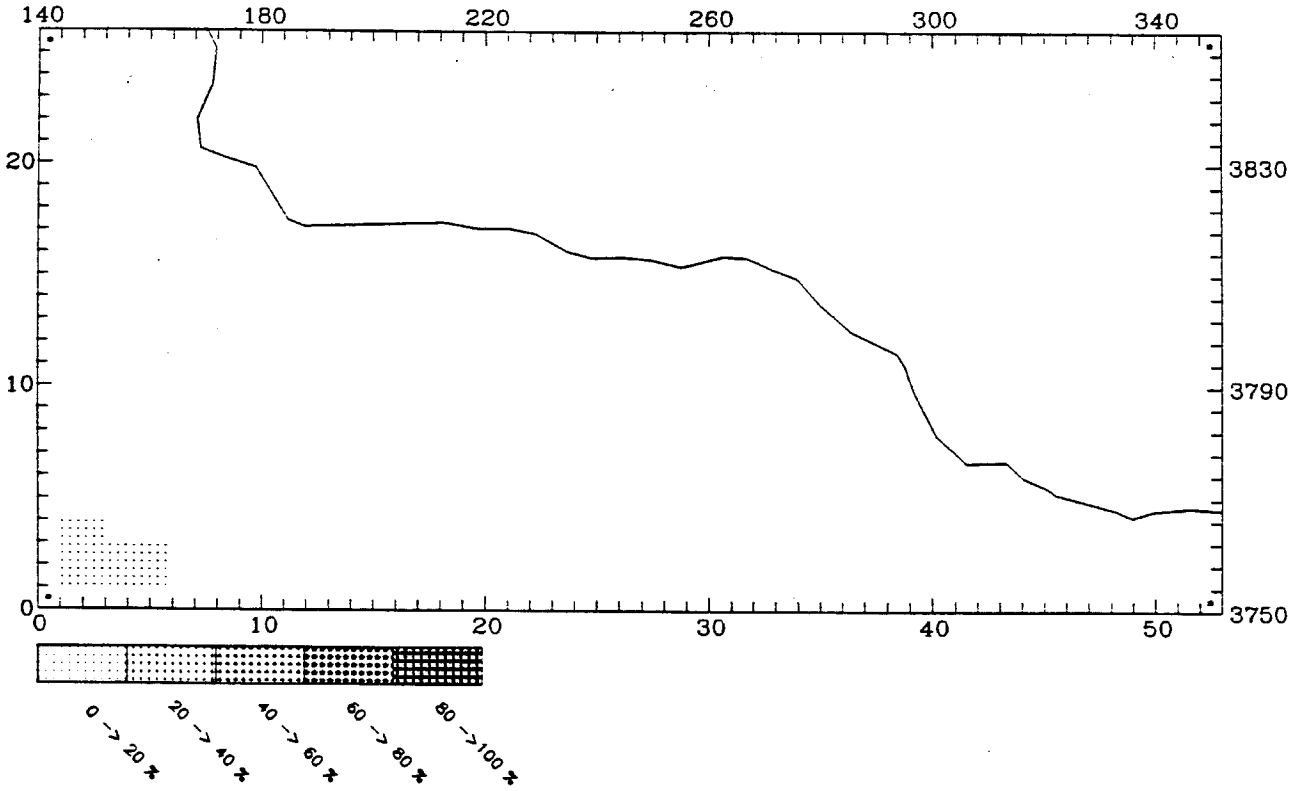

UAM-IV

INTNOX CONTRIBUTION AT: 2300 September 5 LEVEL 1

MAXIMUM CONTRIBUTION IN CELL (32,17) = 42.10 (%)

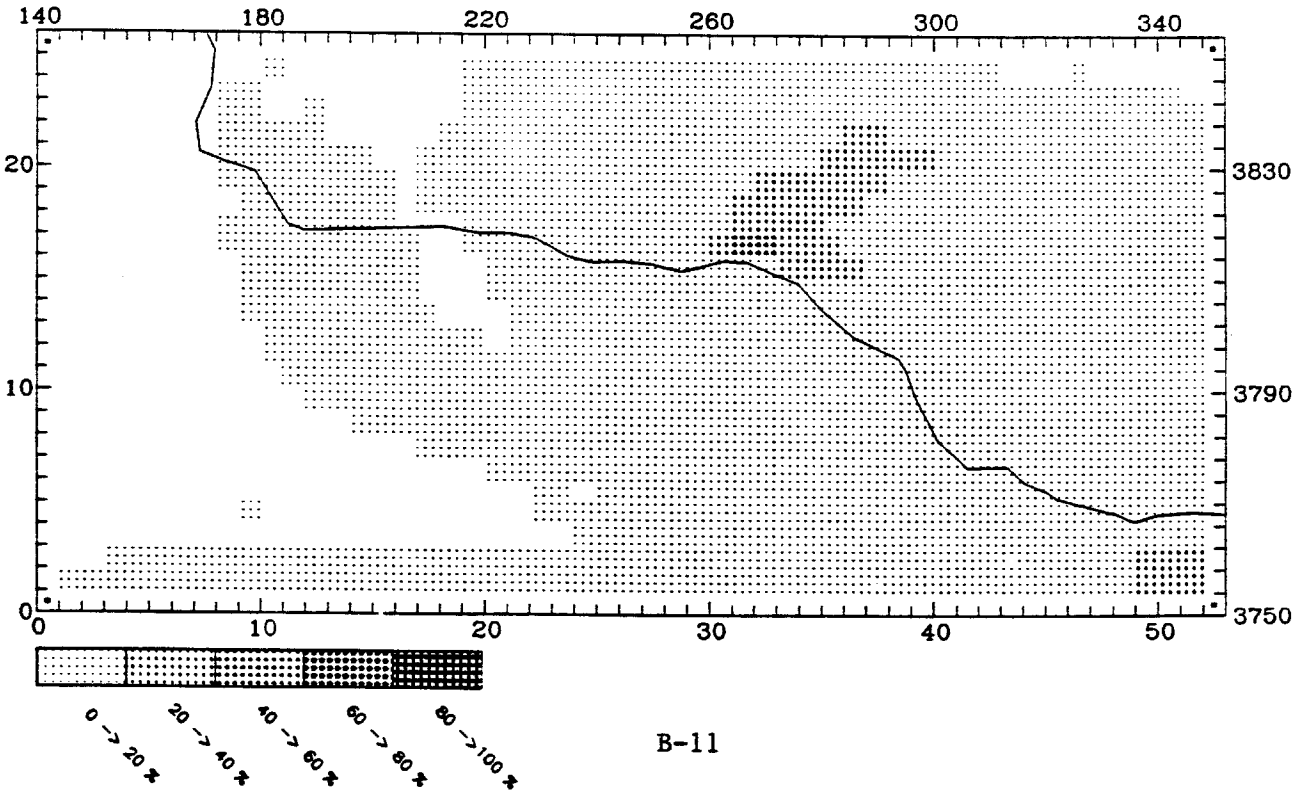

INTHC CONTRIBUTION AT: 2300 September 5 LEVEL 1

MAXIMUM CONTRIBUTION IN CELL (51,20) = 1.27 (%)

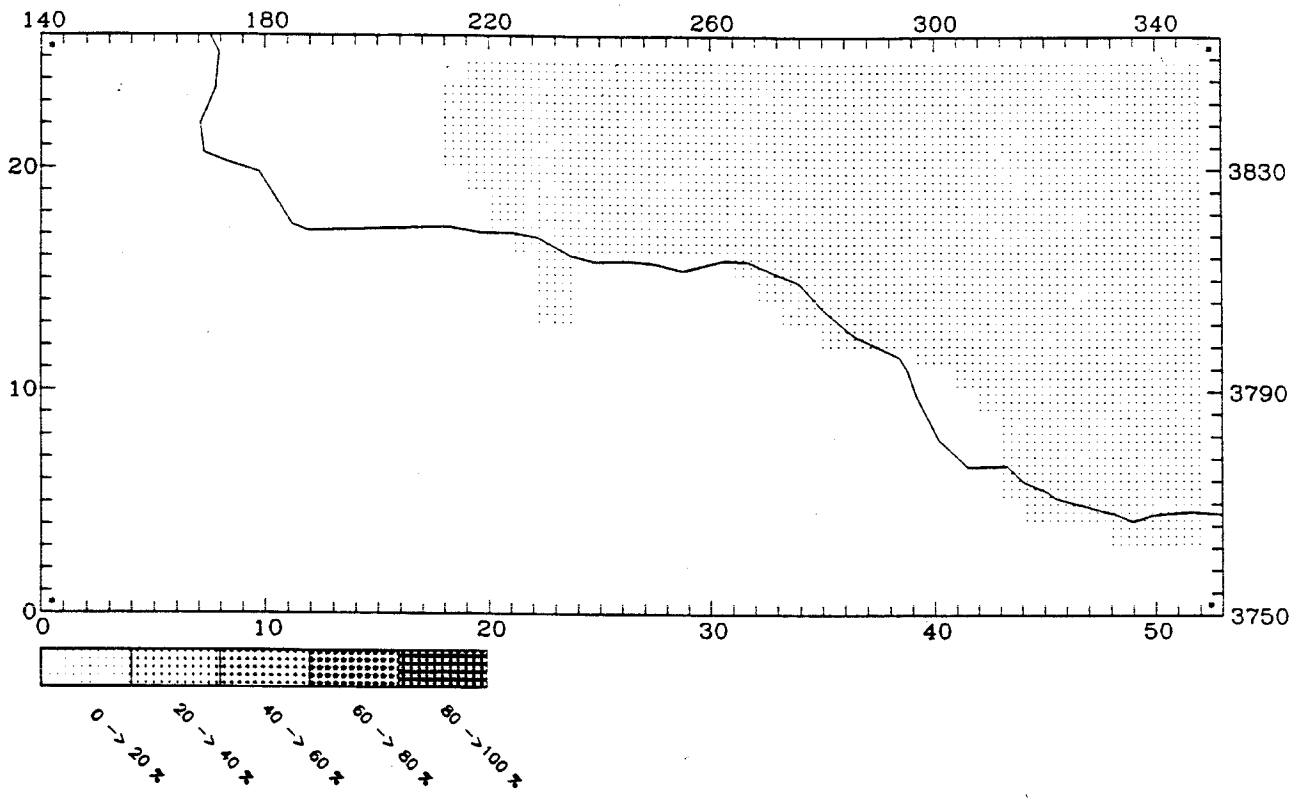

UAM-IV

INTHC CONTRIBUTION AT: 2300 September 5 LEVEL 1

MAXIMUM CONTRIBUTION IN CELL (51,3) = 14.95 (%)

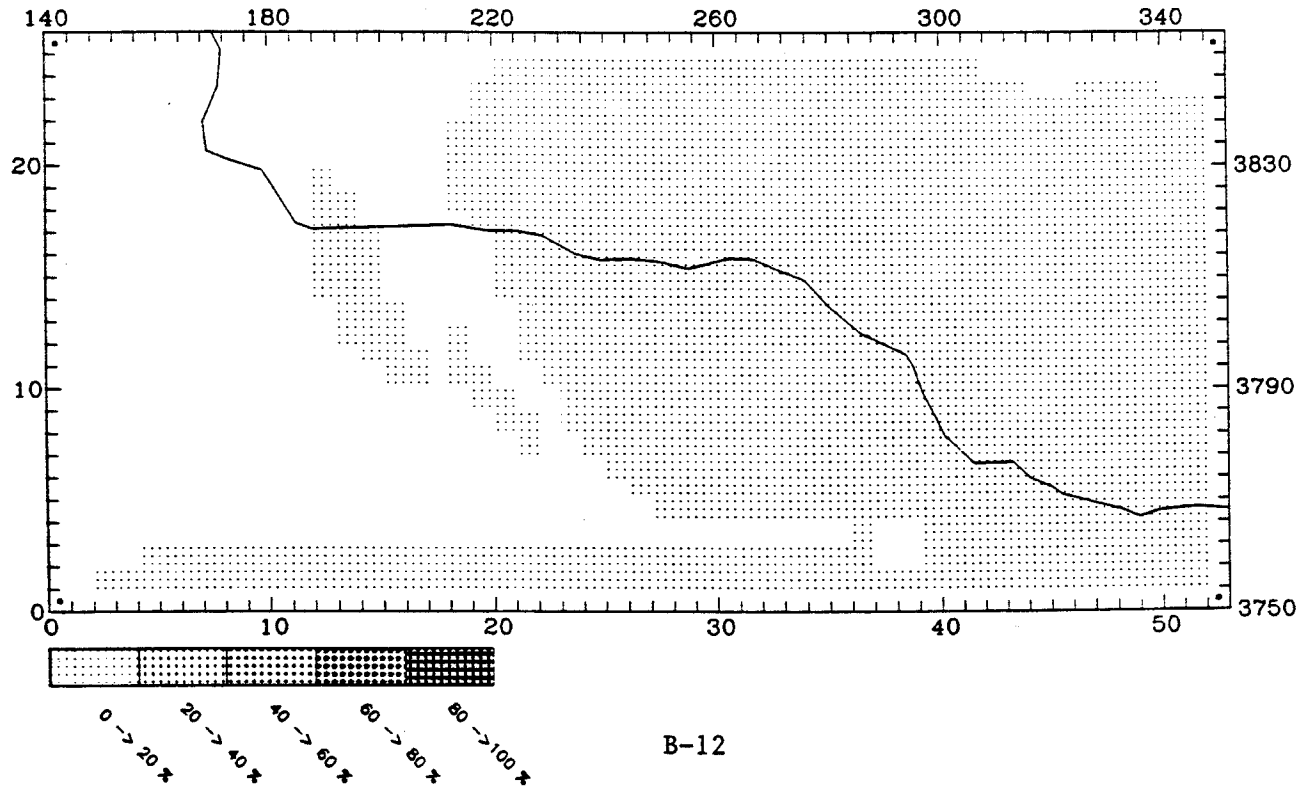

CALGRID–IV

PTARBNOX CONTRIBUTION AT: 2300 September 5 LEVEL 1

MAXIMUM CONTRIBUTION IN CELL (45,2) = 99.91 (%)

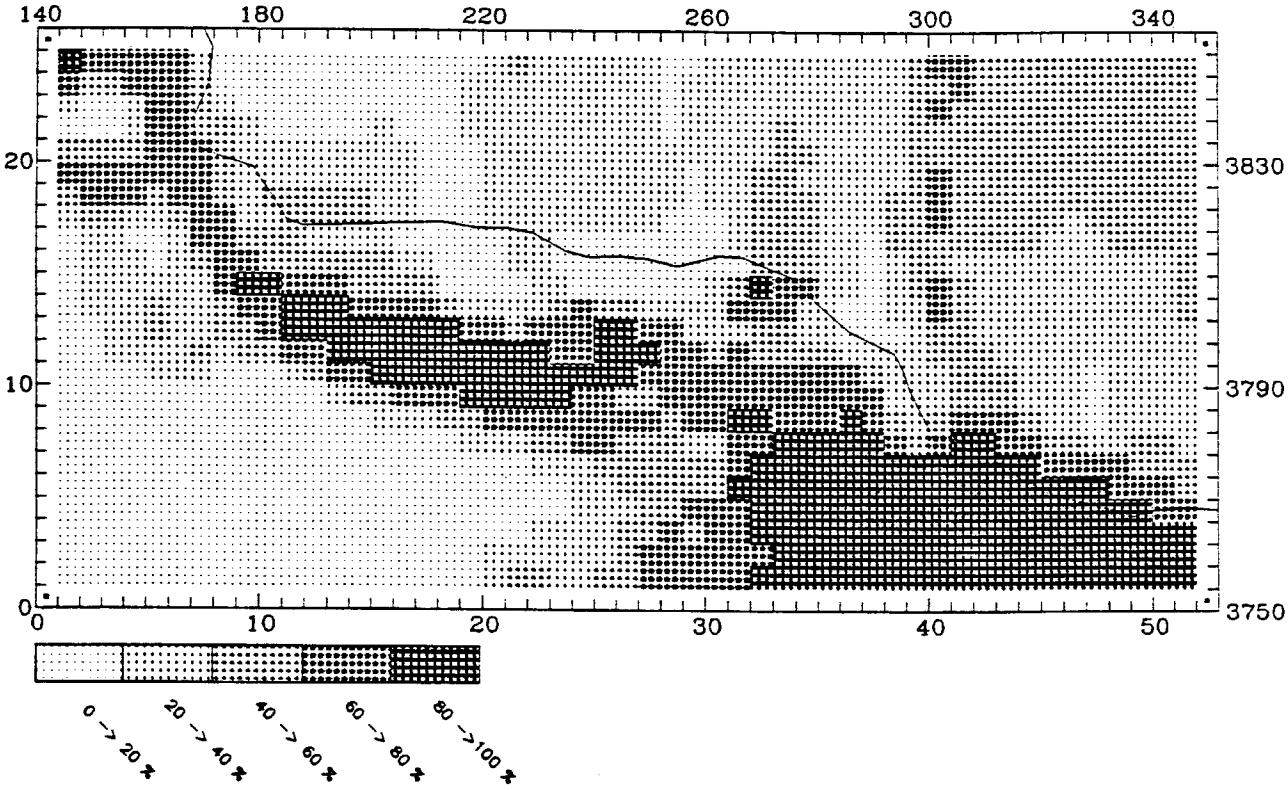

UAM–IV

PTNOX CONTRIBUTION AT: 2300 September 5 LEVEL 1

MAXIMUM CONTRIBUTION IN CELL (33,9) = 61.98 (%)

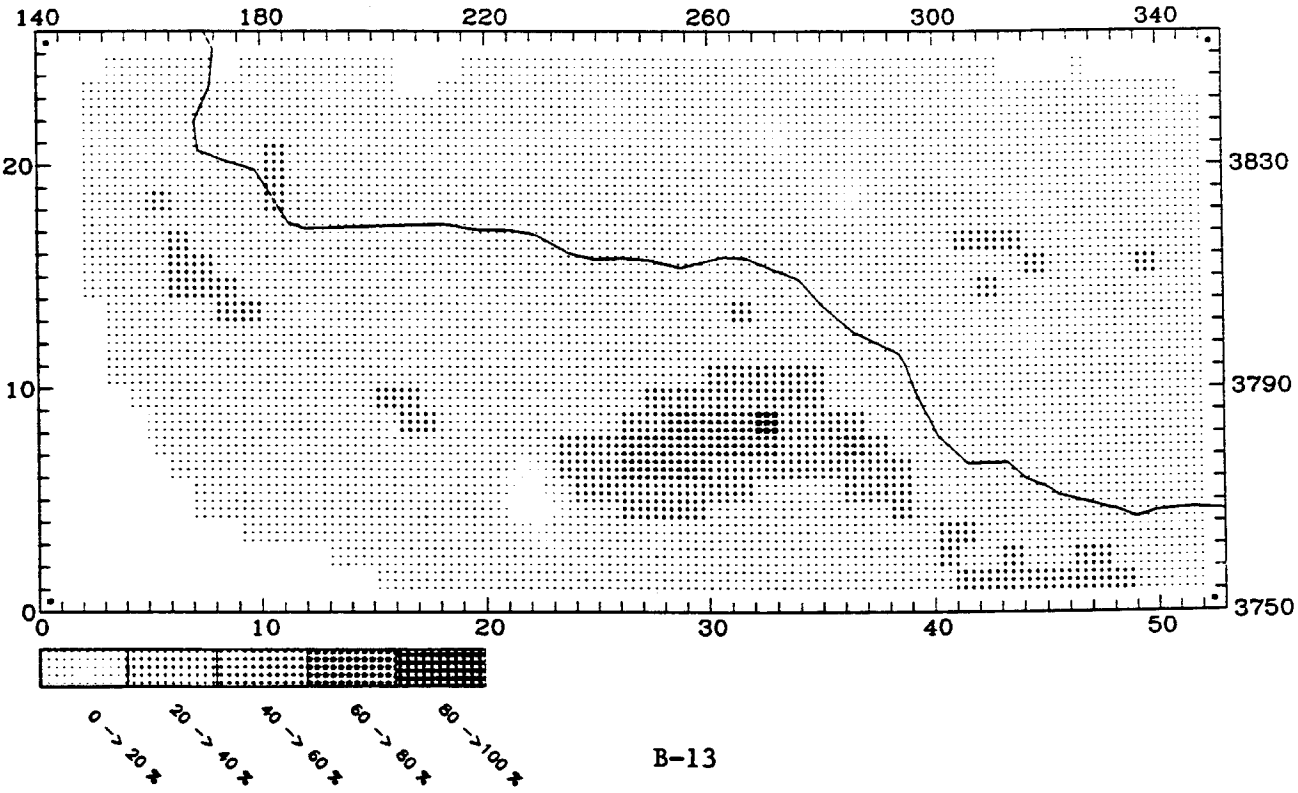

CALGRID–IV

PTARBHC CONTRIBUTION AT: 2300 September 5 LEVEL 1

MAXIMUM CONTRIBUTION IN CELL (44,3) = 6.89 (%)

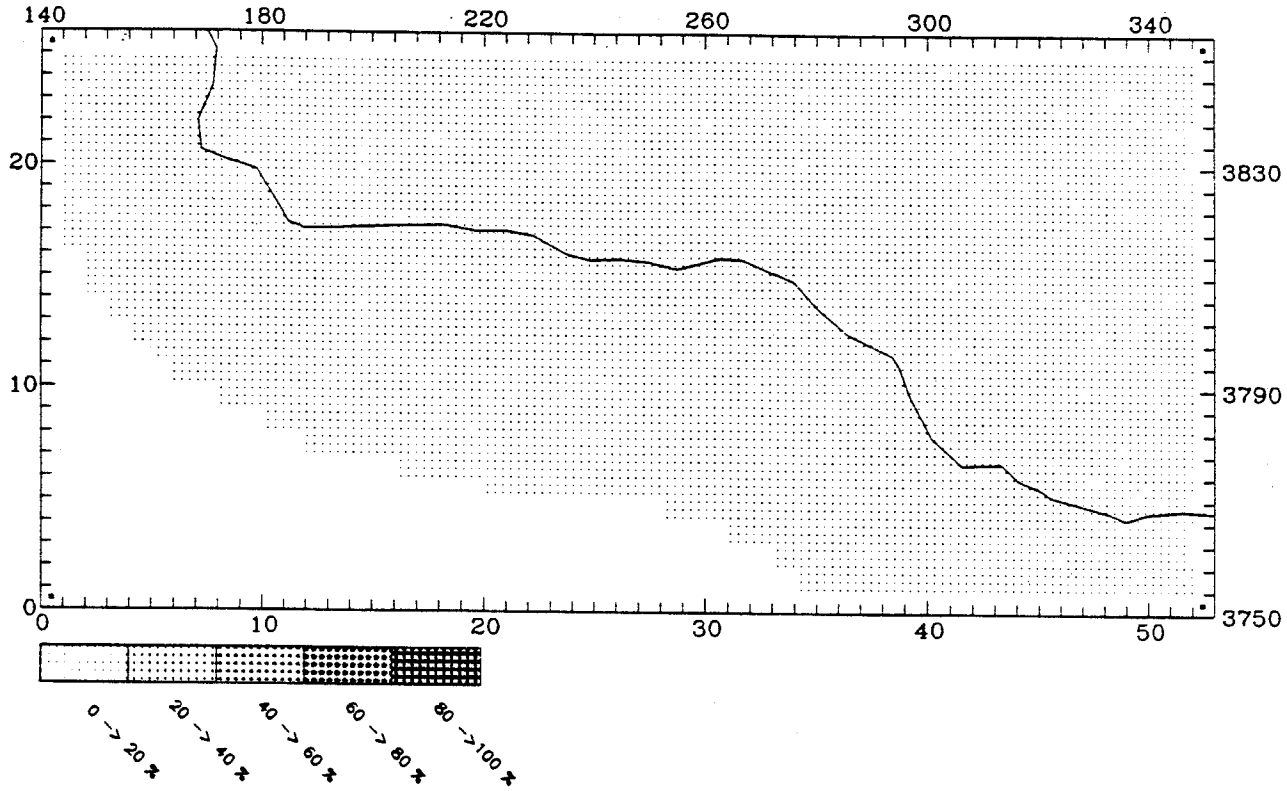

UAM–IV

PTHC CONTRIBUTION AT: 2300 September 5 LEVEL 1

MAXIMUM CONTRIBUTION IN CELL (32,9) = 2.22 (%)

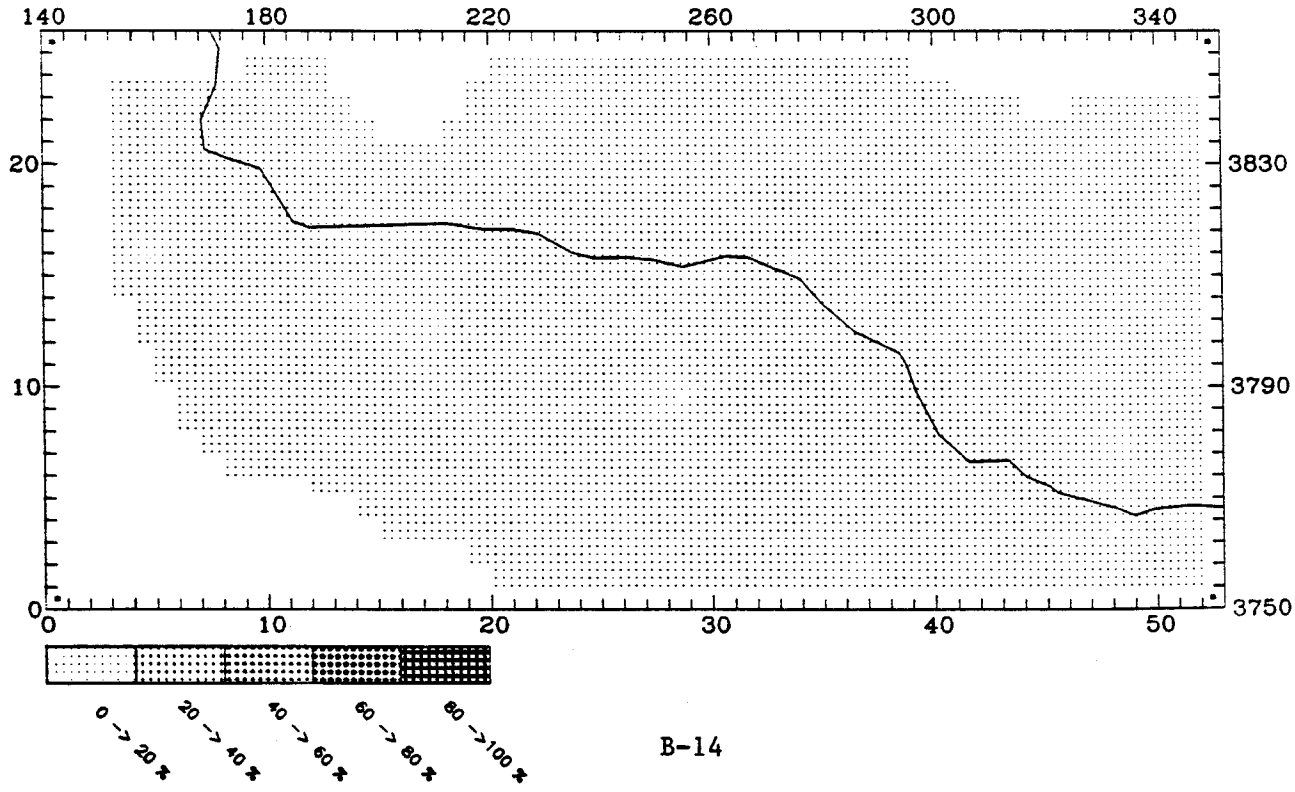

CALGRID–IV

ANOX CONTRIBUTION AT: 2300 September 5 LEVEL 1

MAXIMUM CONTRIBUTION IN CELL (11,9) = 99.75 (%)

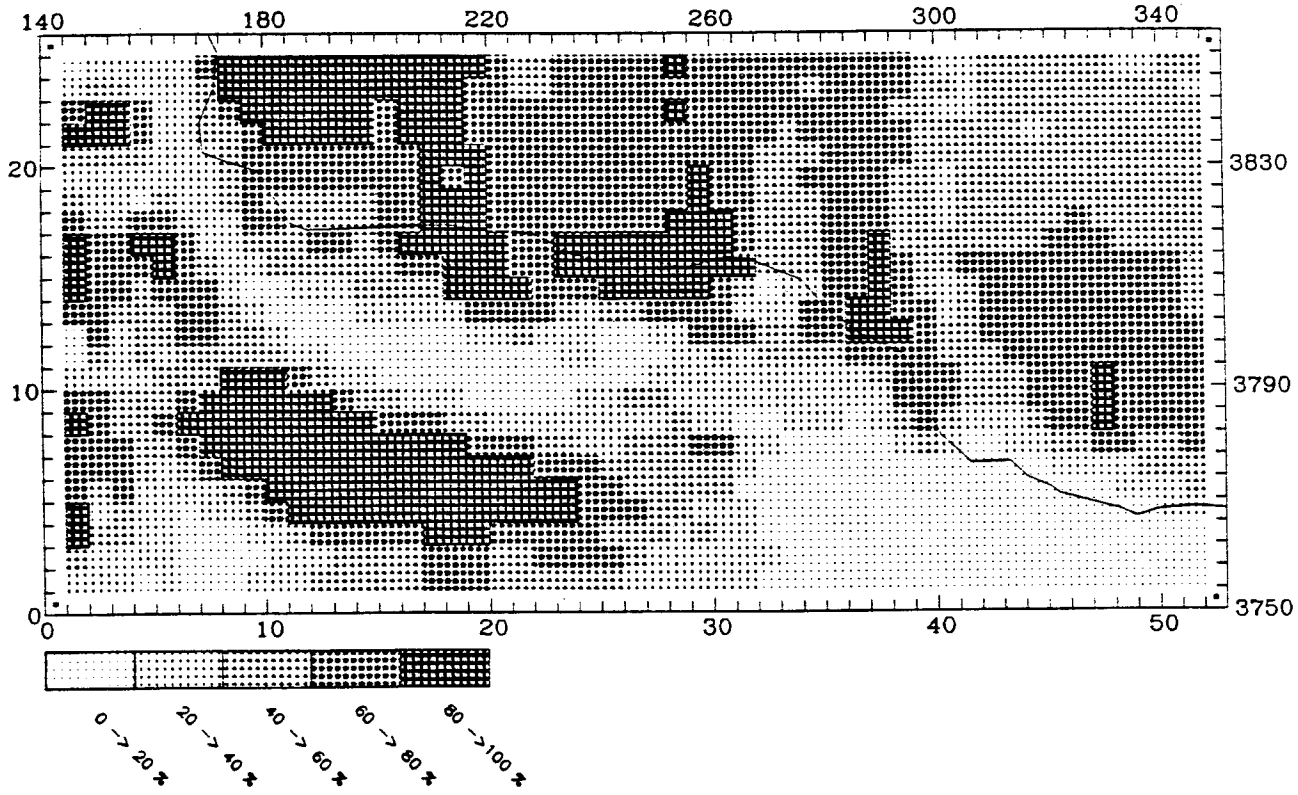

UAM–IV

NOX CONTRIBUTION AT: 2300 September 5 LEVEL 1

MAXIMUM CONTRIBUTION IN CELL (38,13) = 97.66 (%)

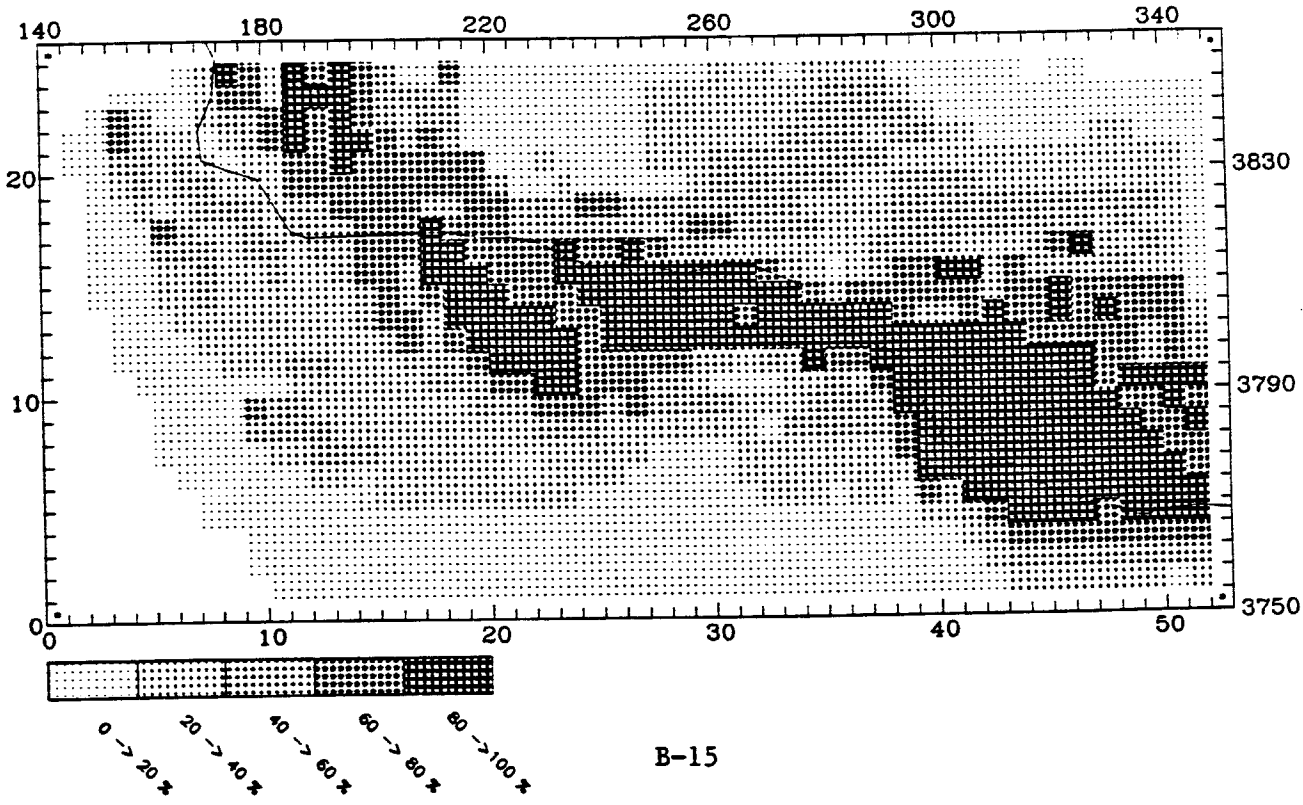

CALGRID–IV

ATHC CONTRIBUTION AT: 2300 September 5 LEVEL 1

MAXIMUM CONTRIBUTION IN CELL (29,16) = 71.54 (%)

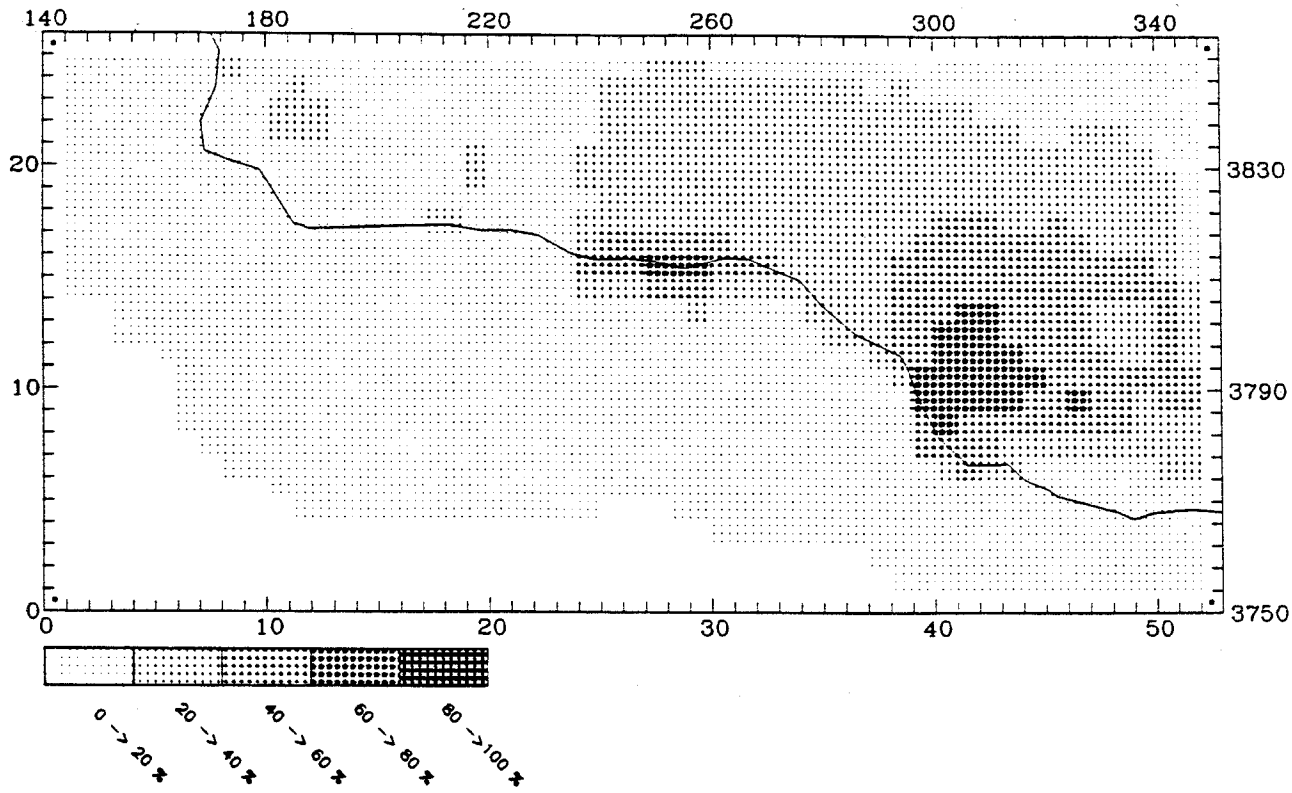

UAM–IV

RHC CONTRIBUTION AT: 2300 September 5 LEVEL 1

MAXIMUM CONTRIBUTION IN CELL (44,10) = 86.46 (%)

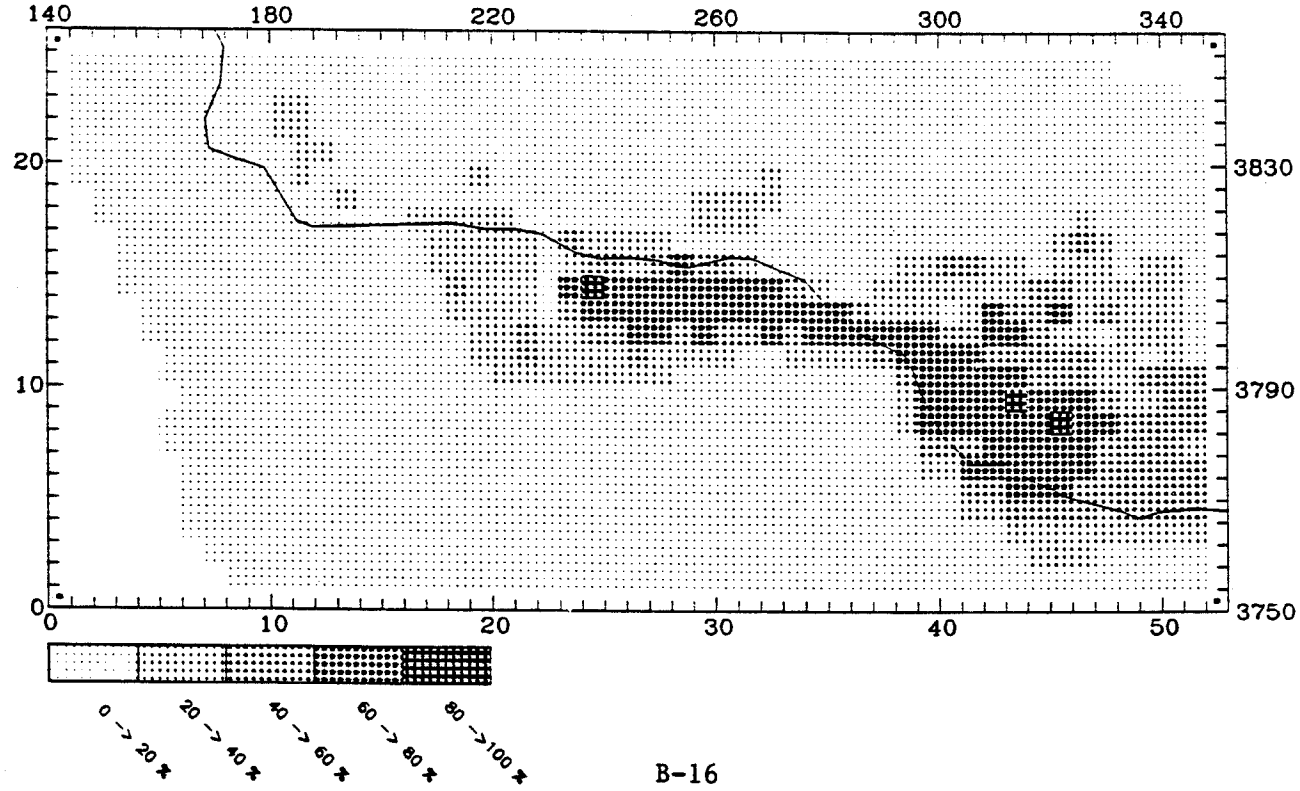

CALGRID–IV

BNDRY NOX CONTRIBUTION AT: 1100 September 6 LEVEL 1

MAXIMUM CONTRIBUTION IN CELL (51,5) = 99.57 (%)

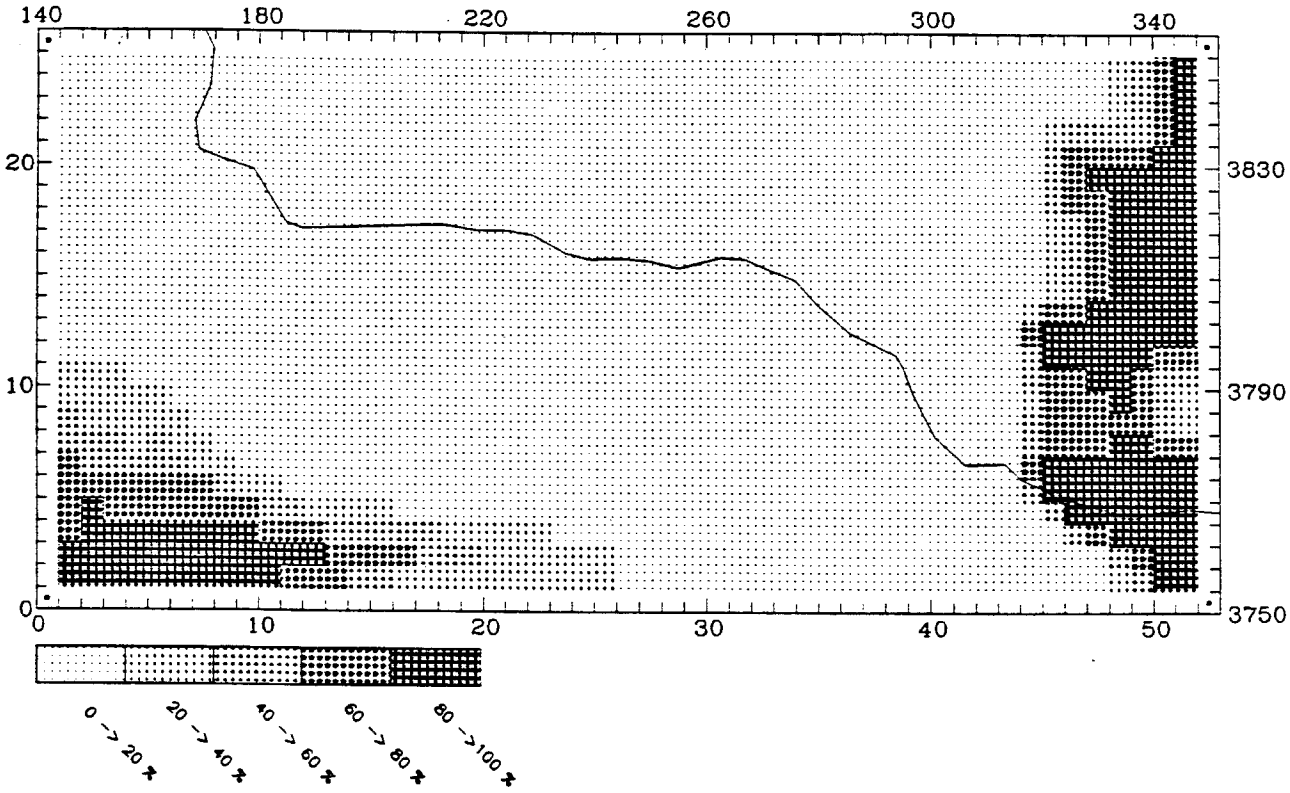

UAM–IV

BNDRY NOX CONTRIBUTION AT: 1100 September 6 LEVEL 1

MAXIMUM CONTRIBUTION IN CELL (2,5) = 100.00 (%)

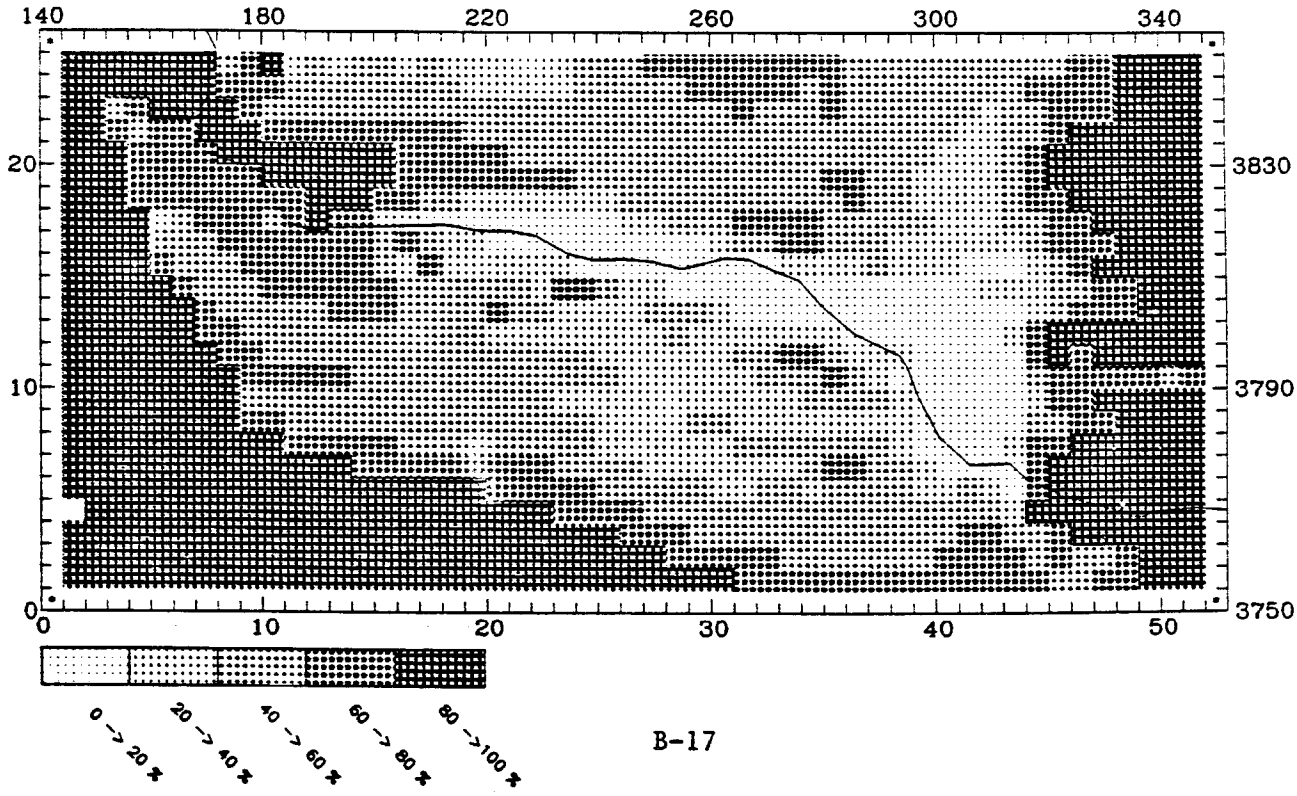

CALGRID–IV

BNDRY RHC CONTRIBUTION AT: 1100 September 6 LEVEL 1

MAXIMUM CONTRIBUTION IN CELL (3,2) = 100.00 (%)

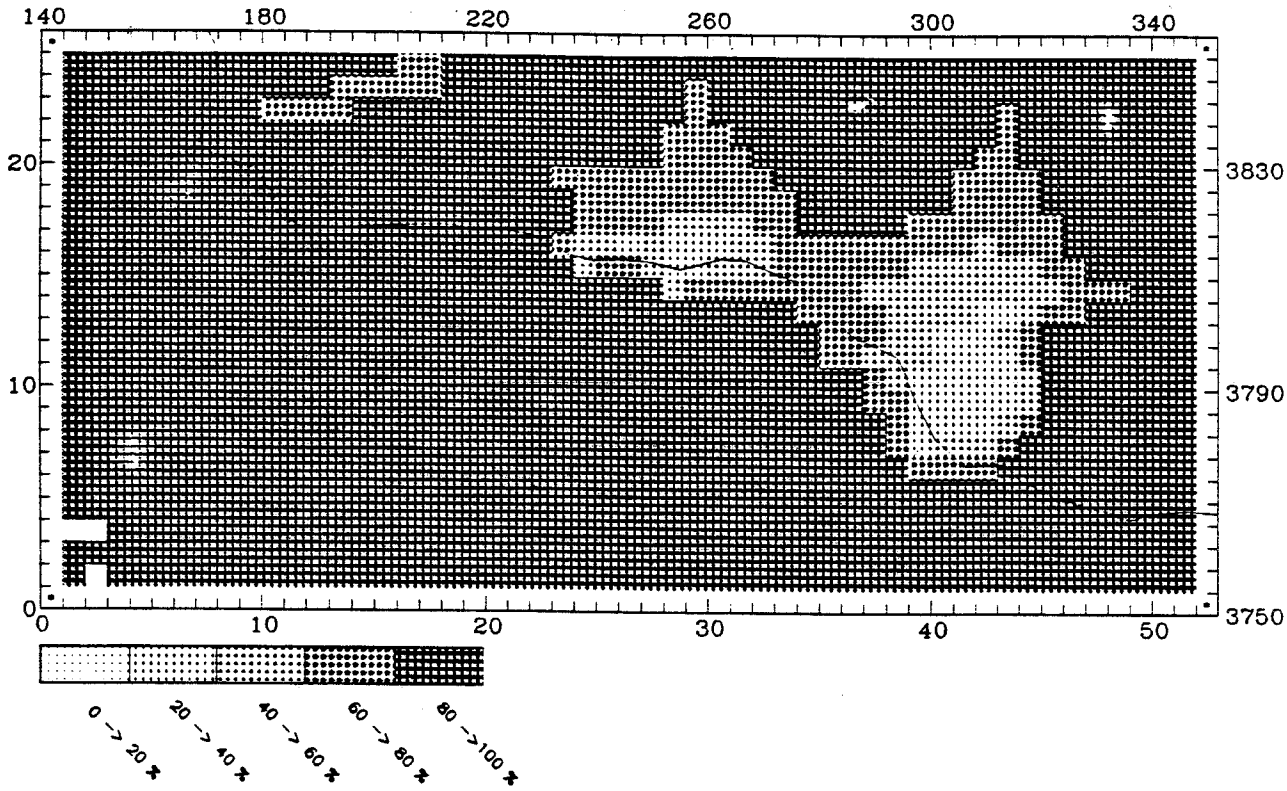

UAM–IV

BNDRY RHC CONTRIBUTION AT: 1100 September 6 LEVEL 1

MAXIMUM CONTRIBUTION IN CELL (3,3) = 100.00 (%)

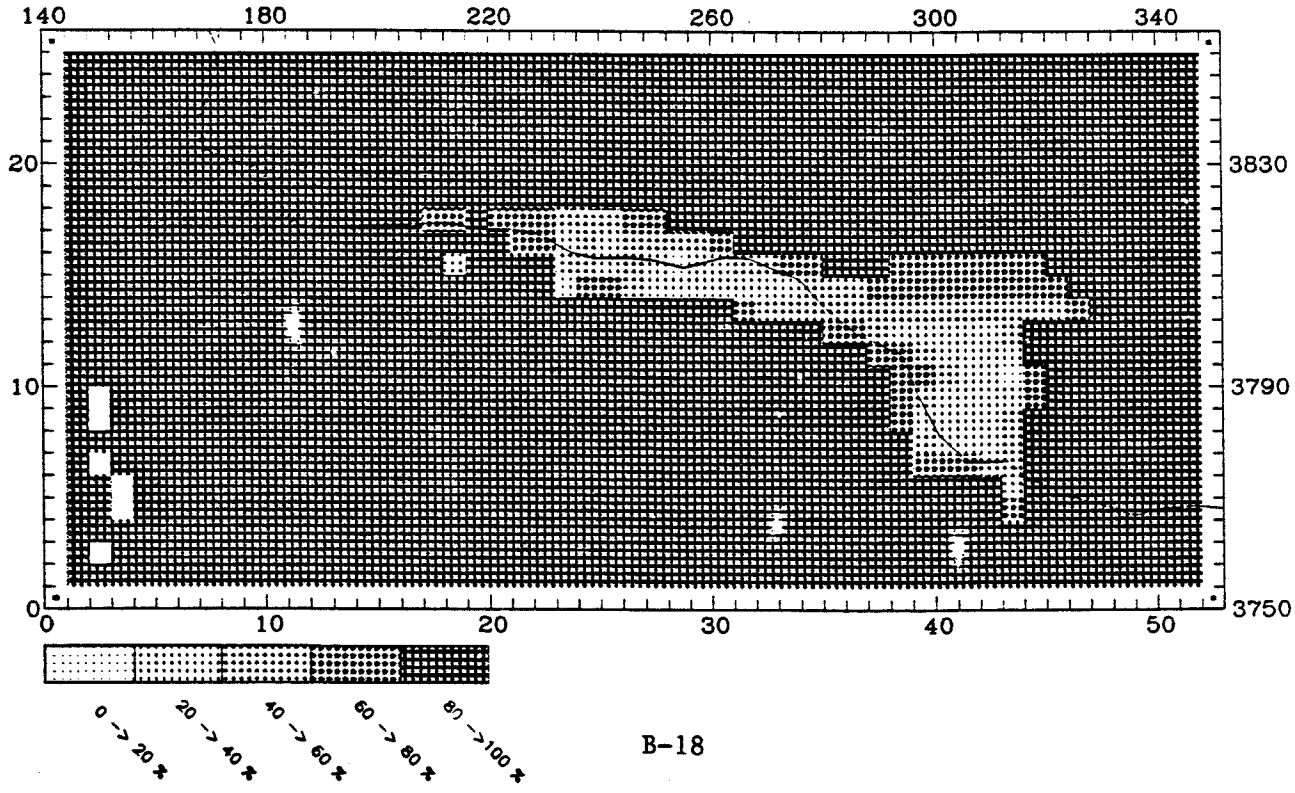

CALGRID–IV

INTNOX CONTRIBUTION AT: 1100 September 6 LEVEL 1

MAXIMUM CONTRIBUTION IN CELL (2,2) = 0.00 (%)

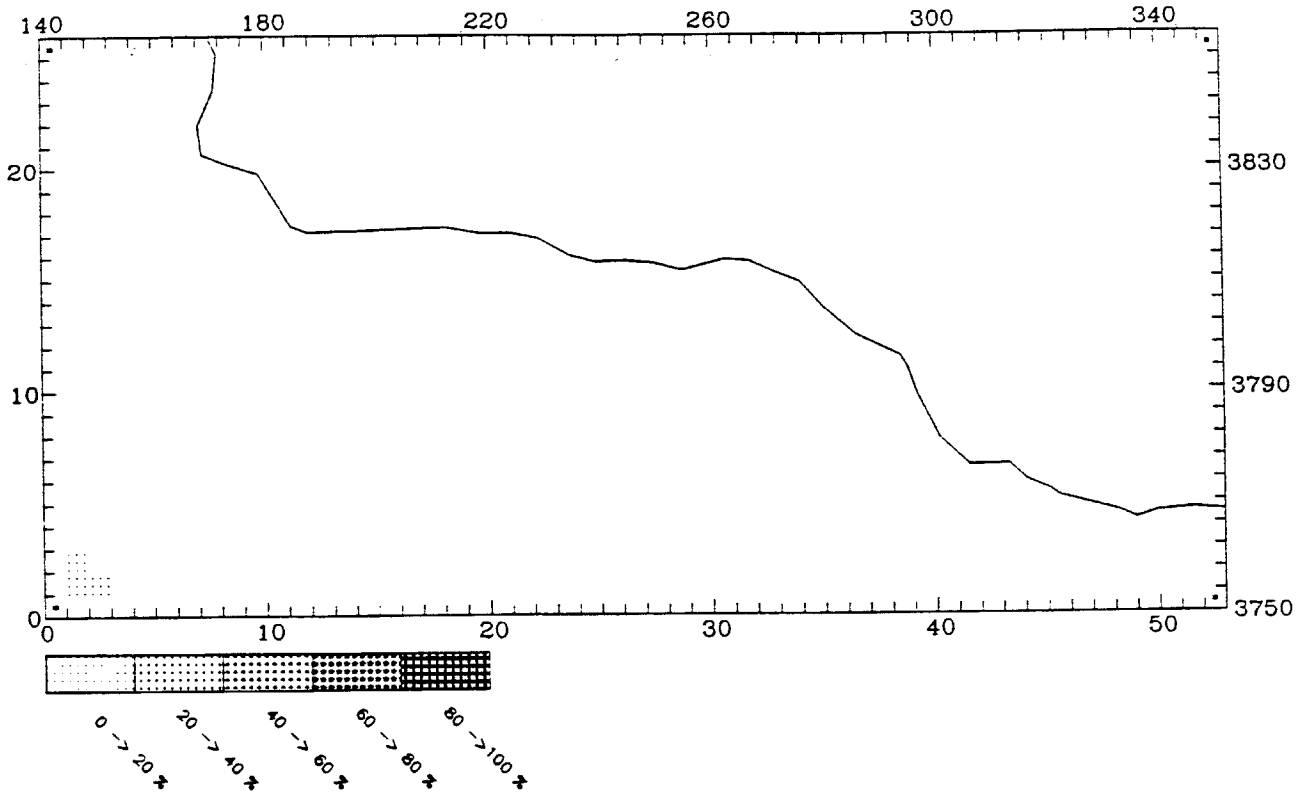

UAM–IV

INTNOX CONTRIBUTION AT: 1100 September 6 LEVEL 1

MAXIMUM CONTRIBUTION IN CELL (45,15) = 3.19 (%)

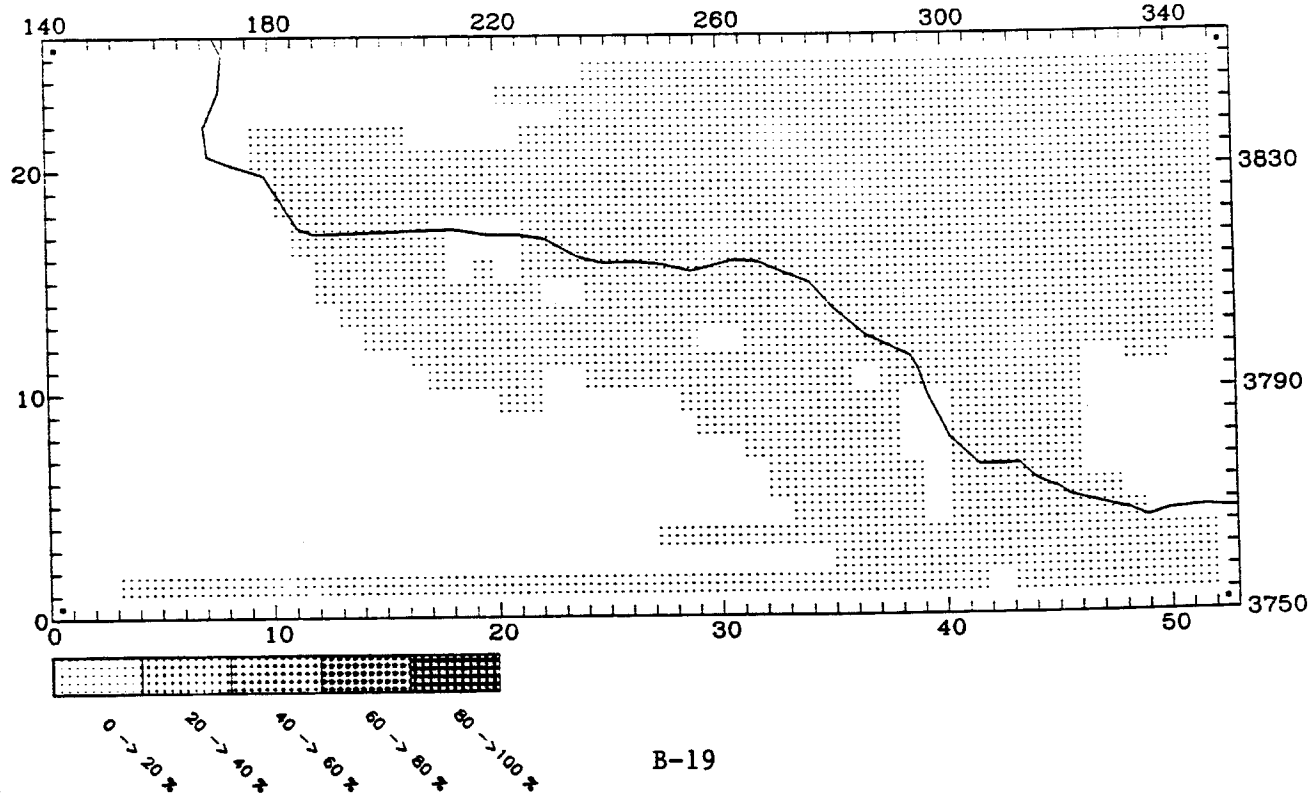

CALGRID–IV

INTHC CONTRIBUTION AT: 1100 September 6 LEVEL 1

MAXIMUM CONTRIBUTION IN CELL (50,23) = 0.02 (%)

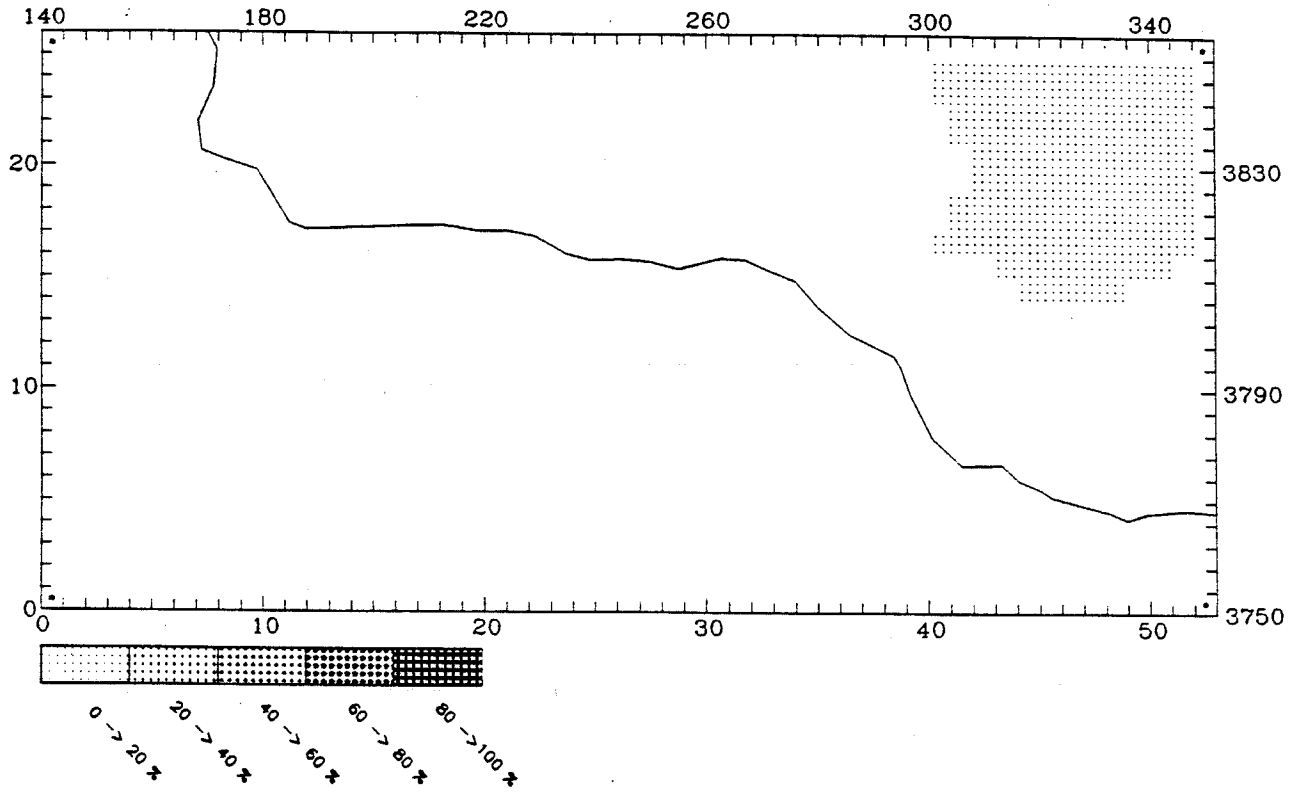

UAM–IV

INTHC CONTRIBUTION AT: 1100 September 6 LEVEL 1

MAXIMUM CONTRIBUTION IN CELL (35,15) = 1.98 (%)

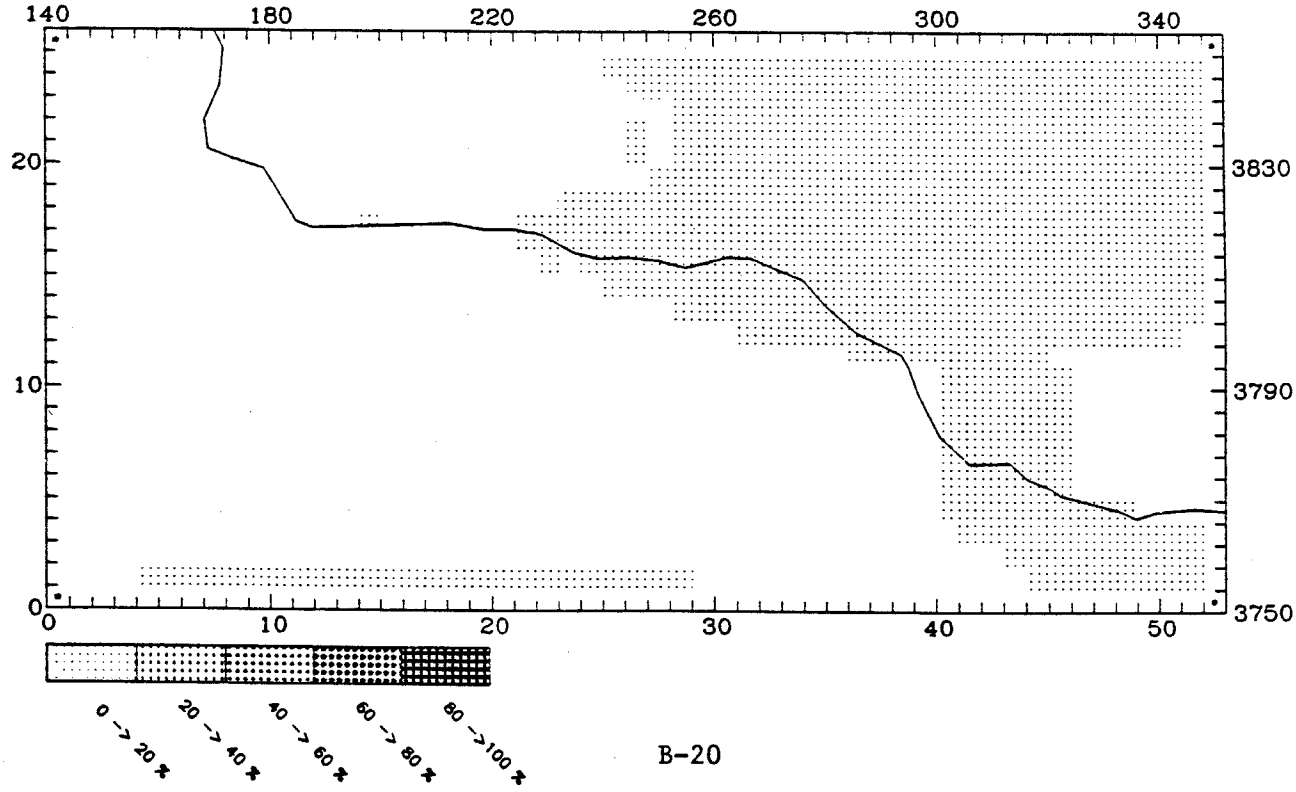

CALGRID–IV

PTARBNOX CONTRIBUTION AT: 1100 September 6 LEVEL 1

MAXIMUM CONTRIBUTION IN CELL (44,2) = 99.82 (%)

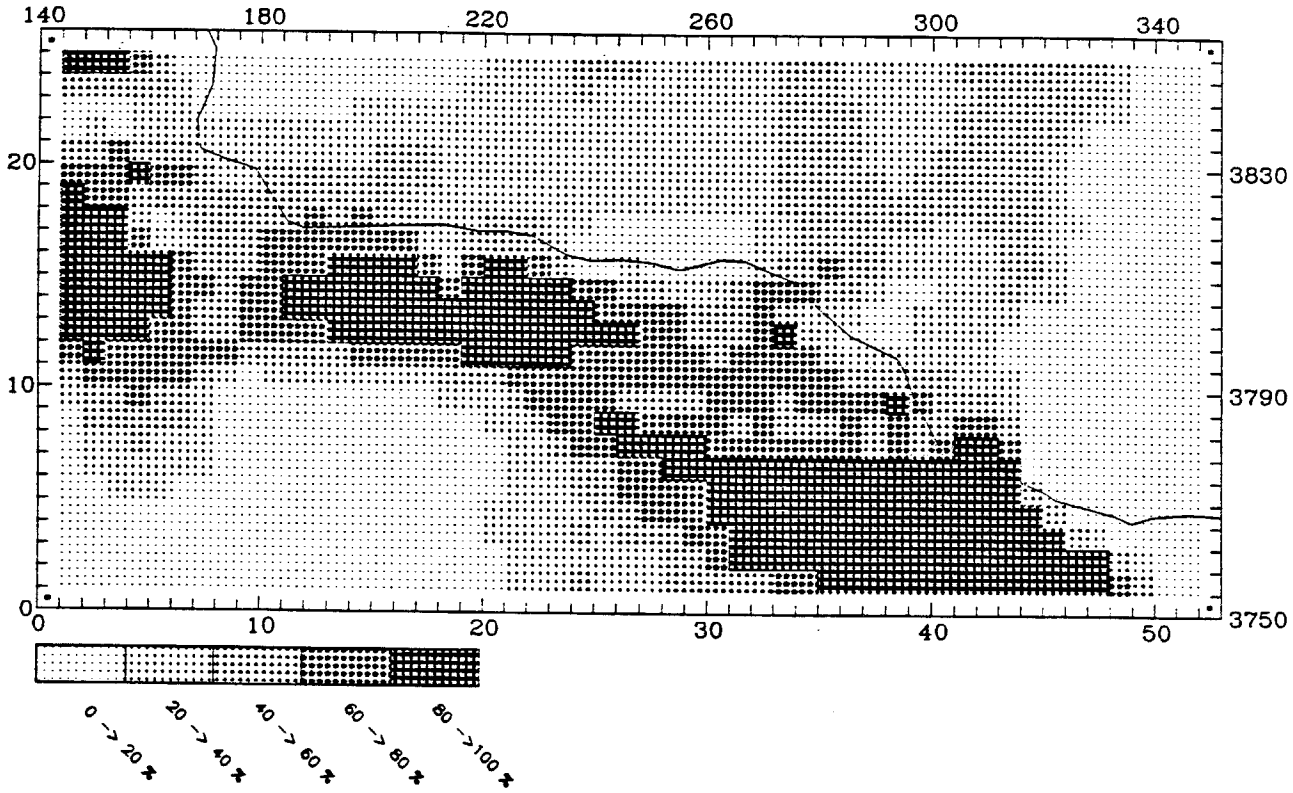

UAM–IV

PTNOX CONTRIBUTION AT: 1100 September 6 LEVEL 1

MAXIMUM CONTRIBUTION IN CELL (33,7) = 61.37 (%)

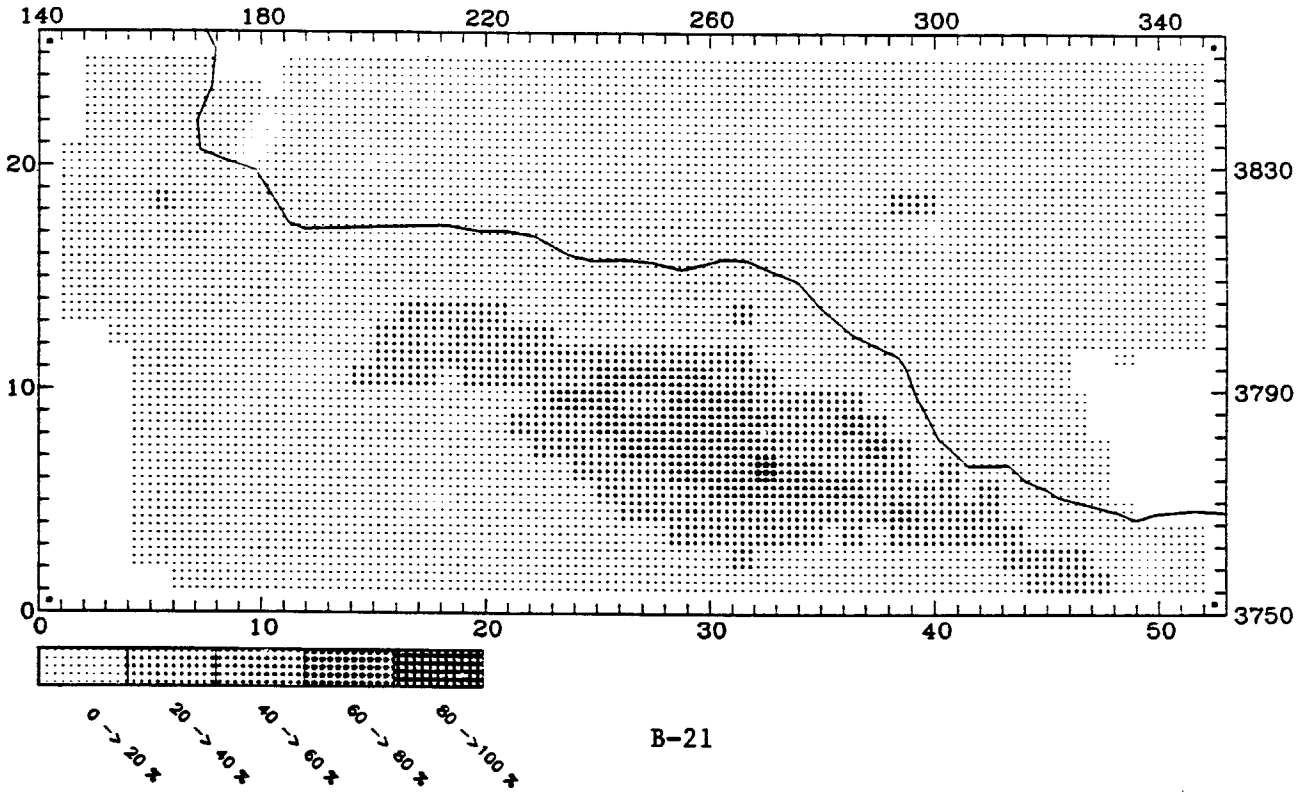

CALGRID–IV

PTARBHC CONTRIBUTION AT: 1100 September 6 LEVEL 1

MAXIMUM CONTRIBUTION IN CELL (33,7) = 3.96 (%)

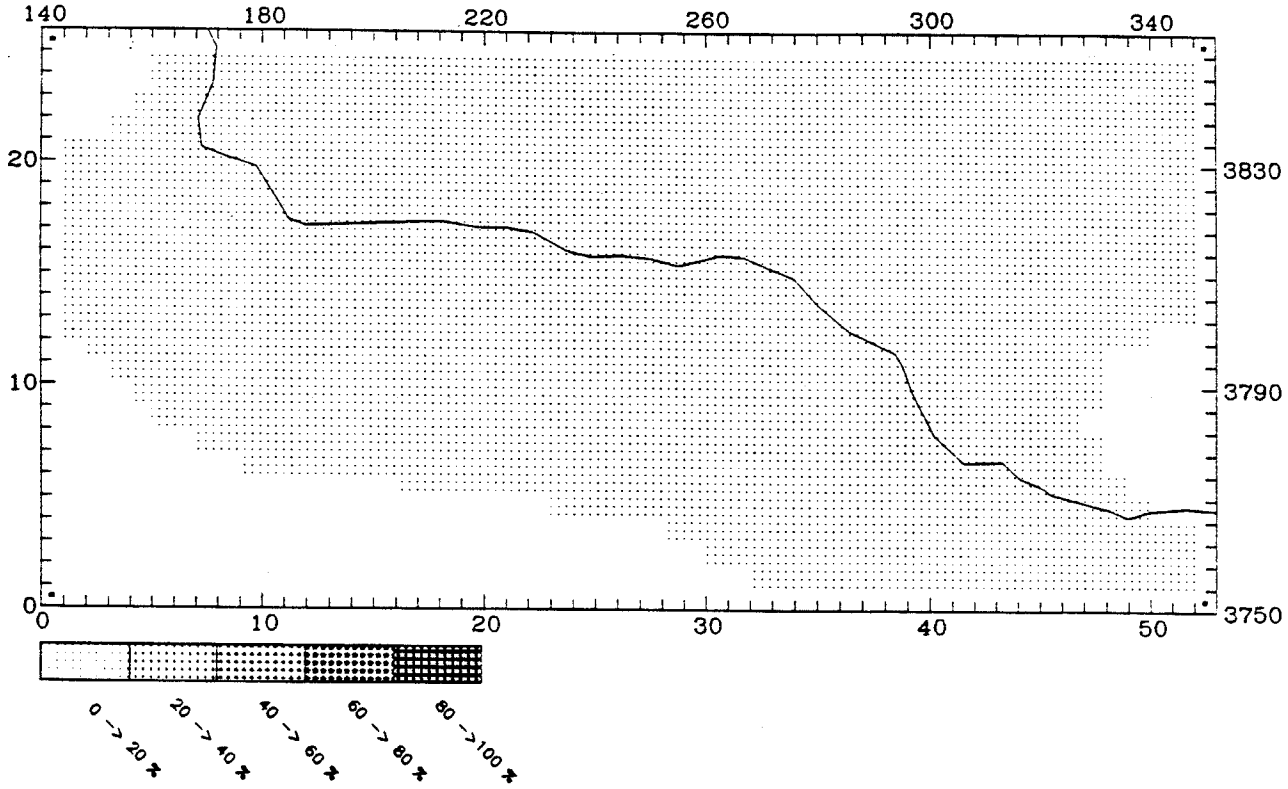

UAM–IV

PTHC CONTRIBUTION AT: 1100 September 6 LEVEL 1

MAXIMUM CONTRIBUTION IN CELL (33,7) = 2.38 (%)

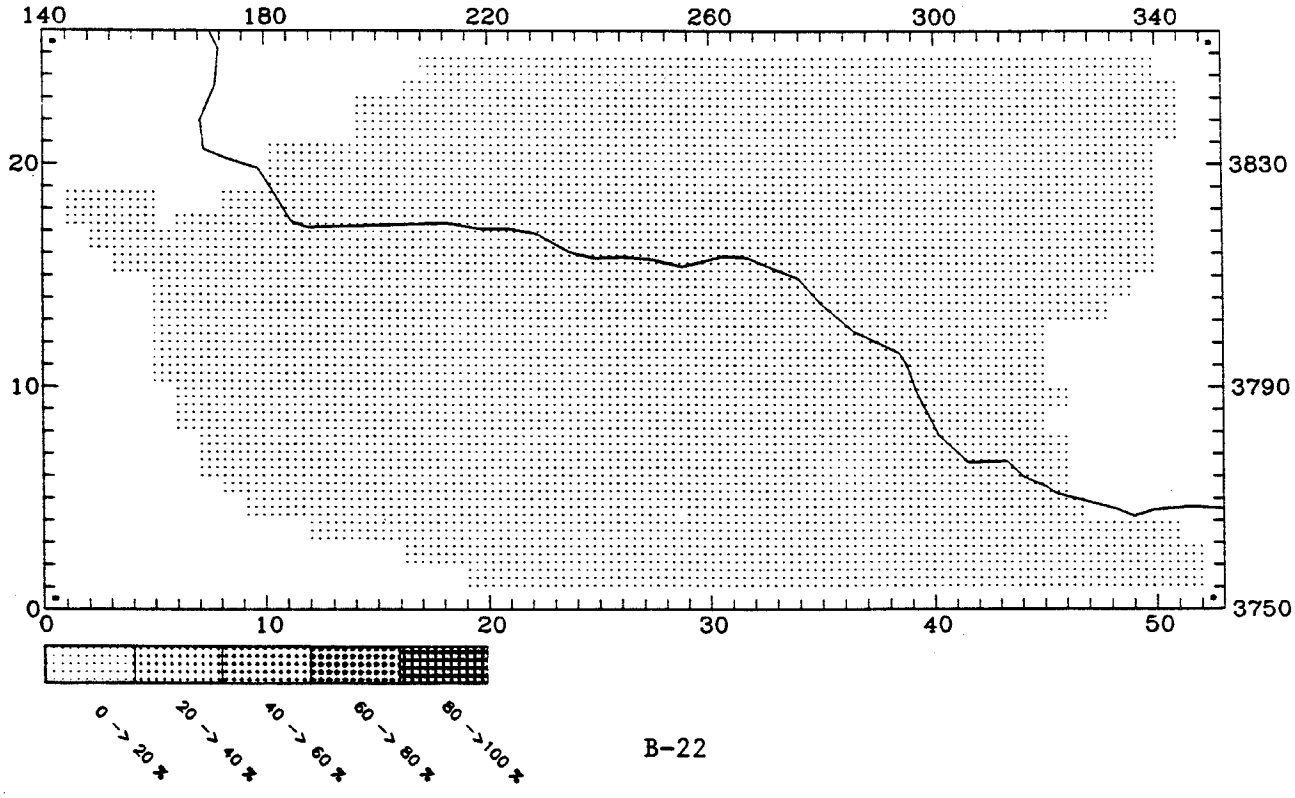

CALGRID–IV

ANOX CONTRIBUTION AT: 1100 September 6 LEVEL 1

MAXIMUM CONTRIBUTION IN CELL (9,25) = 97.51 (%)

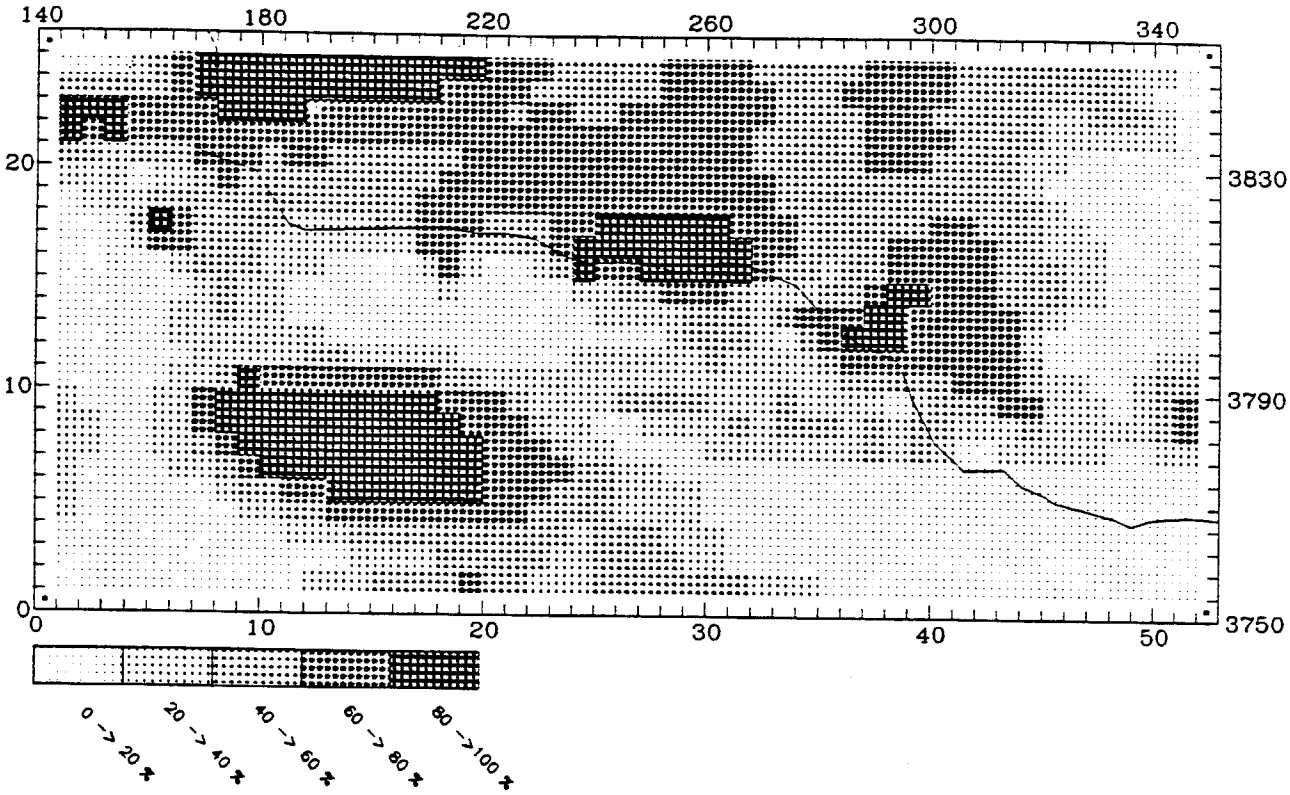

UAM–IV

NOX CONTRIBUTION AT: 1100 September 6 LEVEL 1

MAXIMUM CONTRIBUTION IN CELL (29,16) = 97.05 (%)

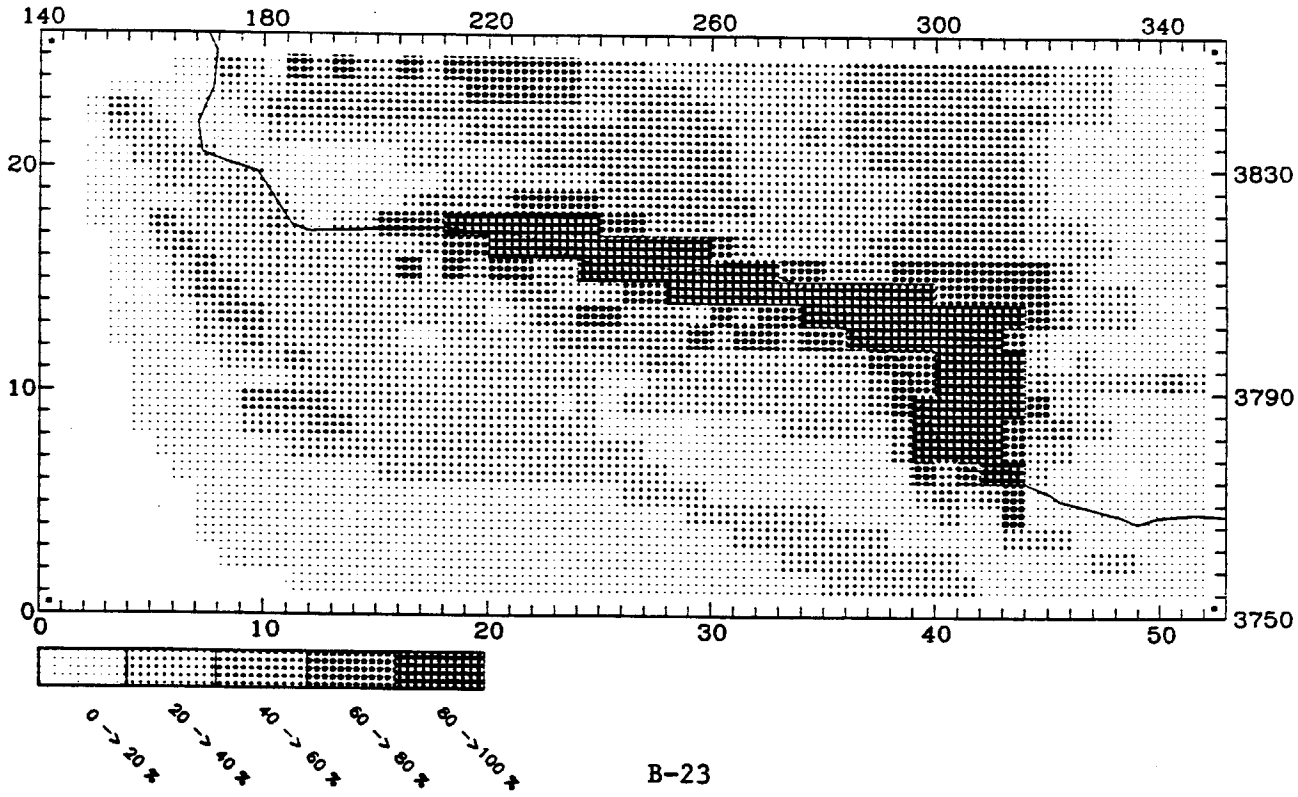

ATHC CONTRIBUTION AT: 1100 September 6 LEVEL 1

MAXIMUM CONTRIBUTION IN CELL (42,12) = 77.29 (%)

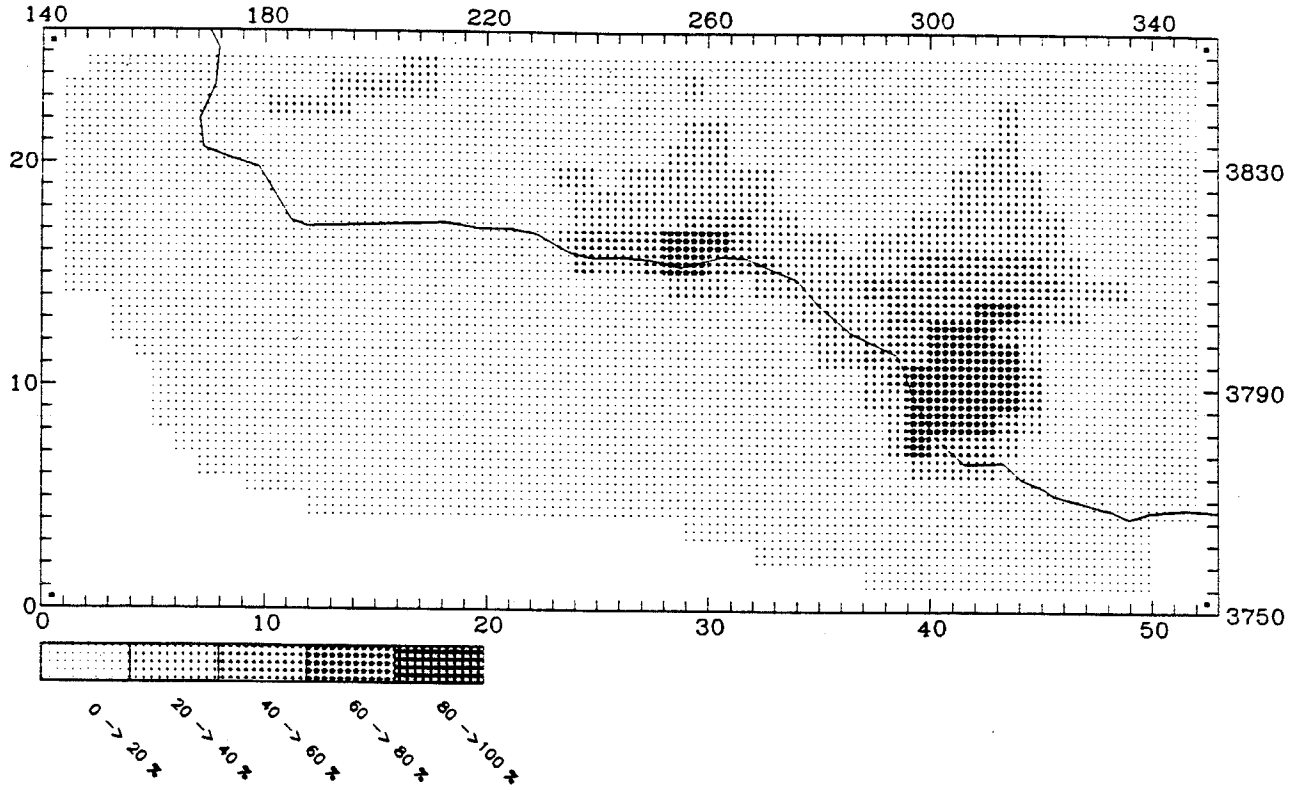

UAM-IV

RHC CONTRIBUTION AT: 1100 September 6 LEVEL 1

MAXIMUM CONTRIBUTION IN CELL (29,16) = 80.49 (%)

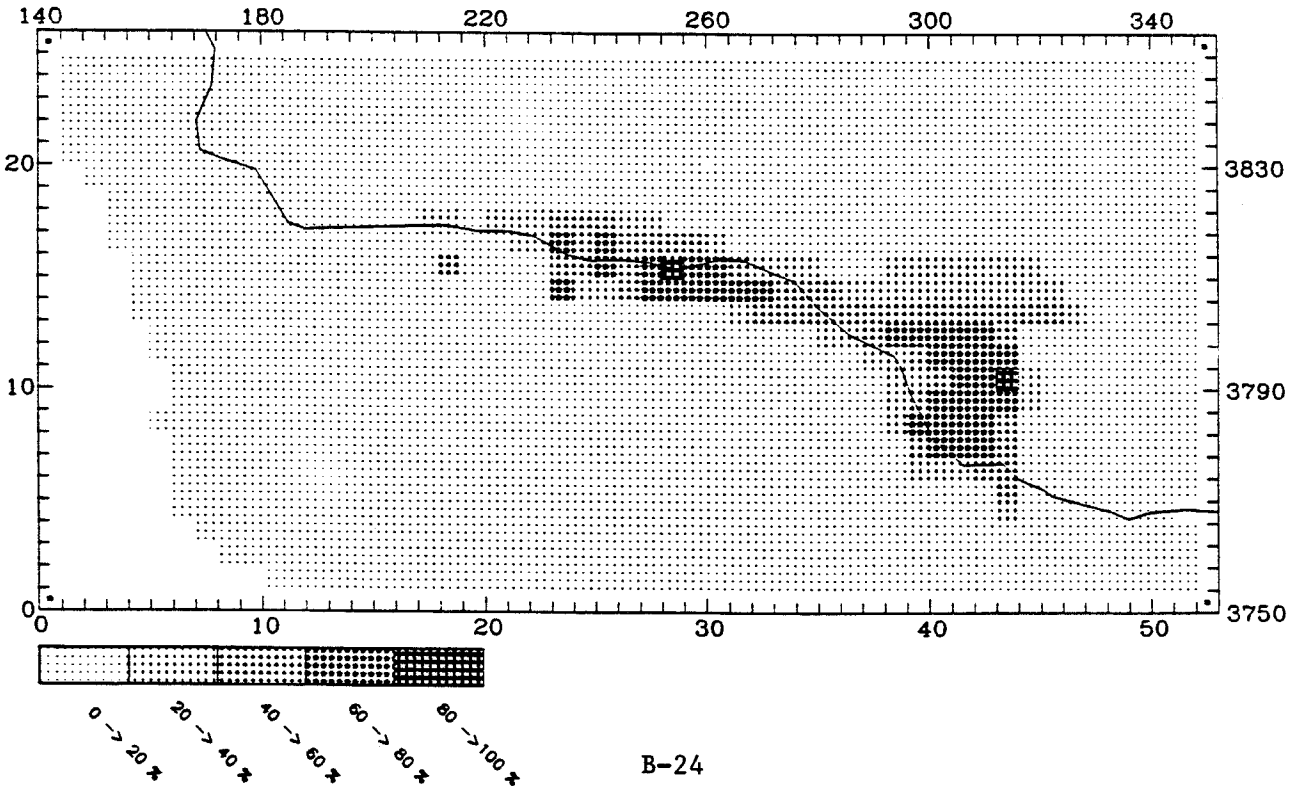

BNDRY NOX CONTRIBUTION AT: 2300 September 6 LEVEL 1

MAXIMUM CONTRIBUTION IN CELL (8,2) = 98.21 (%)

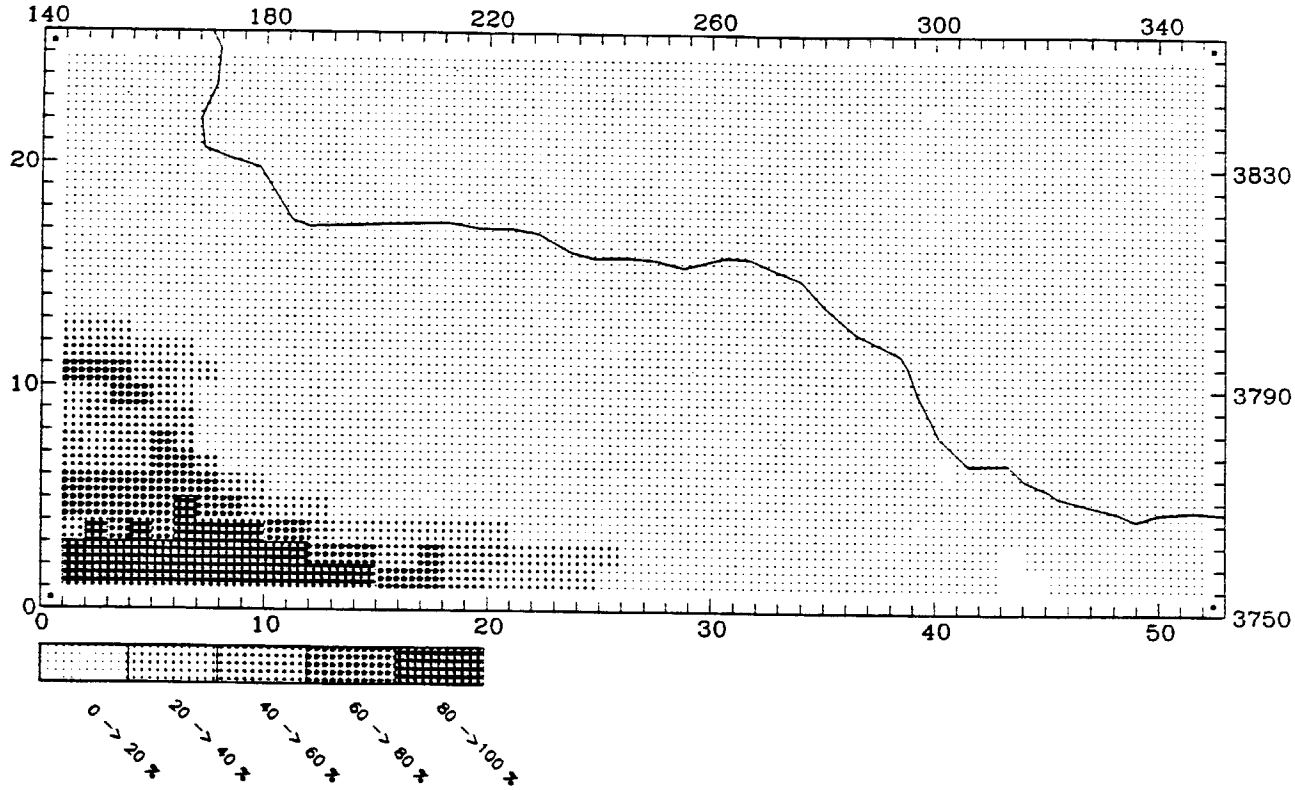

UAM-IV

BNDRY NOX CONTRIBUTION AT: 2300 September 6 LEVEL 1

MAXIMUM CONTRIBUTION IN CELL (5,5) = 100.00 (%)

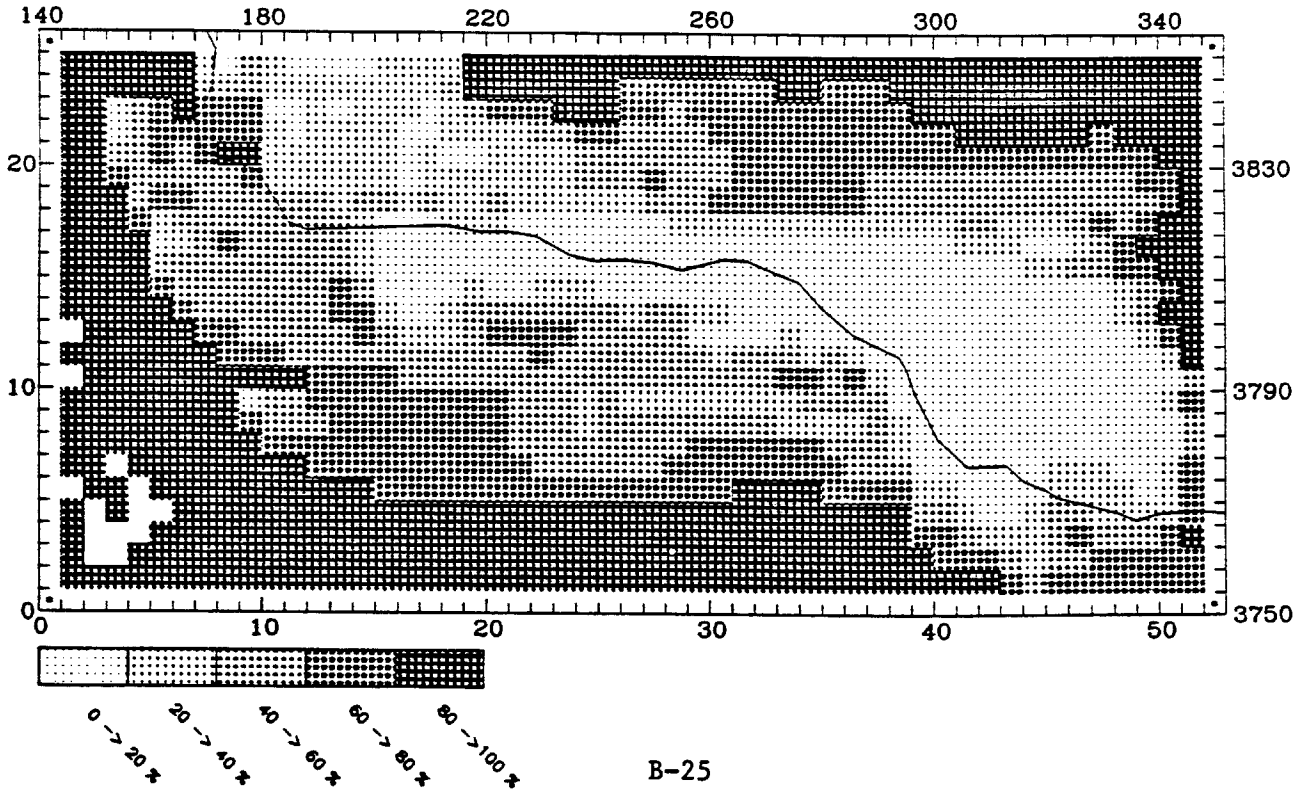

BNDRY RHC CONTRIBUTION AT: 2300 September 6 LEVEL 1

MAXIMUM CONTRIBUTION IN CELL (5,2) = 100.00 (%)

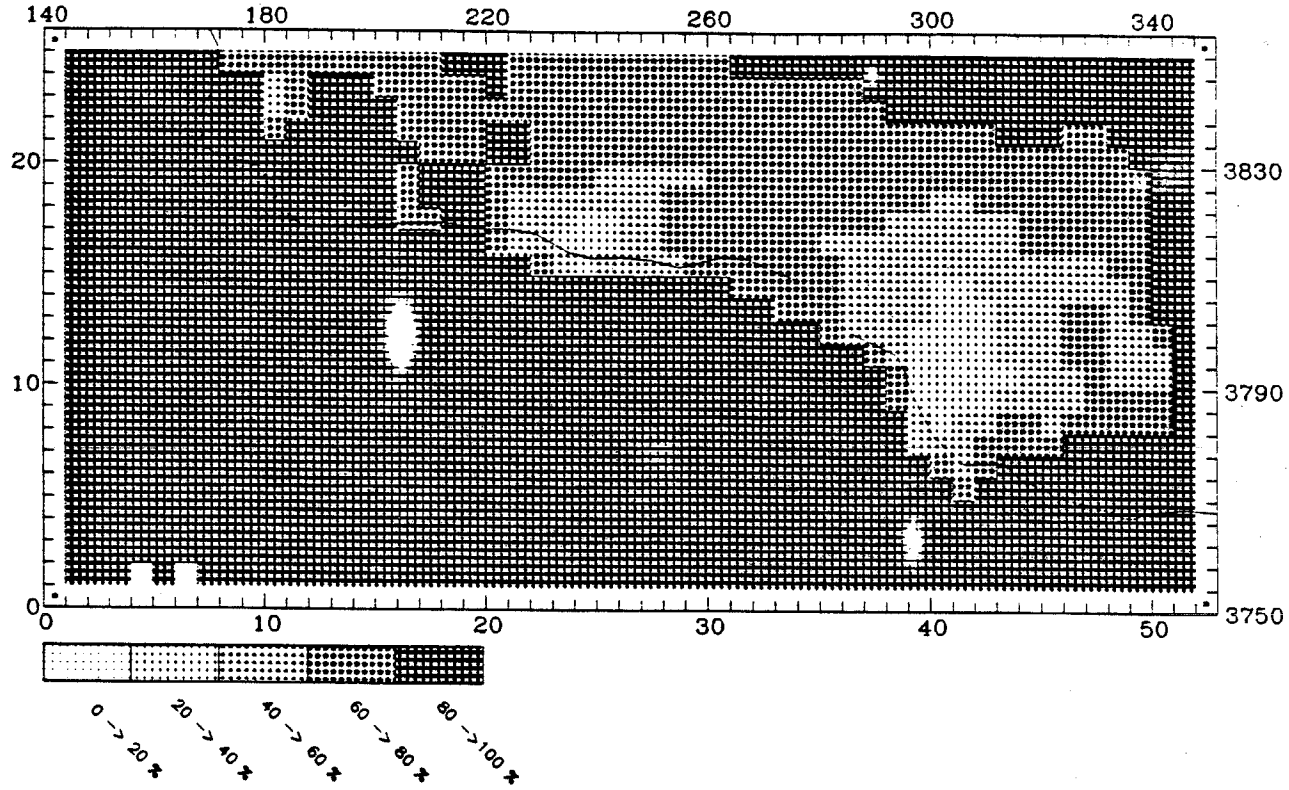

UAM-IV

BNDRY RHC CONTRIBUTION AT: 2300 September 6 LEVEL 1

MAXIMUM CONTRIBUTION IN CELL (2,13) = 100.00 (%)

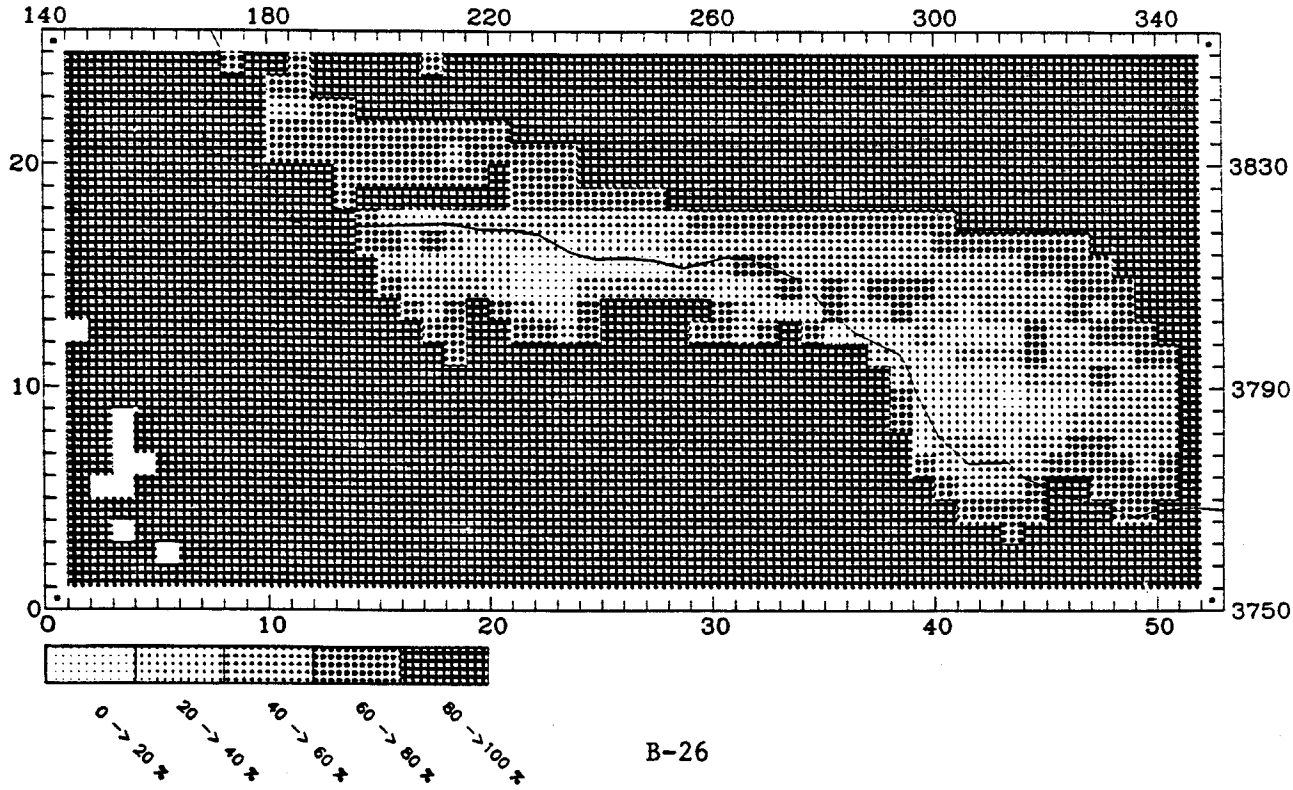

CALGRID–IV

INTNOX CONTRIBUTION AT: 2300 September 6 LEVEL 1

MAXIMUM CONTRIBUTION IN CELL (2,2) = 0.01 (%)

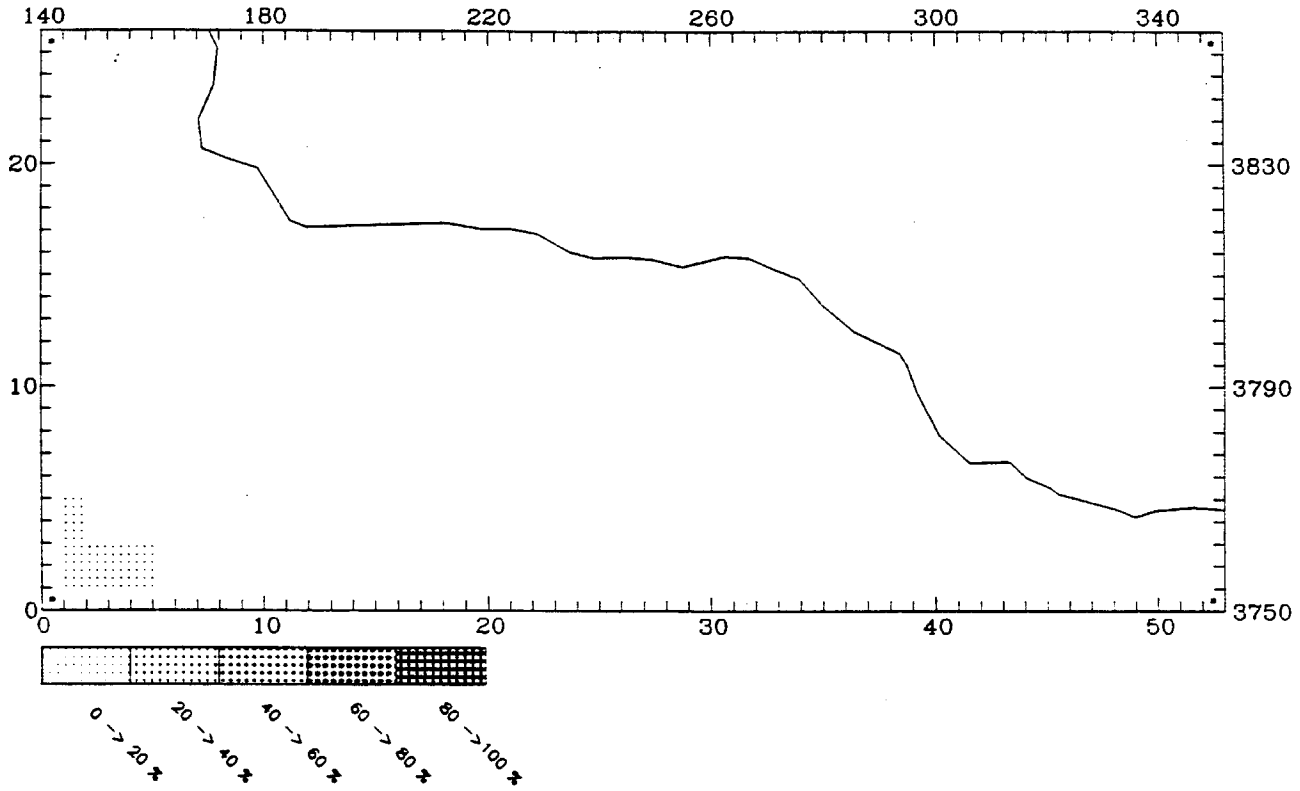

UAM–IV

INTNOX CONTRIBUTION AT: 2300 September 6 LEVEL 1

MAXIMUM CONTRIBUTION IN CELL (49,14) = 0.06 (%)

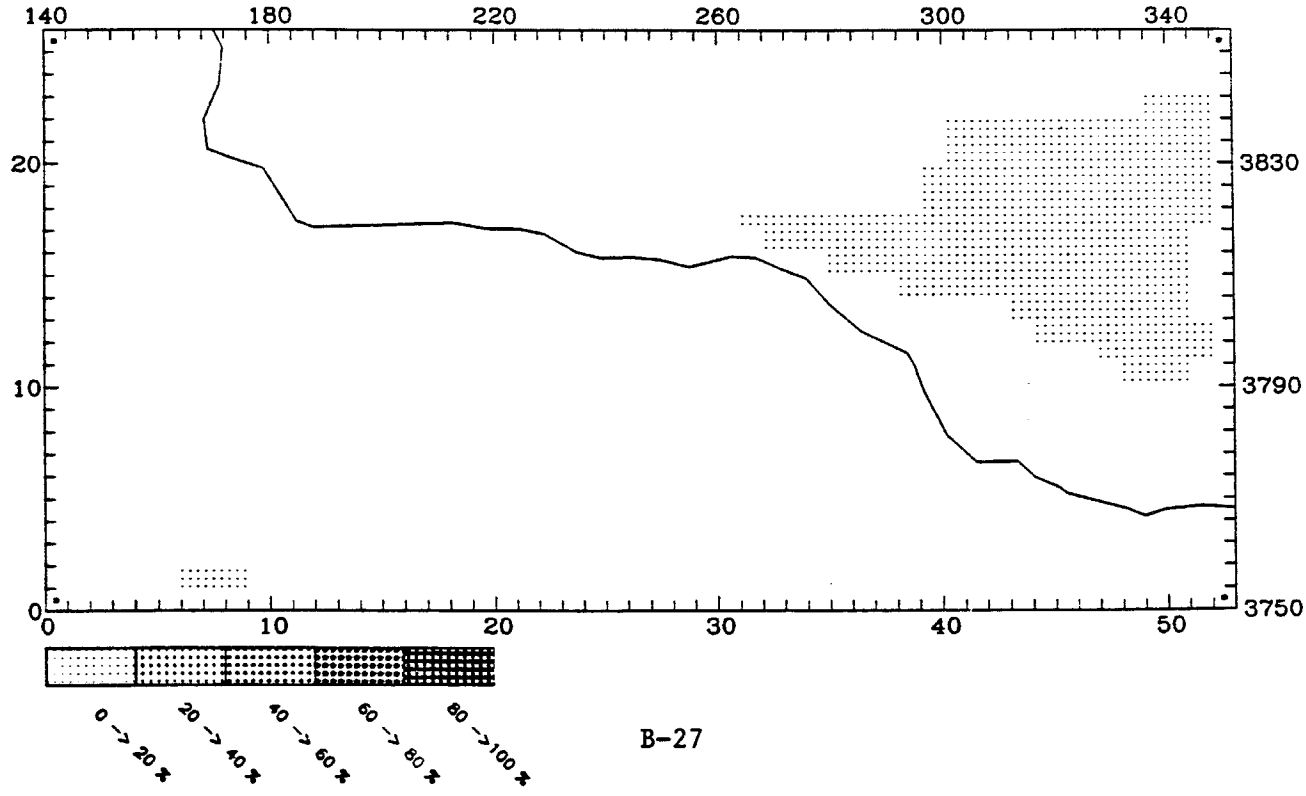

CALGRID–IV

INTHC CONTRIBUTION AT: 2300 September 6 LEVEL 1

MAXIMUM CONTRIBUTION IN CELL (51,21) = 0.00 (%)

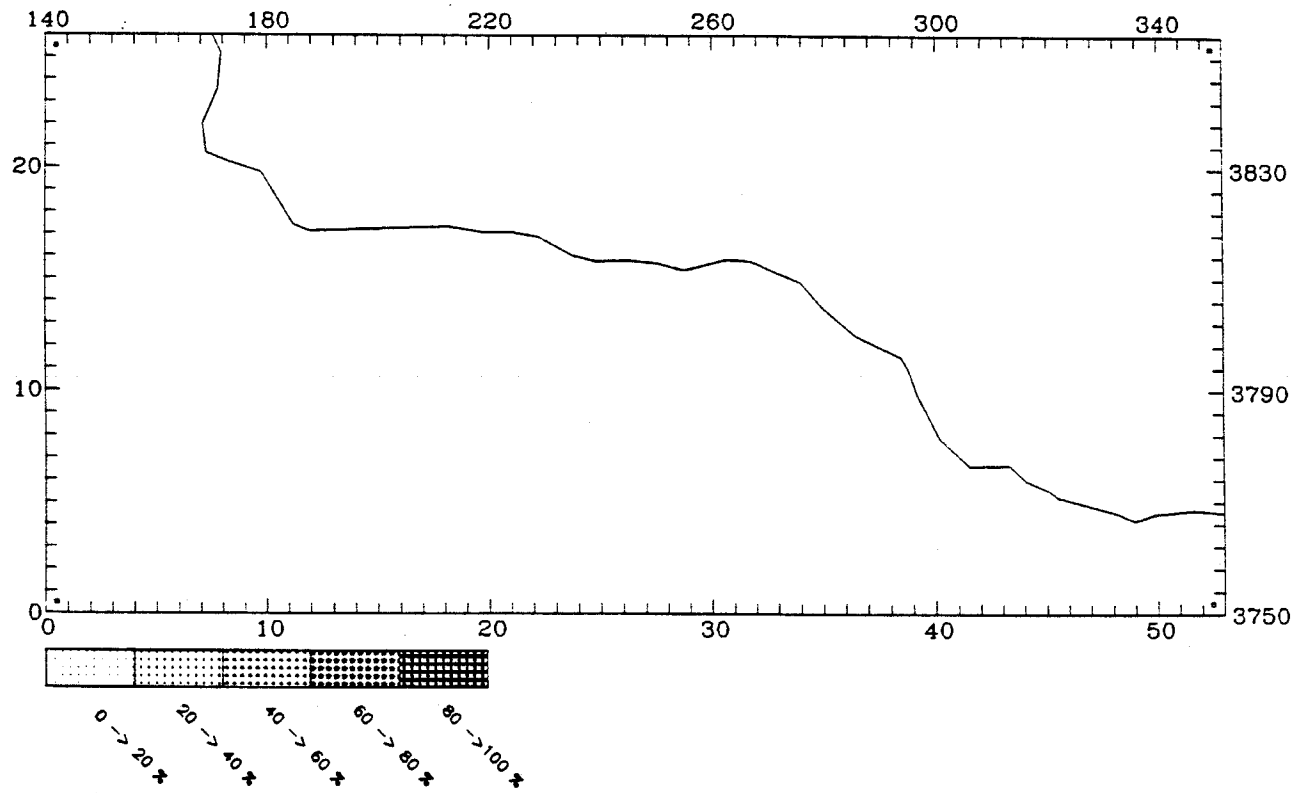

UAM–IV

INTHC CONTRIBUTION AT: 2300 September 6 LEVEL 1

MAXIMUM CONTRIBUTION IN CELL (49,14) = 0.03 (%)

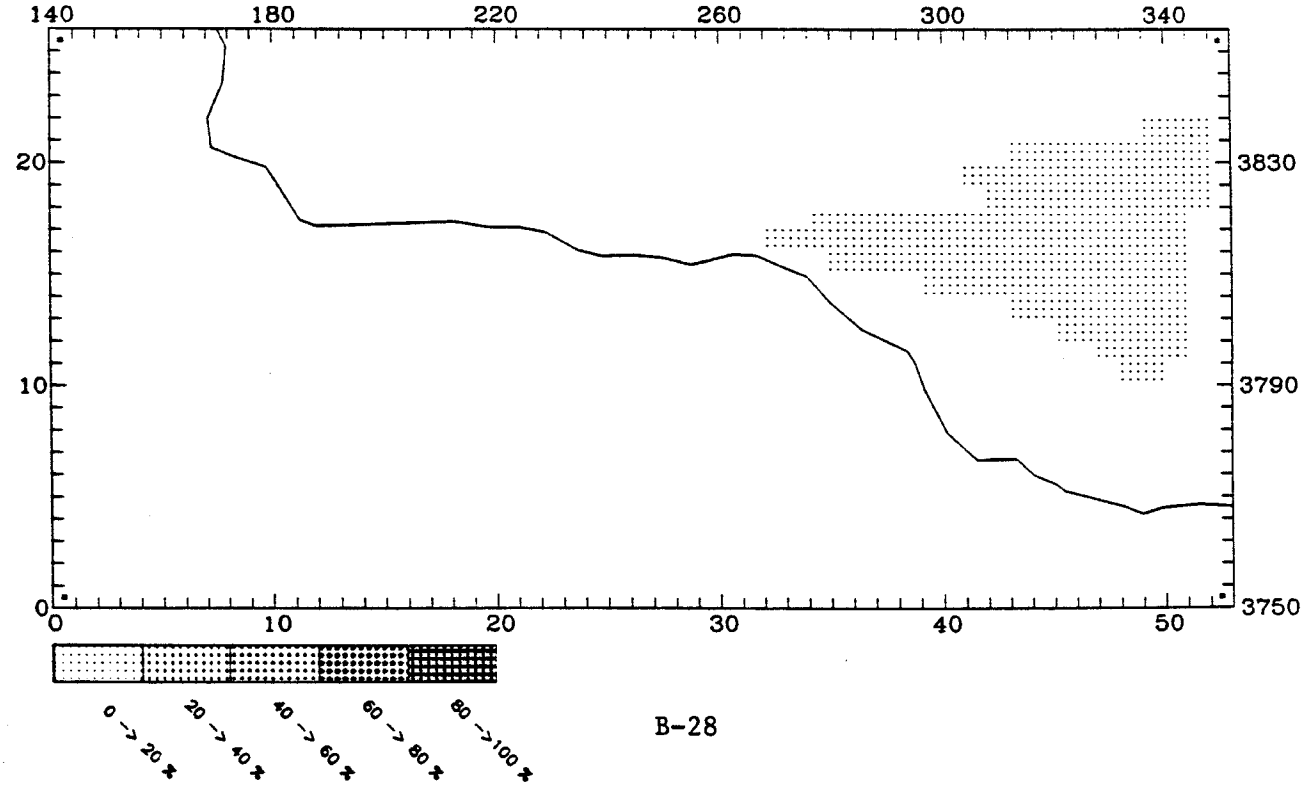

CALGRID-IV

PTARBNOX CONTRIBUTION AT: 2300 September 6 LEVEL 1

MAXIMUM CONTRIBUTION IN CELL (46,2) = 99.89 (%)

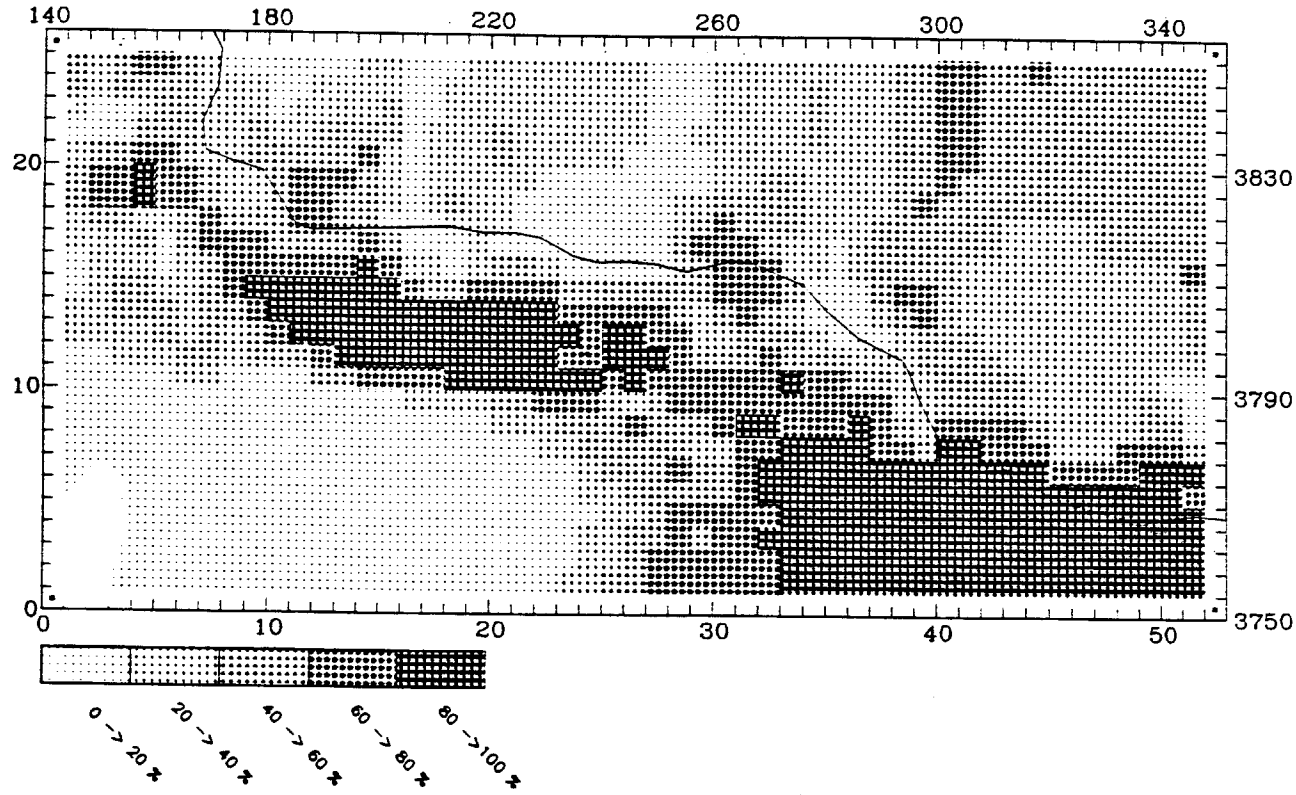

UAM-IV

PTNOX CONTRIBUTION AT: 2300 September 6 LEVEL 1

MAXIMUM CONTRIBUTION IN CELL (25,10) = 54.19 (%)

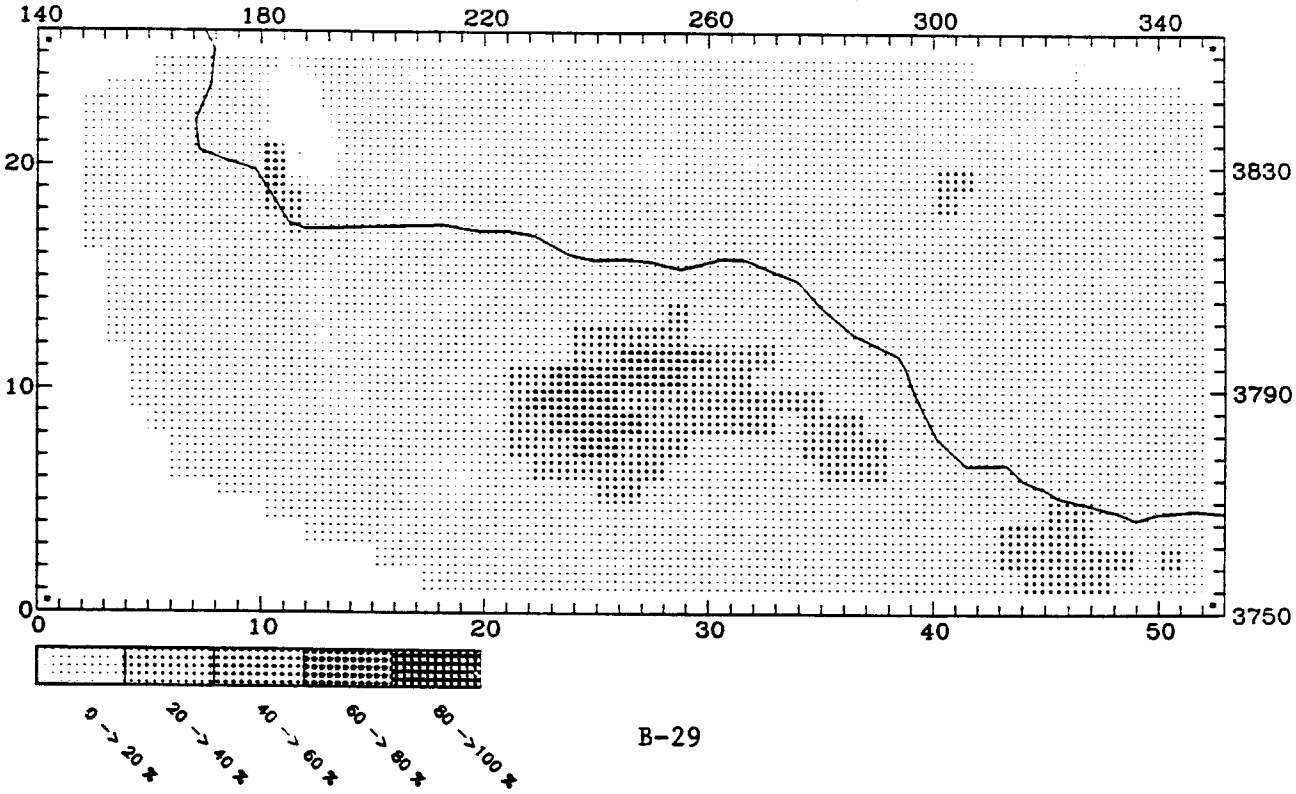

CALGRID–IV

PTARBHC CONTRIBUTION AT: 2300 September 6 LEVEL 1

MAXIMUM CONTRIBUTION IN CELL (44,3) = 7.57 (%)

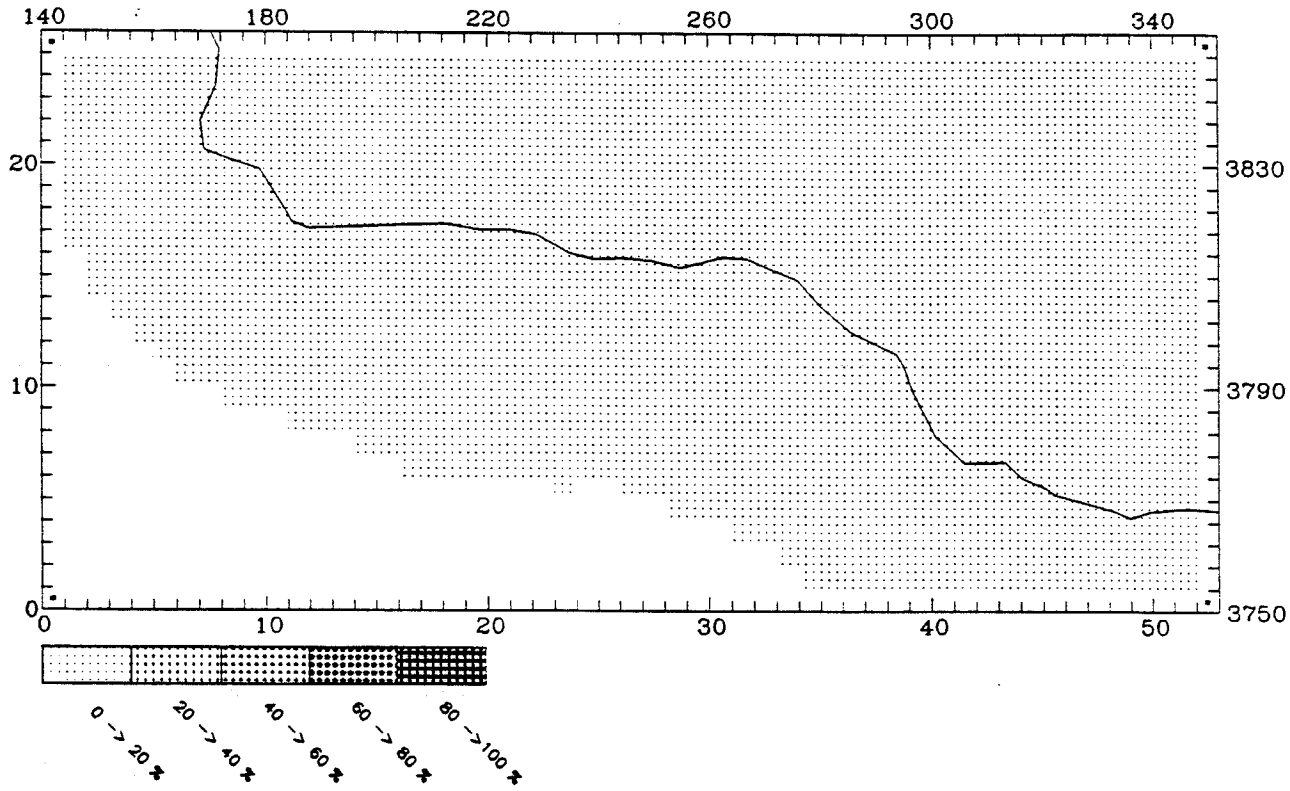

UAM–IV

PTHC CONTRIBUTION AT: 2300 September 6 LEVEL 1

MAXIMUM CONTRIBUTION IN CELL (25,10) = 1.75 (%)

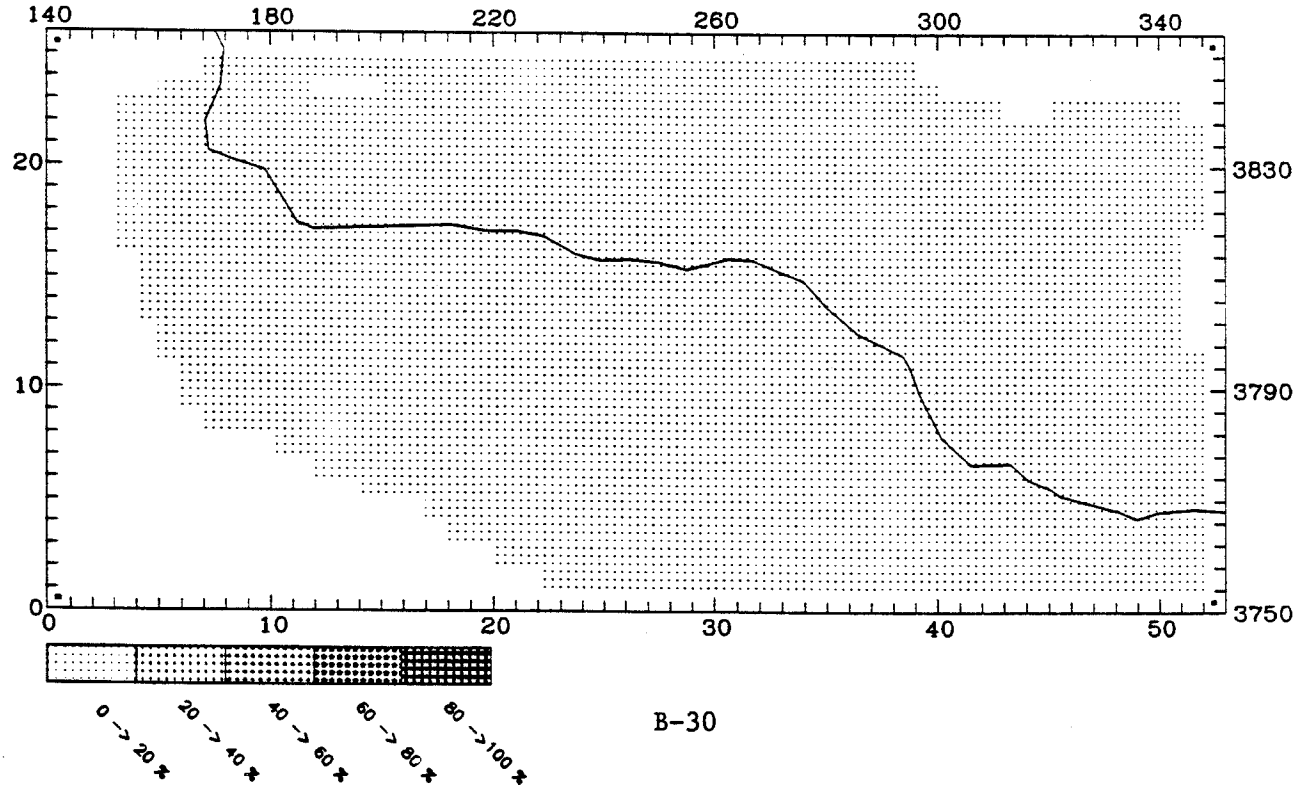

CALGRID–IV

ANOX CONTRIBUTION AT: 2300 September 6 LEVEL 1

MAXIMUM CONTRIBUTION IN CELL (11,9) = 99.83 (%)

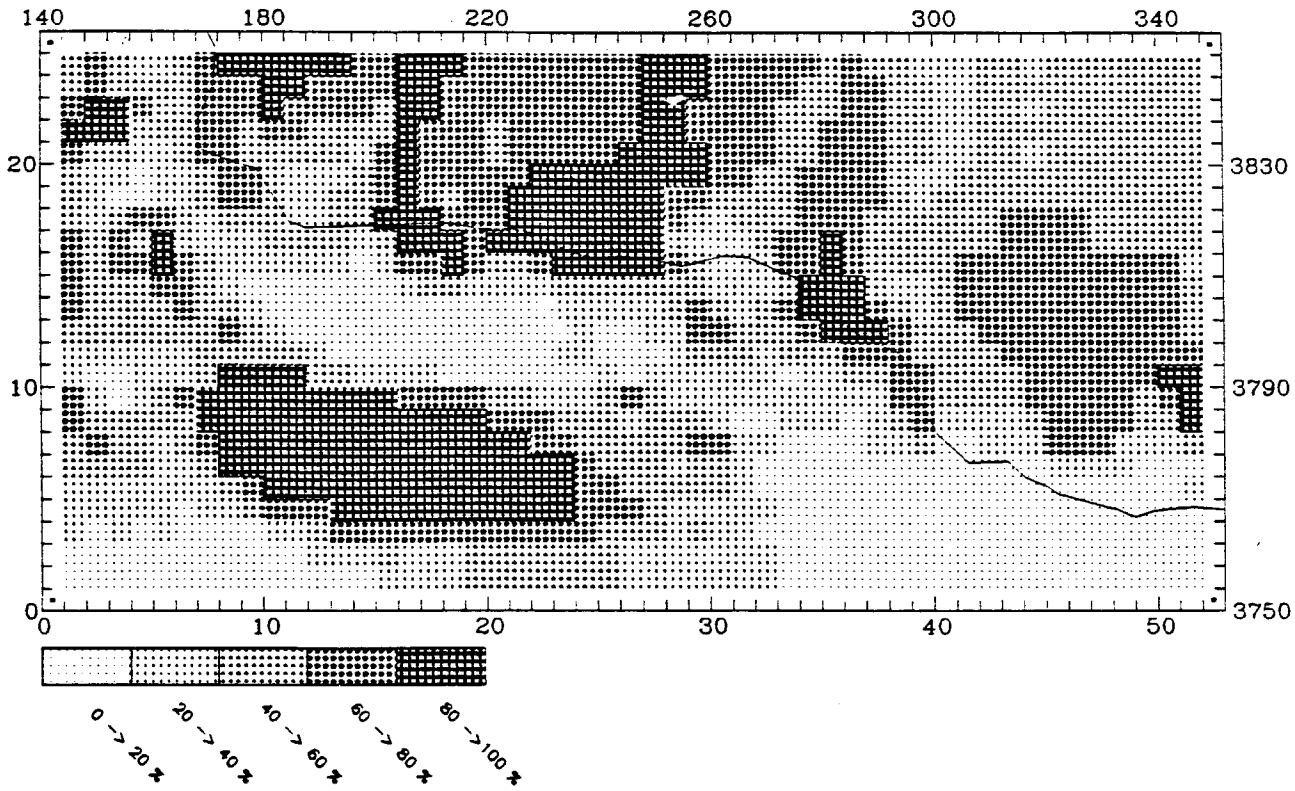

UAM–IV

NOX CONTRIBUTION AT: 2300 September 6 LEVEL 1

MAXIMUM CONTRIBUTION IN CELL (37,13) = 98.88 (%)

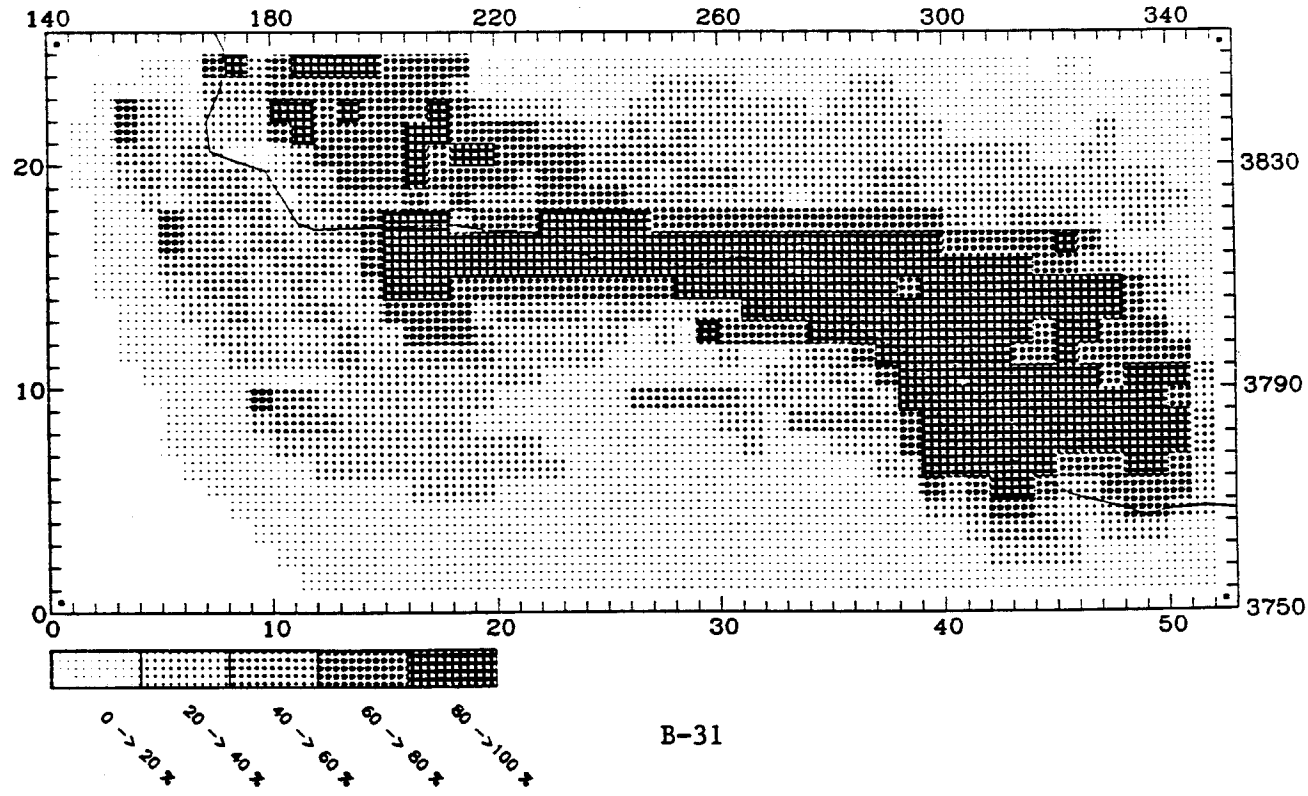

CALGRID-IV

ATHC CONTRIBUTION AT: 2300 September 6 LEVEL 1

MAXIMUM CONTRIBUTION IN CELL (40,10) = 67.16 (%)

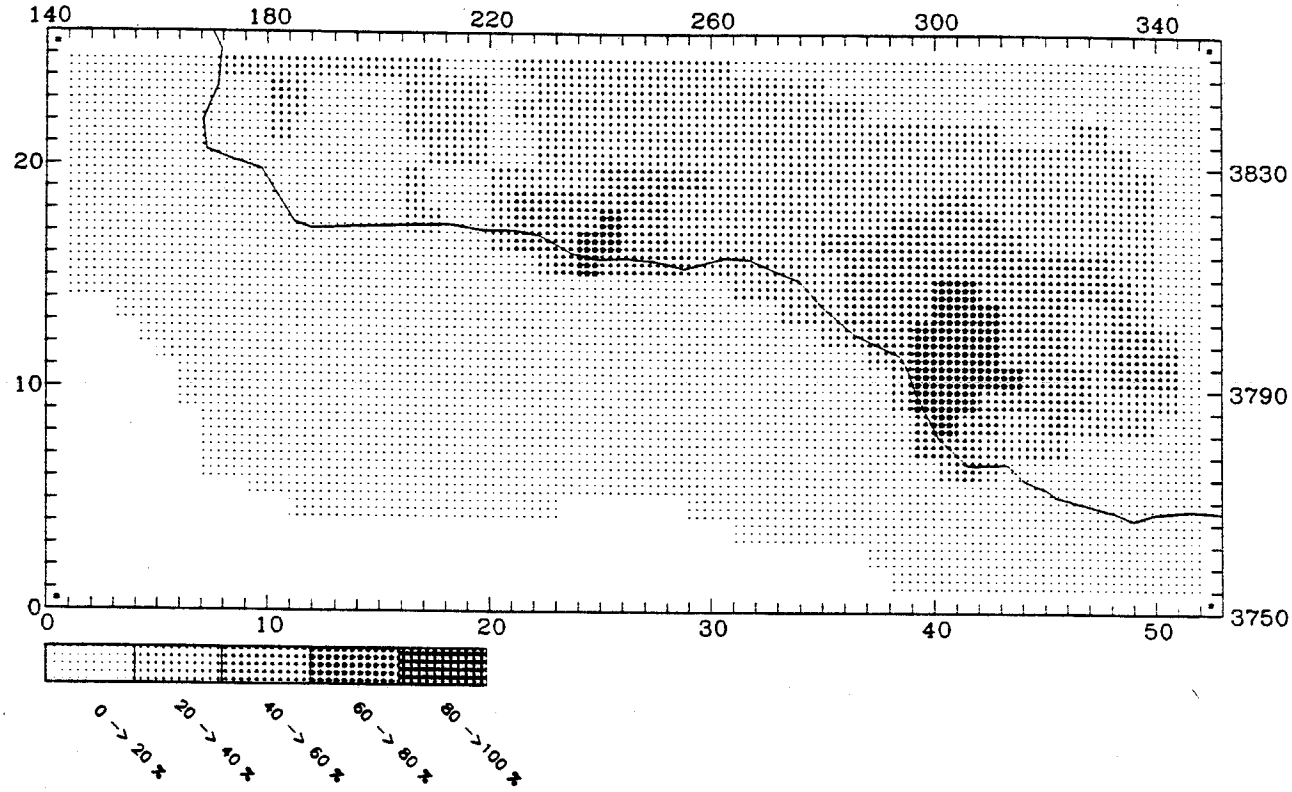

UAM-IV

RHC CONTRIBUTION AT: 2300 September 6 LEVEL 1

MAXIMUM CONTRIBUTION IN CELL (24,15) = 90.18 (%)

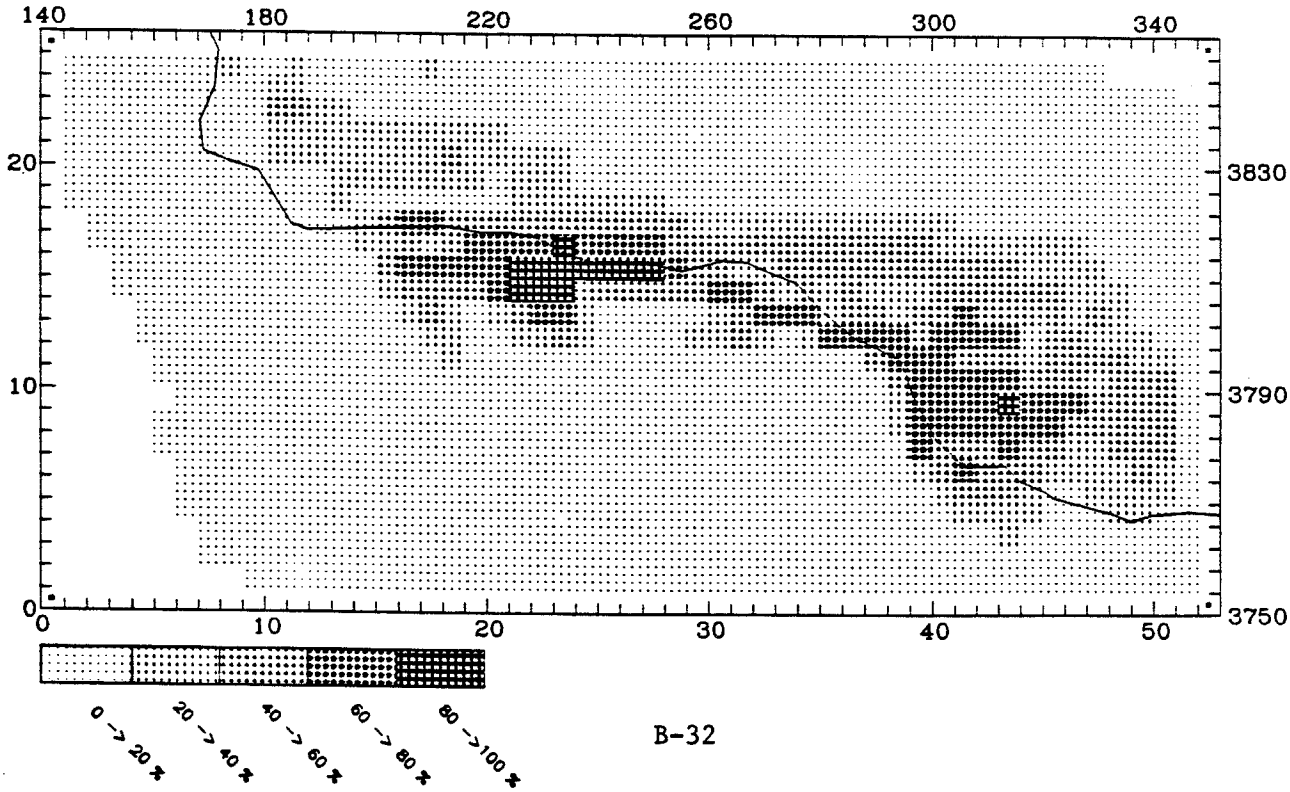

CALGRID–IV

BNDRY NOX CONTRIBUTION AT: 1100 September 7 LEVEL 1

MAXIMUM CONTRIBUTION IN CELL (51,2) = 99.03 (%)

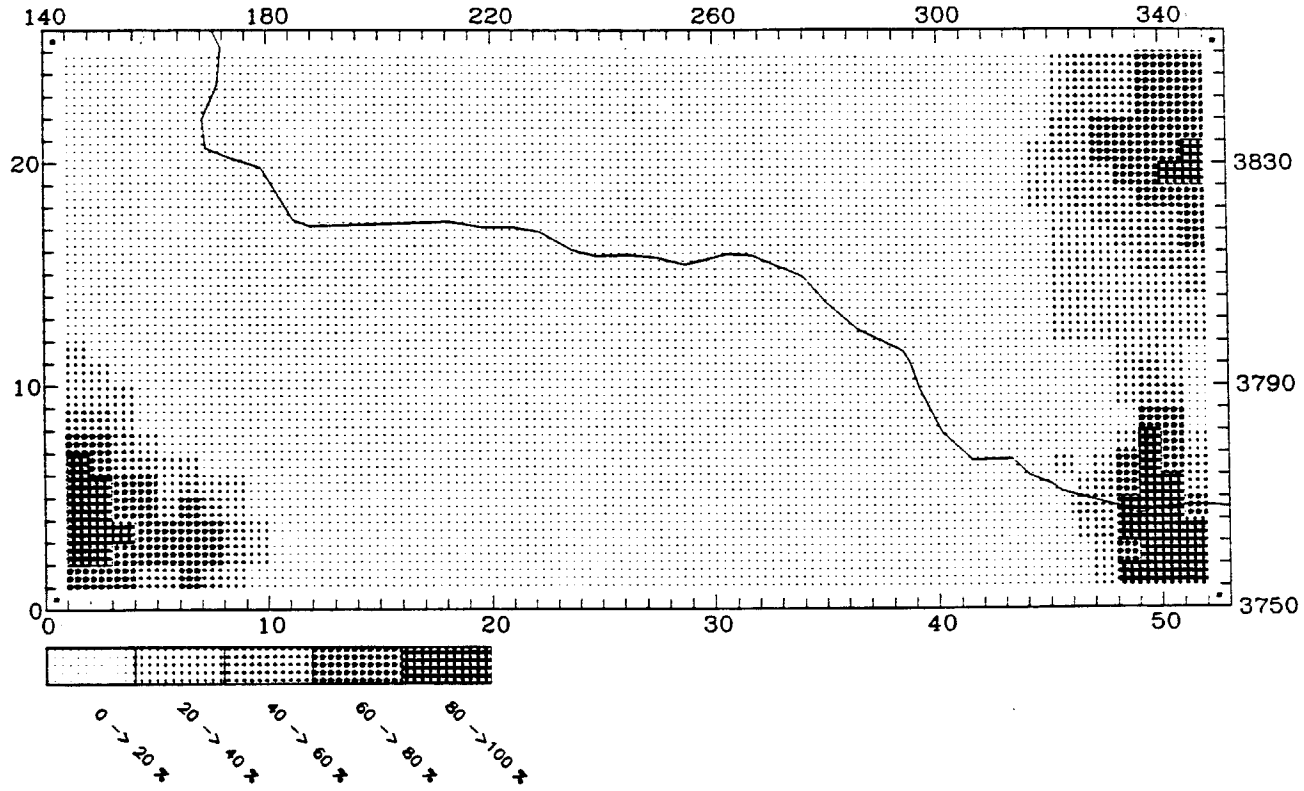

UAM–IV

BNDRY NOX CONTRIBUTION AT: 1100 September 7 LEVEL 1

MAXIMUM CONTRIBUTION IN CELL (2,2) = 100.00 (%)

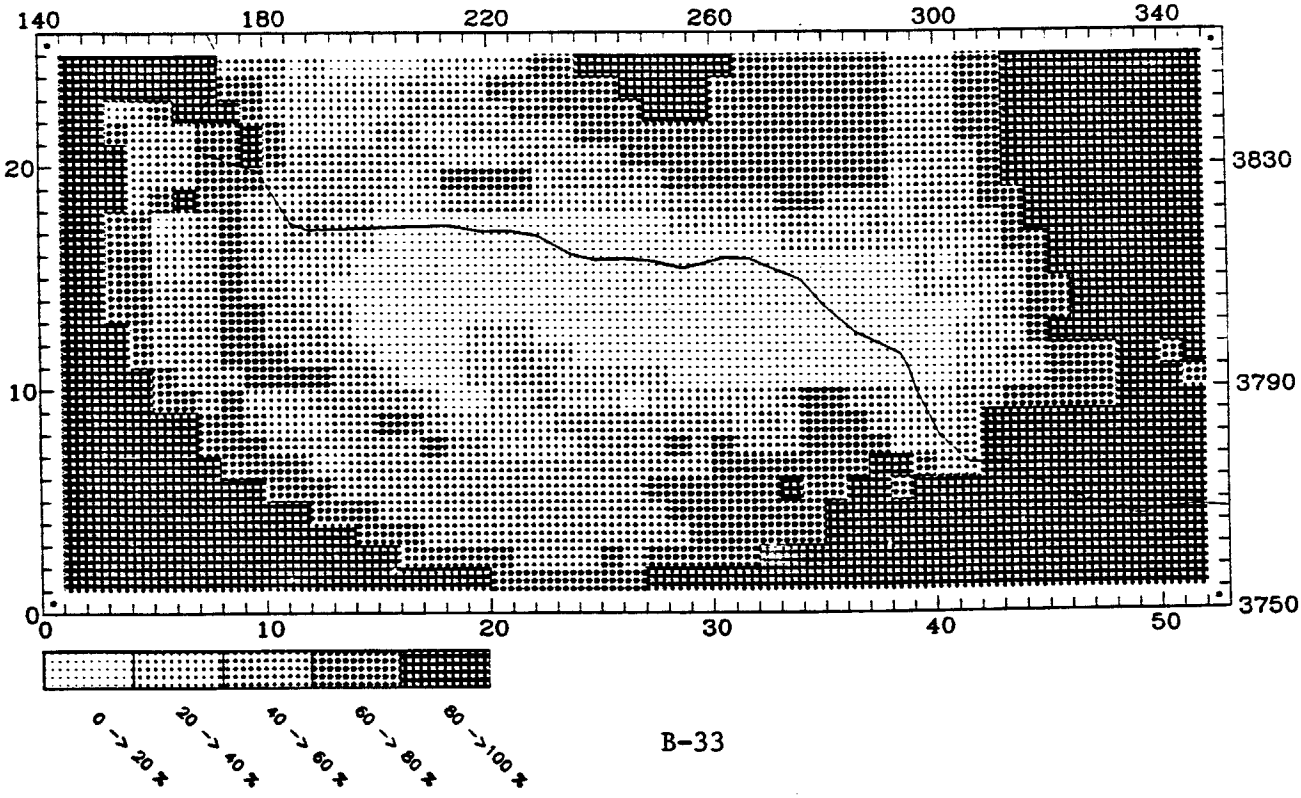

CALGRID–IV

BNDRY RHC CONTRIBUTION AT: 1100 September 7 LEVEL 1

MAXIMUM CONTRIBUTION IN CELL (3,4) = 100.00 (%)

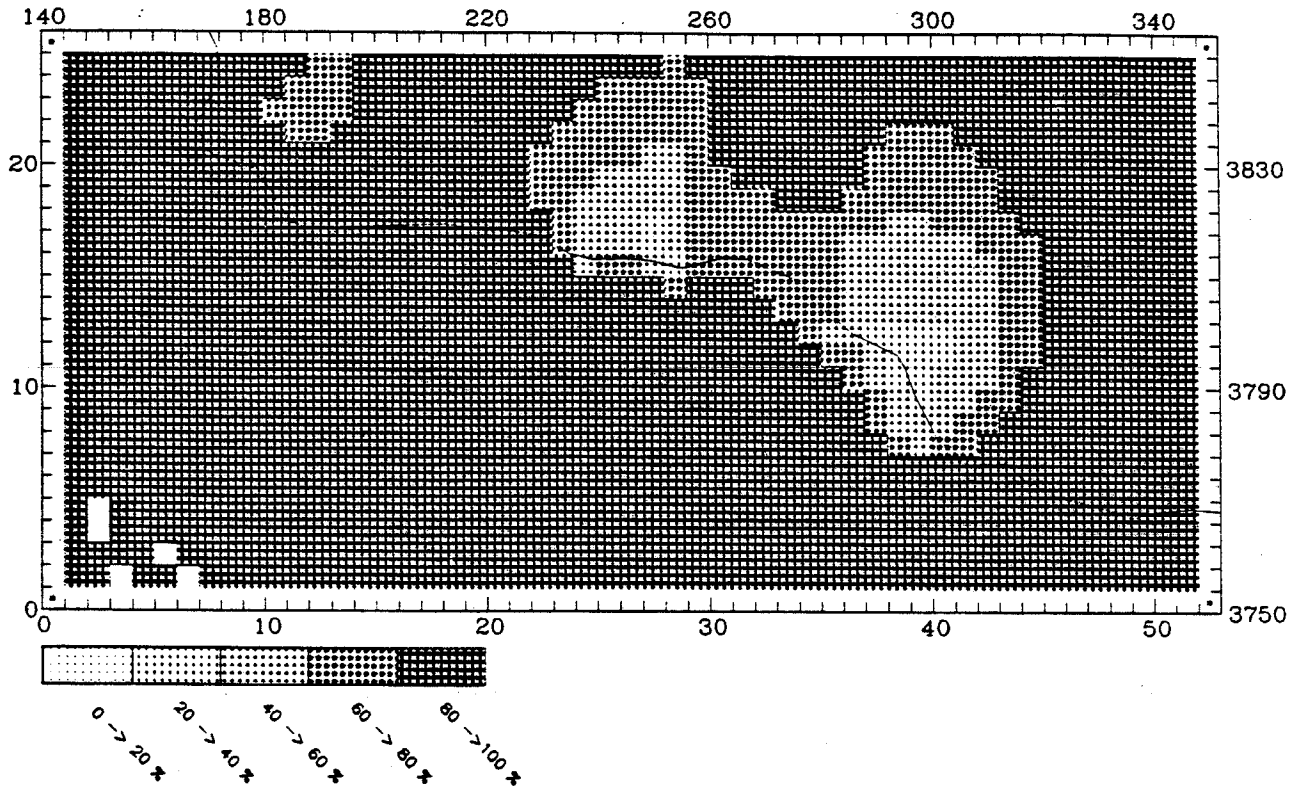

UAM–IV

BNDRY RHC CONTRIBUTION AT: 1100 September 7 LEVEL 1

MAXIMUM CONTRIBUTION IN CELL (2,5) = 100.00 (%)

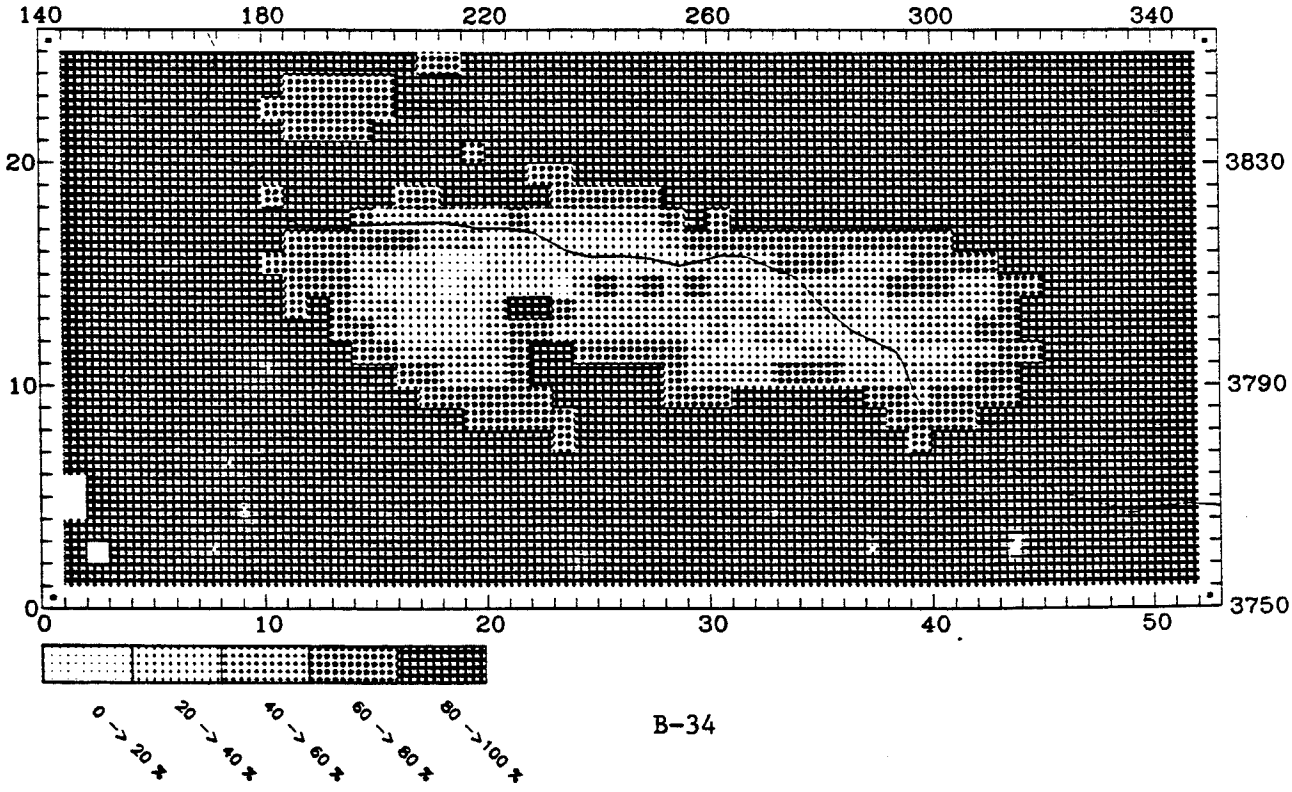

CALGRID–IV

INTNOX CONTRIBUTION AT: 1100 September 7 LEVEL 1

MAXIMUM CONTRIBUTION IN CELL (2,2) = 0.04 (%)

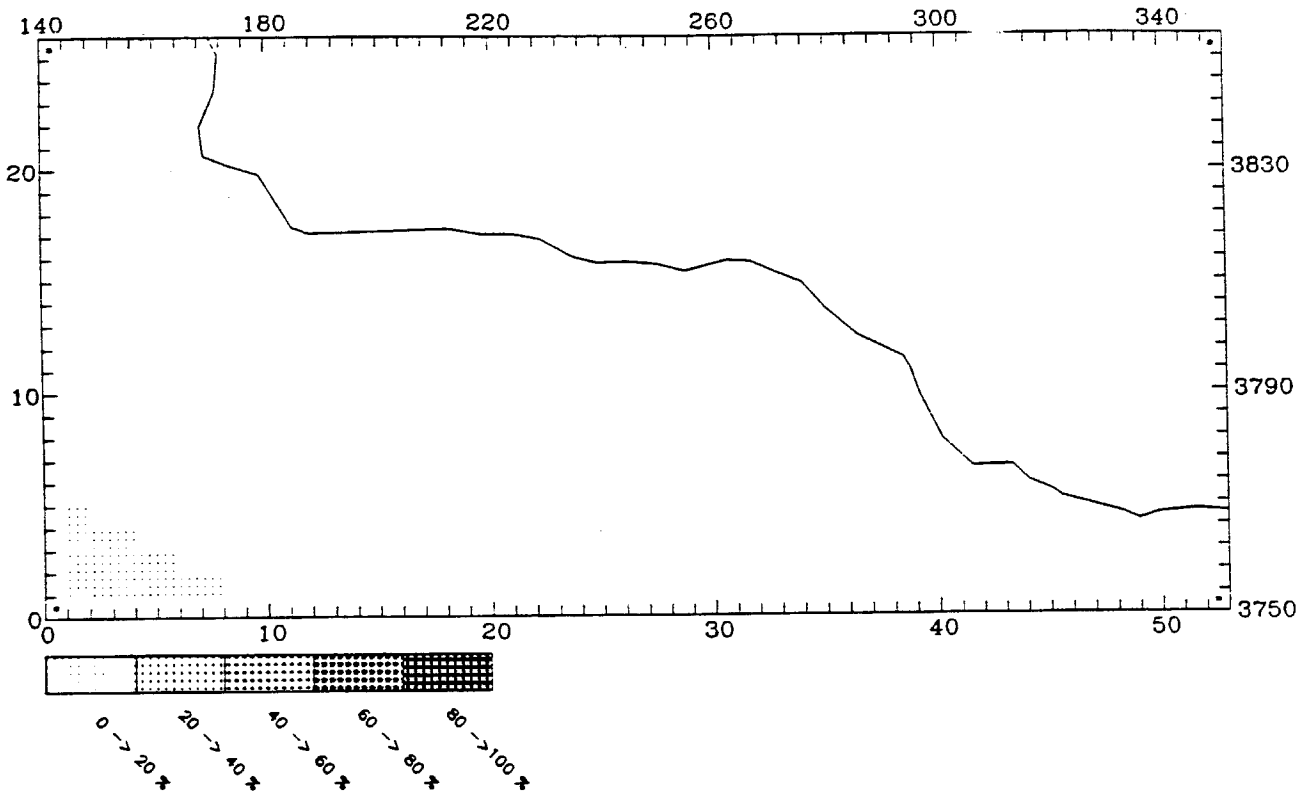

UAM–IV

INTNOX CONTRIBUTION AT: 1100 September 7 LEVEL 1

MAXIMUM CONTRIBUTION IN CELL (40,15) = 0.01 (%)

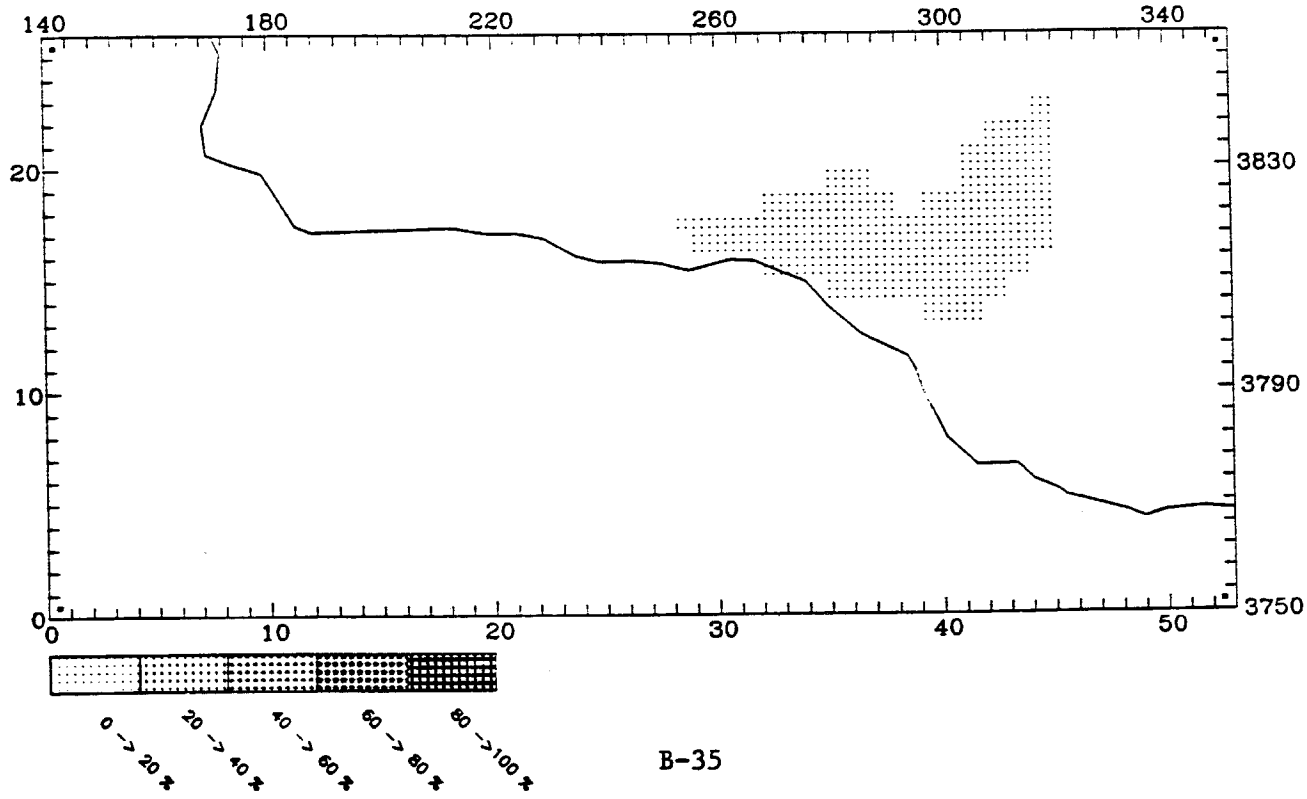

CALGRID–IV

INTHC CONTRIBUTION AT: 1100 September 7 LEVEL 1

MAXIMUM CONTRIBUTION IN CELL (5,23) = 0.00 (%)

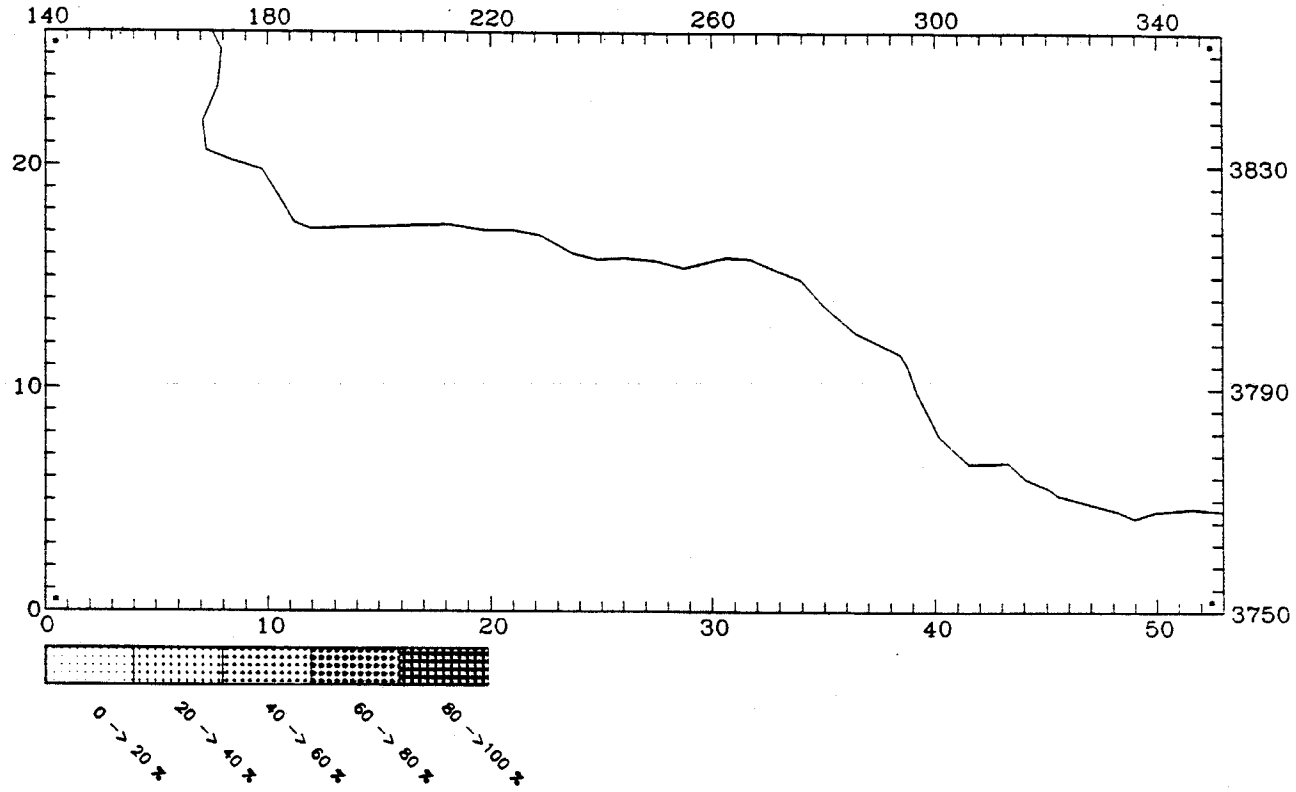

UAM–IV

INTHC CONTRIBUTION AT: 1100 September 7 LEVEL 1

MAXIMUM CONTRIBUTION IN CELL (40,15) = 0.00 (%)

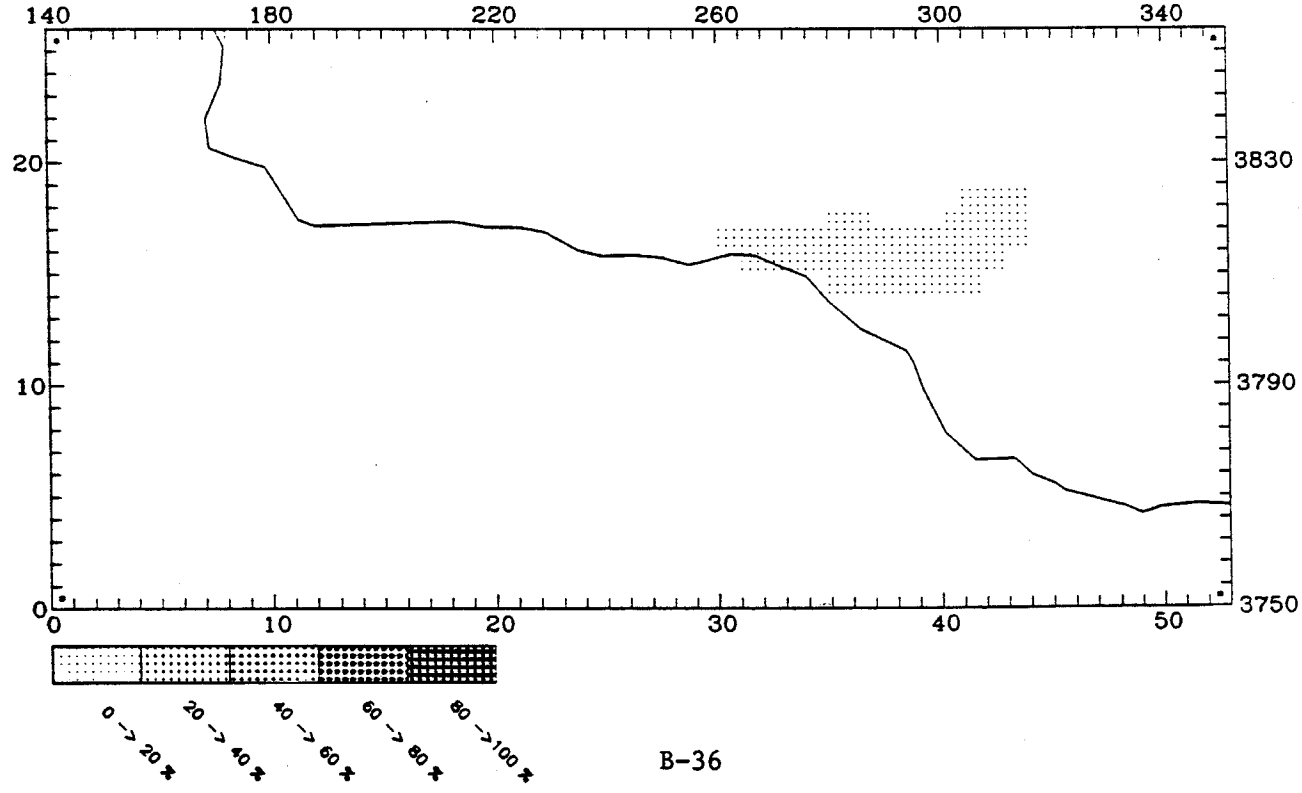

CALGRID–IV

PTARBNOX CONTRIBUTION AT: 1100 September 7 LEVEL 1

MAXIMUM CONTRIBUTION IN CELL (43,3) = 99.89 (%)

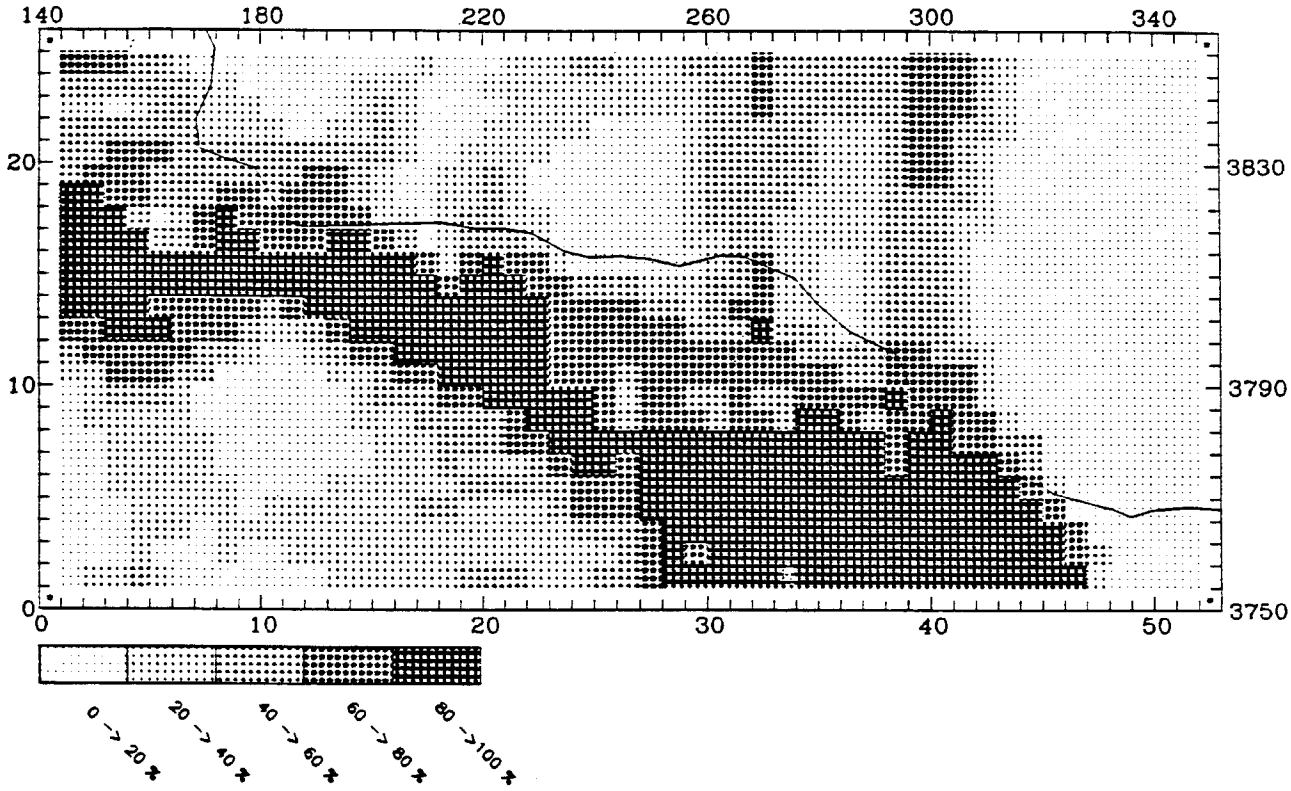

UAM–IV

PTNOX CONTRIBUTION AT: 1100 September 7 LEVEL 1

MAXIMUM CONTRIBUTION IN CELL (41,8) = 41.41 (%)

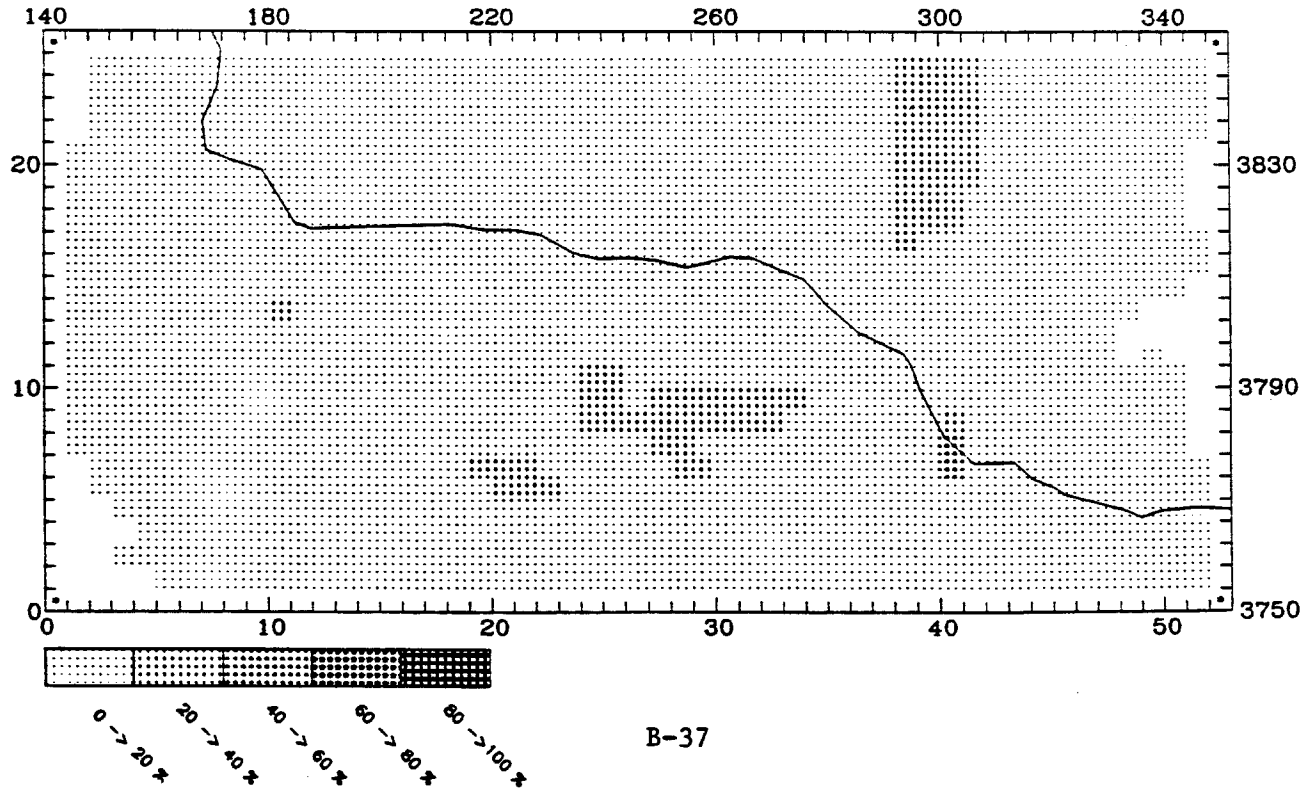

CALGRID–IV

PTARBHC CONTRIBUTION AT: 1100 September 7 LEVEL 1

MAXIMUM CONTRIBUTION IN CELL (33,7) = 3.34 (%)

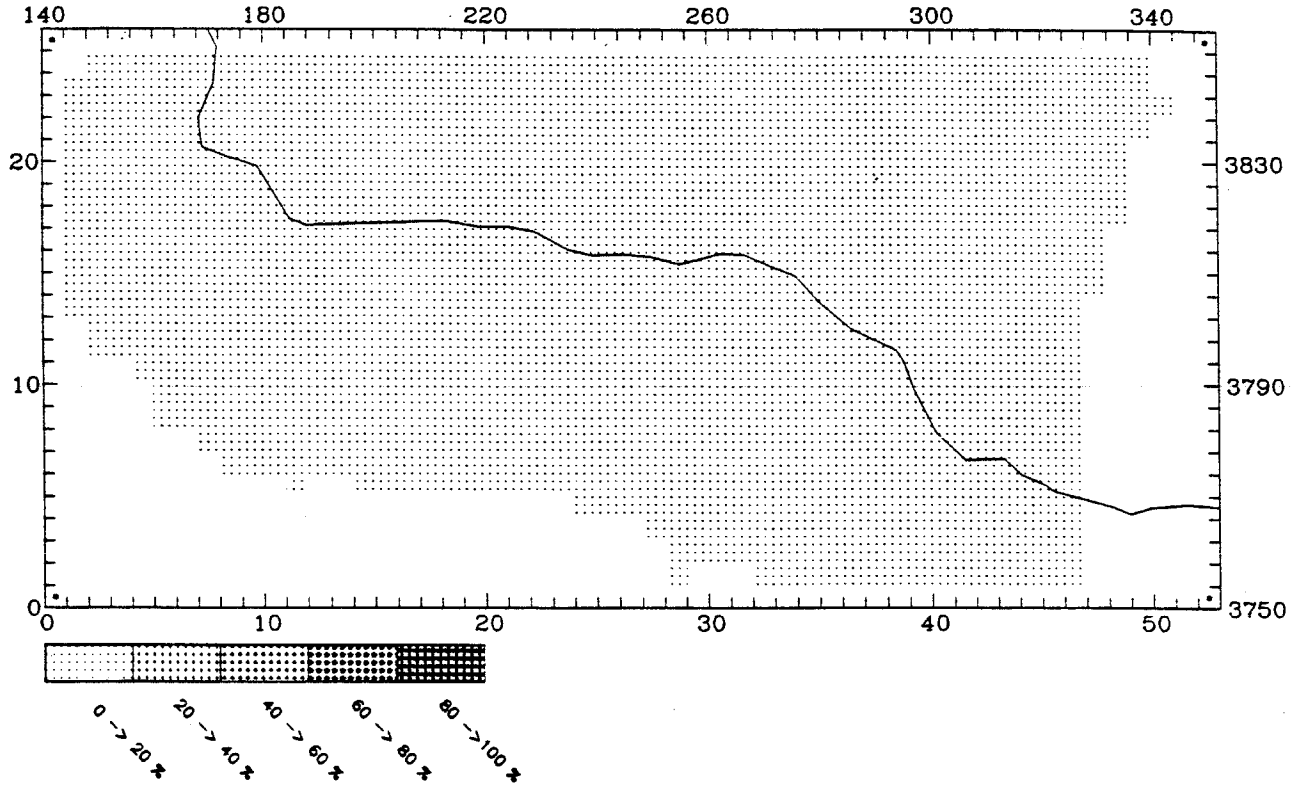

UAM–IV

PTHC CONTRIBUTION AT: 1100 September 7 LEVEL 1

MAXIMUM CONTRIBUTION IN CELL (25,11) = 0.87 (%)

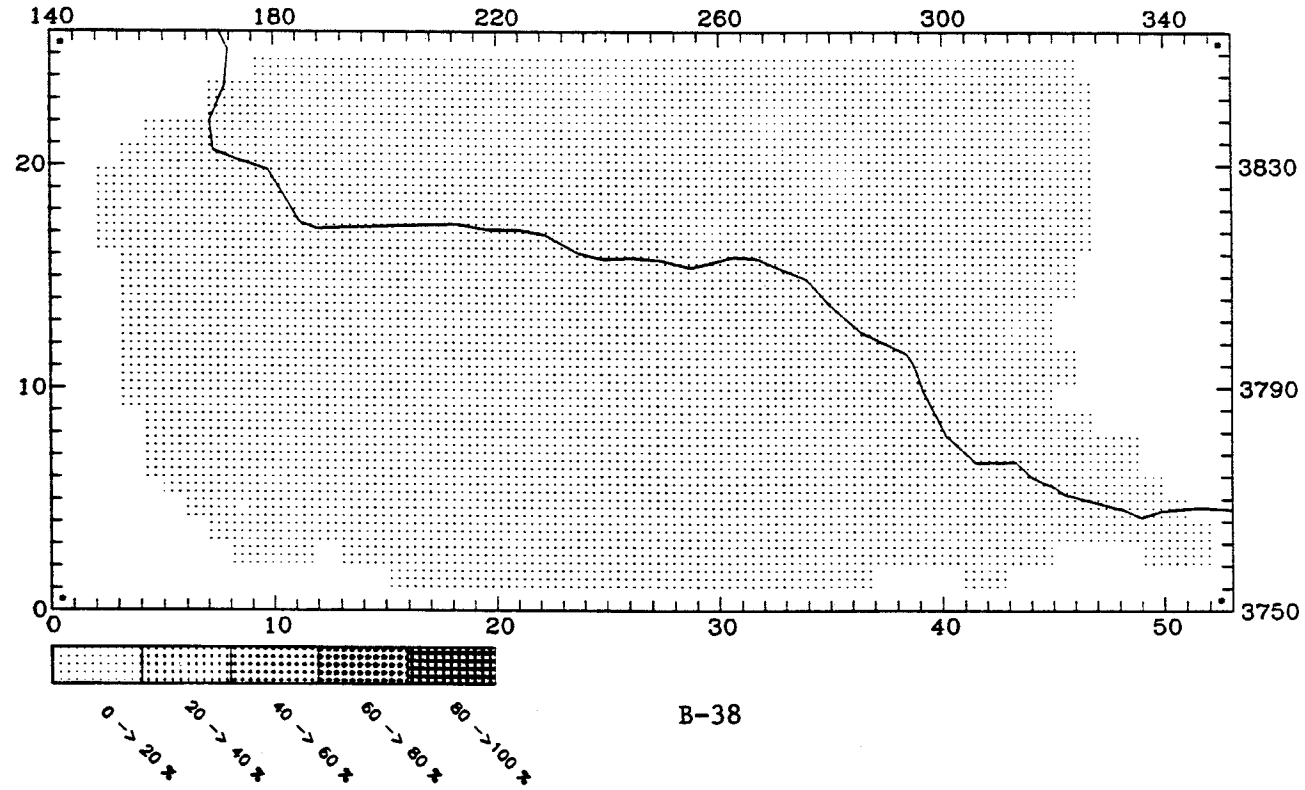

CALGRID–IV

ANOX CONTRIBUTION AT: 1100 September 7 LEVEL 1

MAXIMUM CONTRIBUTION IN CELL (10,10) = 98.91 (%)

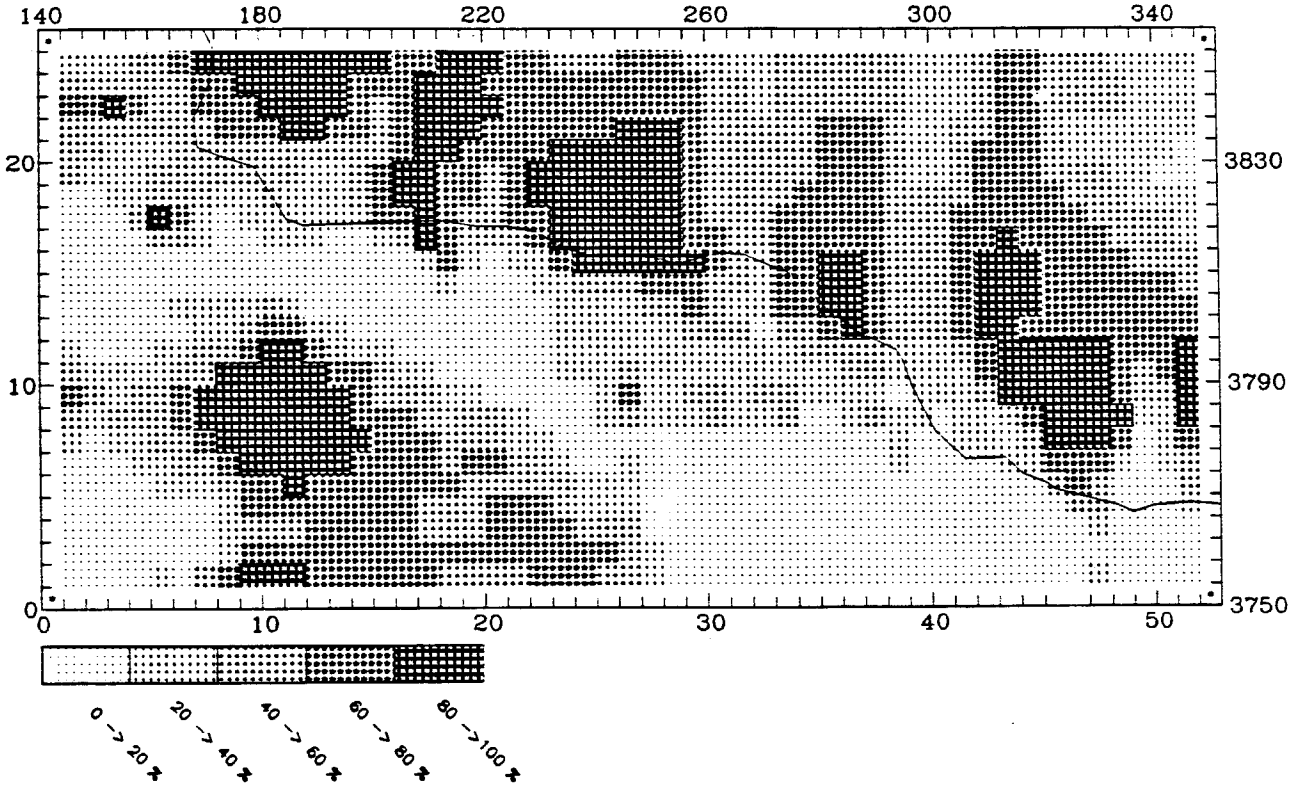

UAM–IV

NOX CONTRIBUTION AT: 1100 September 7 LEVEL 1

MAXIMUM CONTRIBUTION IN CELL (37,13) = 96.60 (%)

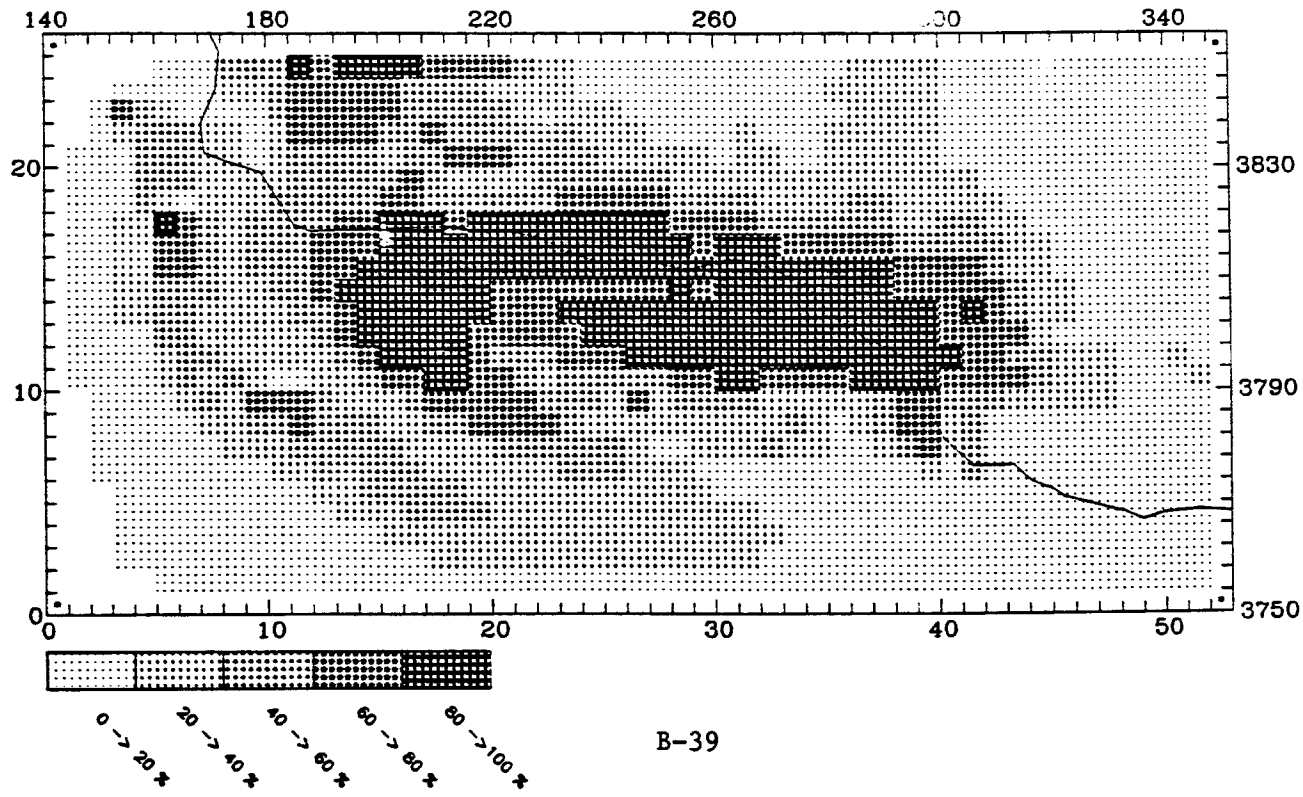

ATHC CONTRIBUTION AT: 1100 September 7 LEVEL 1

MAXIMUM CONTRIBUTION IN CELL (40,13) = 67.48 (%)

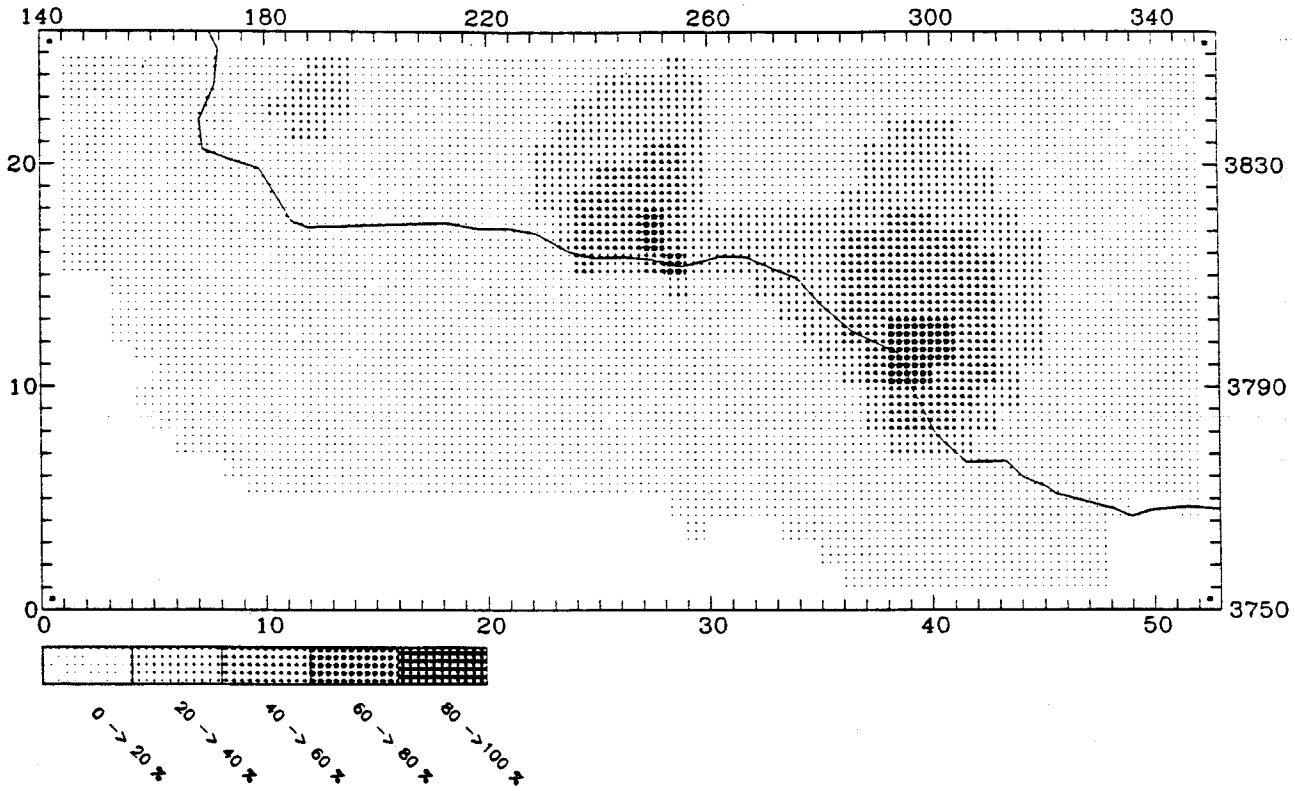

UAM-IV

RHC CONTRIBUTION AT: 1100 September 7 LEVEL 1

MAXIMUM CONTRIBUTION IN CELL (19,16) = 84.38 (%)

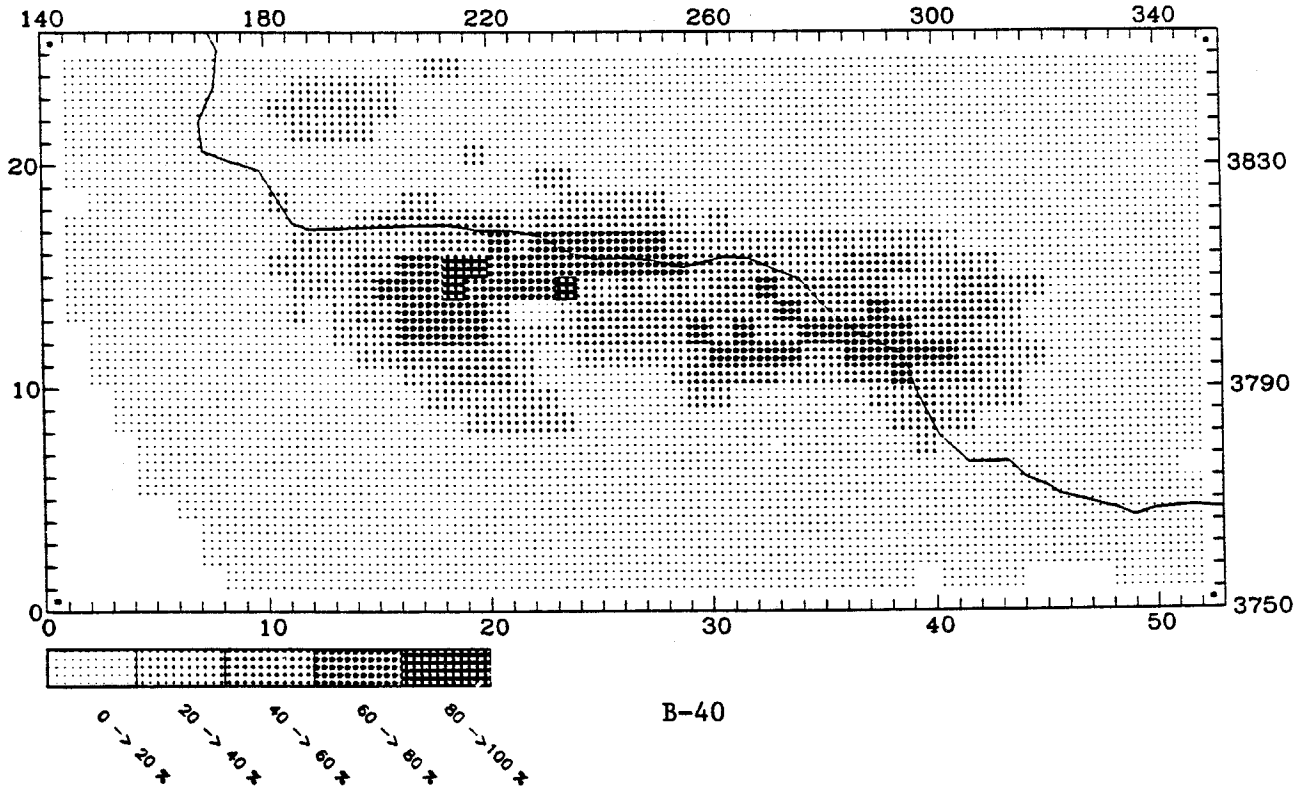

BNDRY NOX CONTRIBUTION AT: 2300 September 7 LEVEL 1

MAXIMUM CONTRIBUTION IN CELL (5,2) = 99.78 (%)

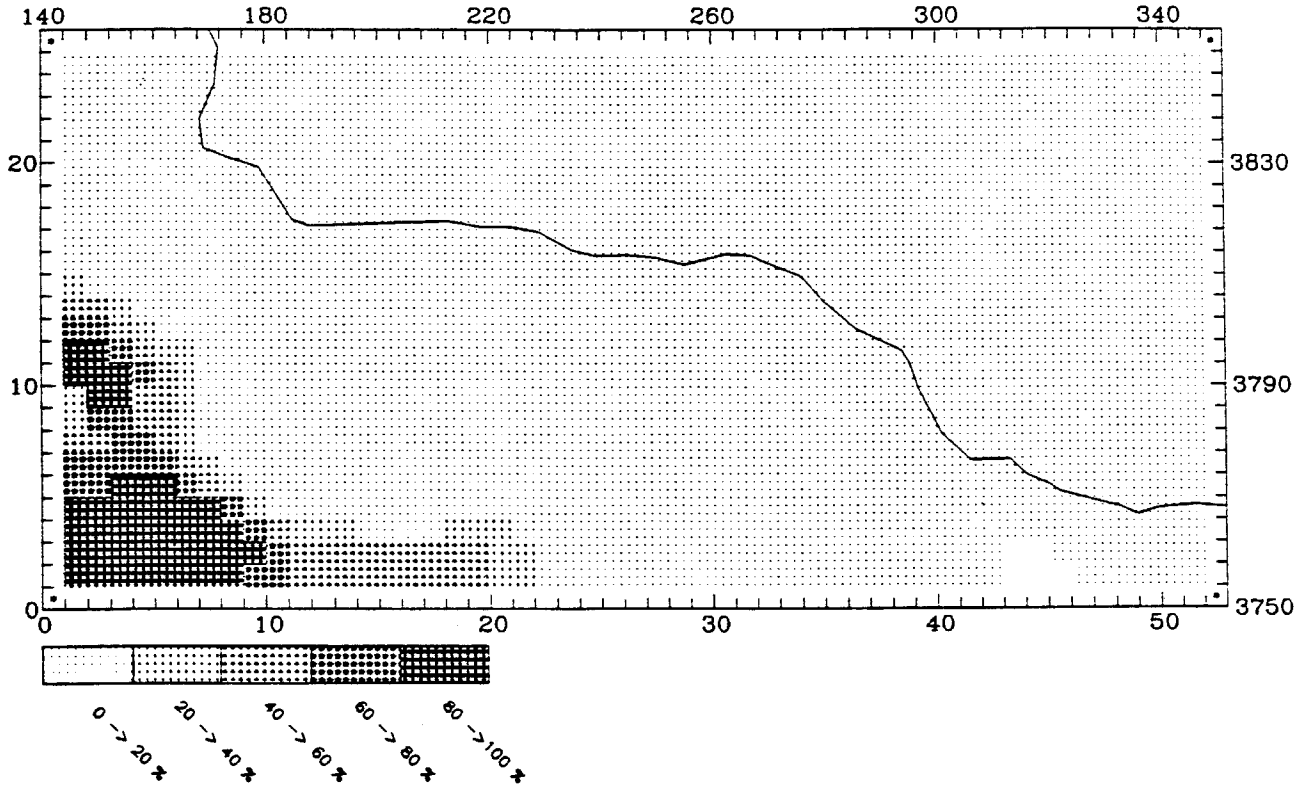

UAM-IV

BNDRY NOX CONTRIBUTION AT: 2300 September 7 LEVEL 1

MAXIMUM CONTRIBUTION IN CELL (3,2) = 100.00 (%)

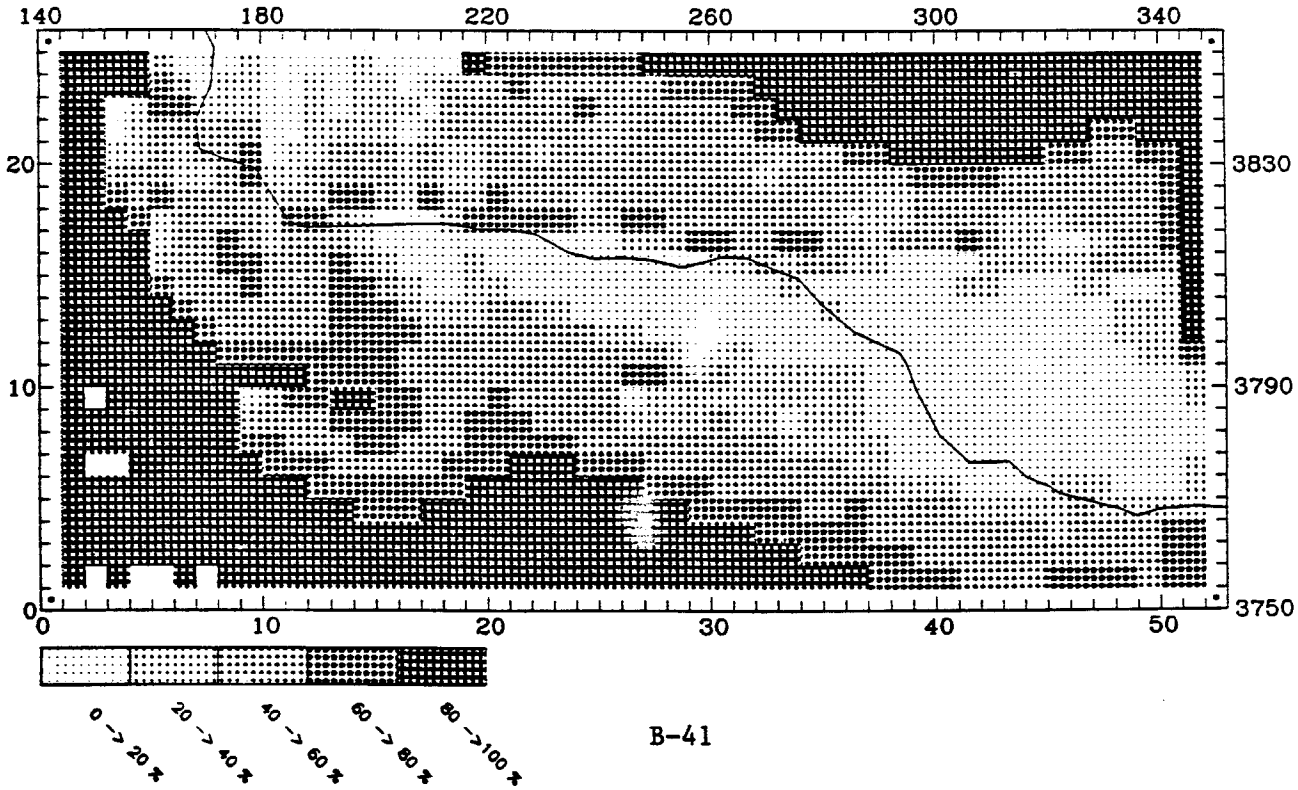

BNDRY RHC CONTRIBUTION AT: 2300 September 7 LEVEL 1

MAXIMUM CONTRIBUTION IN CELL (2,3) = 100.00 (%)

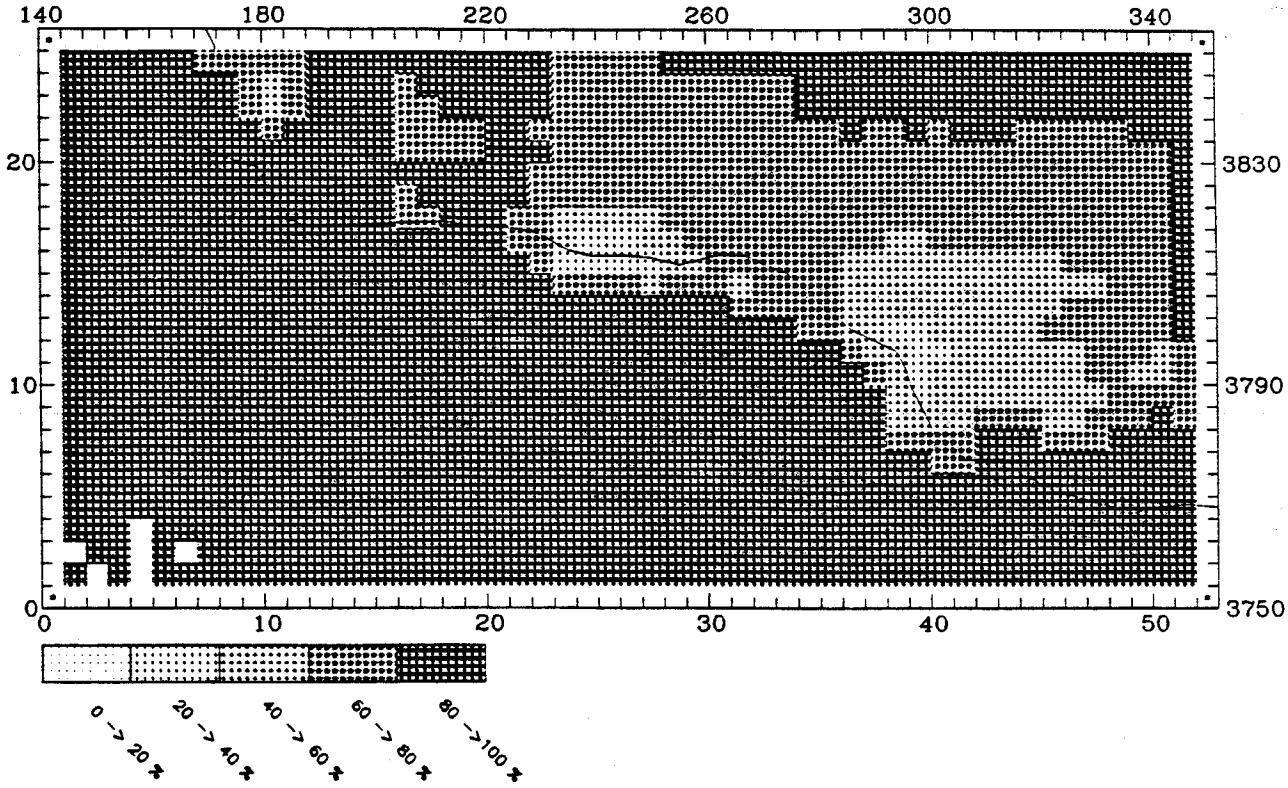

UAM-IV

BNDRY RHC CONTRIBUTION AT: 2300 September 7 LEVEL 1

MAXIMUM CONTRIBUTION IN CELL (2,5) = 100.00 (%)

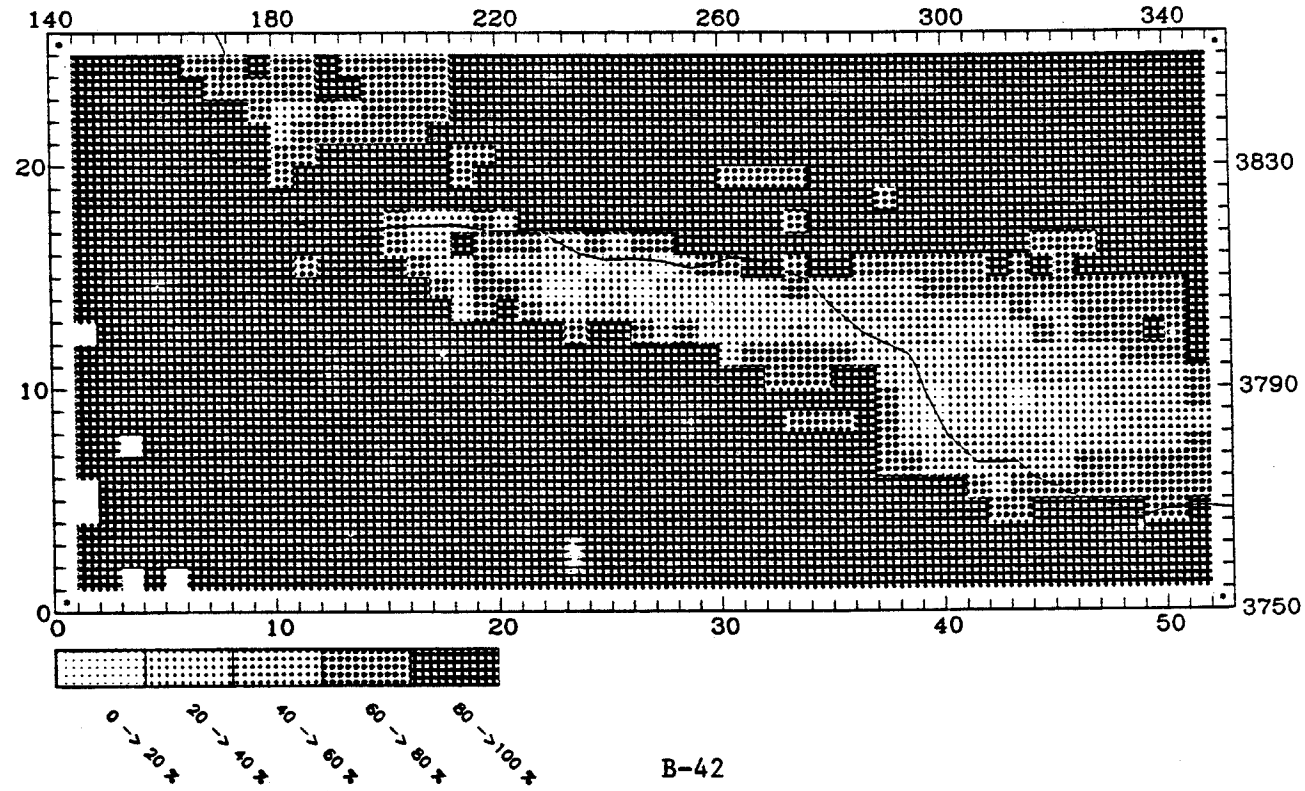

CALGRID–IV

INTNOX CONTRIBUTION AT: 2300 September 7 LEVEL 1

MAXIMUM CONTRIBUTION IN CELL (2,2) = 0.00 (%)

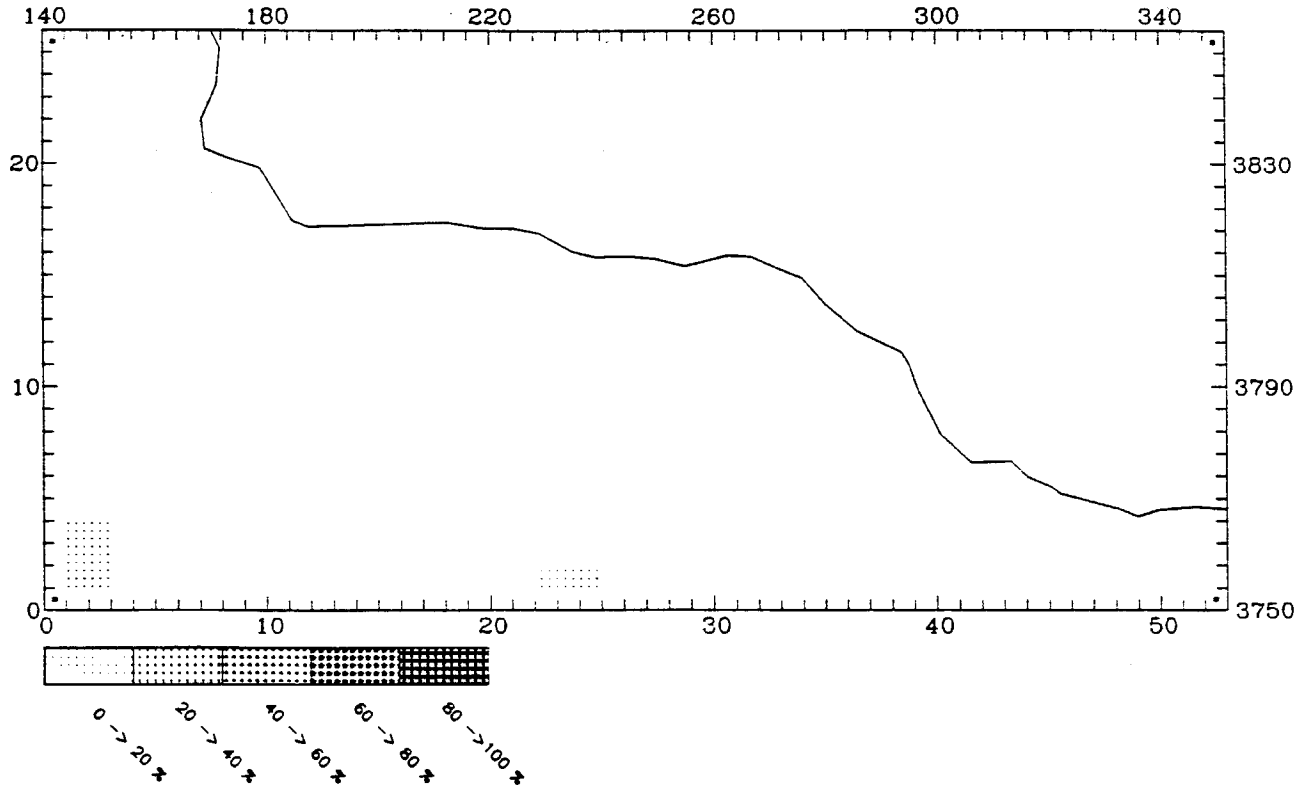

UAM–IV

INTNOX CONTRIBUTION AT: 2300 September 7 LEVEL 1

MAXIMUM CONTRIBUTION IN CELL (36,14) = 0.00 (%)

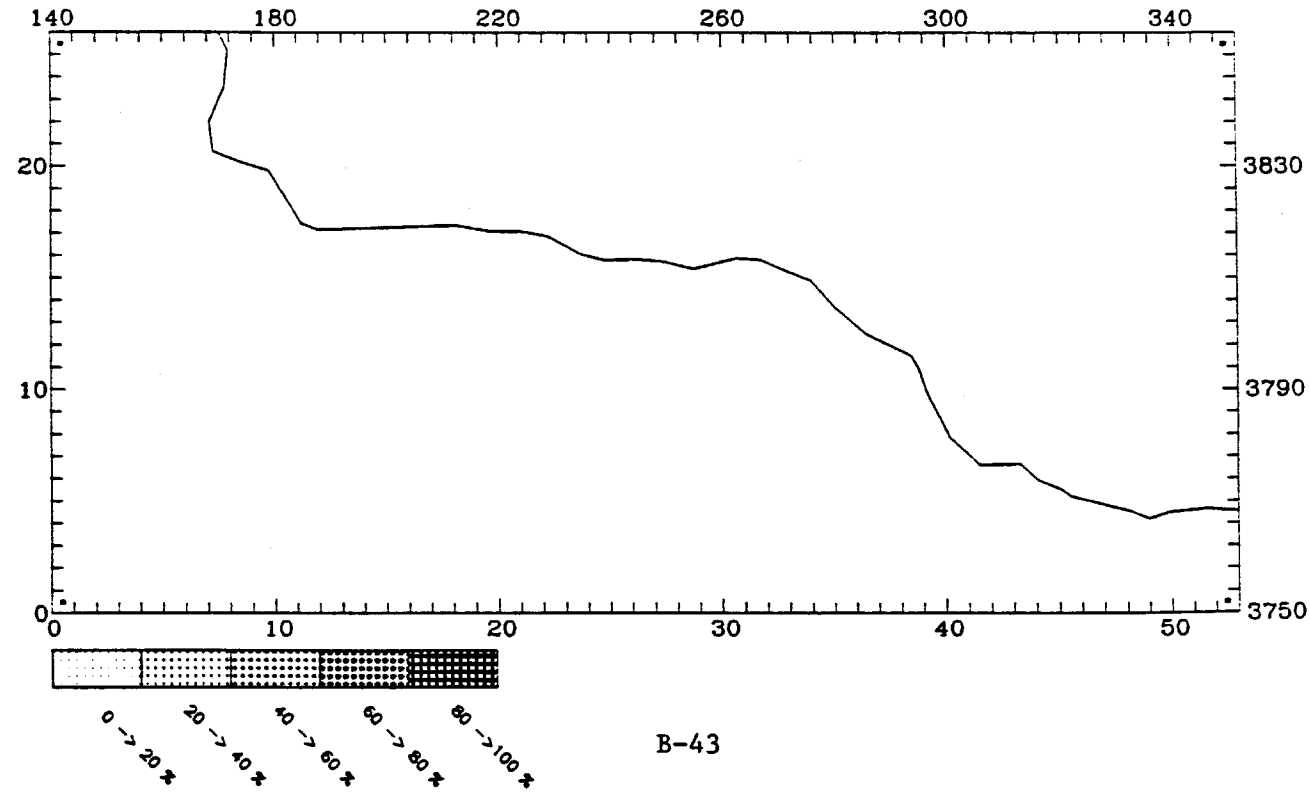

CALGRID–IV

INTHC CONTRIBUTION AT: 2300 September 7 LEVEL 1

MAXIMUM CONTRIBUTION IN CELL (51,24) = 0.00 (%)

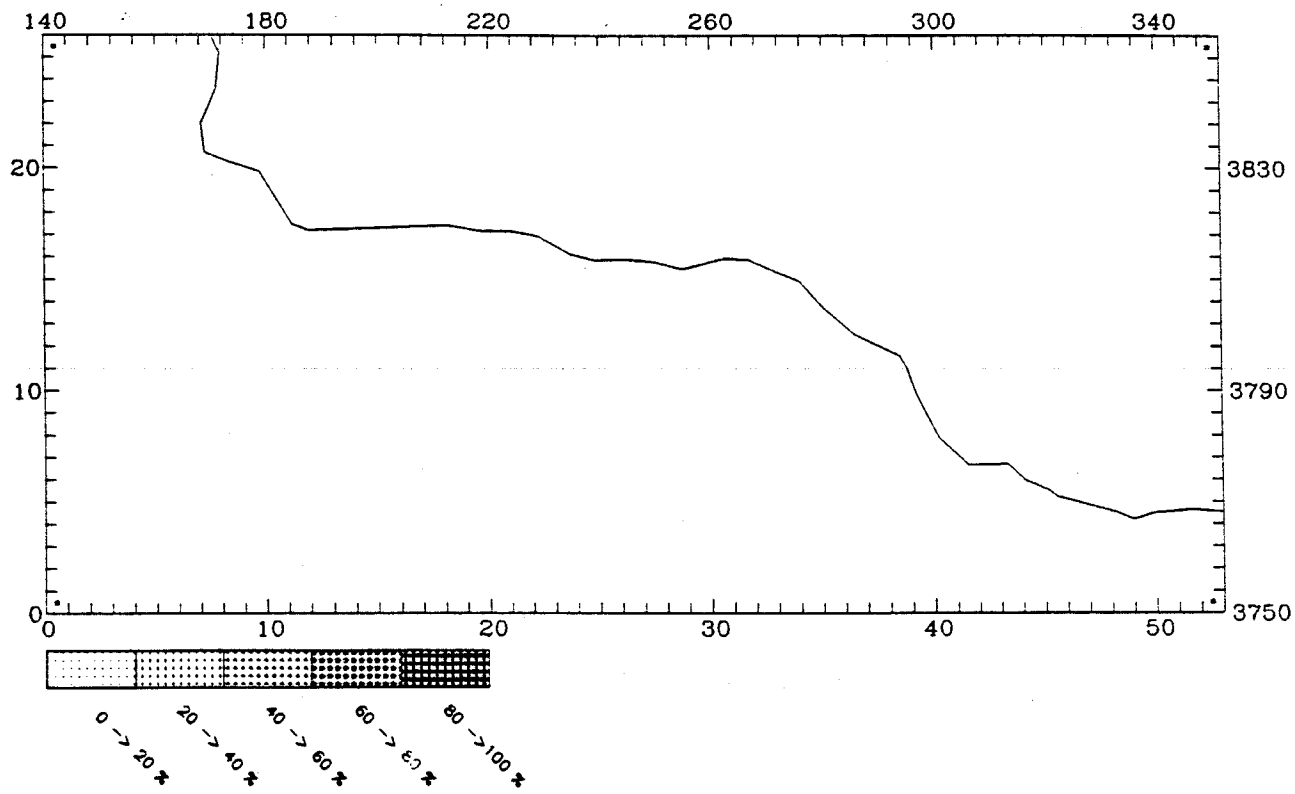

UAM–IV

INTHC CONTRIBUTION AT: 2300 September 7 LEVEL 1

MAXIMUM CONTRIBUTION IN CELL (38,14) = 0.00 (%)

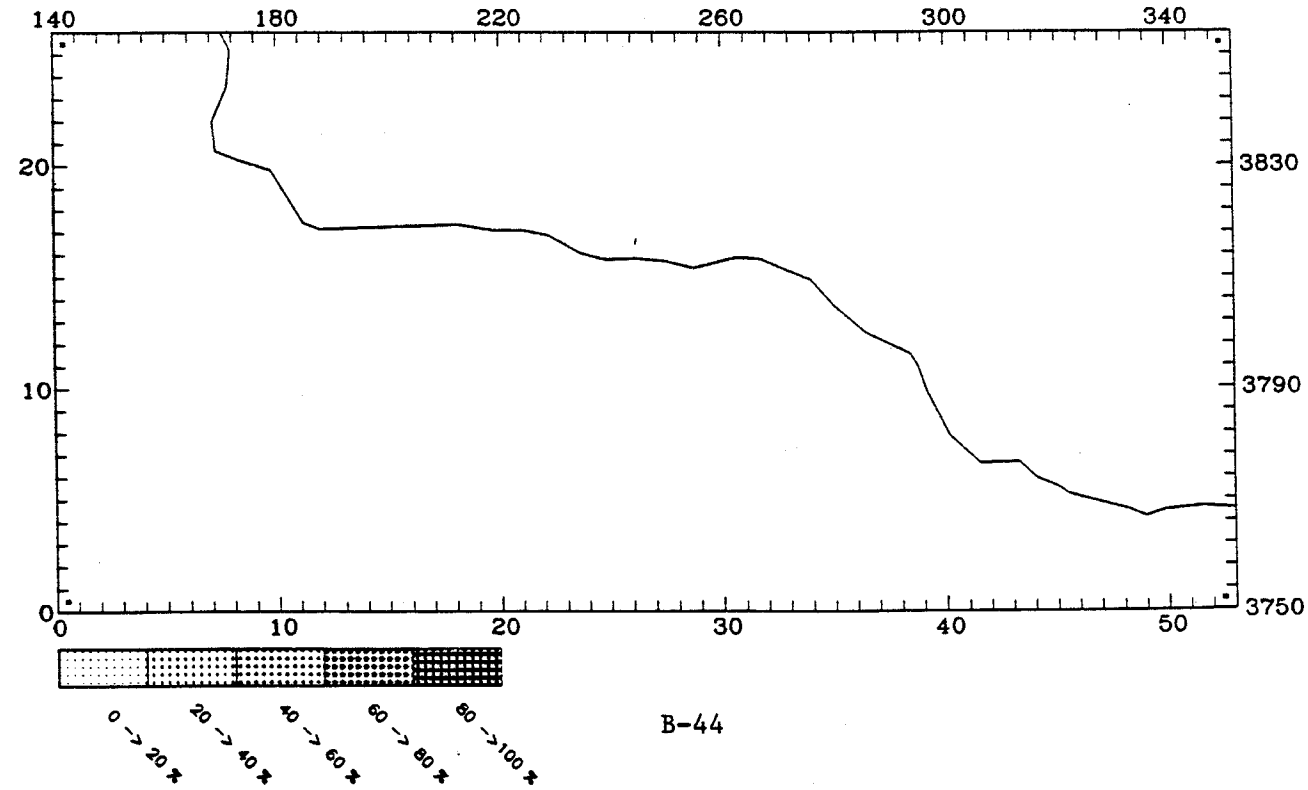

CALGRID–IV

PTARBNOX CONTRIBUTION AT: 2300 September 7 LEVEL 1

MAXIMUM CONTRIBUTION IN CELL (46,2) = 99.95 (%)

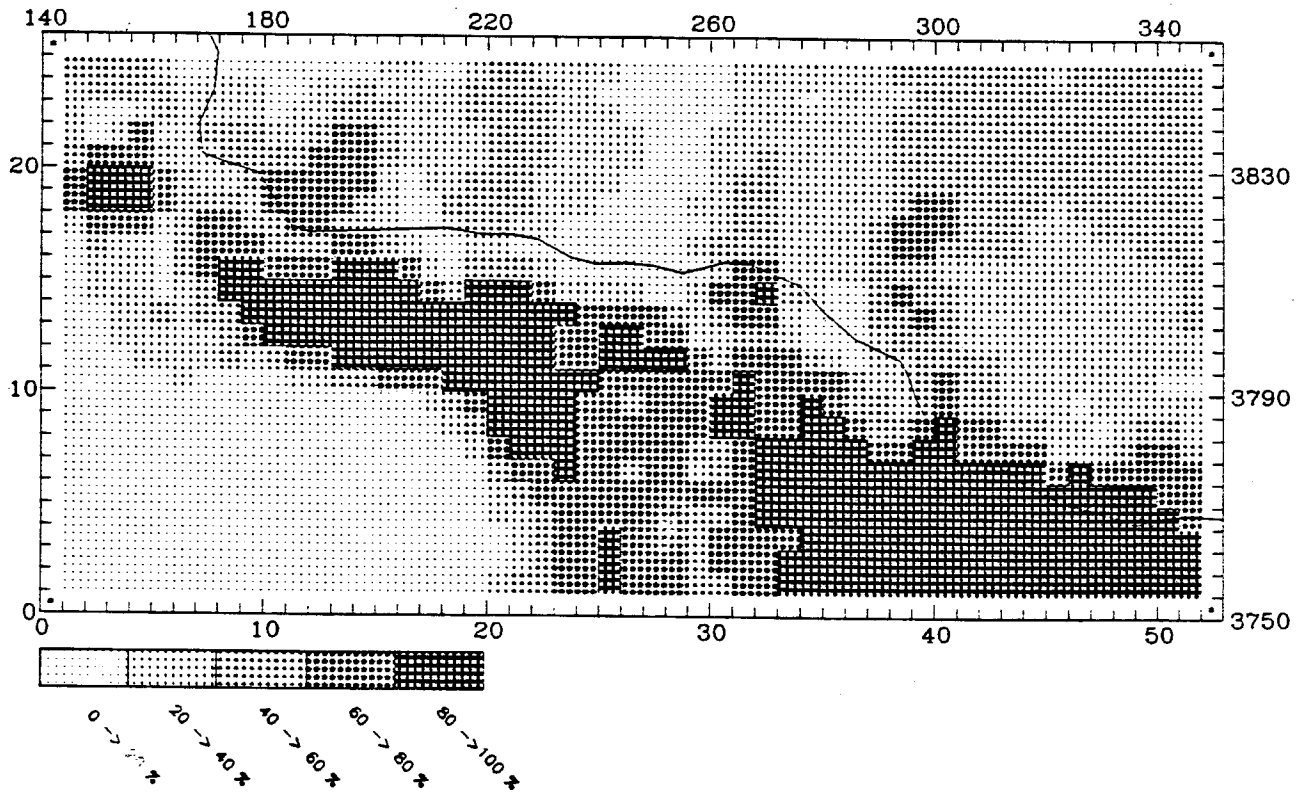

UAM–IV

PTNOX CONTRIBUTION AT: 2300 September 7 LEVEL 1

MAXIMUM CONTRIBUTION IN CELL (11,20) = 44.07 (%)

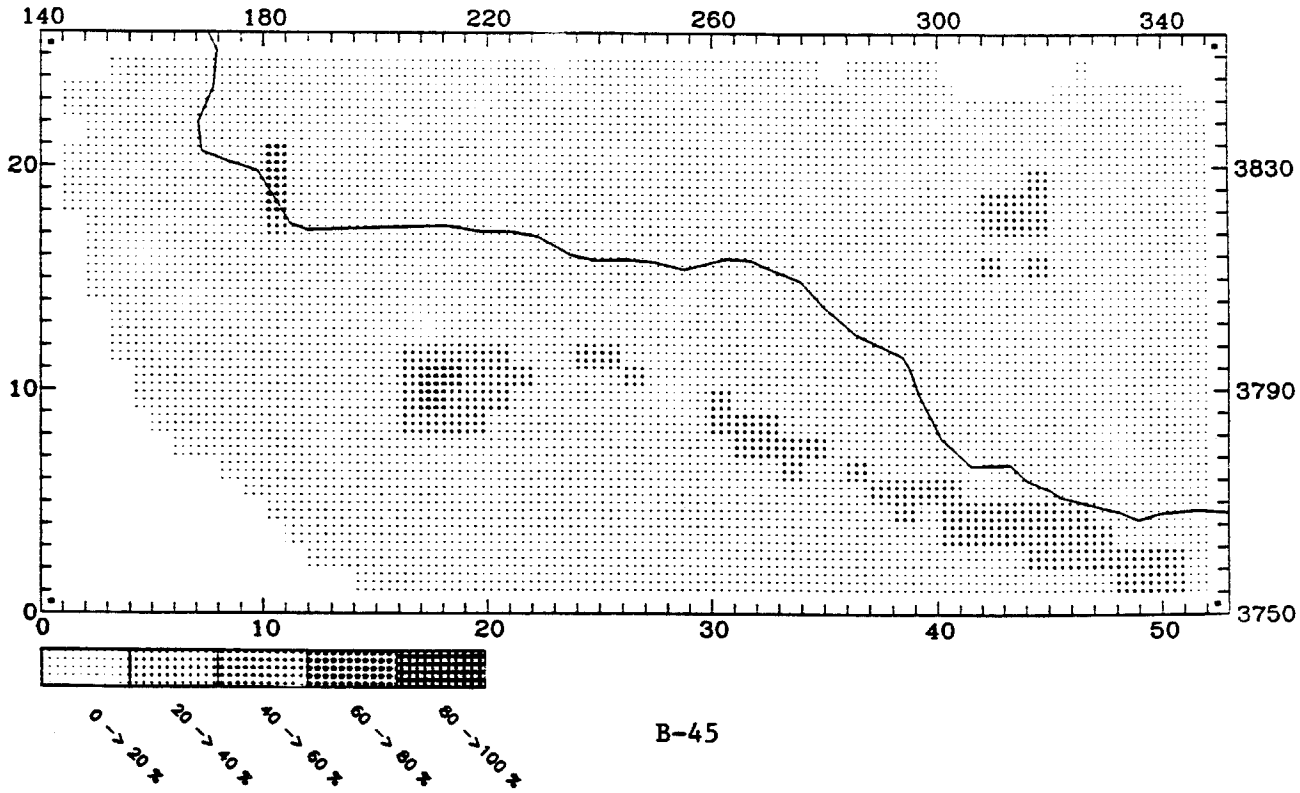

CALGRID–IV

PTARBHC CONTRIBUTION AT: 2300 September 7 LEVEL 1

MAXIMUM CONTRIBUTION IN CELL (44,3) = 5.60 (%)

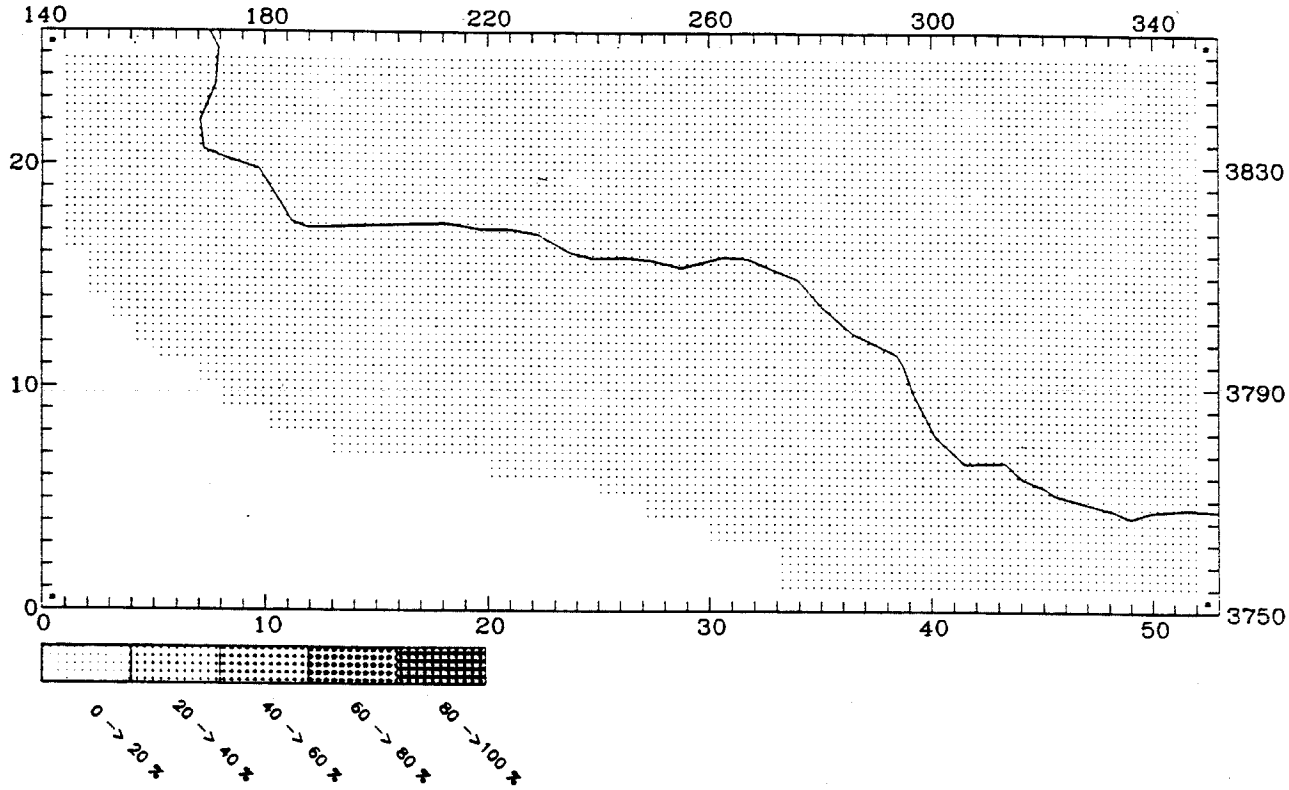

UAM–IV

PTHC CONTRIBUTION AT: 2300 September 7 LEVEL 1

MAXIMUM CONTRIBUTION IN CELL (33,9) = 1.12 (%)

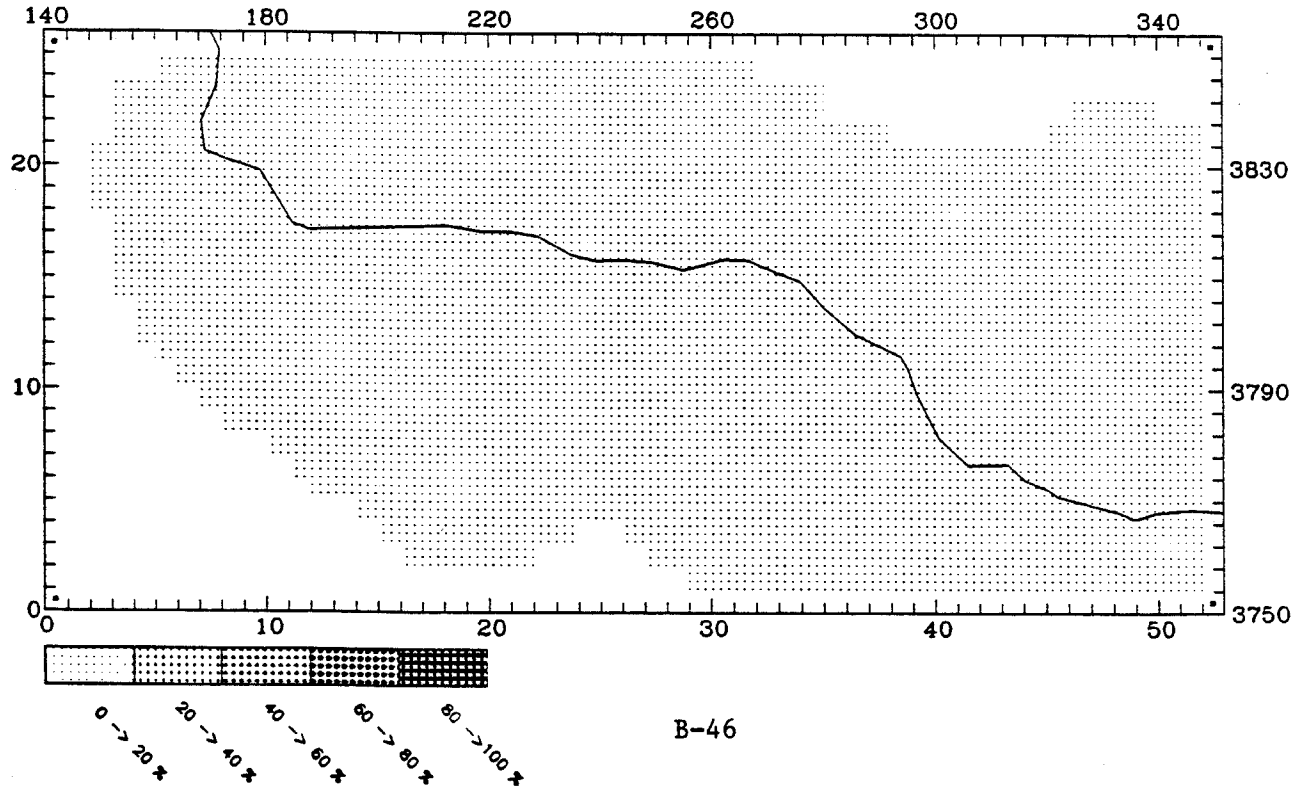

CALGRID–IV

ANOX CONTRIBUTION AT: 2300 September 7 LEVEL 1

MAXIMUM CONTRIBUTION IN CELL (11,9) = 99.88 (%)

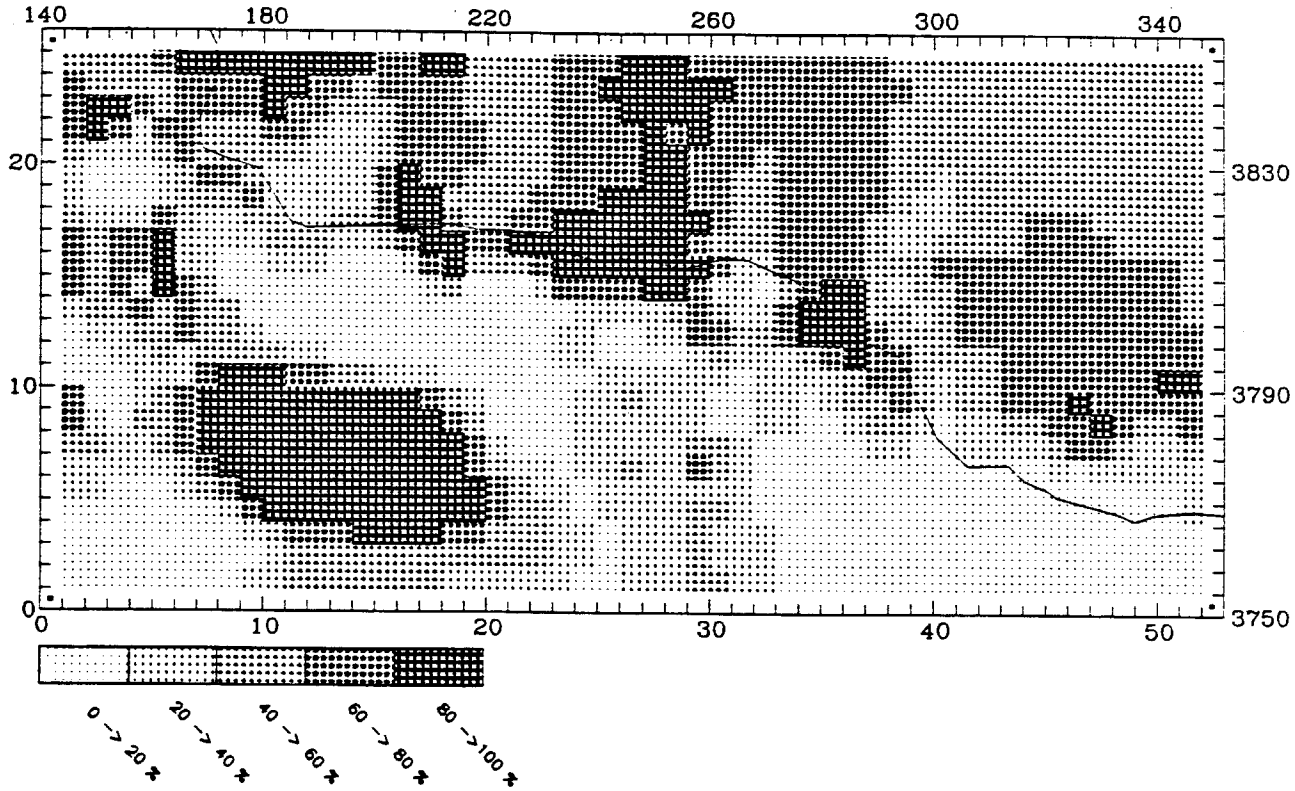

UAM–IV

NOX CONTRIBUTION AT: 2300 September 7 LEVEL 1

MAXIMUM CONTRIBUTION IN CELL (37,13) = 98.42 (%)

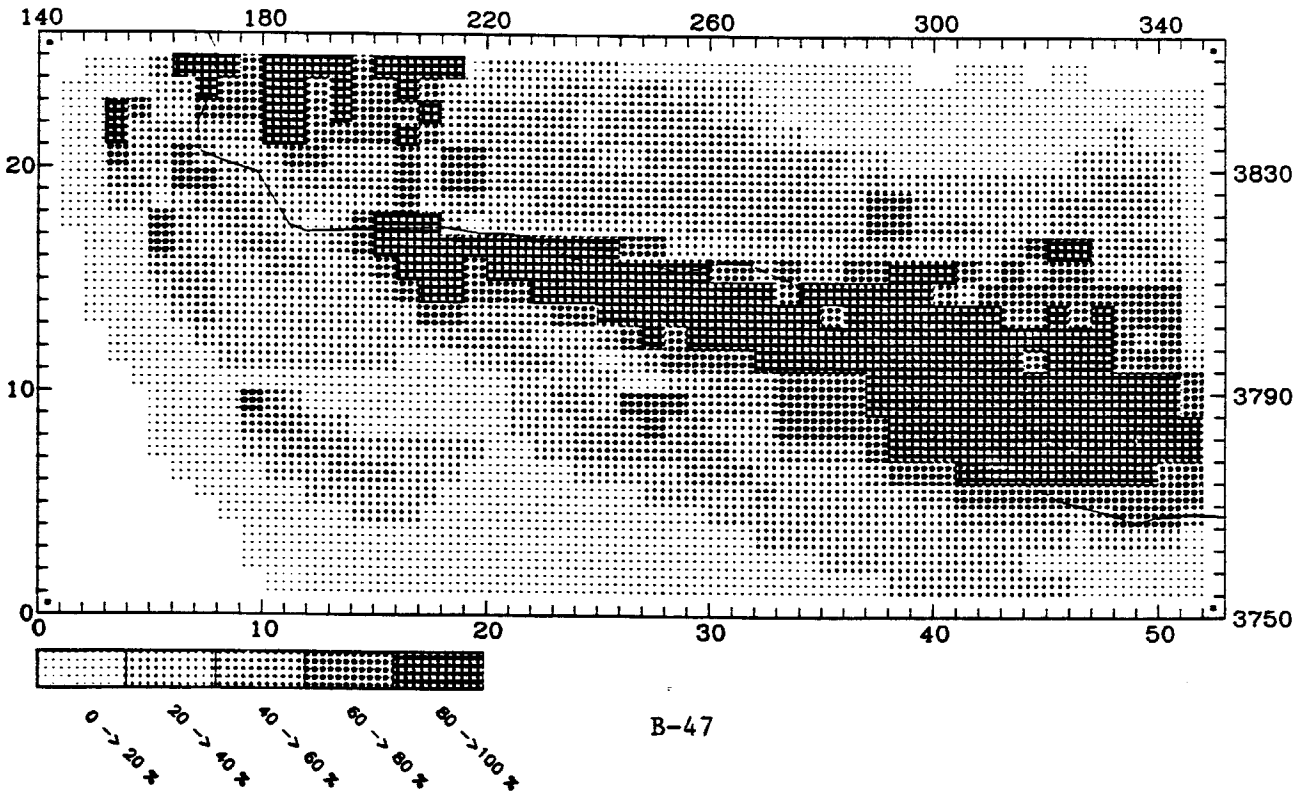

CALGRID–IV

ATHC CONTRIBUTION AT: 2300 September 7 LEVEL 1

MAXIMUM CONTRIBUTION IN CELL (28,16) = 75.10 (%)

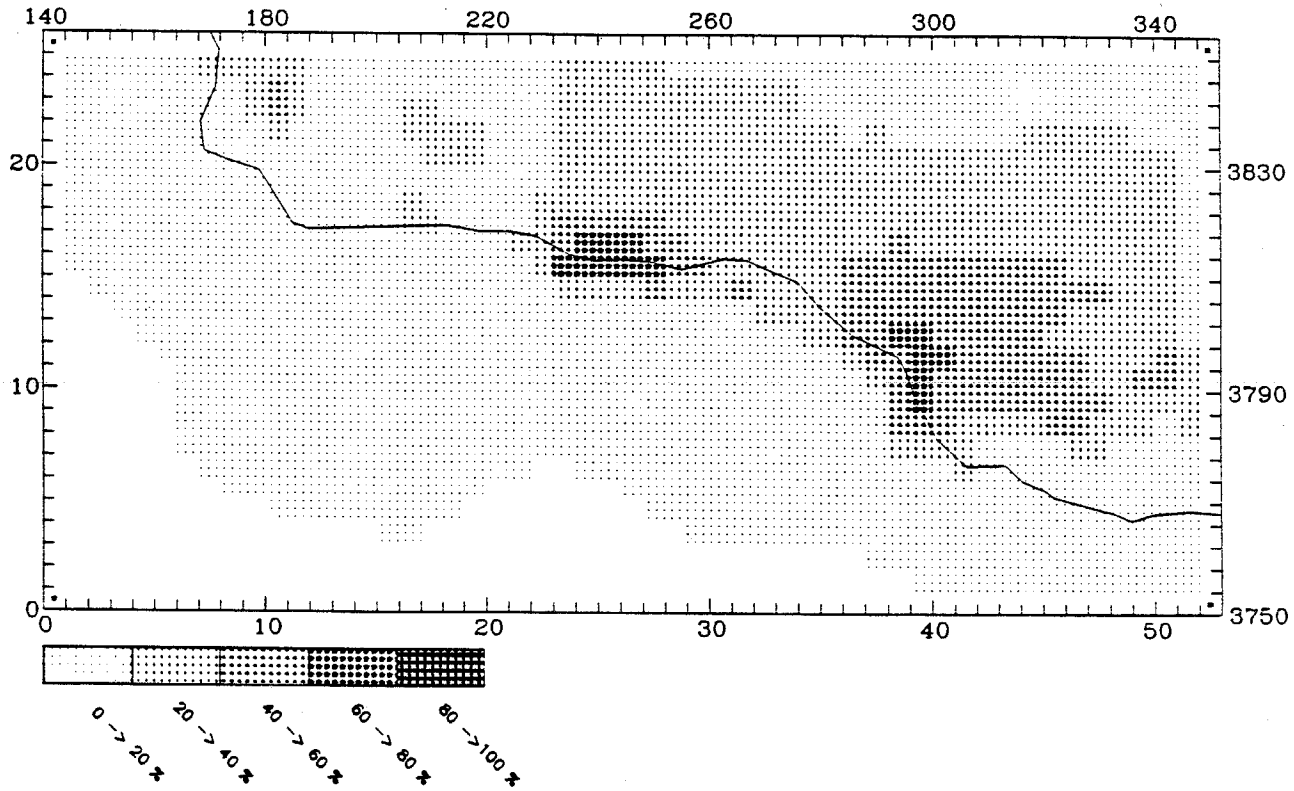

UAM–IV

RHC CONTRIBUTION AT: 2300 September 7 LEVEL 1

MAXIMUM CONTRIBUTION IN CELL (24,15) = 93.97 (%)

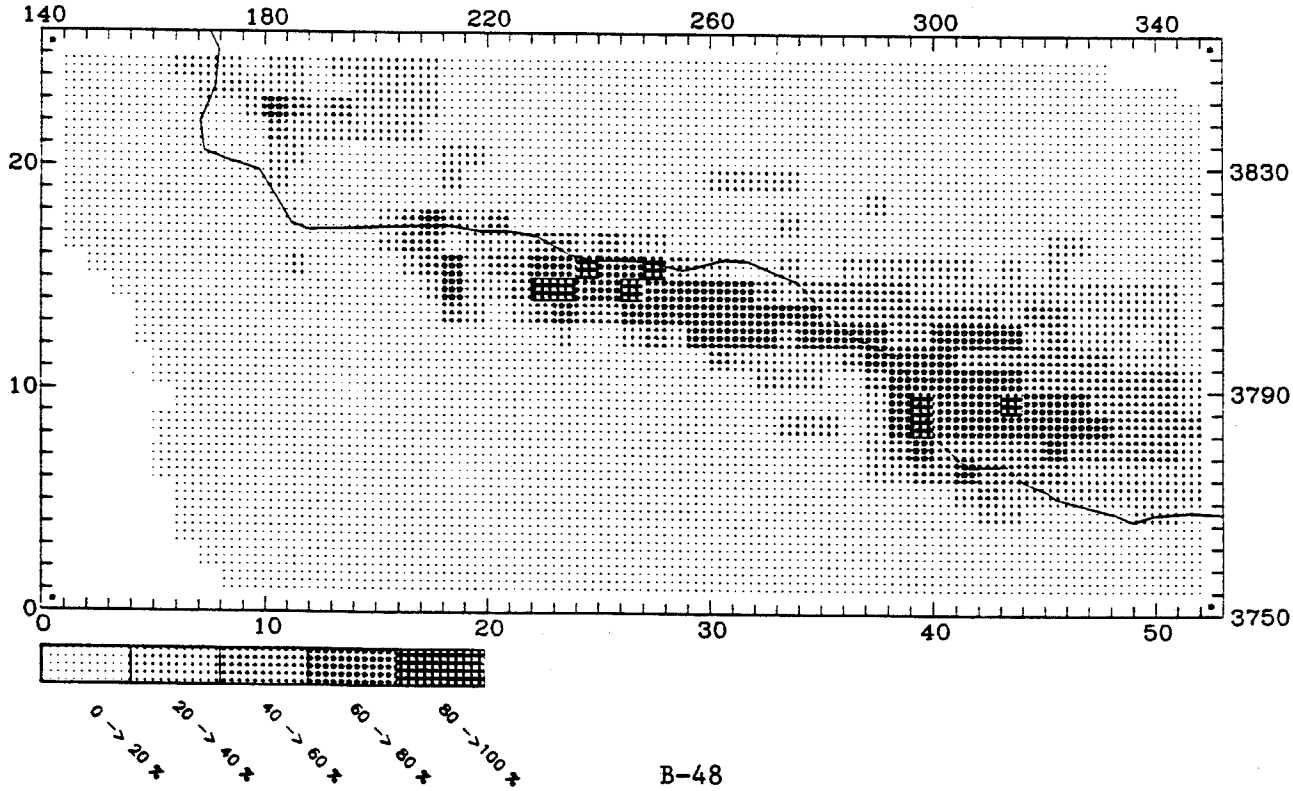

Appendix C

CALGRID AND UAM-IV WEIGHTED-TRACER SIMULATION RESULTS FOR 16-17 SEPTEMBER 1984

CALGRID–IV

BNDRY NOX CONTRIBUTION AT: 1100 September 16 LEVEL 1

MAXIMUM CONTRIBUTION IN CELL (3,2) = 71.23 (%)

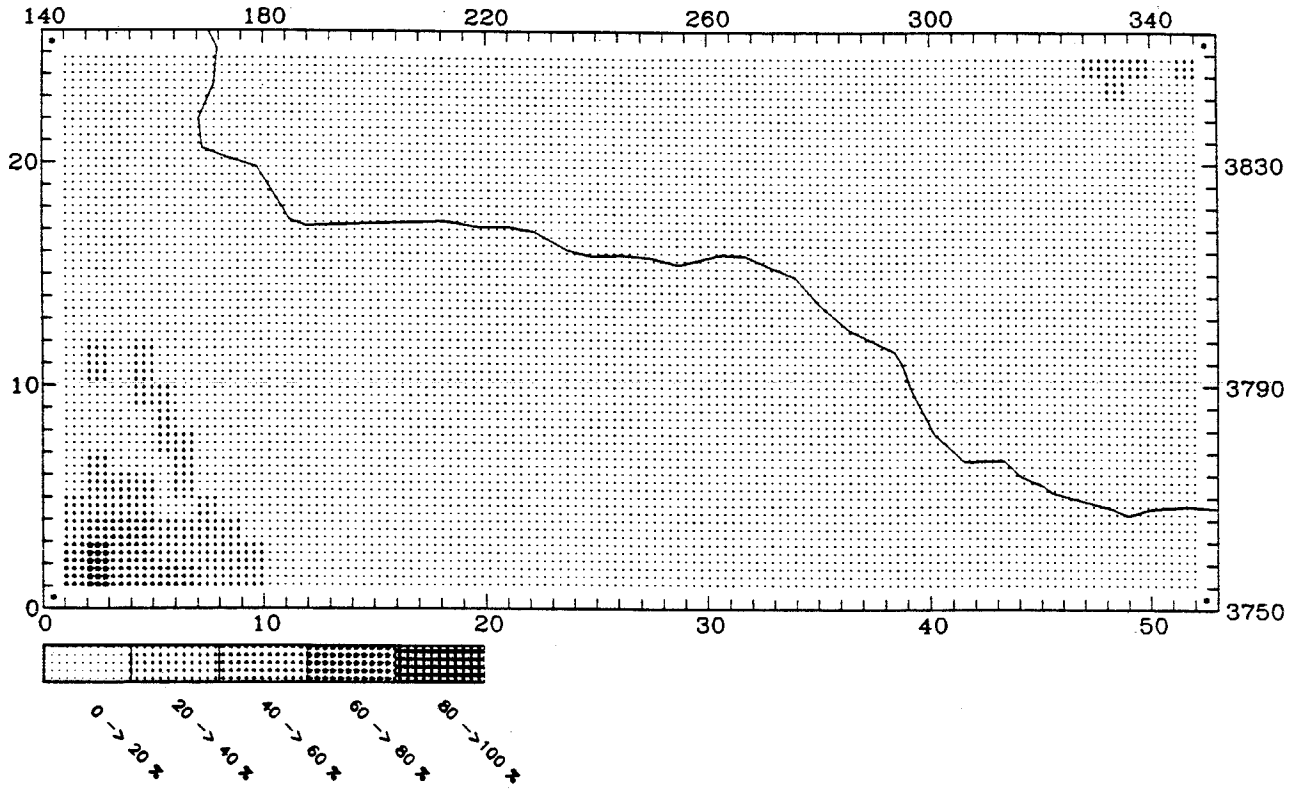

UAM–IV

BNDRY NOX CONTRIBUTION AT: 1100 September 16 LEVEL 1

MAXIMUM CONTRIBUTION IN CELL (2,4) = 100.00 (%)

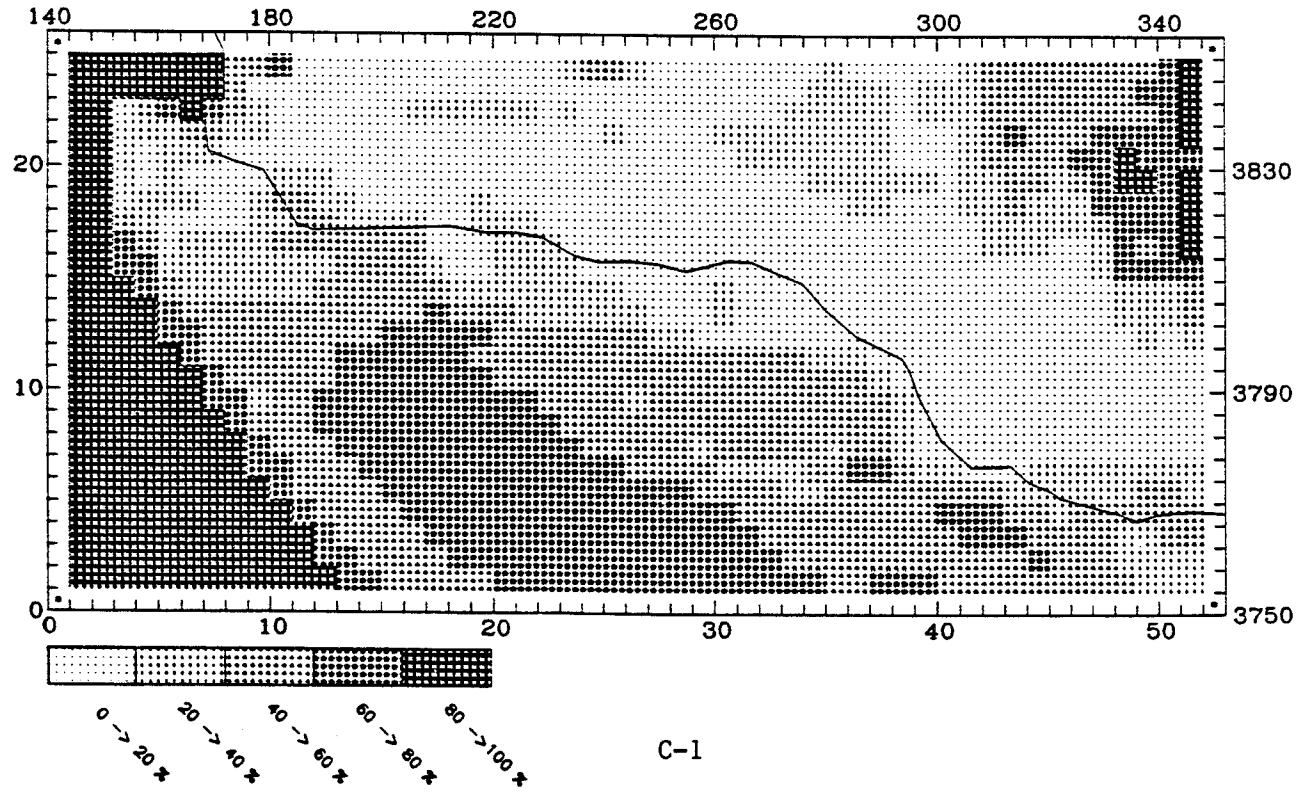

CALGRID–IV

BNDRY RHC CONTRIBUTION AT: 1100 September 16 LEVEL 1

MAXIMUM CONTRIBUTION IN CELL (2,5) = 100.00 (%)

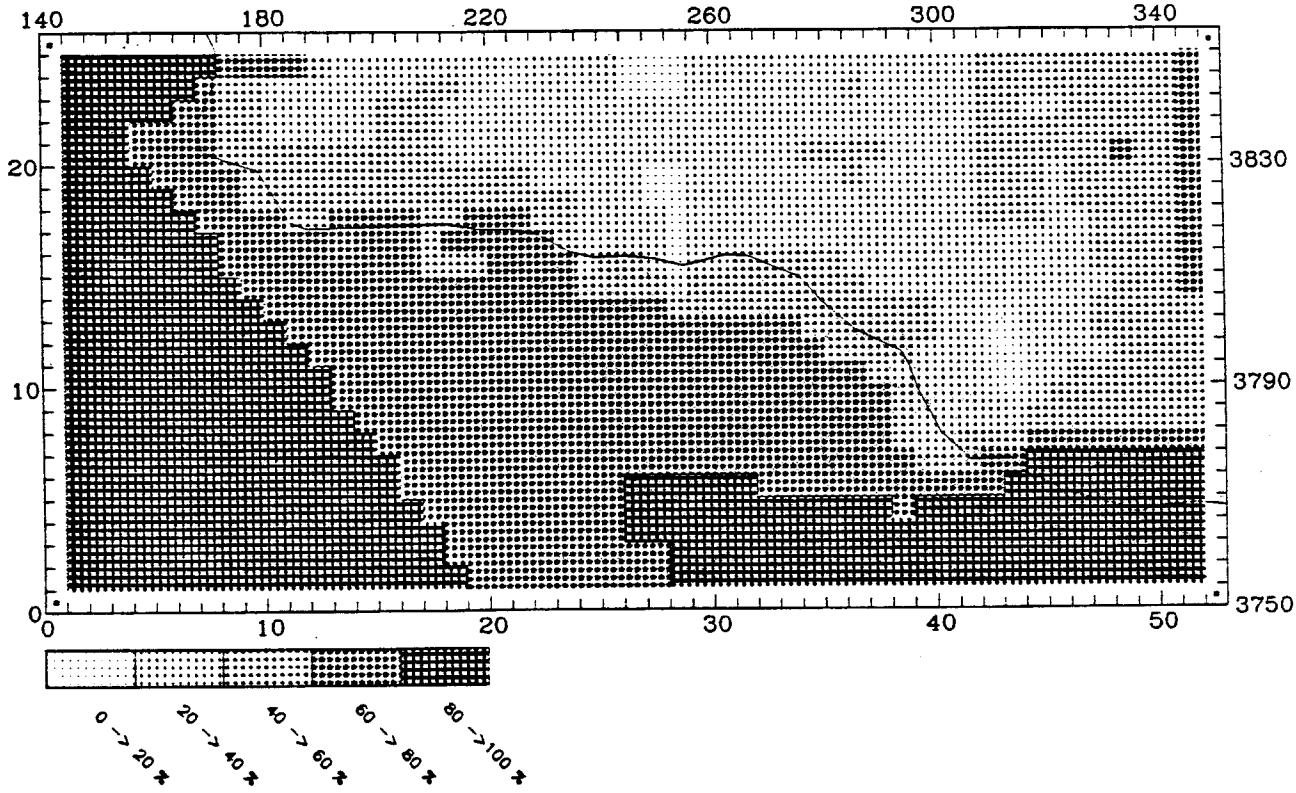

UAM–IV

BNDRY RHC CONTRIBUTION AT: 1100 September 16 LEVEL 1

MAXIMUM CONTRIBUTION IN CELL (2,4) = 100.00 (%)

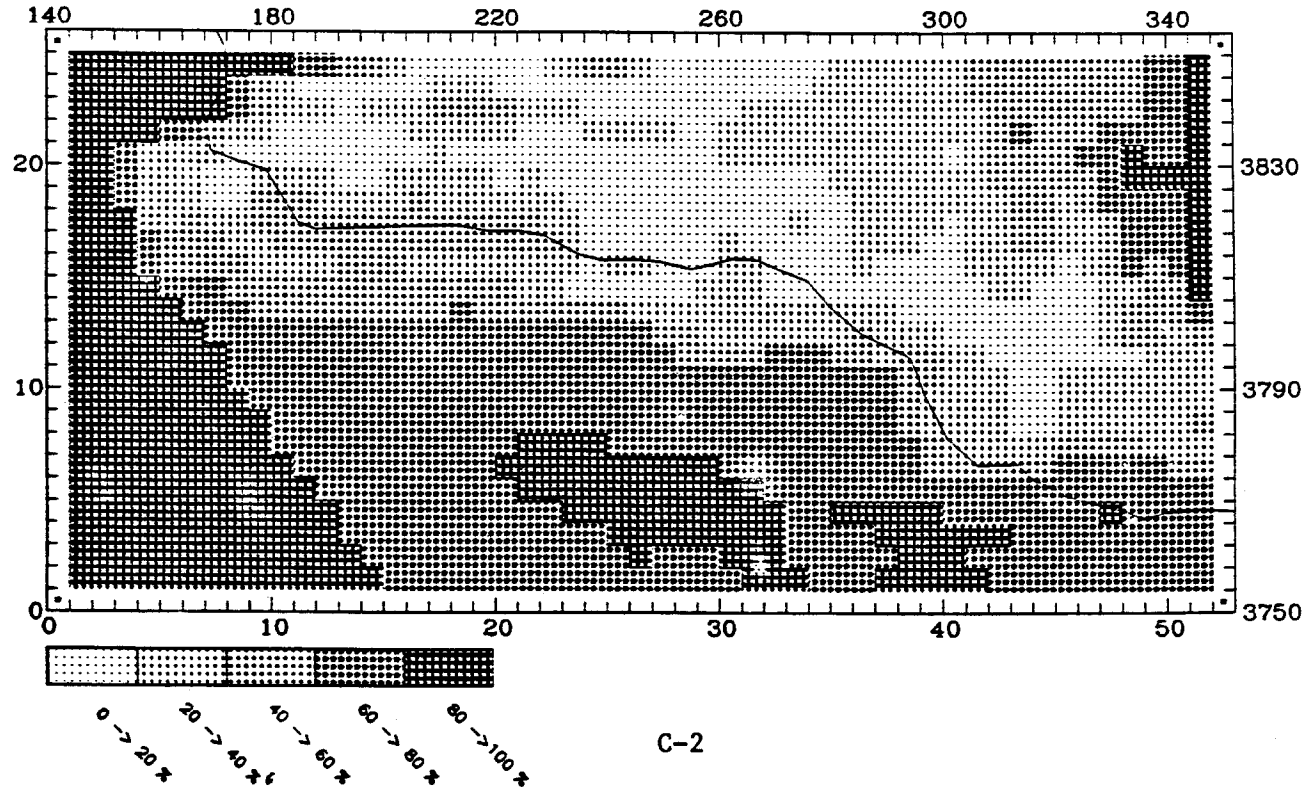

CALGRID–IV

INTNOX CONTRIBUTION AT: 1100 September 16 LEVEL 1

MAXIMUM CONTRIBUTION IN CELL (27,25) = 63.08 (%)

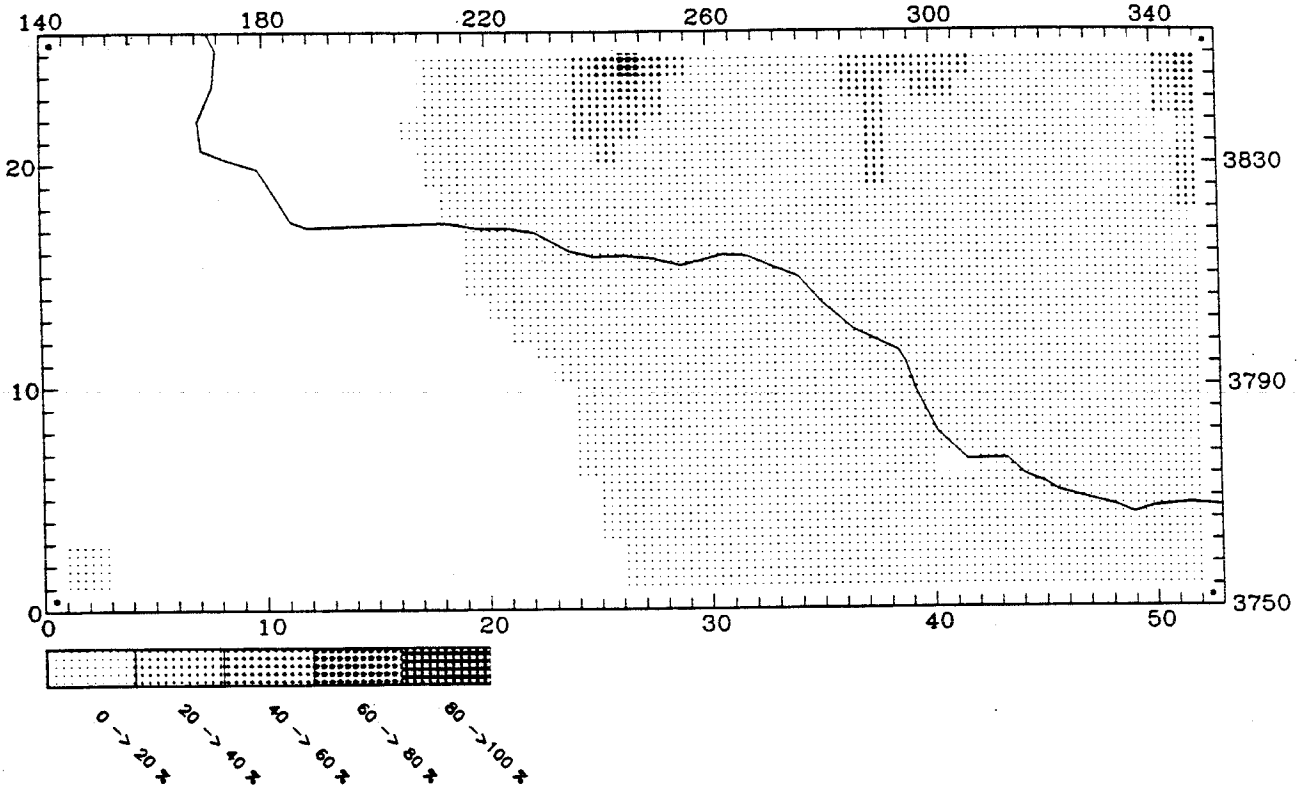

UAM–IV

INTNOX CONTRIBUTION AT: 1100 September 16 LEVEL 1

MAXIMUM CONTRIBUTION IN CELL (29,24) = 93.84 (%)

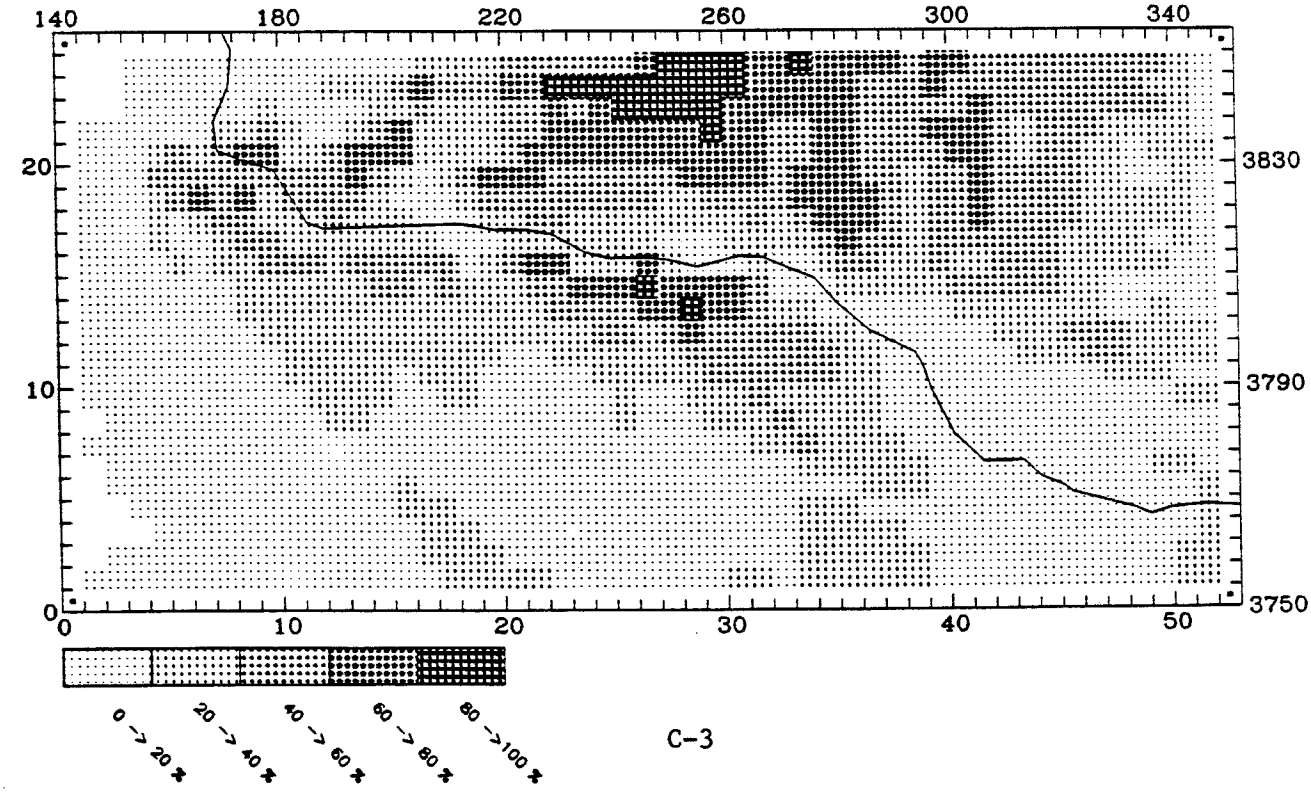

INTHC CONTRIBUTION AT: 1100 September 16 LEVEL 1

MAXIMUM CONTRIBUTION IN CELL (27,25) = 71.44 (%)

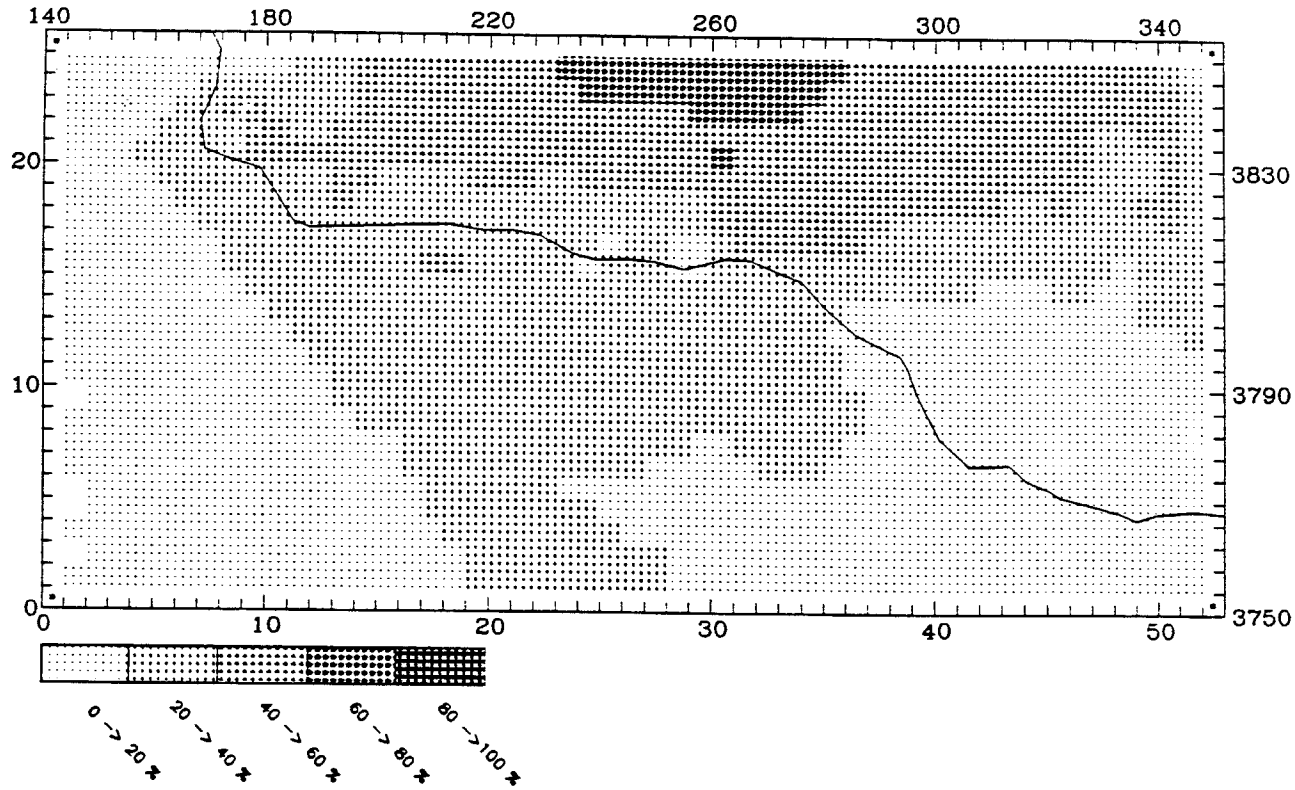

UAM-IV

INTHC CONTRIBUTION AT: 1100 September 16 LEVEL 1

MAXIMUM CONTRIBUTION IN CELL (29,24) = 90.92 (%)

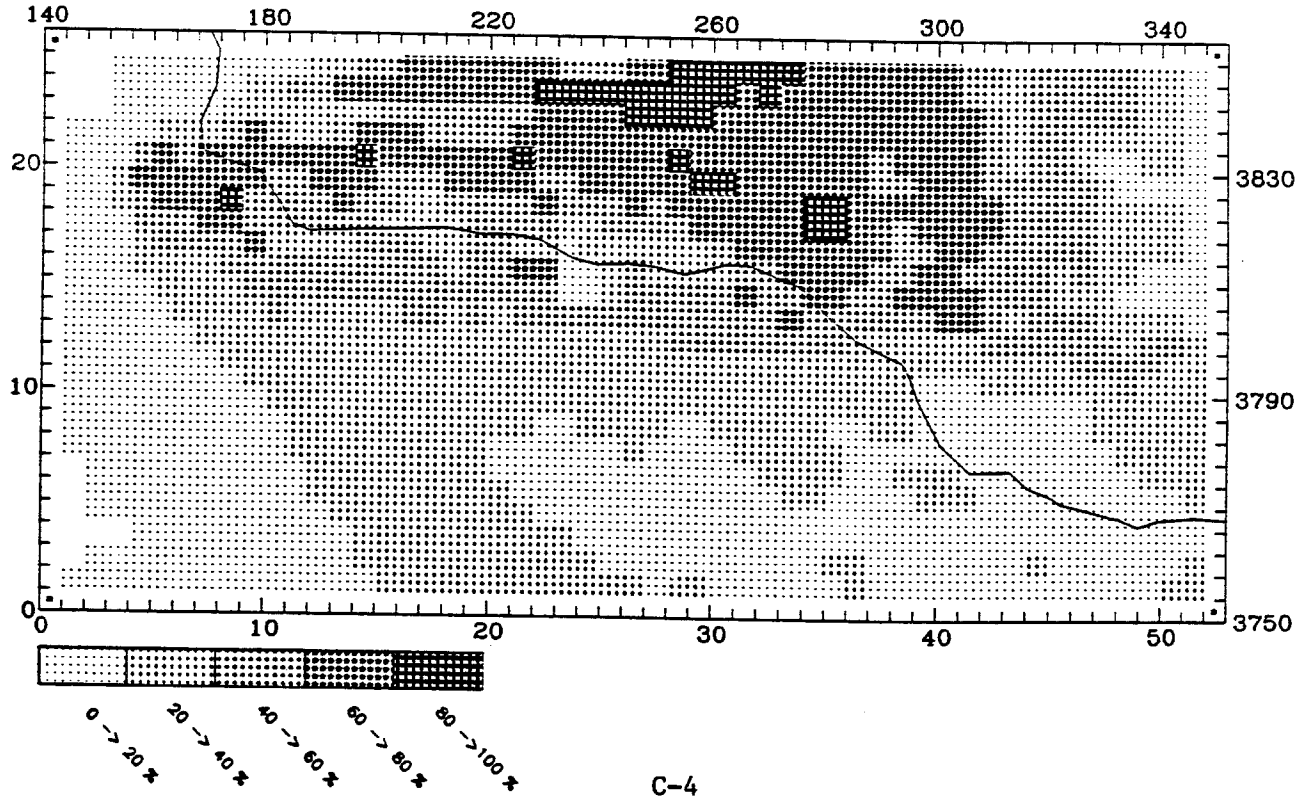

PTARBNOX CONTRIBUTION AT: 1100 September 16 LEVEL 1

MAXIMUM CONTRIBUTION IN CELL (2,16) = 98.80 (%)

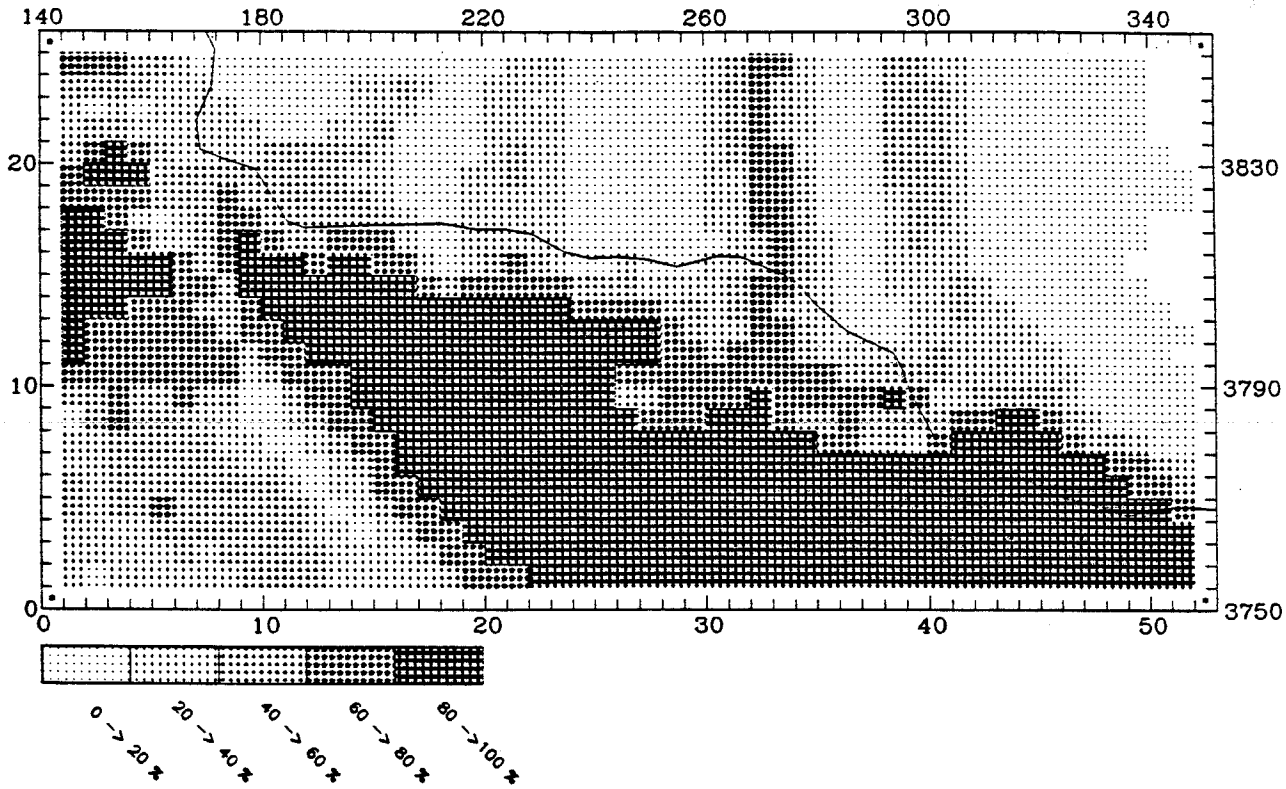

UAM-IV

PTNOX CONTRIBUTION AT: 1100 September 16 LEVEL 1

MAXIMUM CONTRIBUTION IN CELL (33,7) = 50.11 (%)

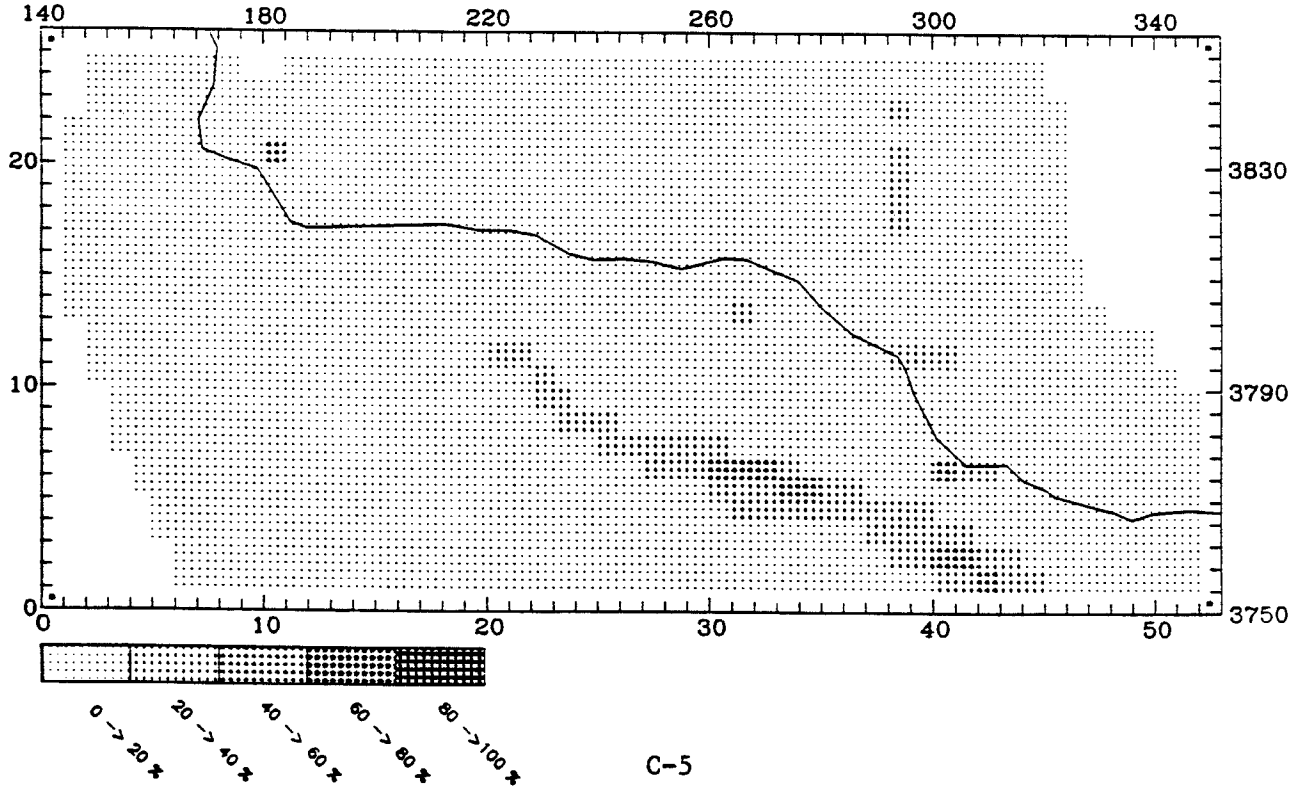

PTARBHC CONTRIBUTION AT: 1100 September 16 LEVEL 1

MAXIMUM CONTRIBUTION IN CELL (33,7) = 5.61 (%)

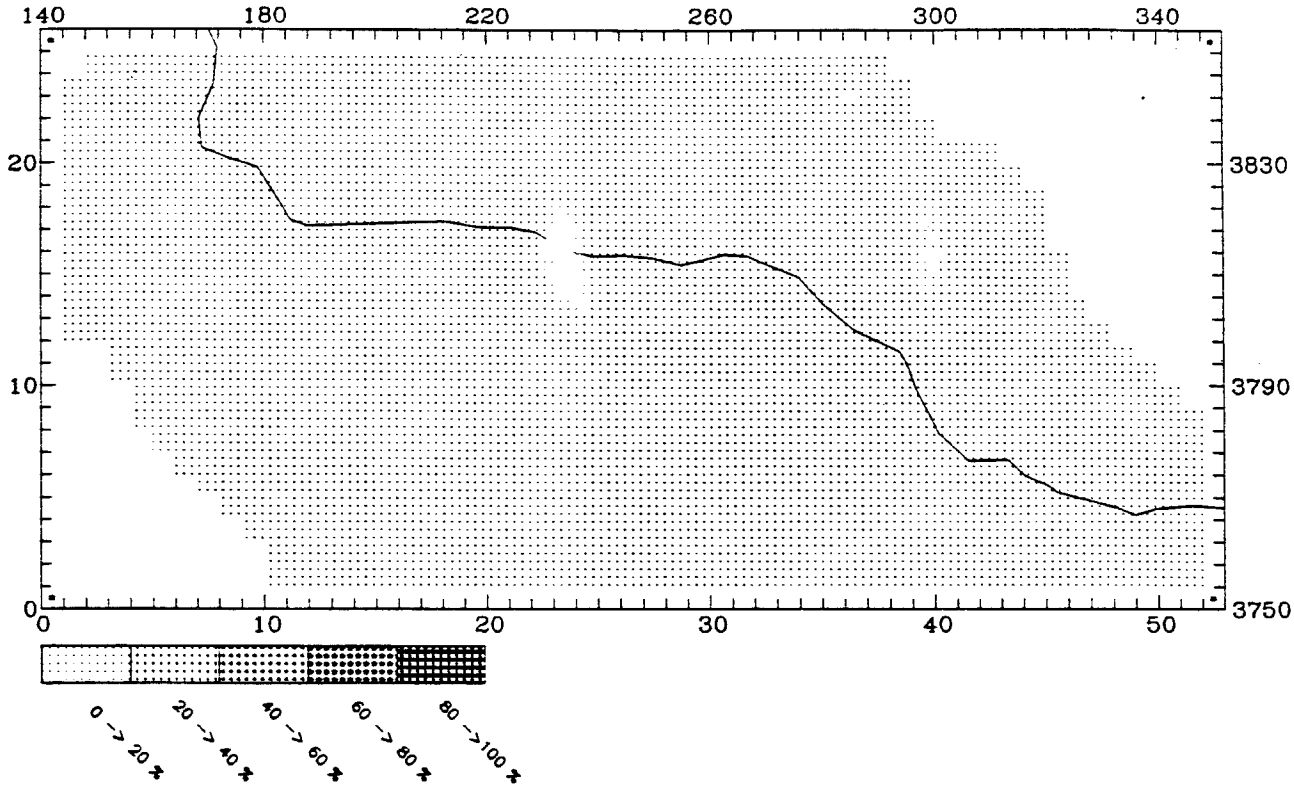

UAM-IV

PTHC CONTRIBUTION AT: 1100 September 16 LEVEL 1

MAXIMUM CONTRIBUTION IN CELL (33,7) = 2.86 (%)

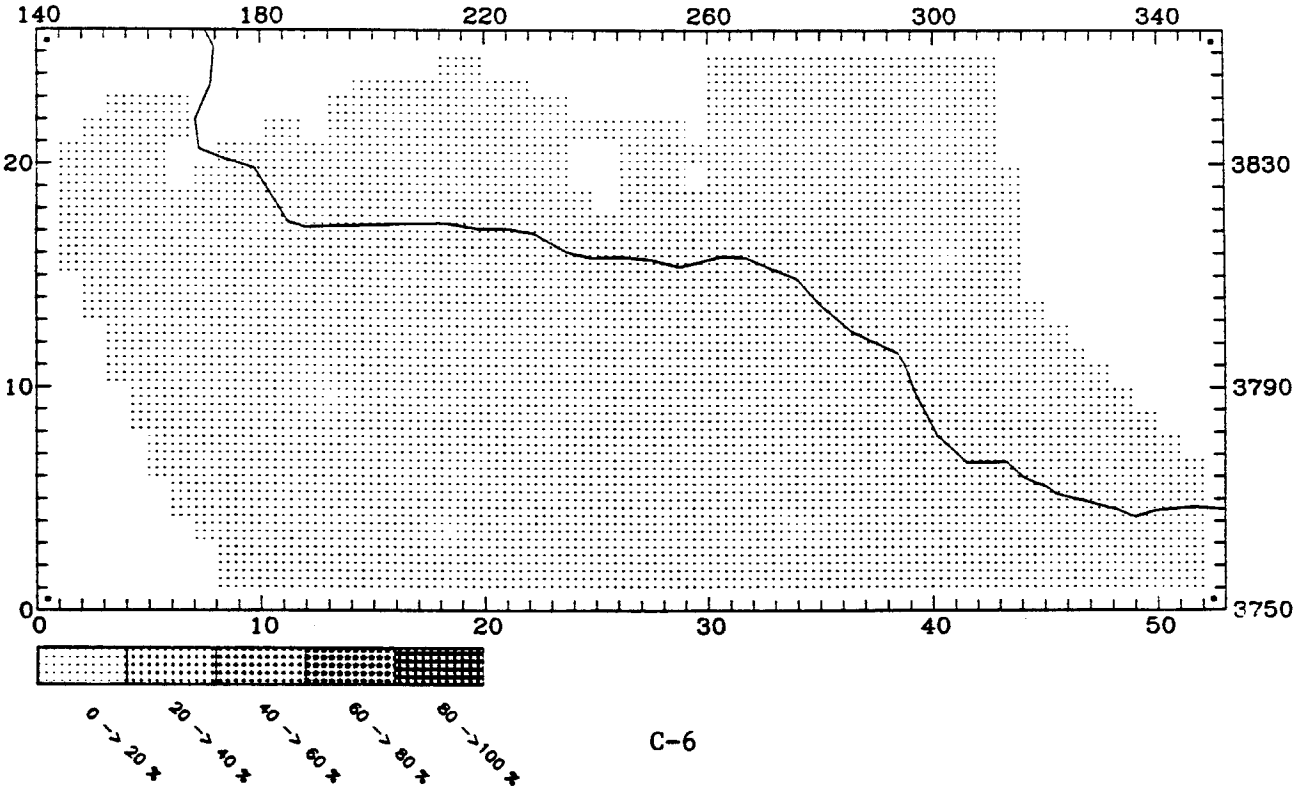

CALGRID–IV

ANOX CONTRIBUTION AT: 1100 September 16 LEVEL 1

MAXIMUM CONTRIBUTION IN CELL (51,11) = 99.65 (%)

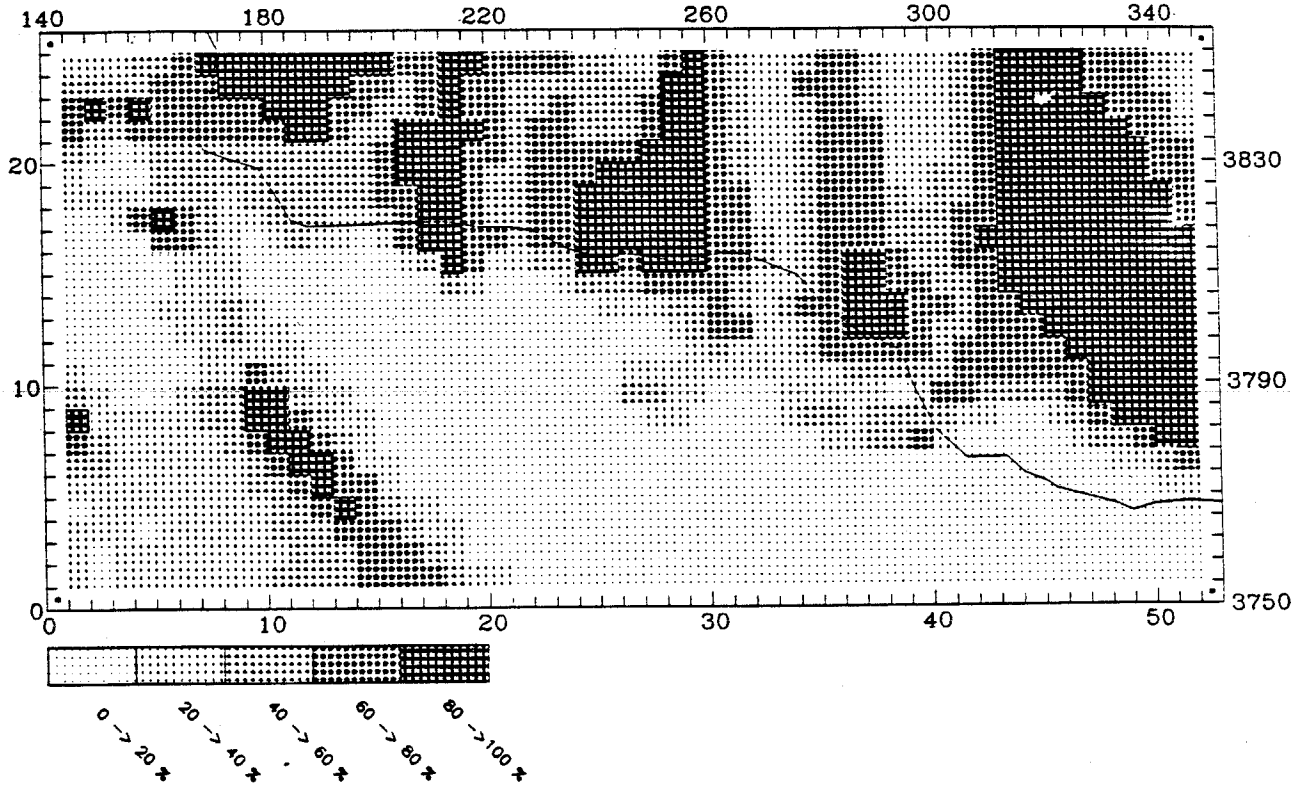

UAM–IV

NOX CONTRIBUTION AT: 1100 September 16 LEVEL 1

MAXIMUM CONTRIBUTION IN CELL (45,10) = 87.44 (%)

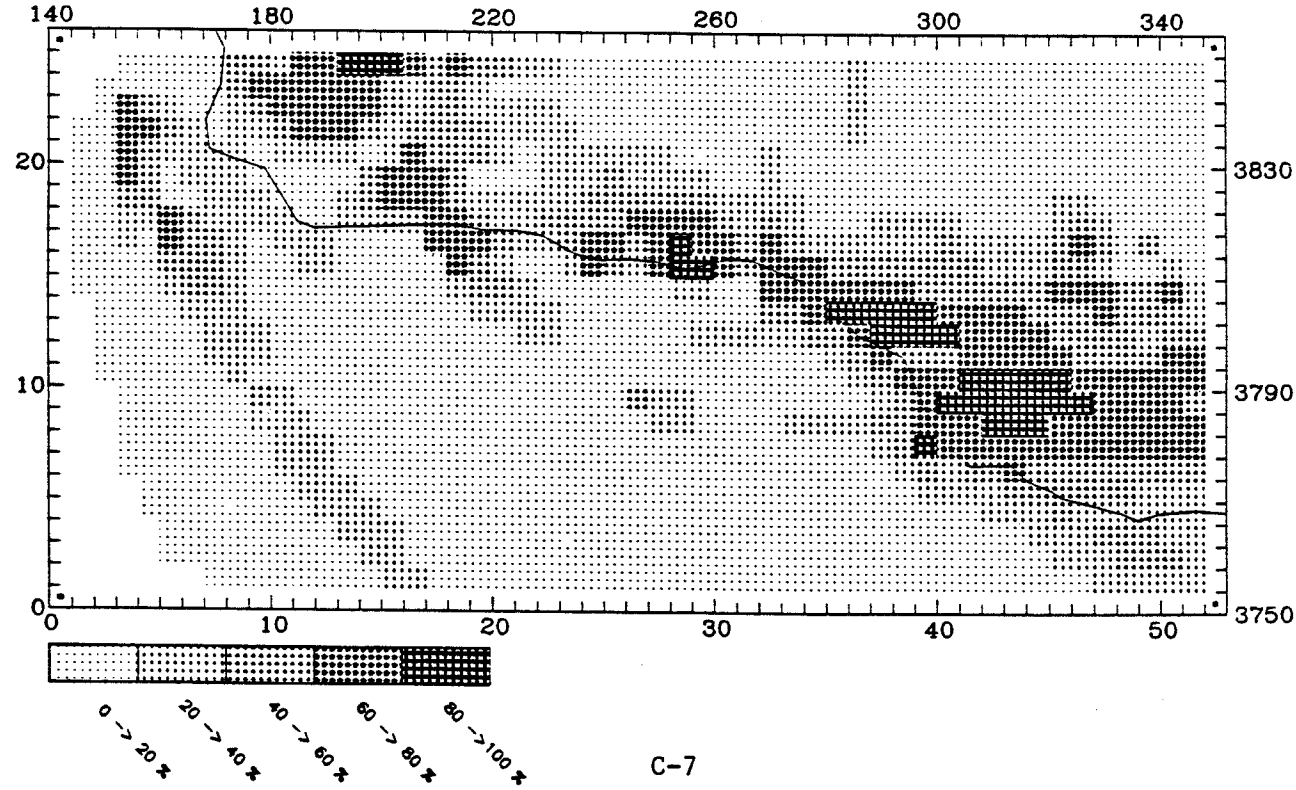

CALGRID–IV

ATHC CONTRIBUTION AT: 1100 September 16 LEVEL 1

MAXIMUM CONTRIBUTION IN CELL (44,11) = 75.23 (%)

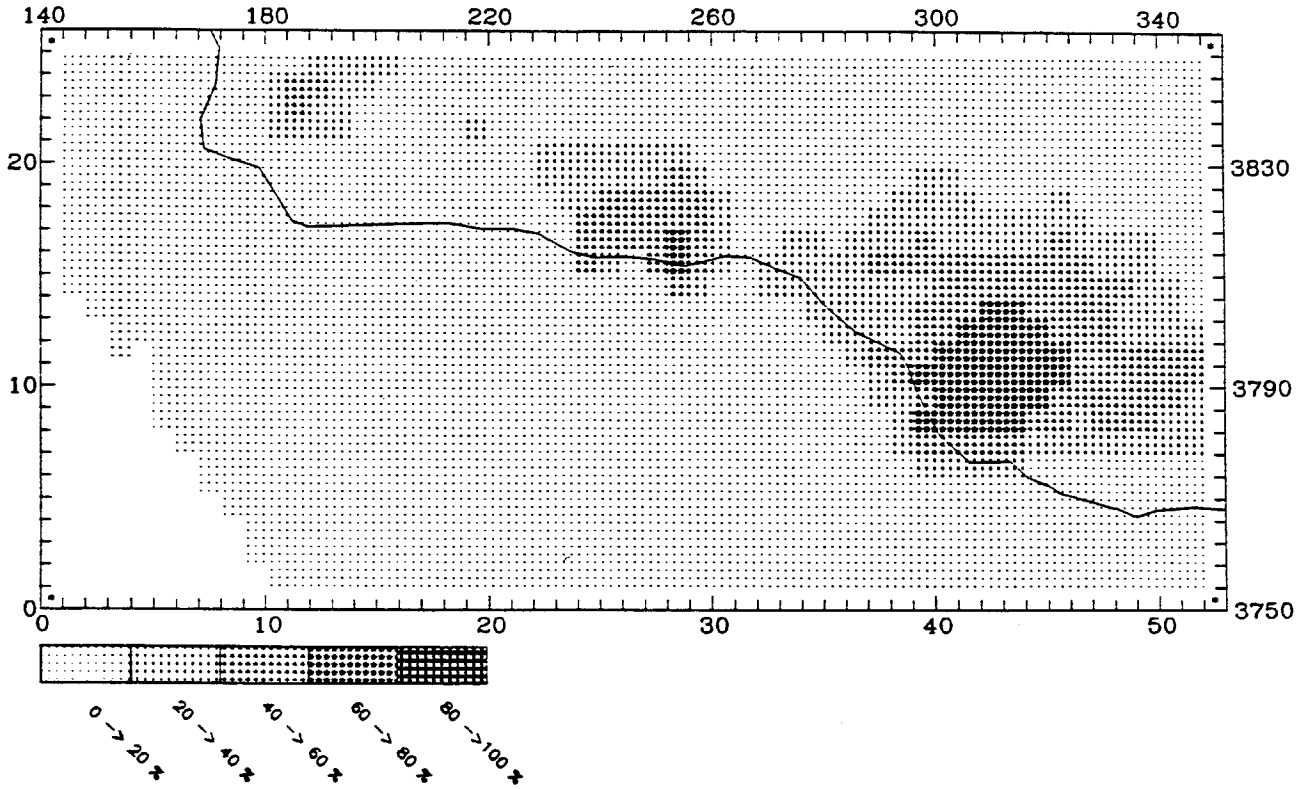

UAM–IV

RHC CONTRIBUTION AT: 1100 September 16 LEVEL 1

MAXIMUM CONTRIBUTION IN CELL (24,15) = 74.16 (%)

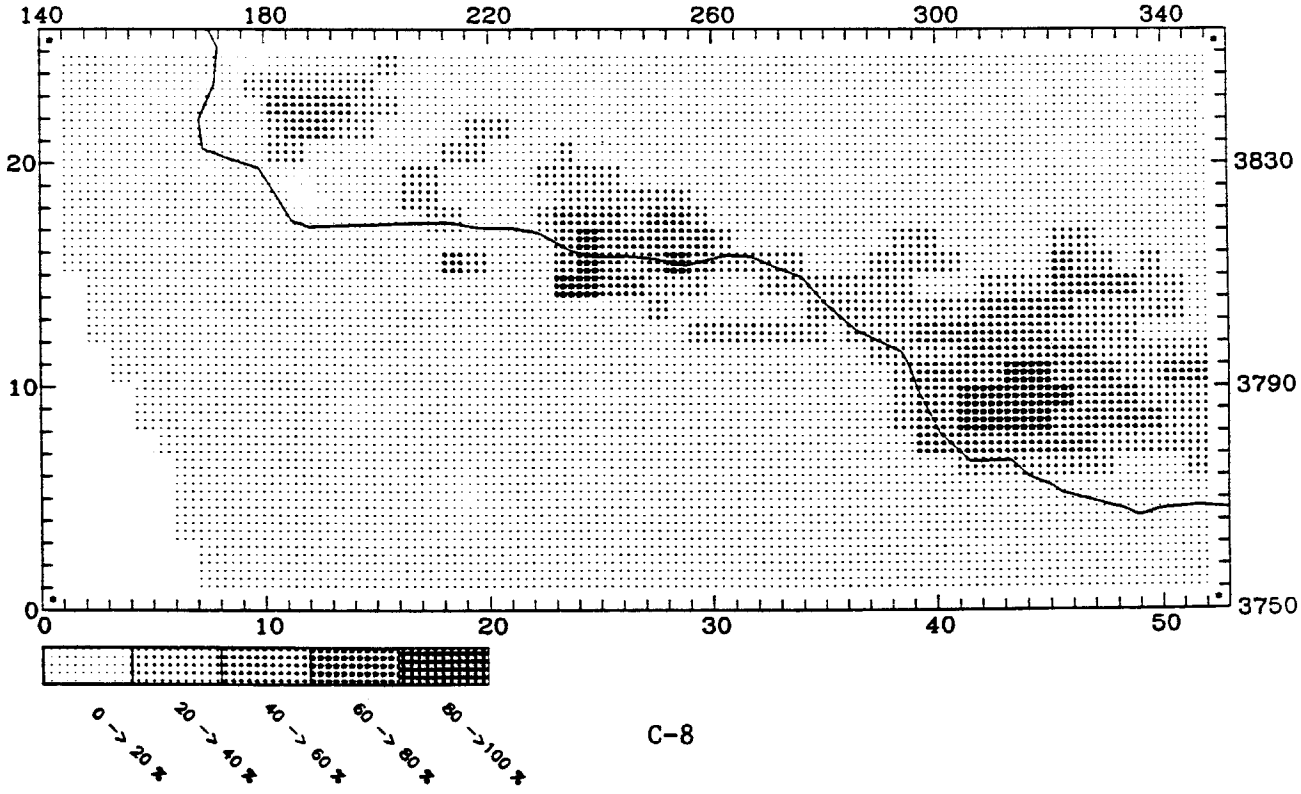

CALGRID–IV

BNDRY NOX CONTRIBUTION AT: 2300 September 16 LEVEL 1

MAXIMUM CONTRIBUTION IN CELL (3,11) = 92.75 (%)

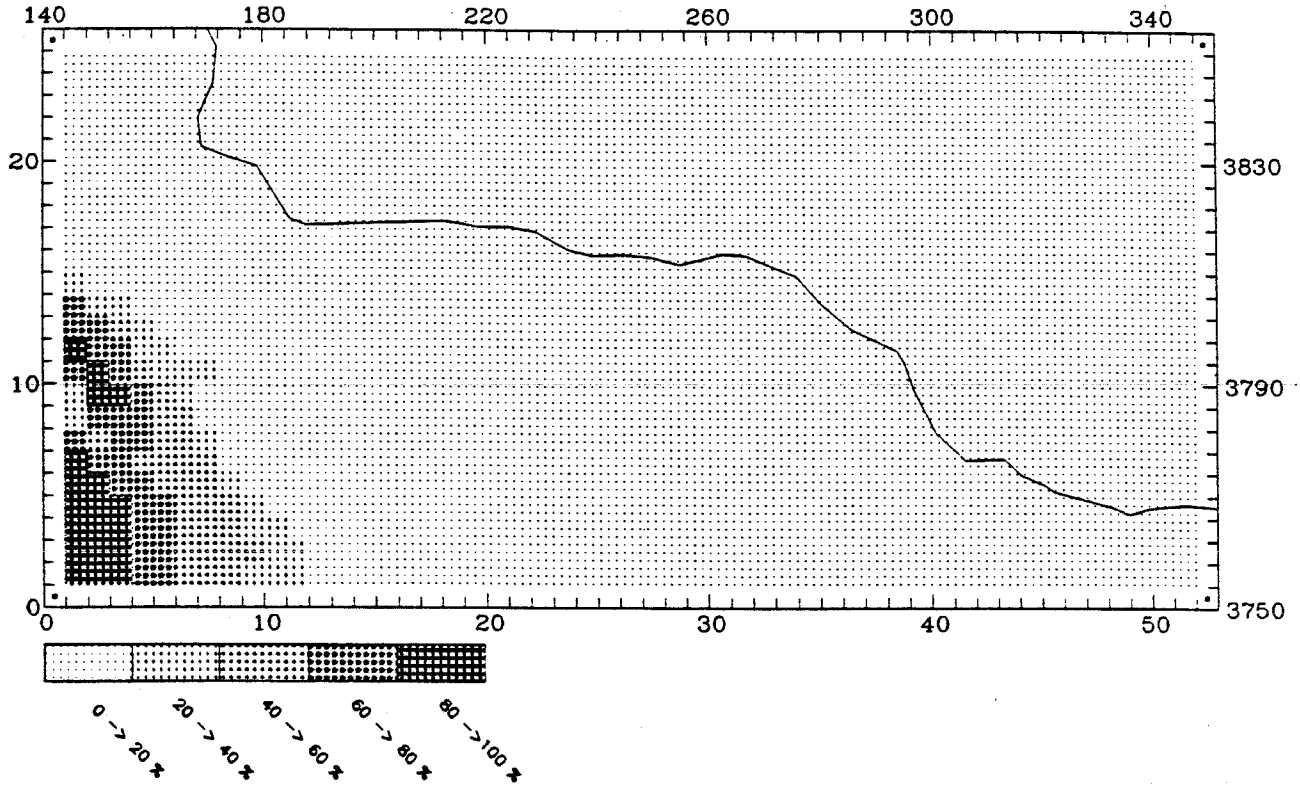

UAM–IV

BNDRY NOX CONTRIBUTION AT: 2300 September 16 LEVEL 1

MAXIMUM CONTRIBUTION IN CELL (3,8) = 100.00 (%)

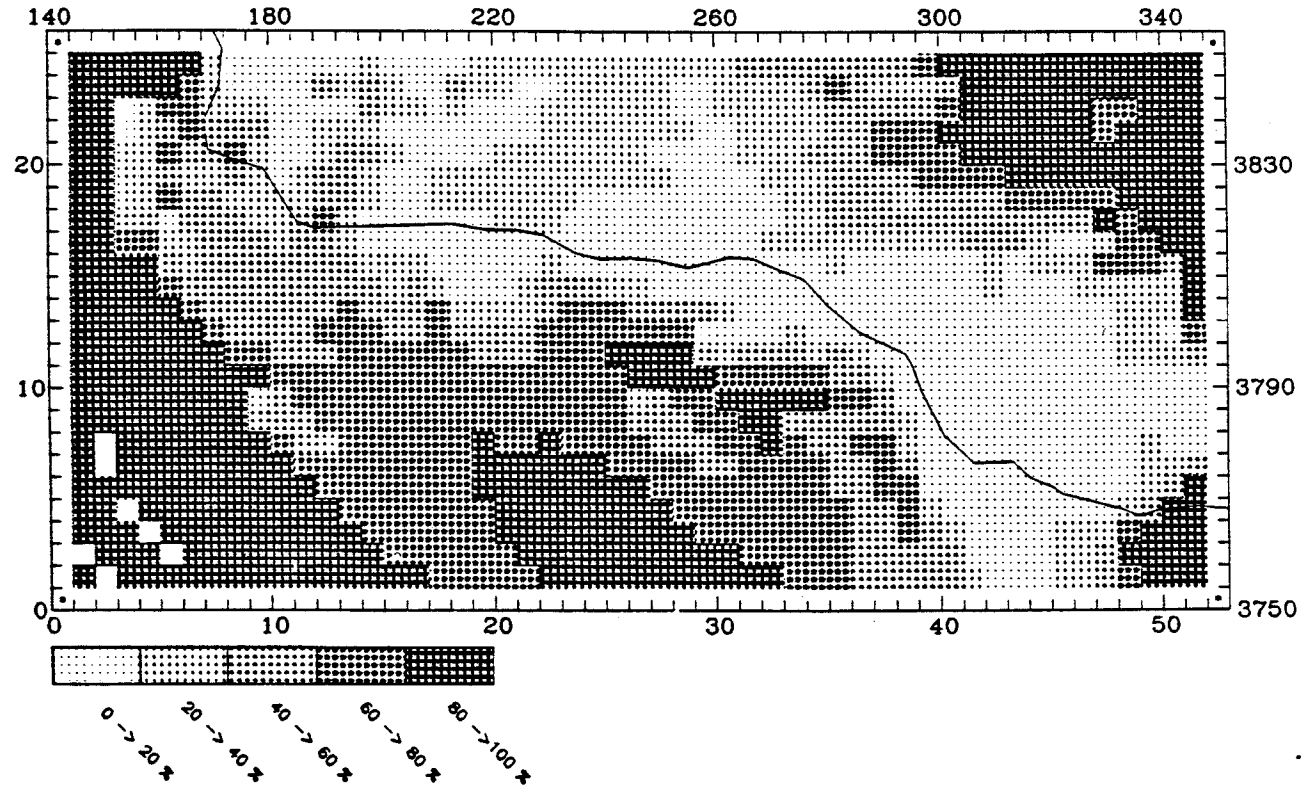

CALGRID–IV

BNDRY RHC CONTRIBUTION AT: 2300 September 16 LEVEL 1

MAXIMUM CONTRIBUTION IN CELL (2,2) = 100.00 (%)

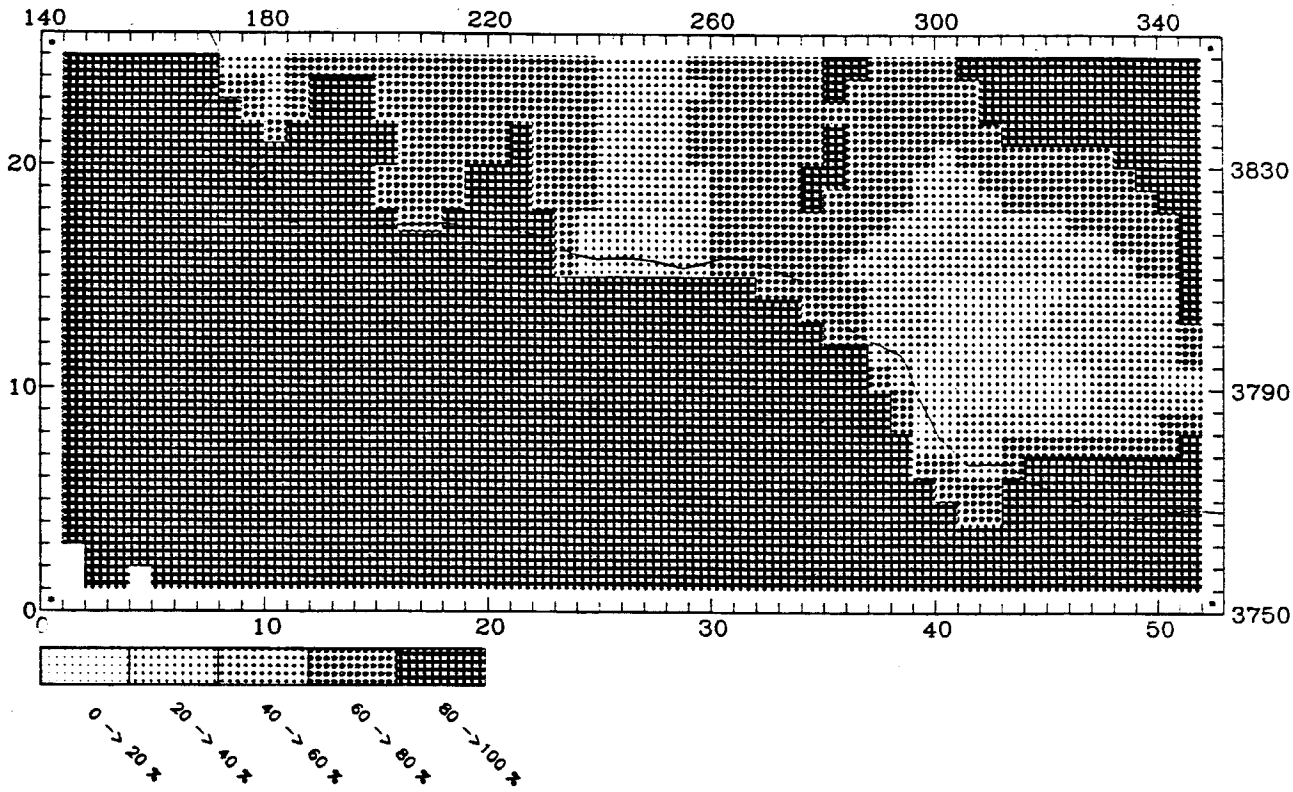

UAM–IV

BNDRY RHC CONTRIBUTION AT: 2300 September 16 LEVEL 1

MAXIMUM CONTRIBUTION IN CELL (2,2) = 100.00 (%)

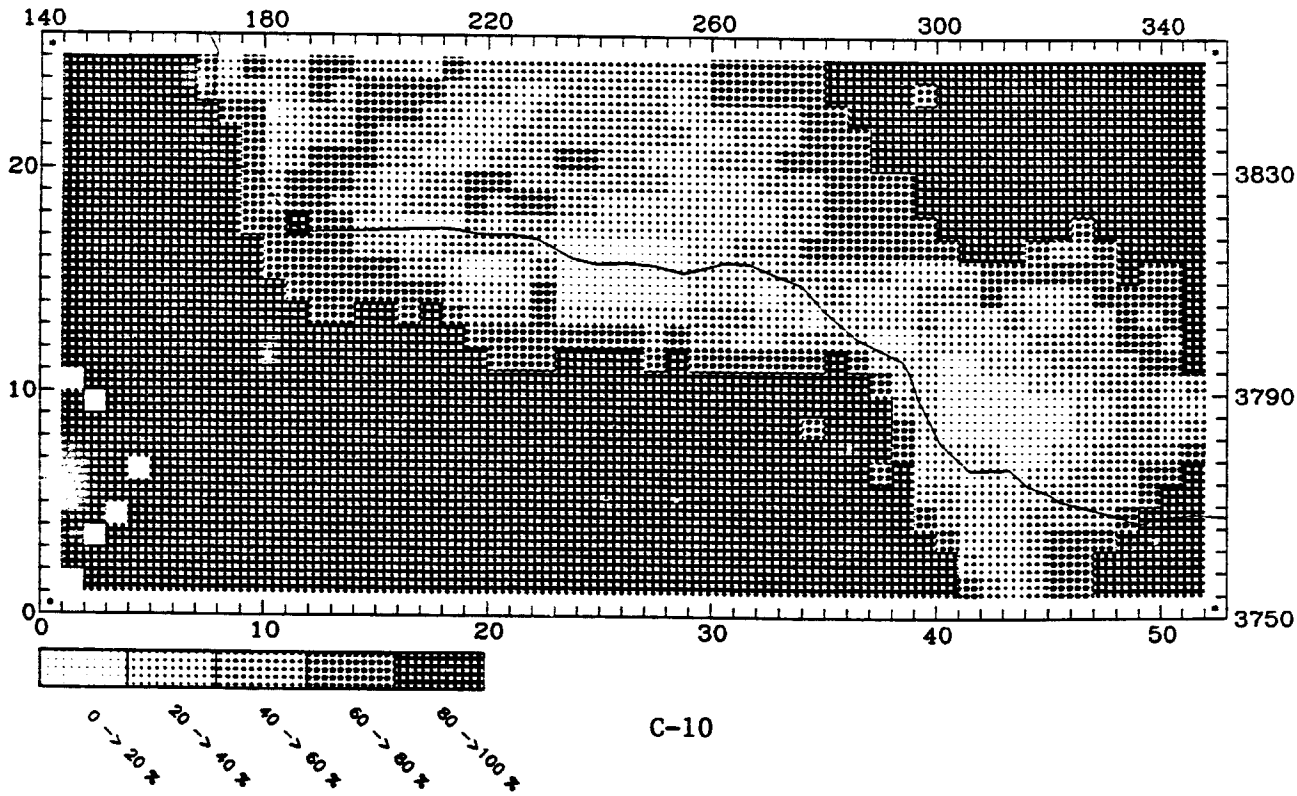

CALGRID–IV

INTNOX CONTRIBUTION AT: 2300 September 16 LEVEL 1

MAXIMUM CONTRIBUTION IN CELL (52,25) = 0.09 (%)

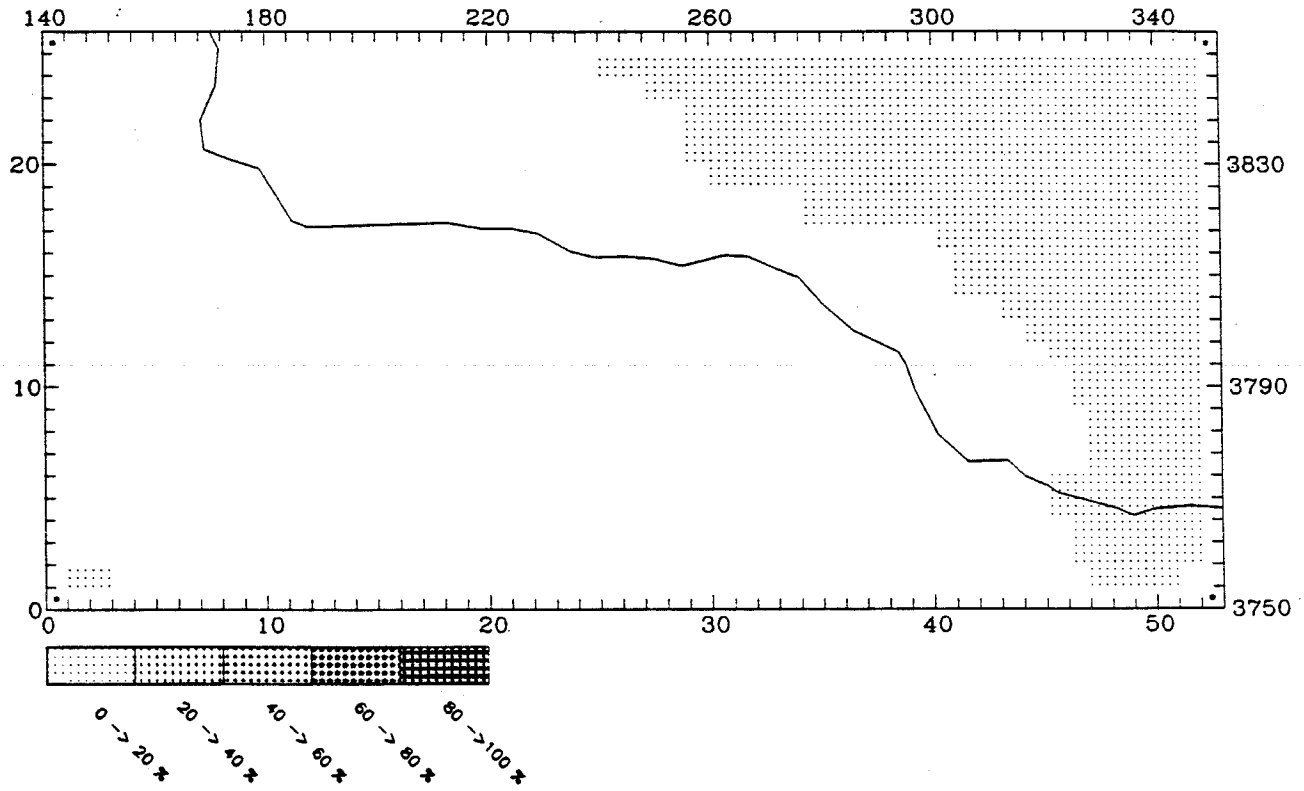

UAM–IV

INTNOX CONTRIBUTION AT: 2300 September 16 LEVEL 1

MAXIMUM CONTRIBUTION IN CELL (24,25) = 29.90 (%)

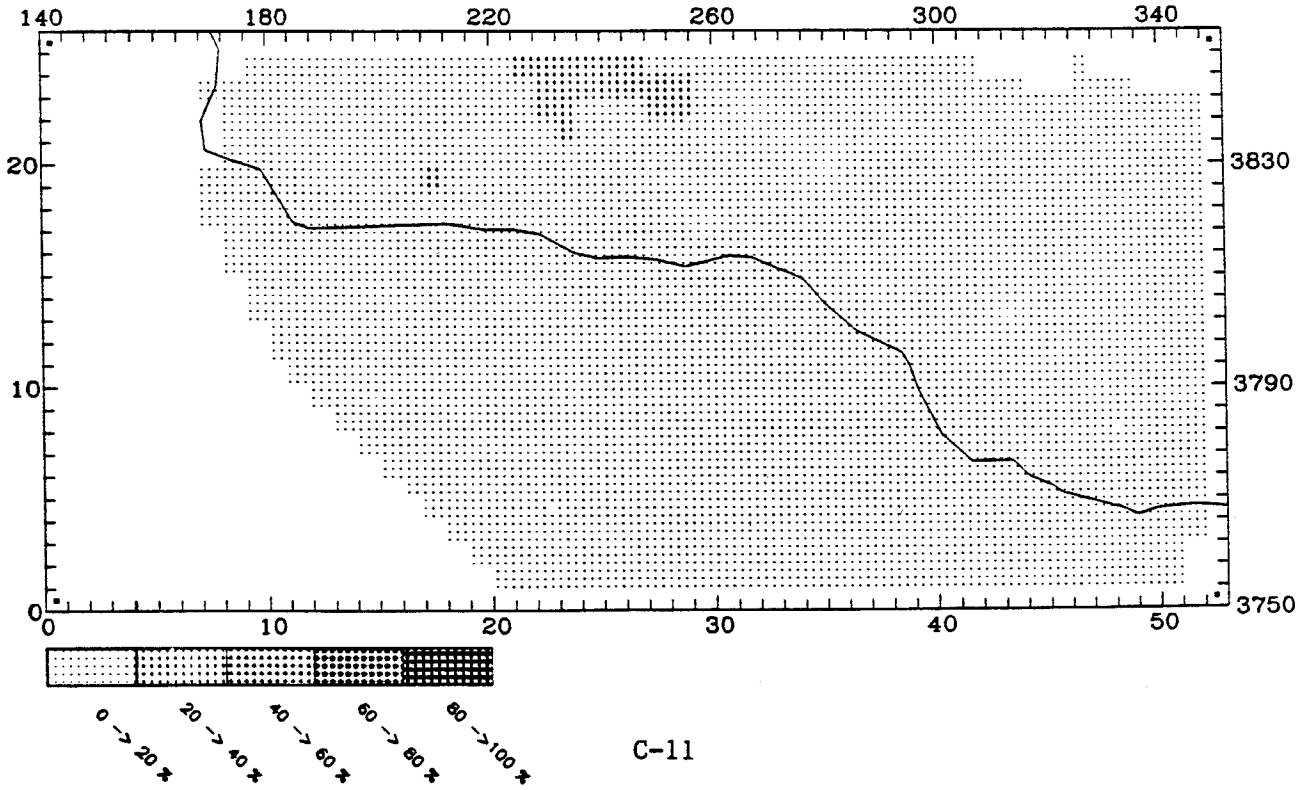

CALGRID–IV

INTHC CONTRIBUTION AT: 2300 September 16 LEVEL 1

MAXIMUM CONTRIBUTION IN CELL (18,25) = 5.19 (%)

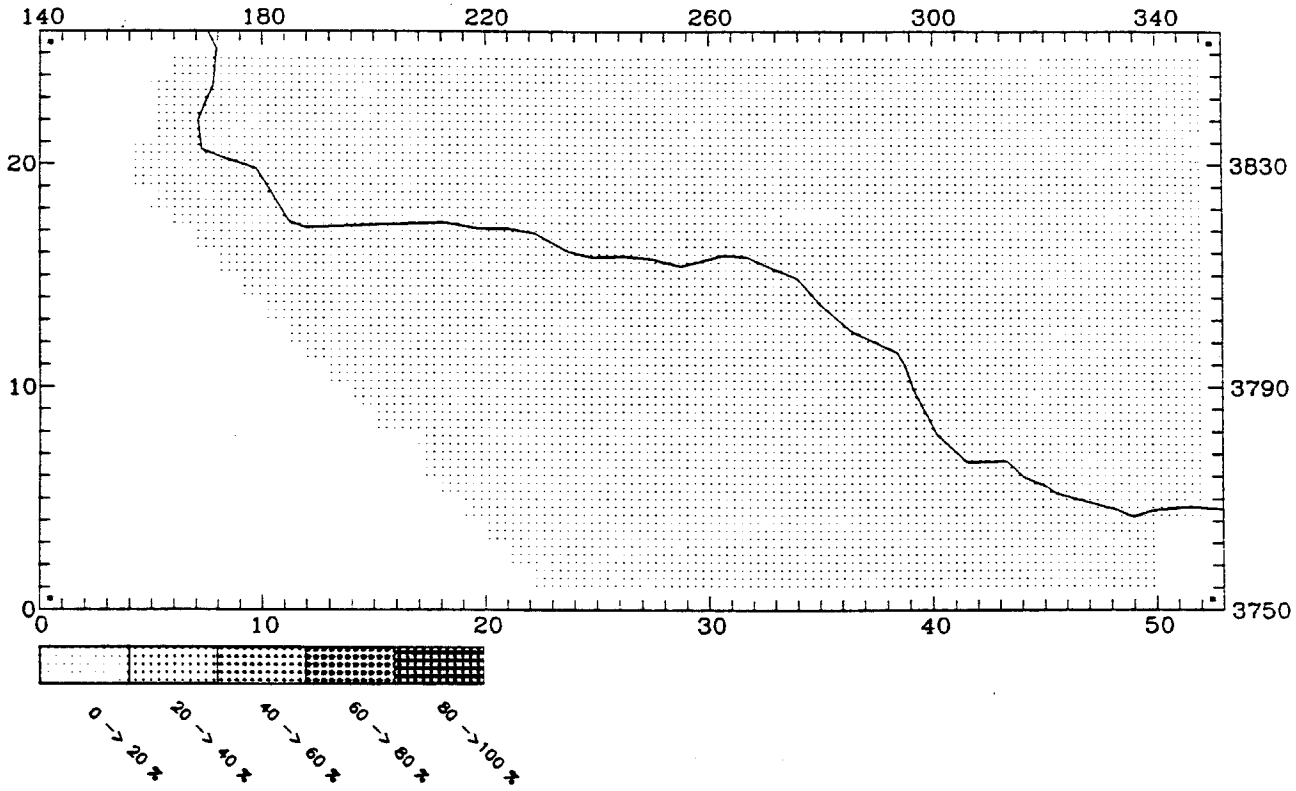

UAM–IV

INTHC CONTRIBUTION AT: 2300 September 16 LEVEL 1

MAXIMUM CONTRIBUTION IN CELL (18,20) = 40.61 (%)

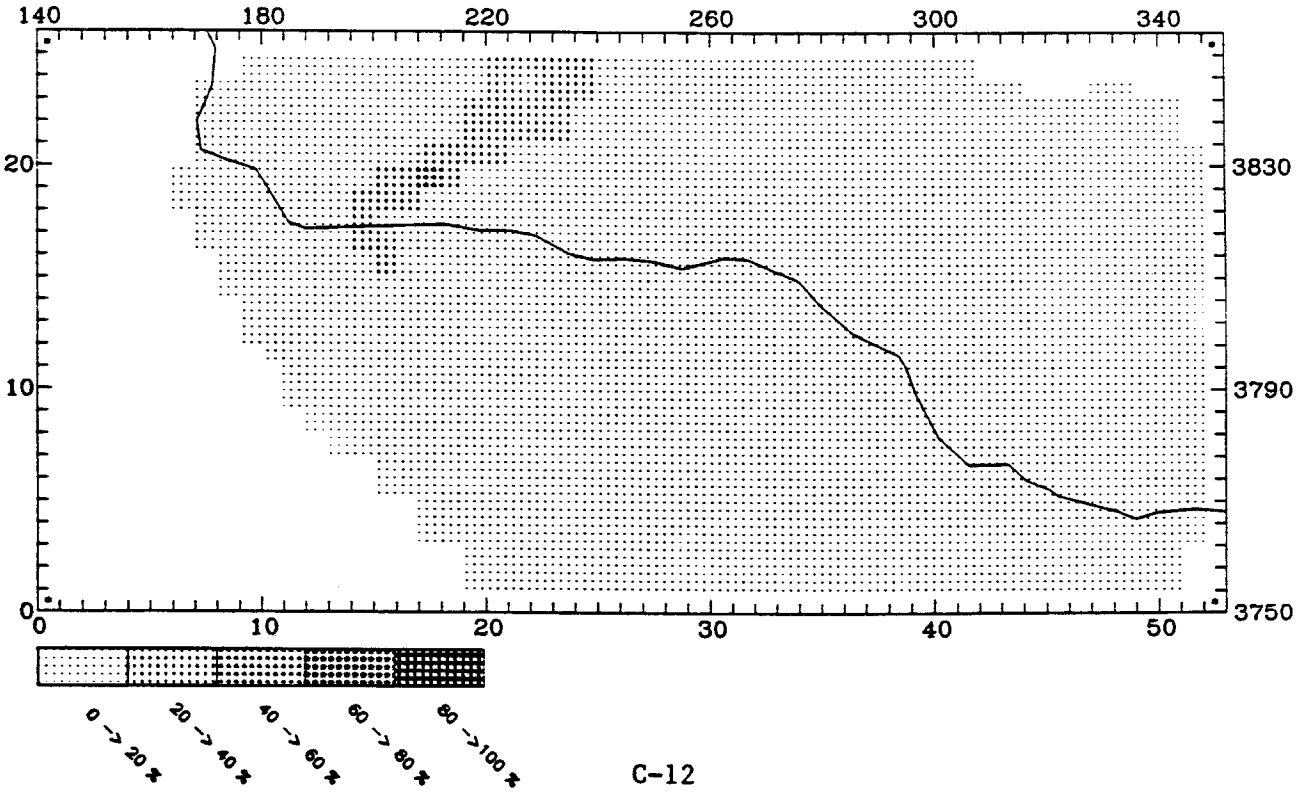

CALGRID–IV

PTARBNOX CONTRIBUTION AT: 2300 September 16 LEVEL 1

MAXIMUM CONTRIBUTION IN CELL (46,2) = 99.42 (%)

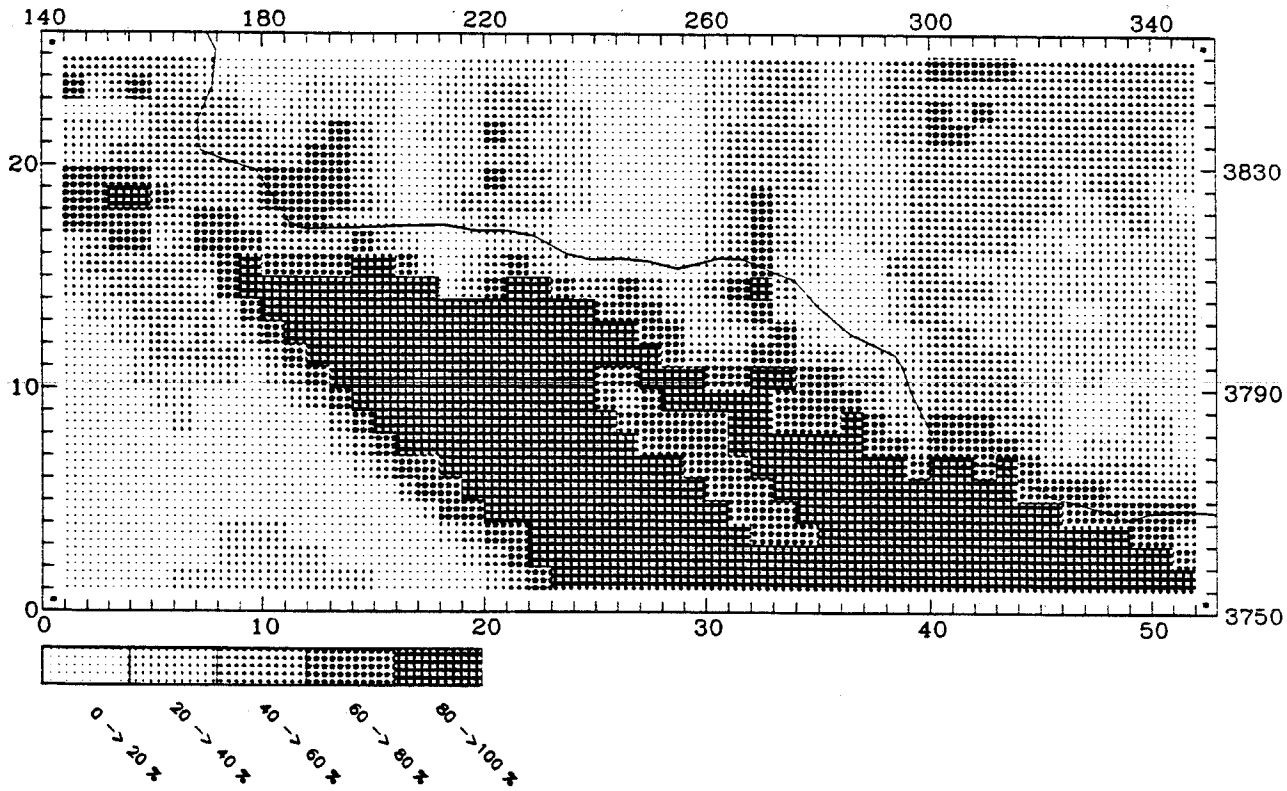

UAM–IV

PTNOX CONTRIBUTION AT: 2300 September 16 LEVEL 1

MAXIMUM CONTRIBUTION IN CELL (32,14) = 79.58 (%)

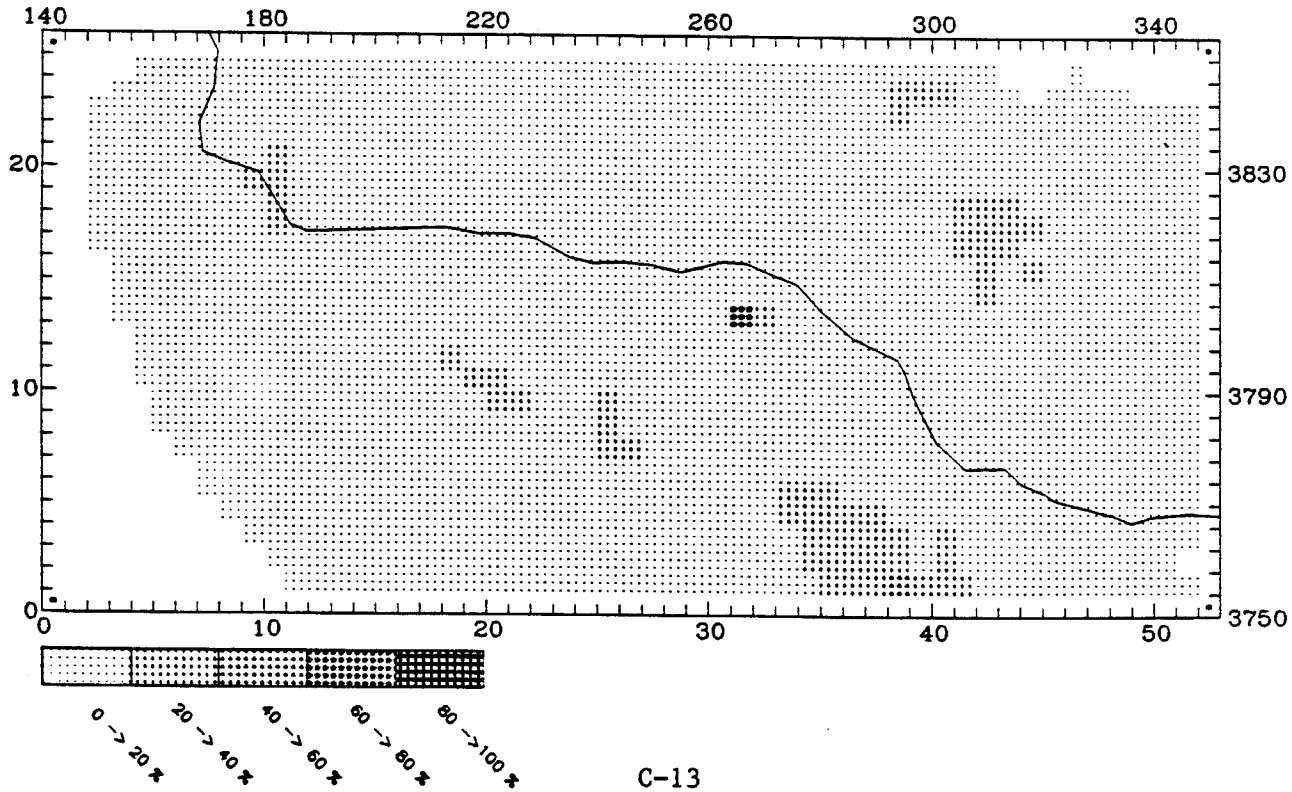

CALGRID–IV

PTARBHC CONTRIBUTION AT: 2300 September 16 LEVEL 1

MAXIMUM CONTRIBUTION IN CELL (43,3) = 9.43 (%)

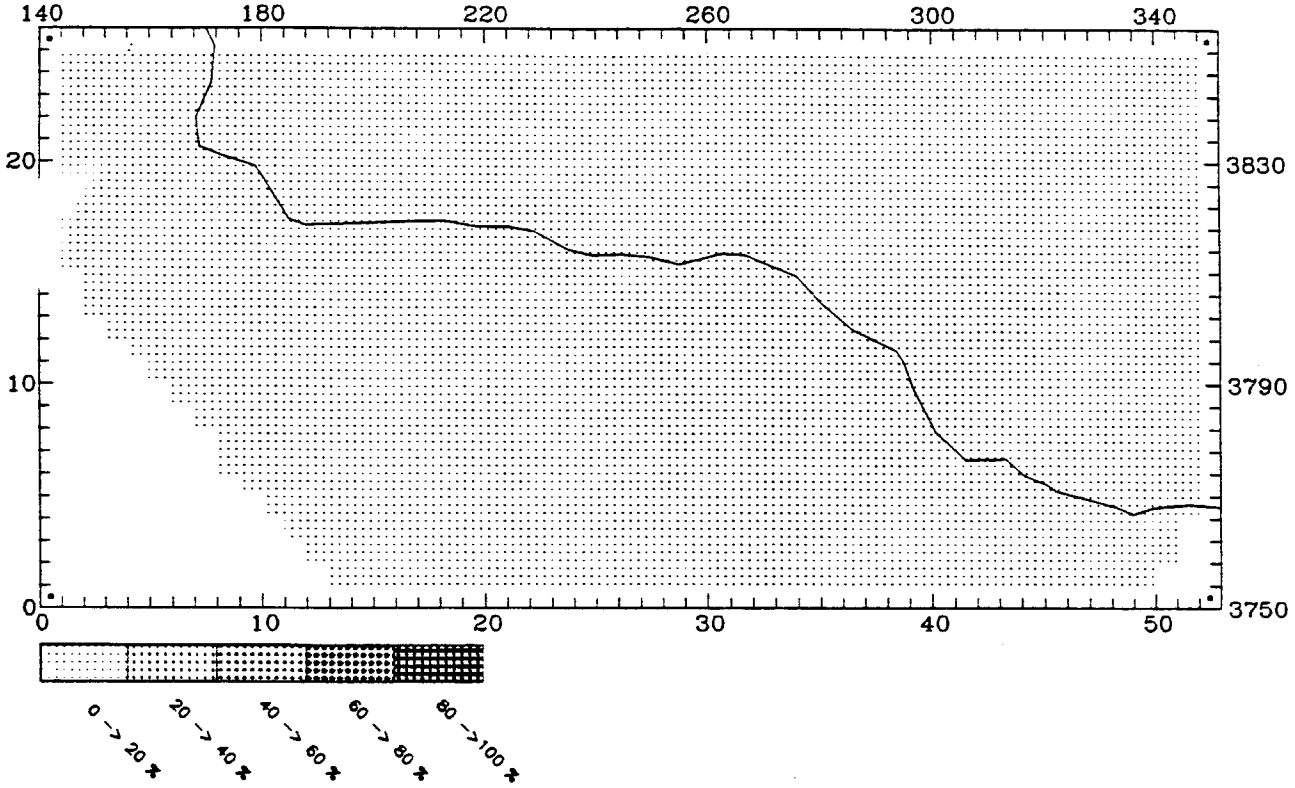

UAM–IV

PTHC CONTRIBUTION AT: 2300 September 16 LEVEL 1

MAXIMUM CONTRIBUTION IN CELL (38,3) = 1.53 (%)

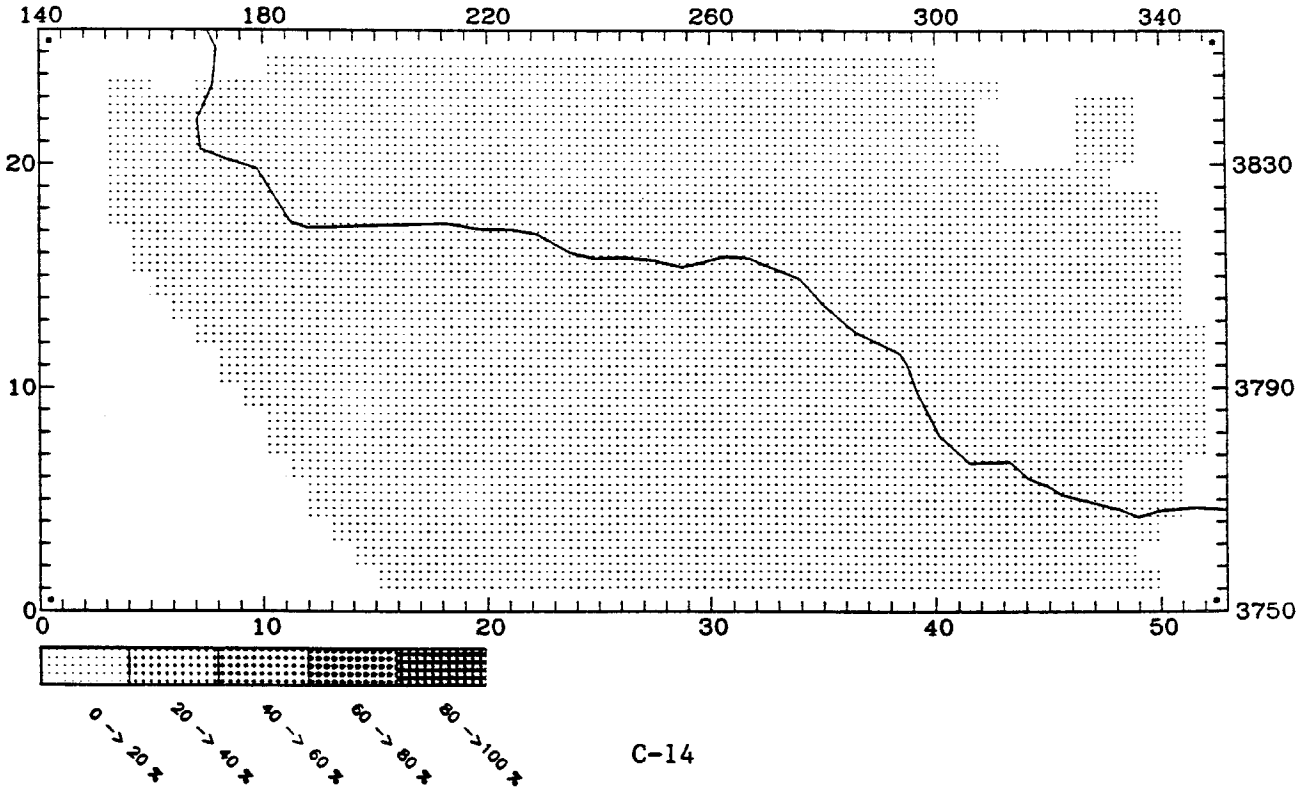

CALGRID–IV

ANOX CONTRIBUTION AT: 2300 September 16 LEVEL 1

MAXIMUM CONTRIBUTION IN CELL (10,9) = 98.65 (%)

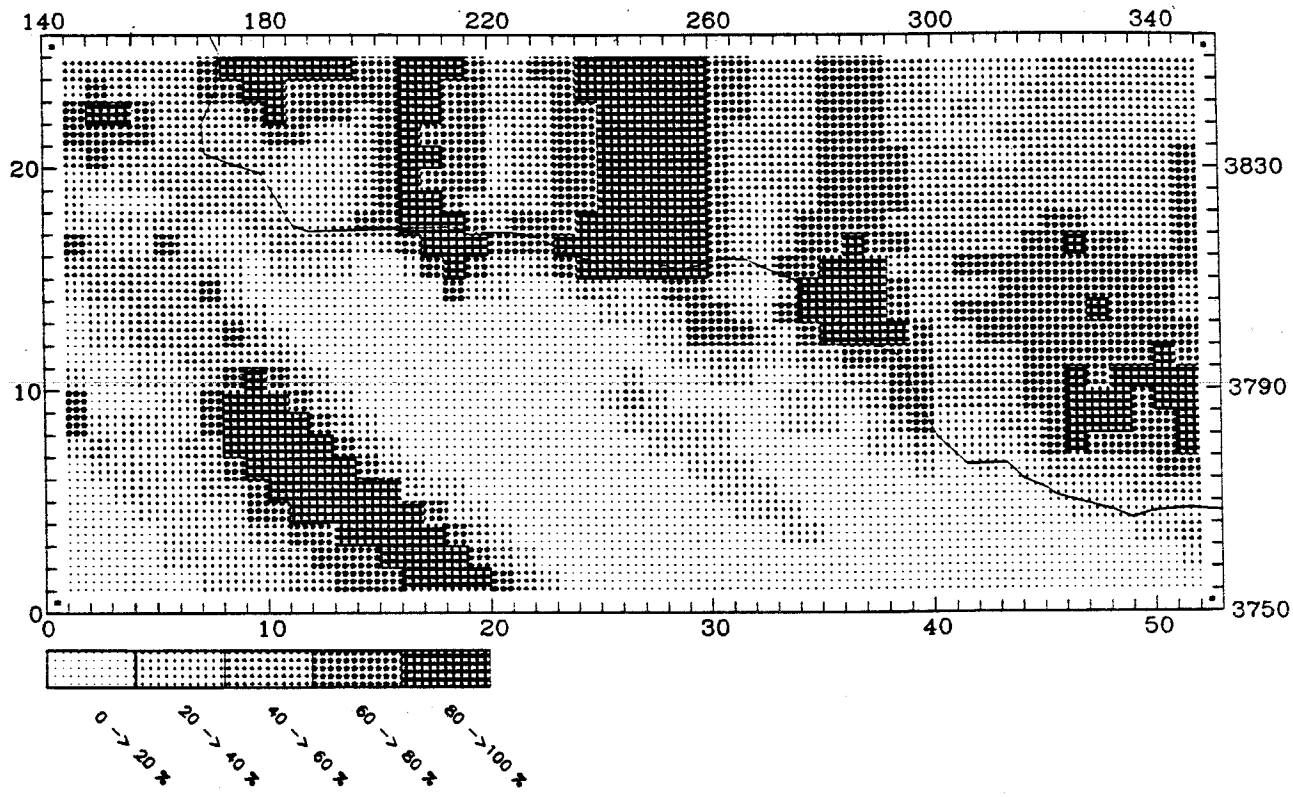

UAM–IV

NOX CONTRIBUTION AT: 2300 September 16 LEVEL 1

MAXIMUM CONTRIBUTION IN CELL (28,16) = 98.30 (%)

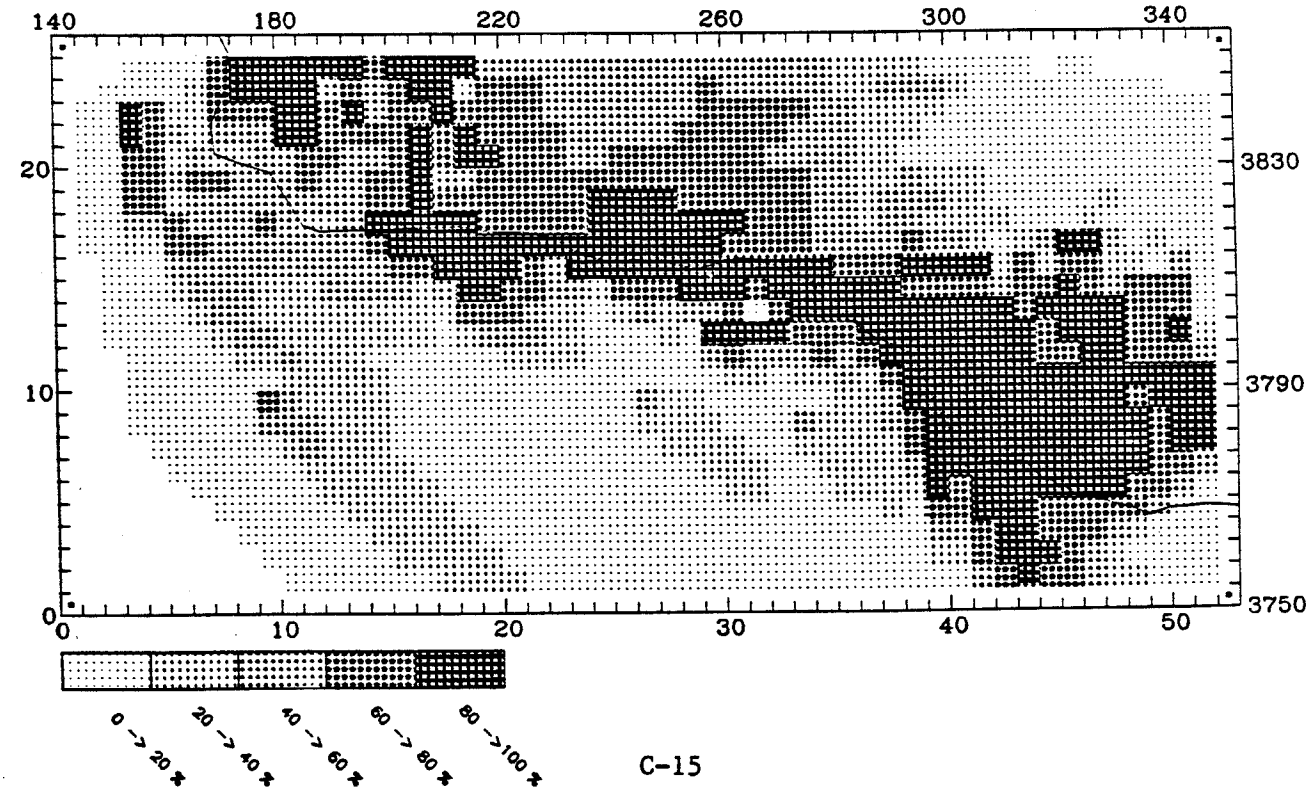

CALGRID–IV

ATHC CONTRIBUTION AT: 2300 September 16 LEVEL 1

MAXIMUM CONTRIBUTION IN CELL (25,16) = 70.73 (%)

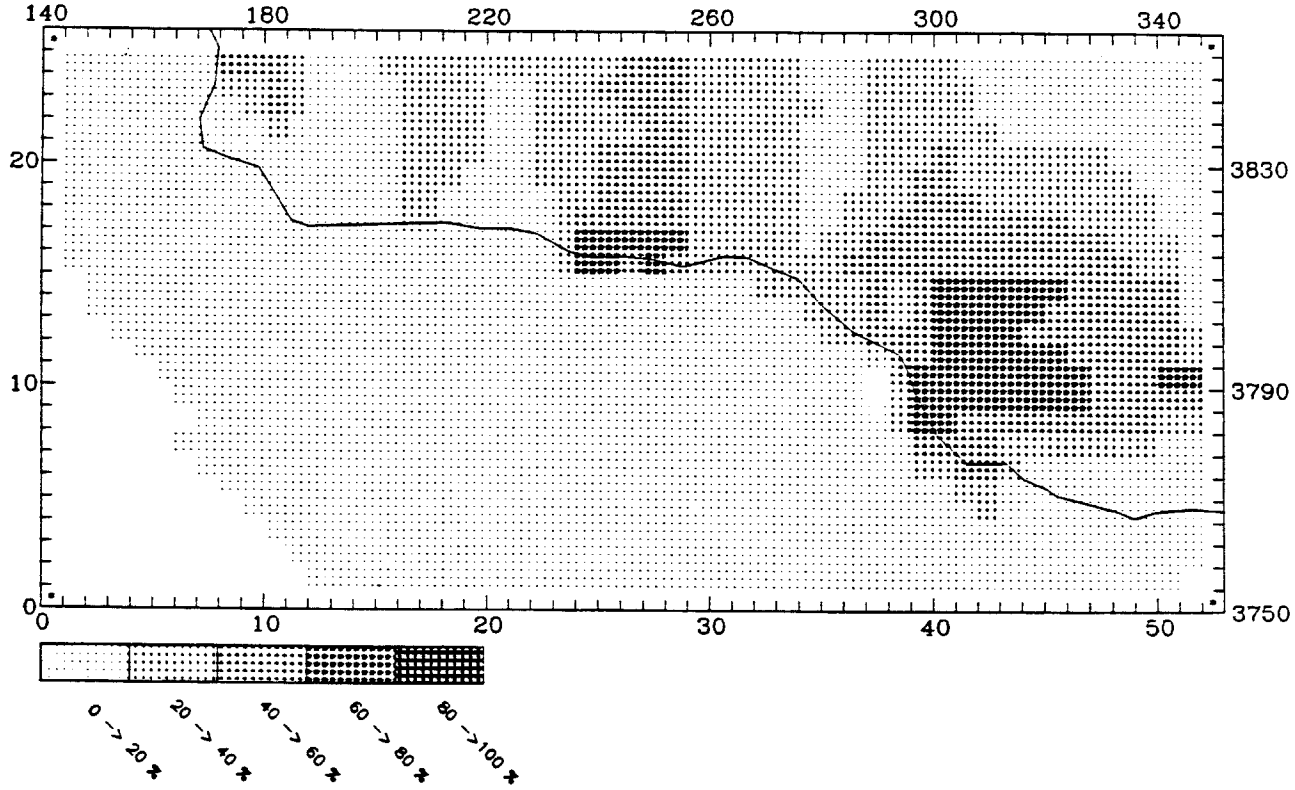

UAM–IV

RHC CONTRIBUTION AT: 2300 September 16 LEVEL 1

MAXIMUM CONTRIBUTION IN CELL (28,16) = 93.73 (%)

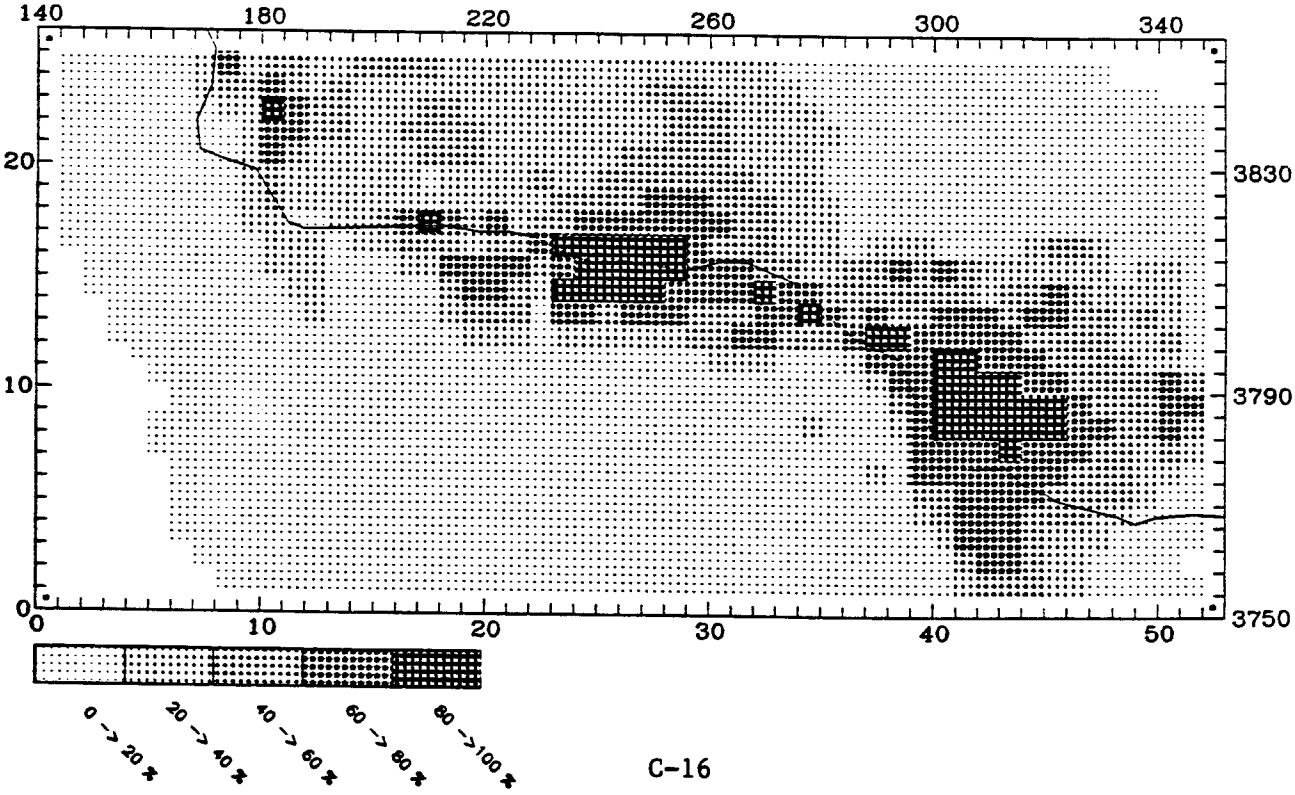

CALGRID–IV

BNDRY NOX CONTRIBUTION AT: 1100 September 17 LEVEL 1

MAXIMUM CONTRIBUTION IN CELL (3,2) = 99.80 (%)

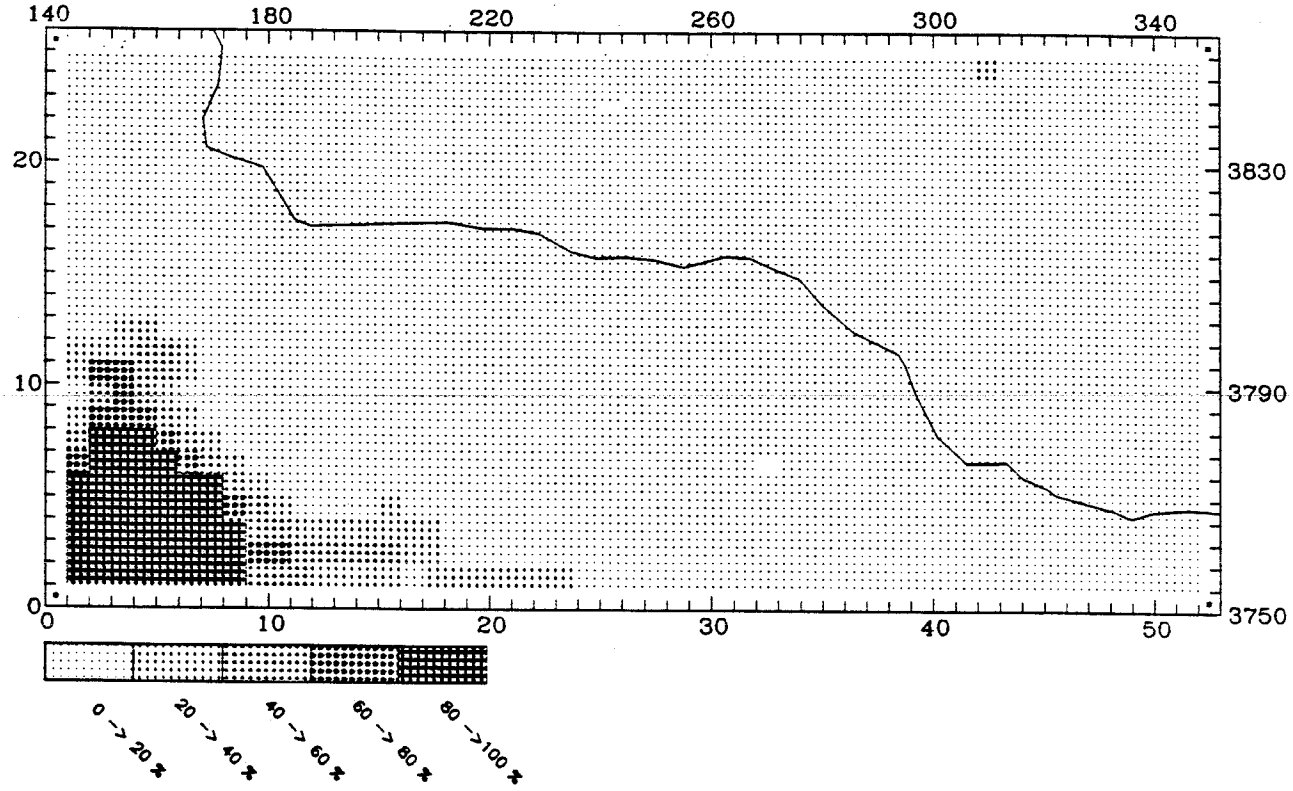

UAM–IV

BNDRY NOX CONTRIBUTION AT: 1100 September 17 LEVEL 1

MAXIMUM CONTRIBUTION IN CELL (2,2) = 100.00 (%)

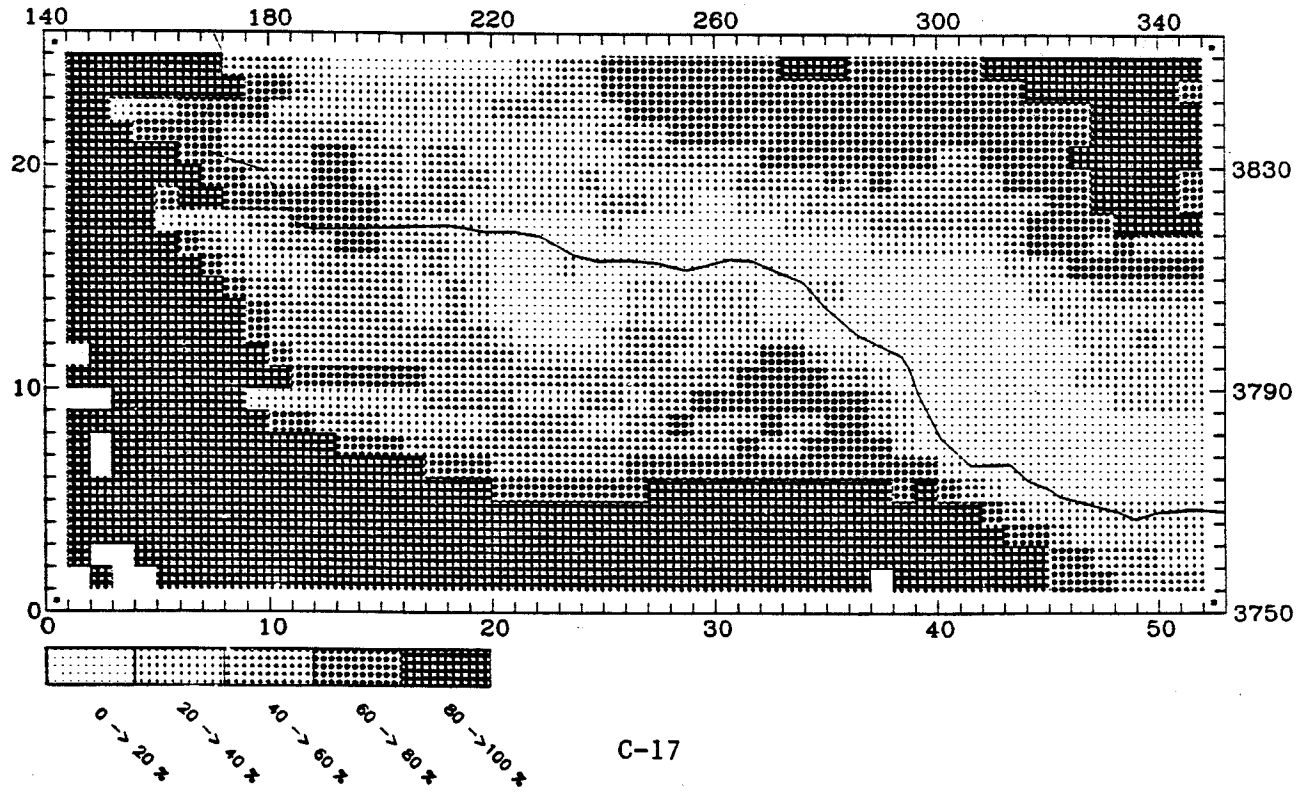

BNDRY RHC CONTRIBUTION AT: 1100 September 17 LEVEL 1

MAXIMUM CONTRIBUTION IN CELL (7,3) = 100.00 (%)

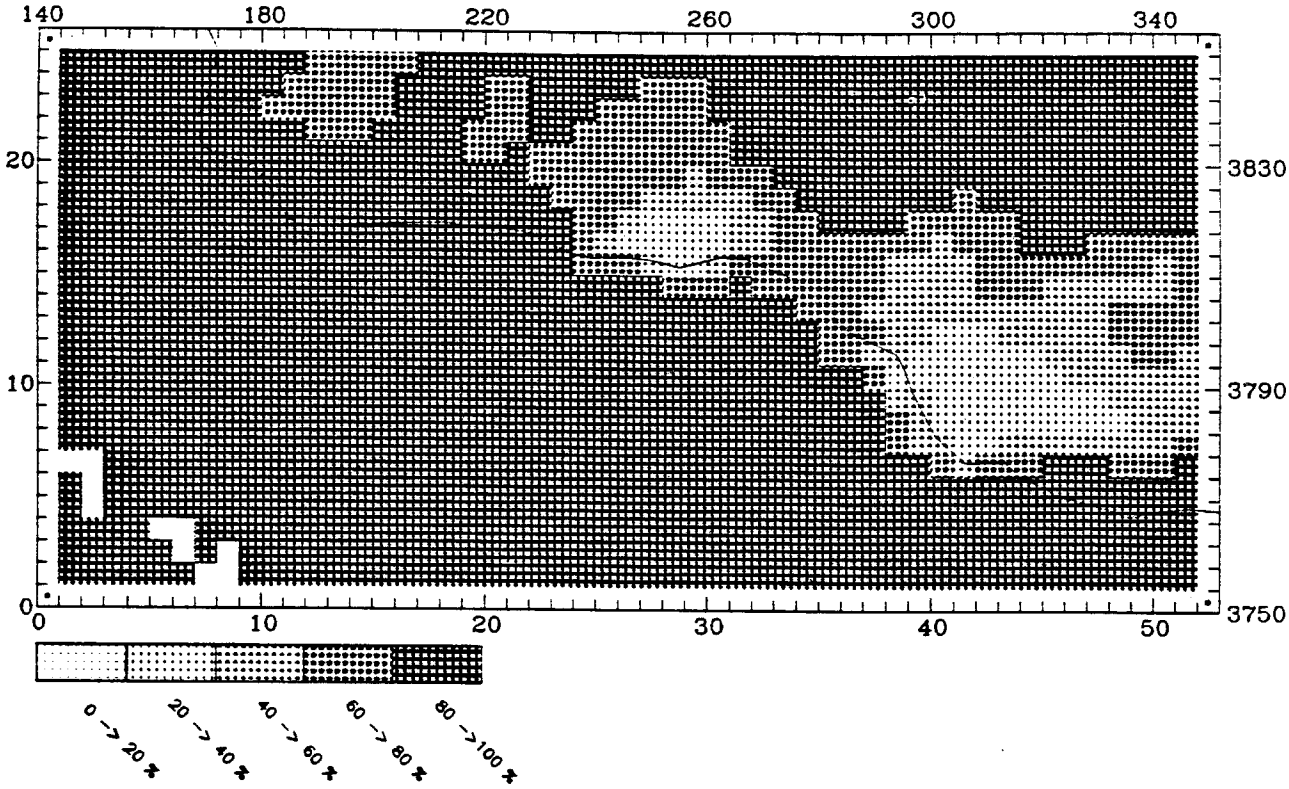

UAM-IV

BNDRY RHC CONTRIBUTION AT: 1100 September 17 LEVEL 1

MAXIMUM CONTRIBUTION IN CELL (2,2) = 100.00 (%)

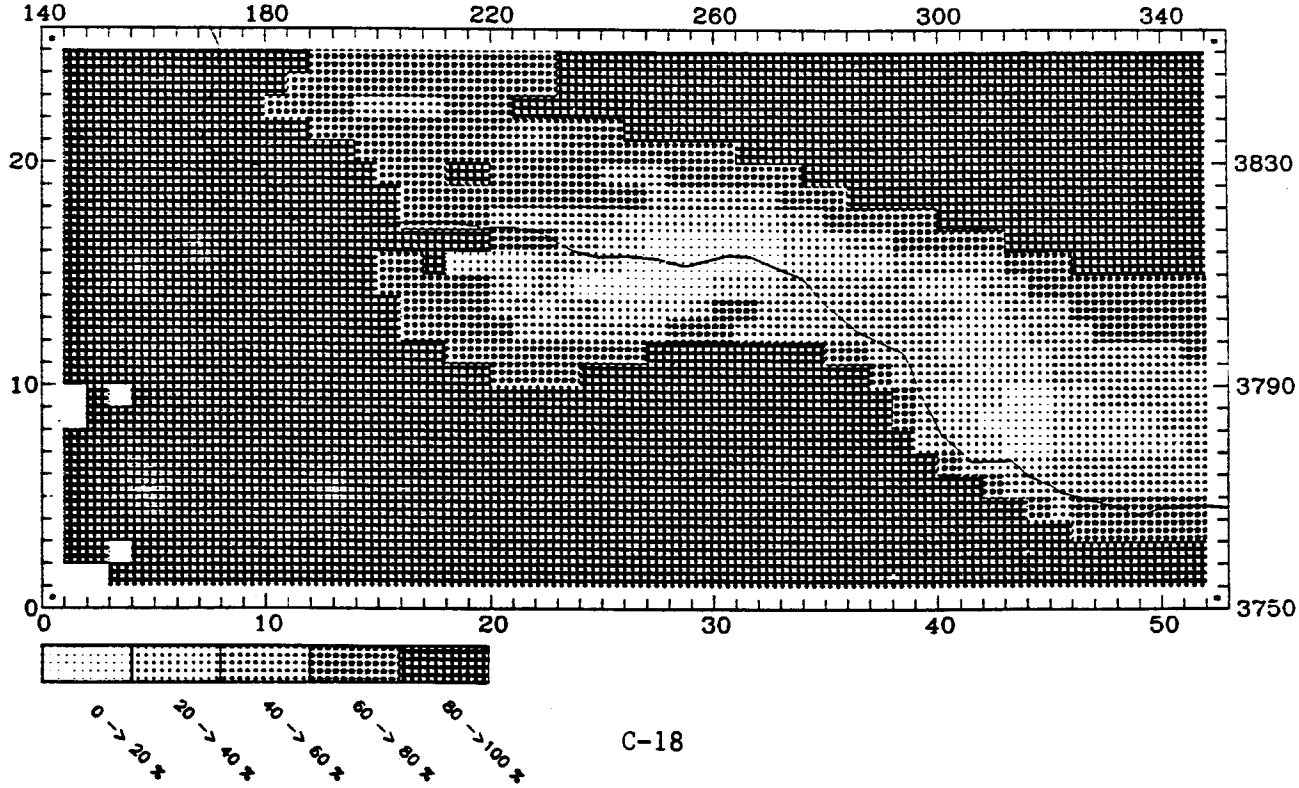

INTNOX CONTRIBUTION AT: 1100 September 17 LEVEL 1

MAXIMUM CONTRIBUTION IN CELL (4,2) = 0.01 (%)

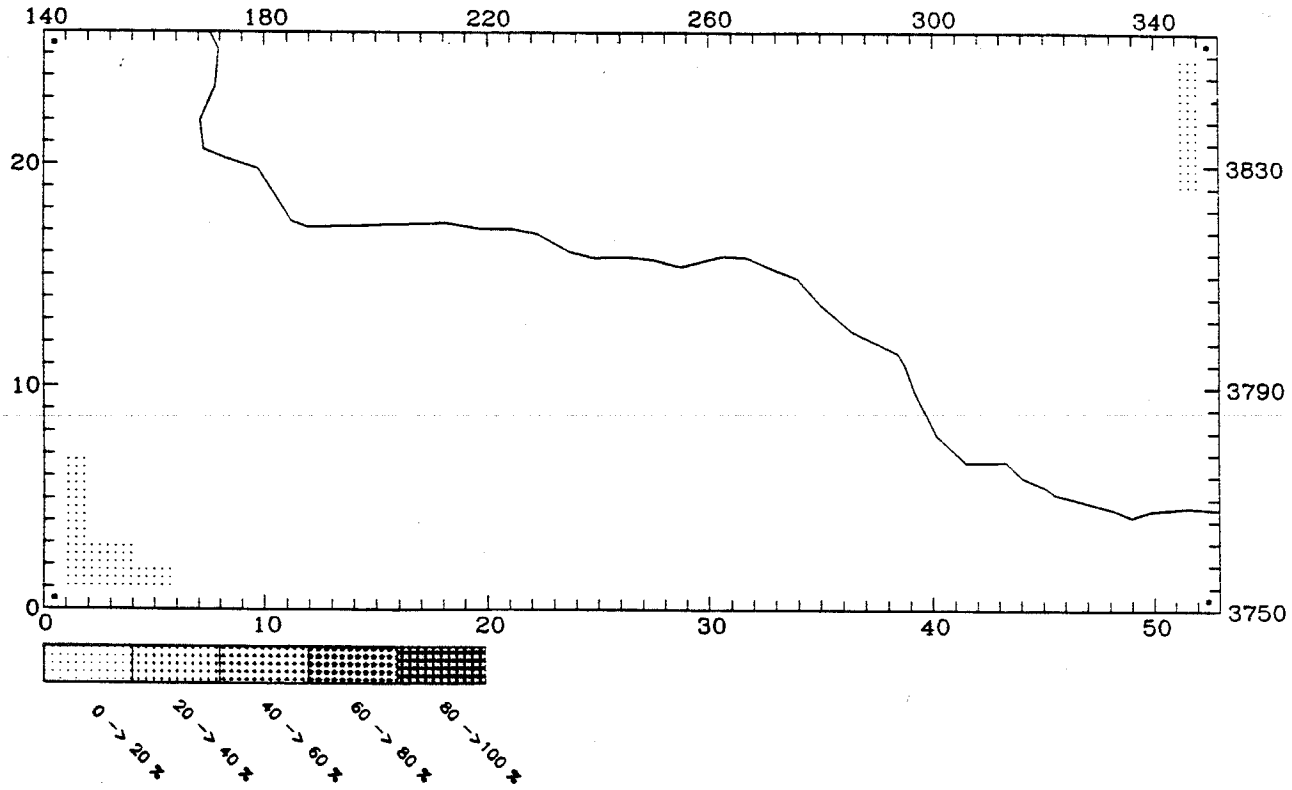

UAM-IV

INTNOX CONTRIBUTION AT: 1100 September 17 LEVEL 1

MAXIMUM CONTRIBUTION IN CELL (20,14) = 3.23 (%)

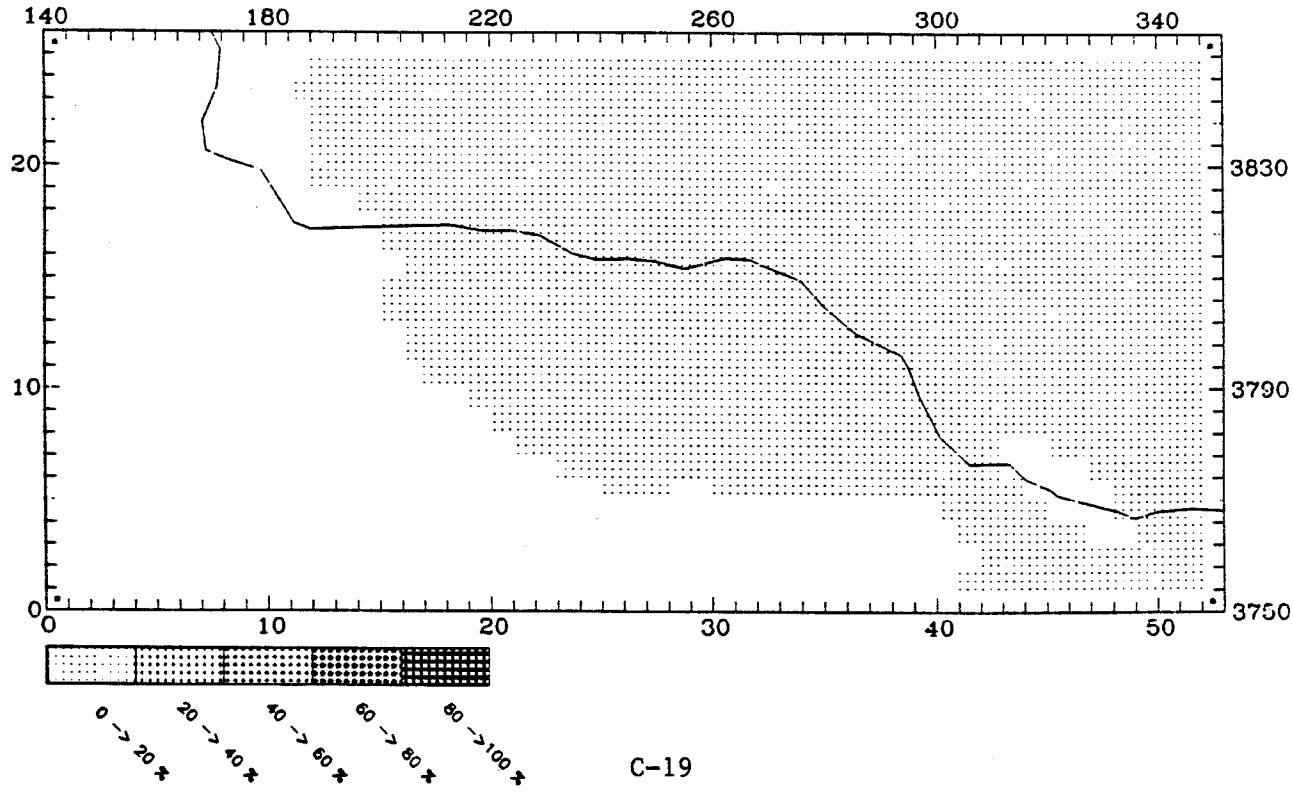

INTHC CONTRIBUTION AT: 1100 September 17 LEVEL 1

MAXIMUM CONTRIBUTION IN CELL (51,24) = 0.05 (%)

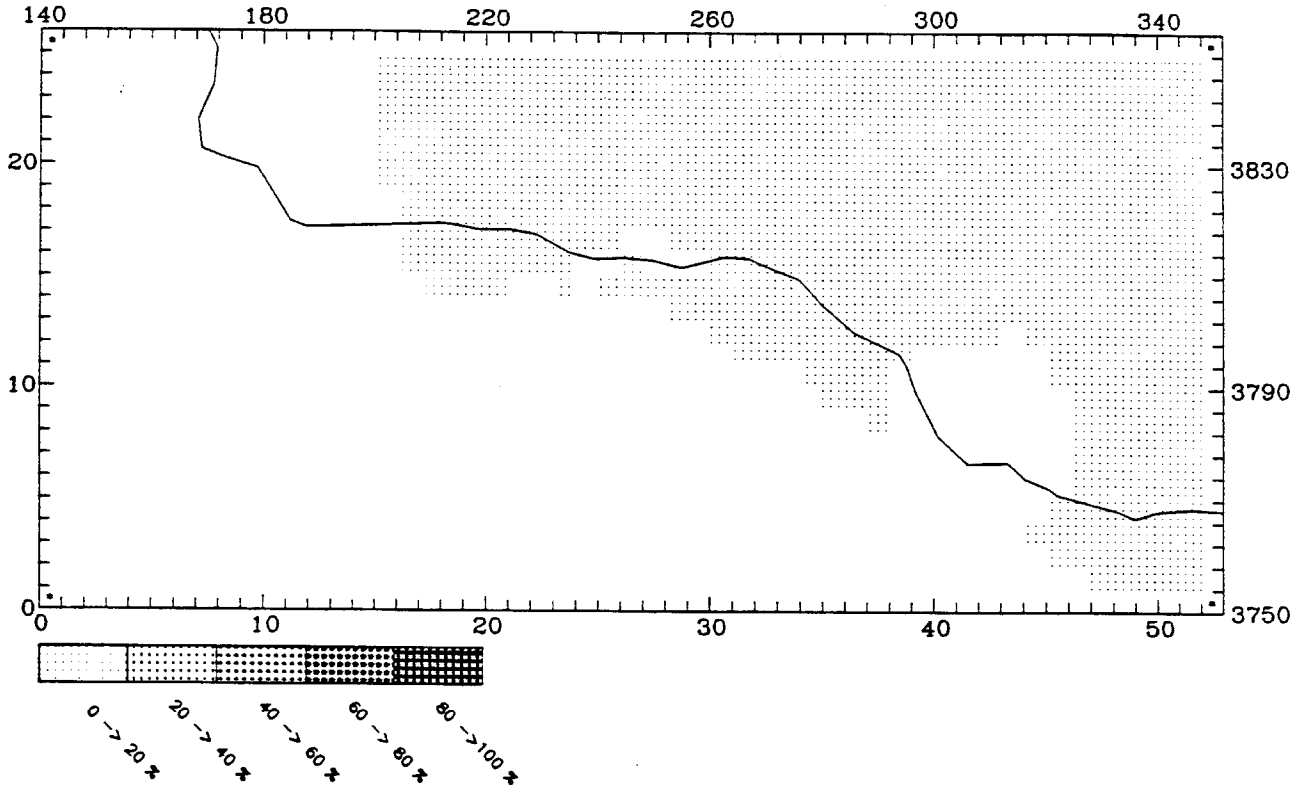

UAM-IV

INTHC CONTRIBUTION AT: 1100 September 17 LEVEL 1

MAXIMUM CONTRIBUTION IN CELL (21,14) = 9.18 (%)

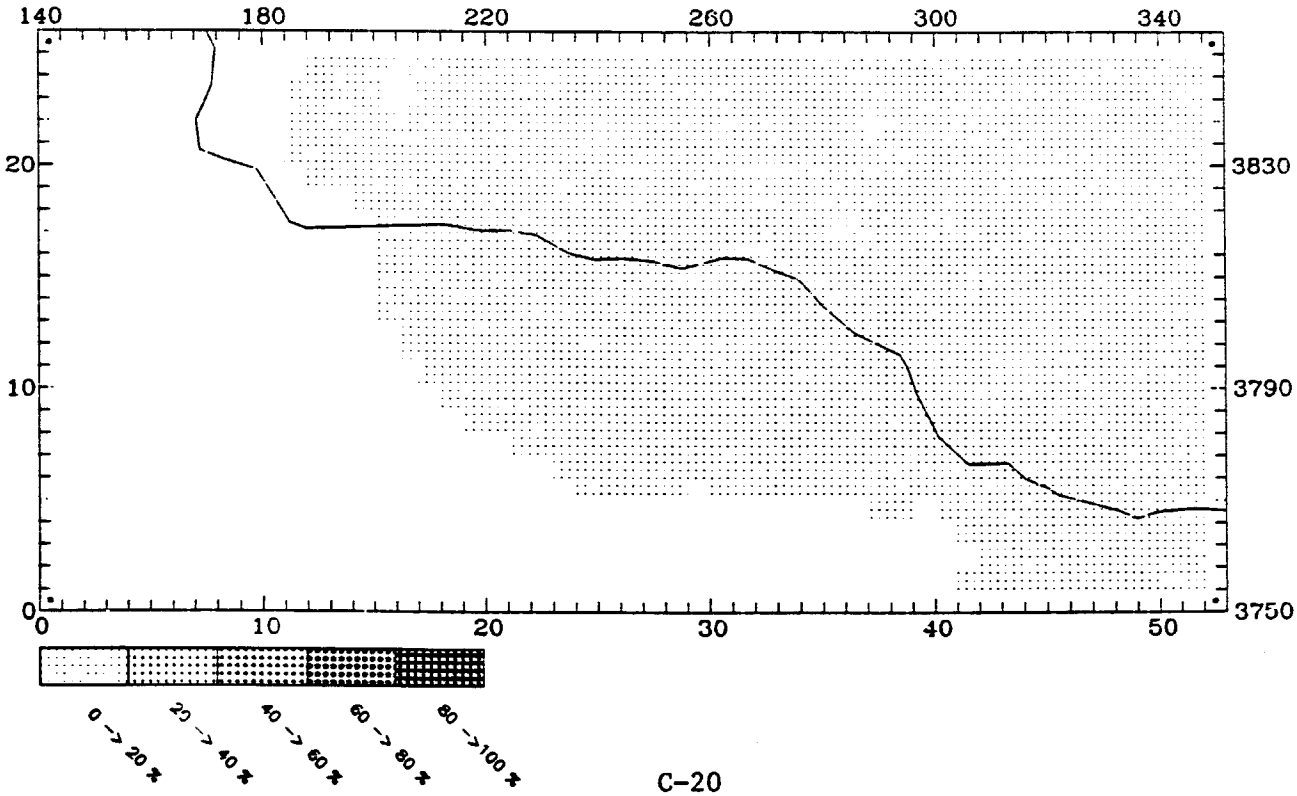

PTARBNOX CONTRIBUTION AT: 1100 September 17 LEVEL 1

MAXIMUM CONTRIBUTION IN CELL (43,2) = 99.94 (%)

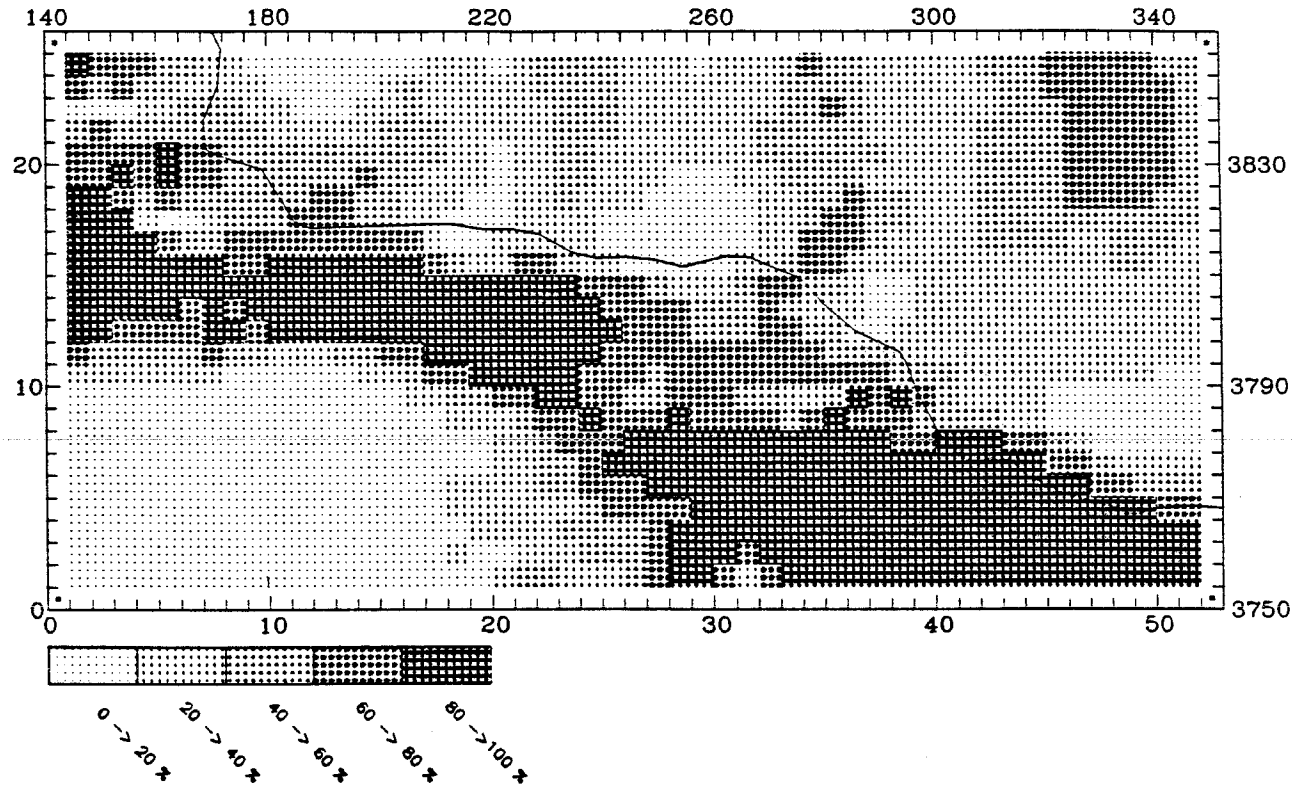

UAM-IV

PTNOX CONTRIBUTION AT: 1100 September 17 LEVEL 1

MAXIMUM CONTRIBUTION IN CELL (34,8) = 42.43 (%)

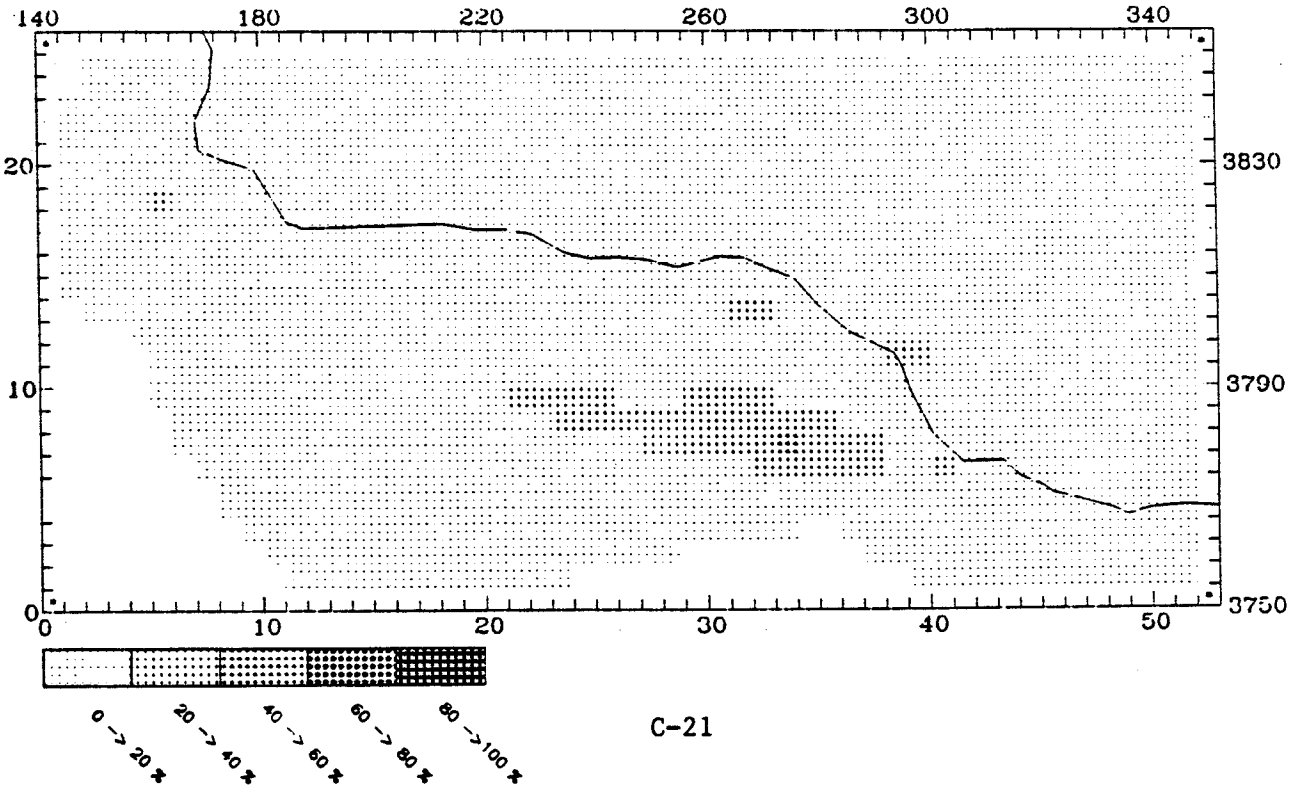

PTARBHC CONTRIBUTION AT: 1100 September 17 LEVEL 1

MAXIMUM CONTRIBUTION IN CELL (43,3) = 4.31 (%)

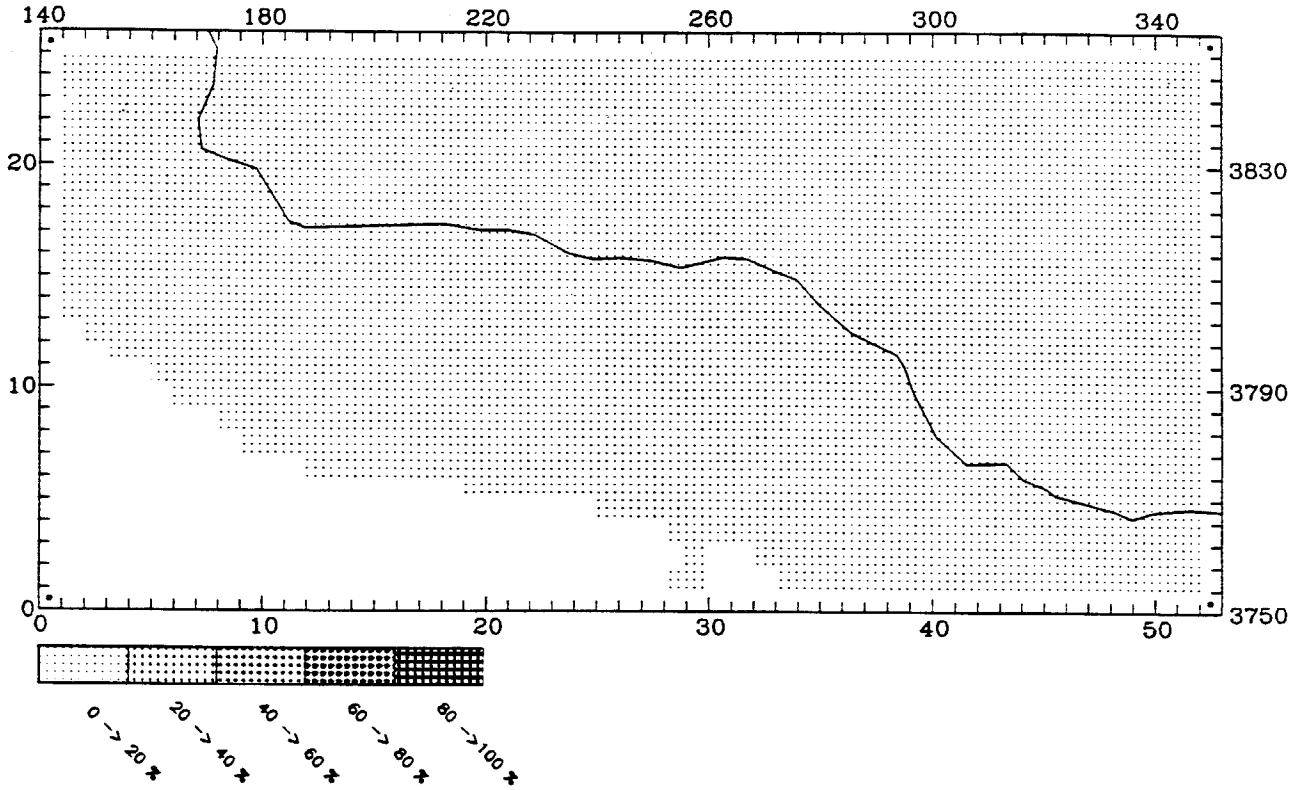

UAM-IV

PTHC CONTRIBUTION AT: 1100 September 17 LEVEL 1

MAXIMUM CONTRIBUTION IN CELL (26,9) = 1.96 (%)

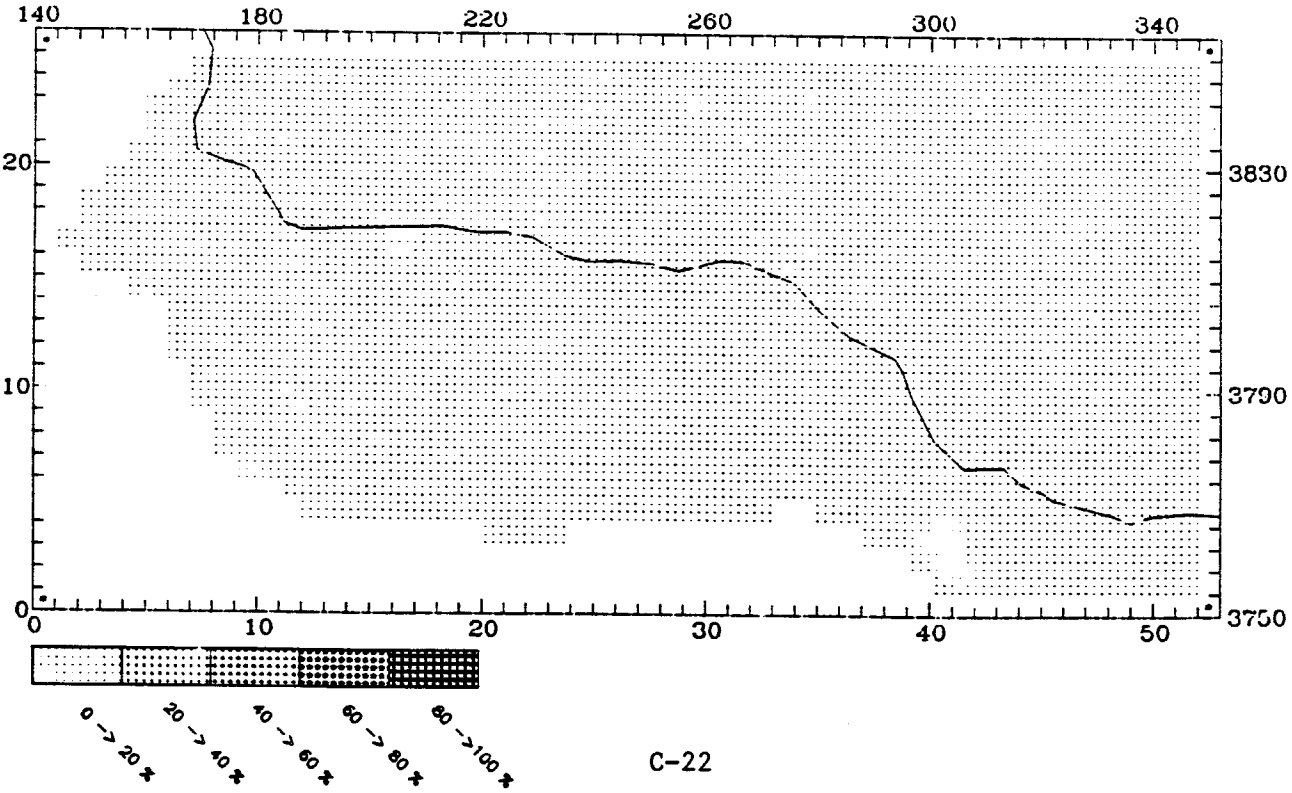

ANOX CONTRIBUTION AT: 1100 September 17 LEVEL 1

MAXIMUM CONTRIBUTION IN CELL (11,10) = 99.43 (%)

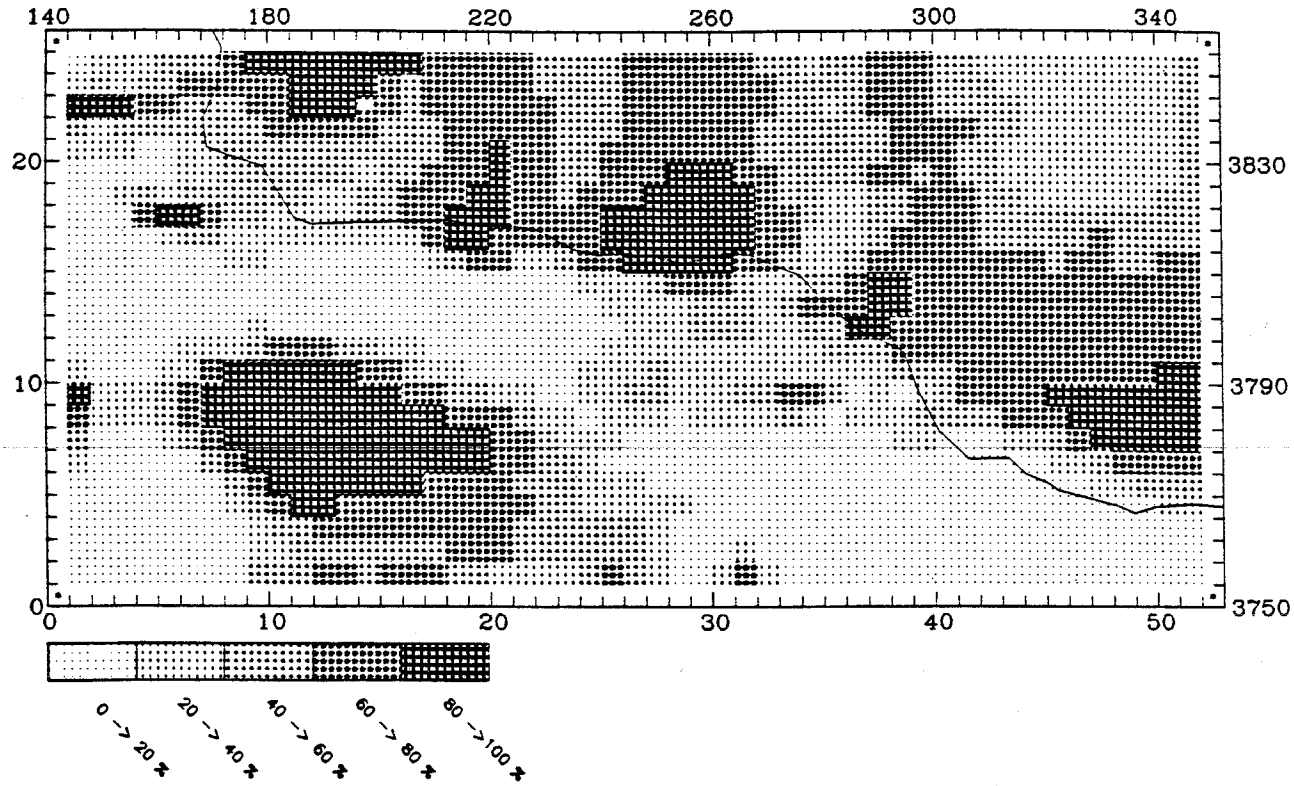

UAM—IV

NOX CONTRIBUTION AT: 1100 September 17 LEVEL 1

MAXIMUM CONTRIBUTION IN CELL (33,16) = 95.98 (%)

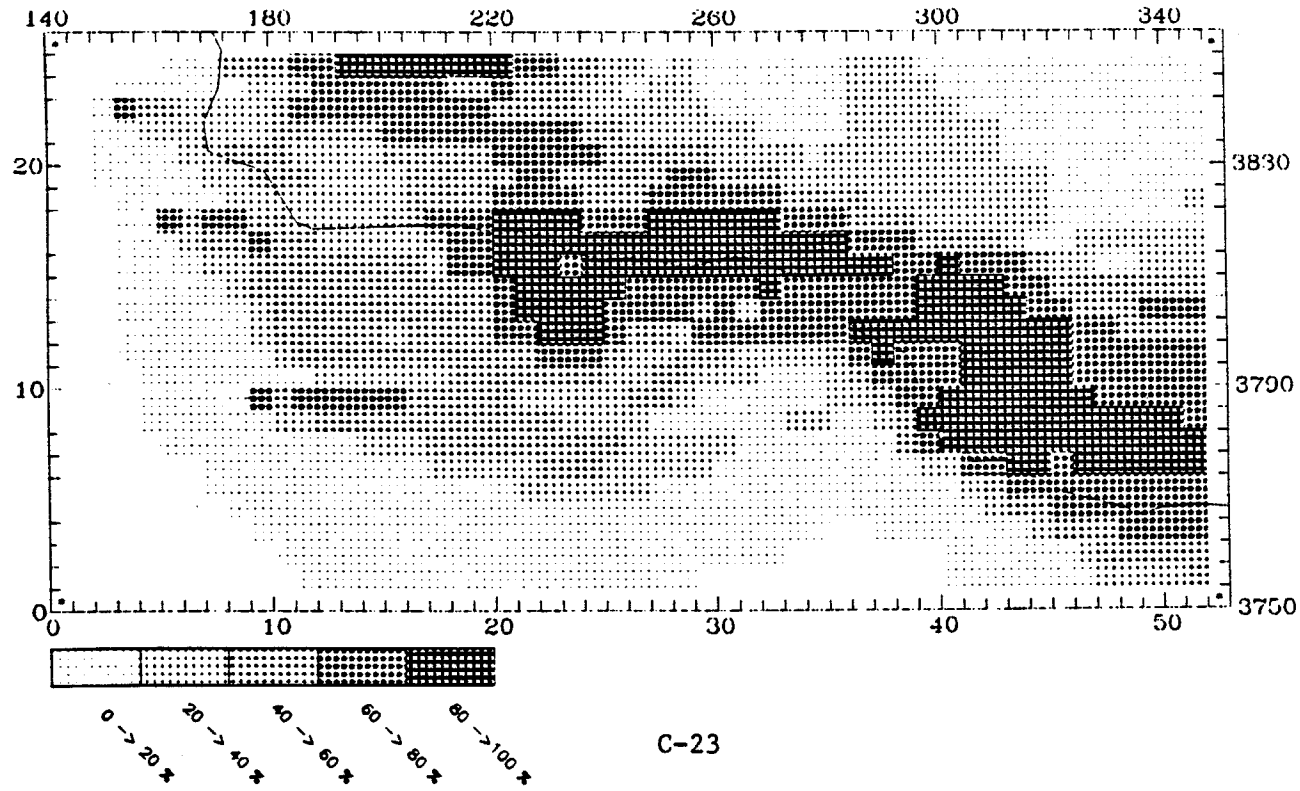

ATHC CONTRIBUTION AT: 1100 September 17 LEVEL 1

MAXIMUM CONTRIBUTION IN CELL (43,10) = 78.33 (%)

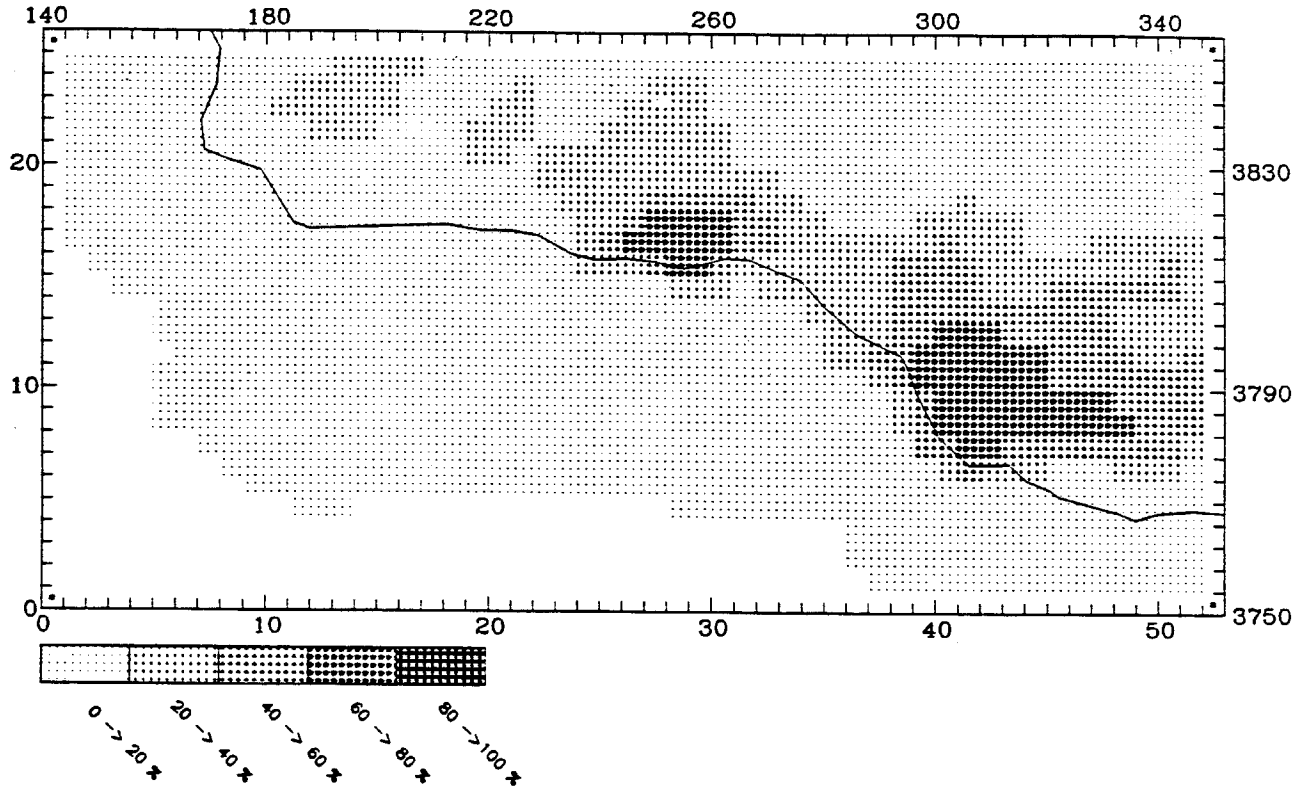

UAM-IV

RHC CONTRIBUTION AT: 1100 September 17 LEVEL 1

MAXIMUM CONTRIBUTION IN CELL (27,15) = 88.91 (%)

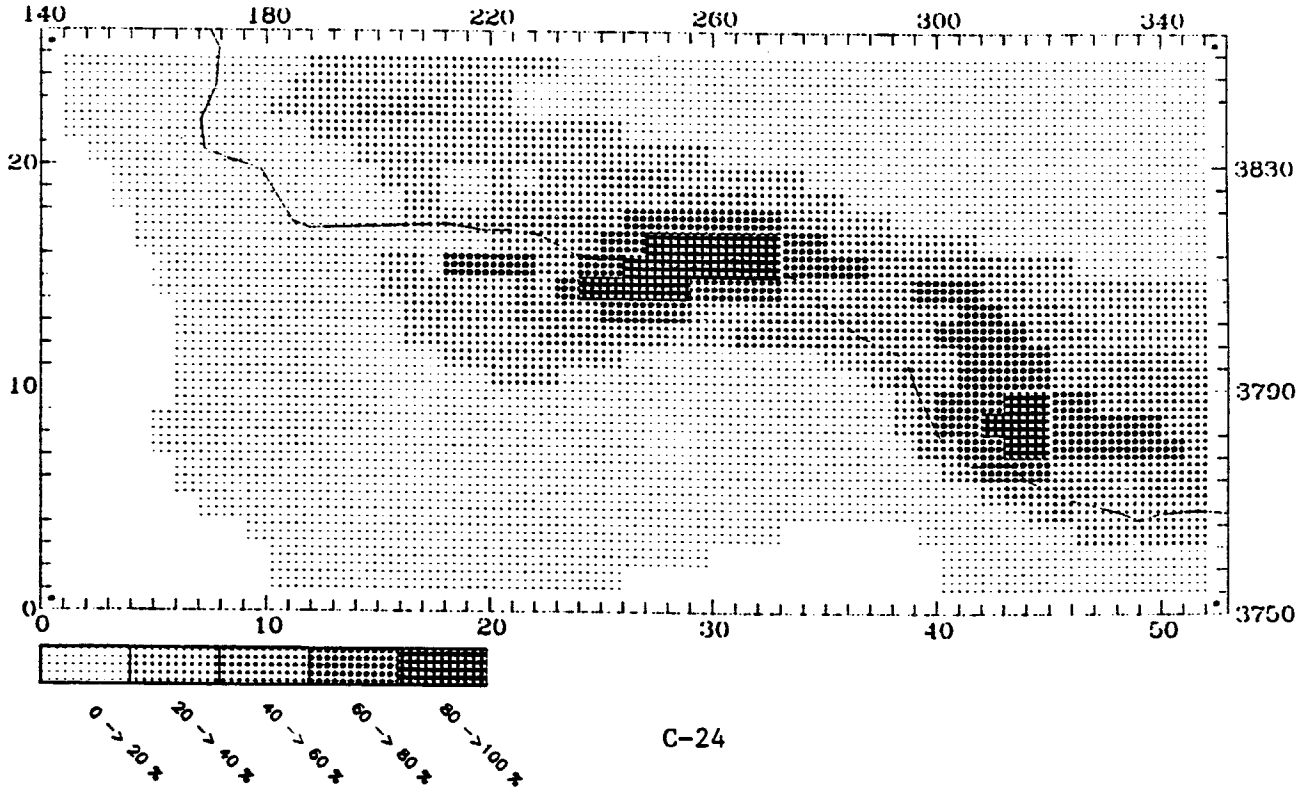

Appendix D

COMPARISON OF CALGRID AND UAM-IV PHOTOCHEMICAL SENSITIVITY AND WEIGHTED-TRACER SIMULATION RESULTS ON 7 AND 17 SEPTEMBER 1984

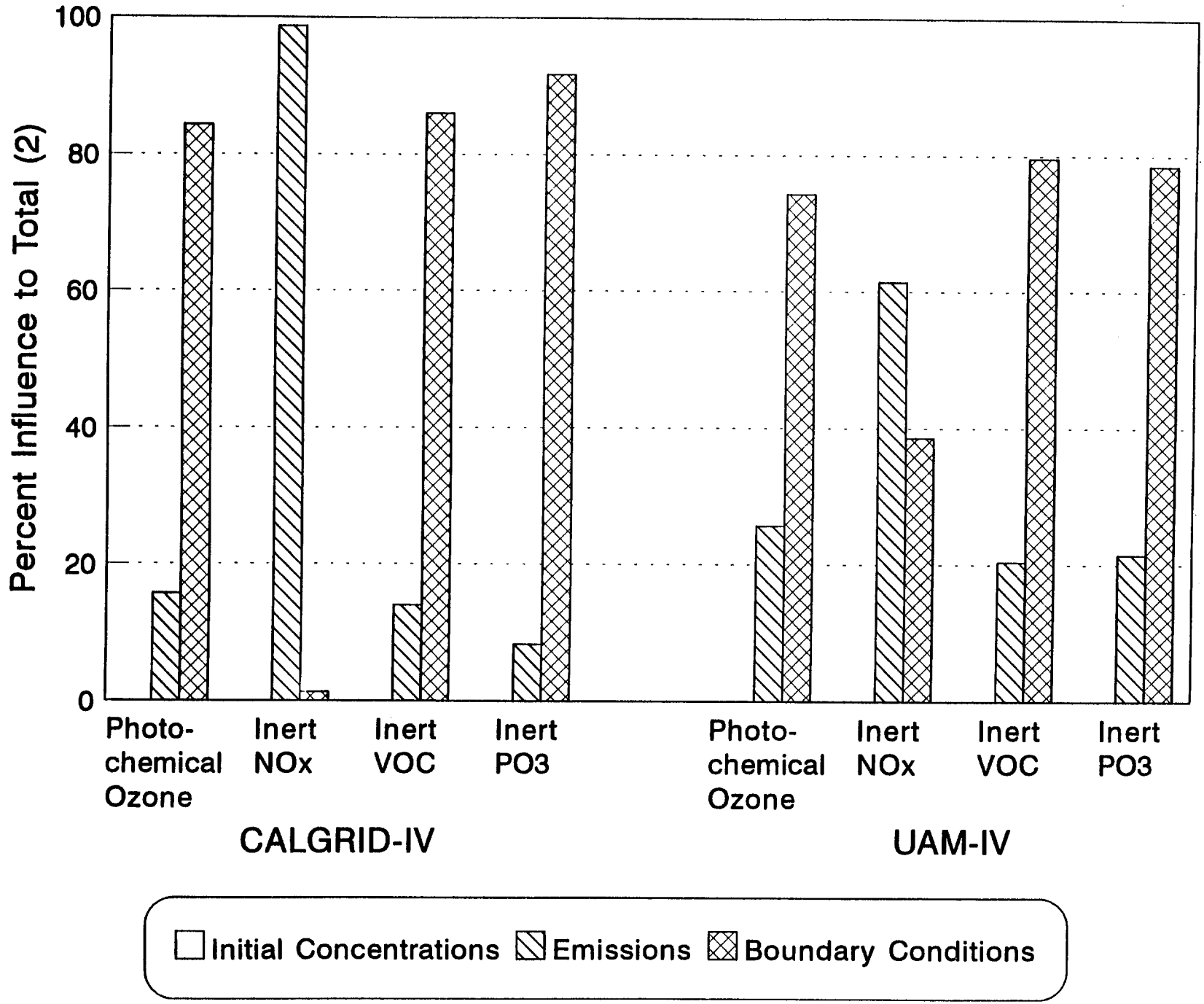

Relative influence of emissions, initial concentrations, and boundary conditions to total for photochemical and inert weighte racer CALGRID-IV and UAM-IV simulation on September 7, 1984, at Santa Ynez ozone monitor.

rem\calgrid8

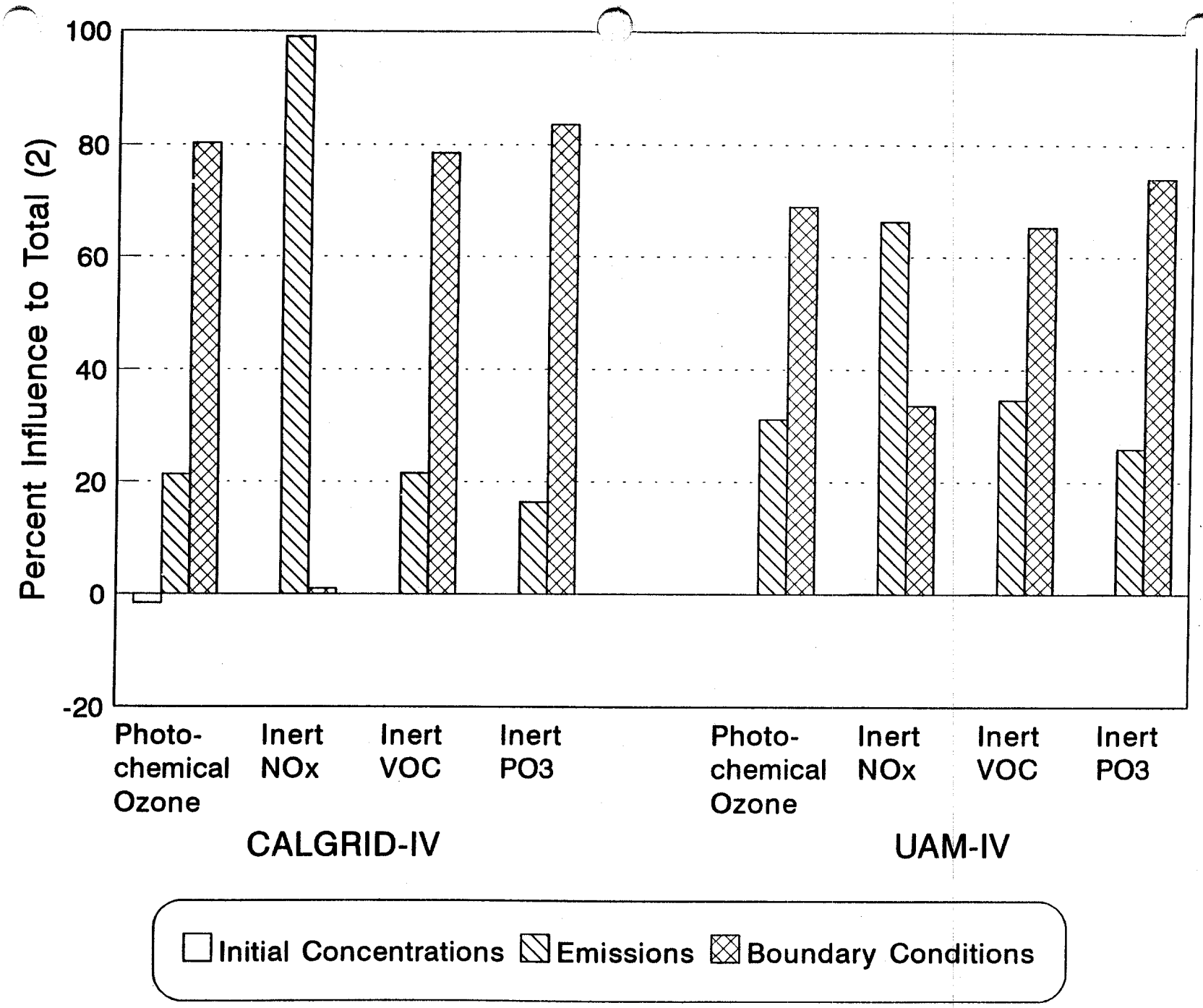

Relative influence of emissions, initial concentrations, and boundary conditions to total for photochemical and inert weighted-tracer CALGRID-IV and UAM-IV simulations on September 17, 1984, at Santa Ynez ozone monitor.

rem\calgrd17

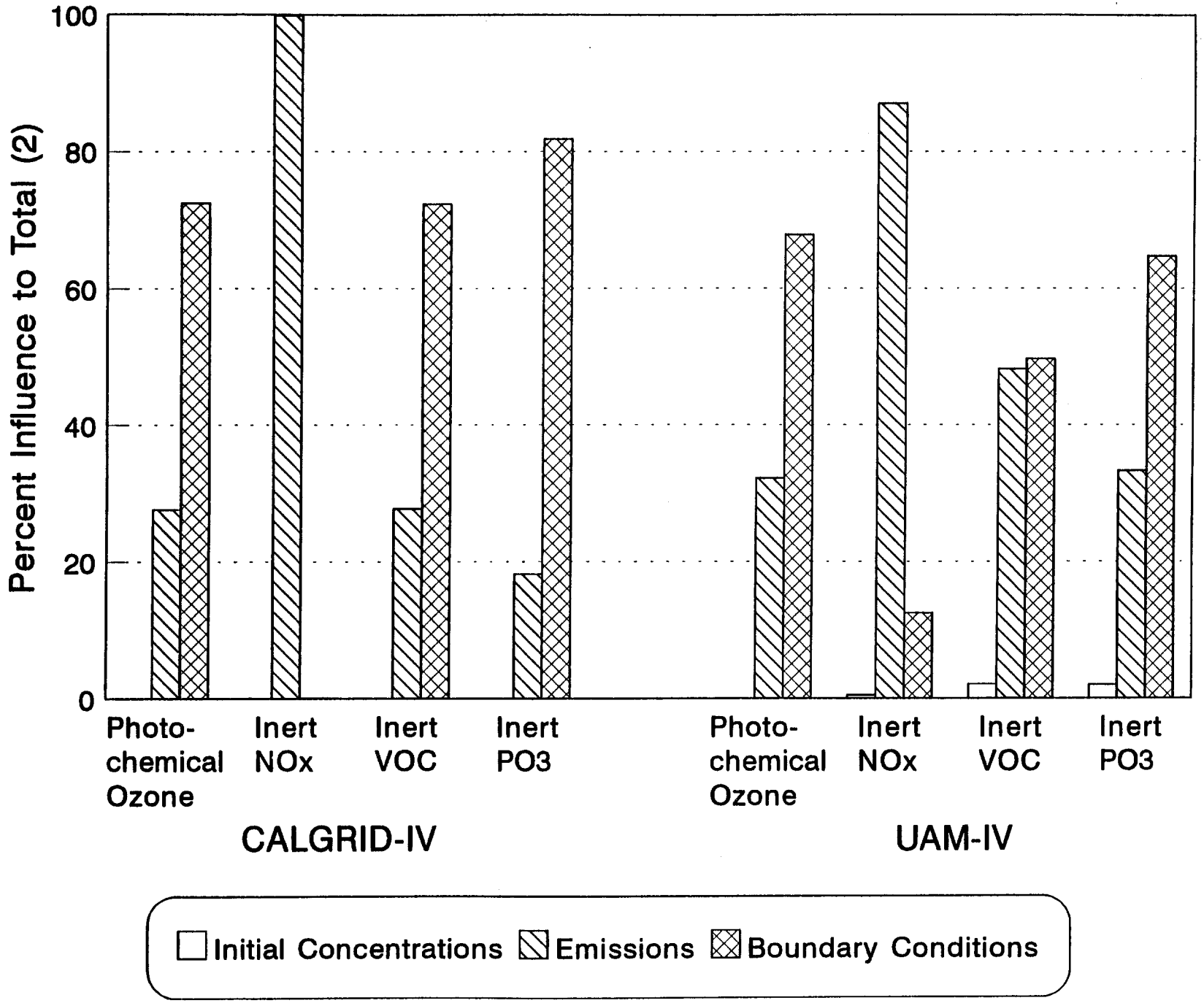

Relative influence of emissions, initial concentrations, and boundary conditions to total for photochemical and inert weighted tracer CALGRID-IV and UAM-IV simulations on September 17, 1984, at Goleta ozone monitor.

rem\calgrd11

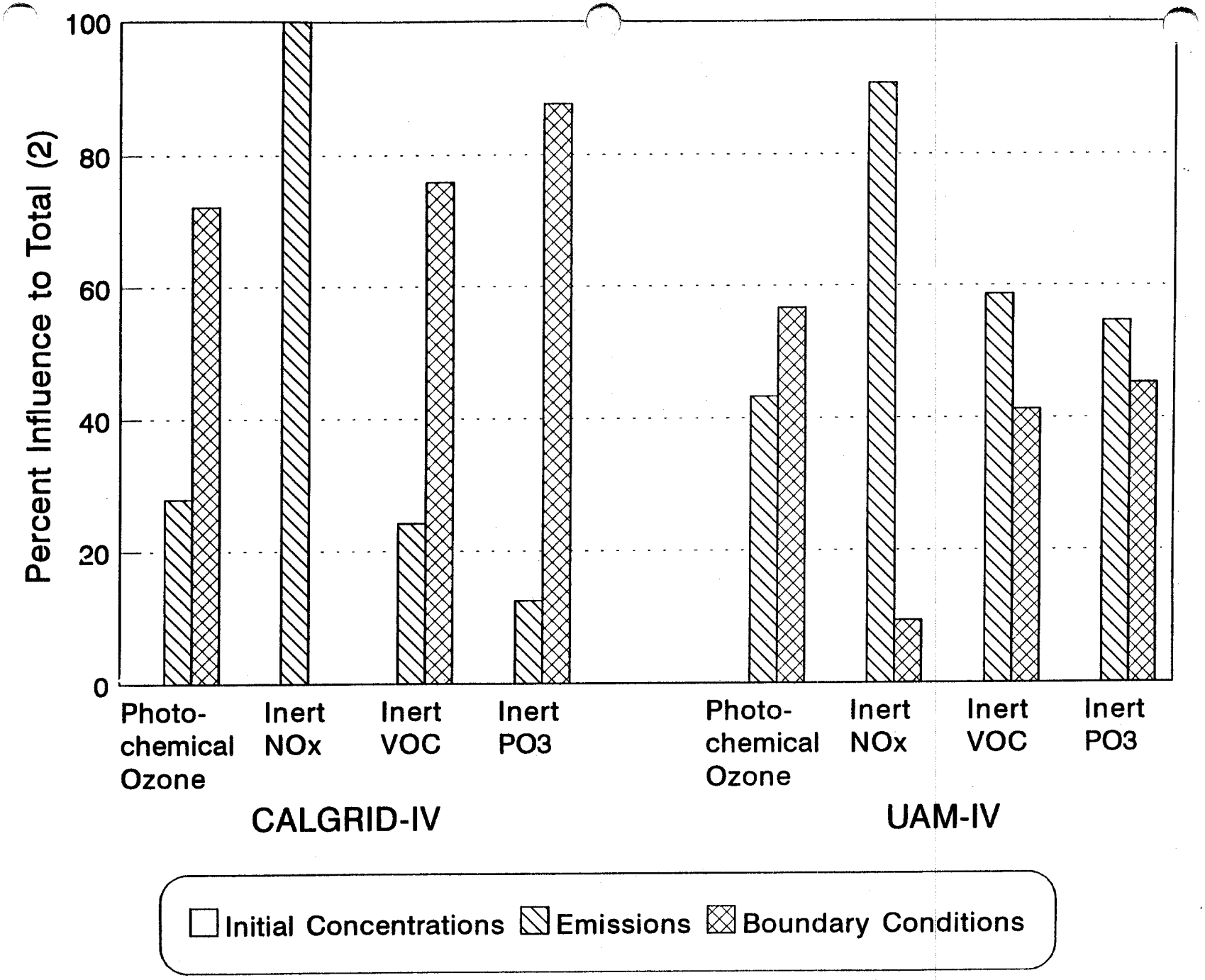

Relative influence of emissions, initial concentrations, and boundary conditions to total for photochemical and inert weighted-tracer CALGRID-IV and UAM-IV simulations on September 7, 1984, at Goleta ozone monitor.

rem\calgrid2

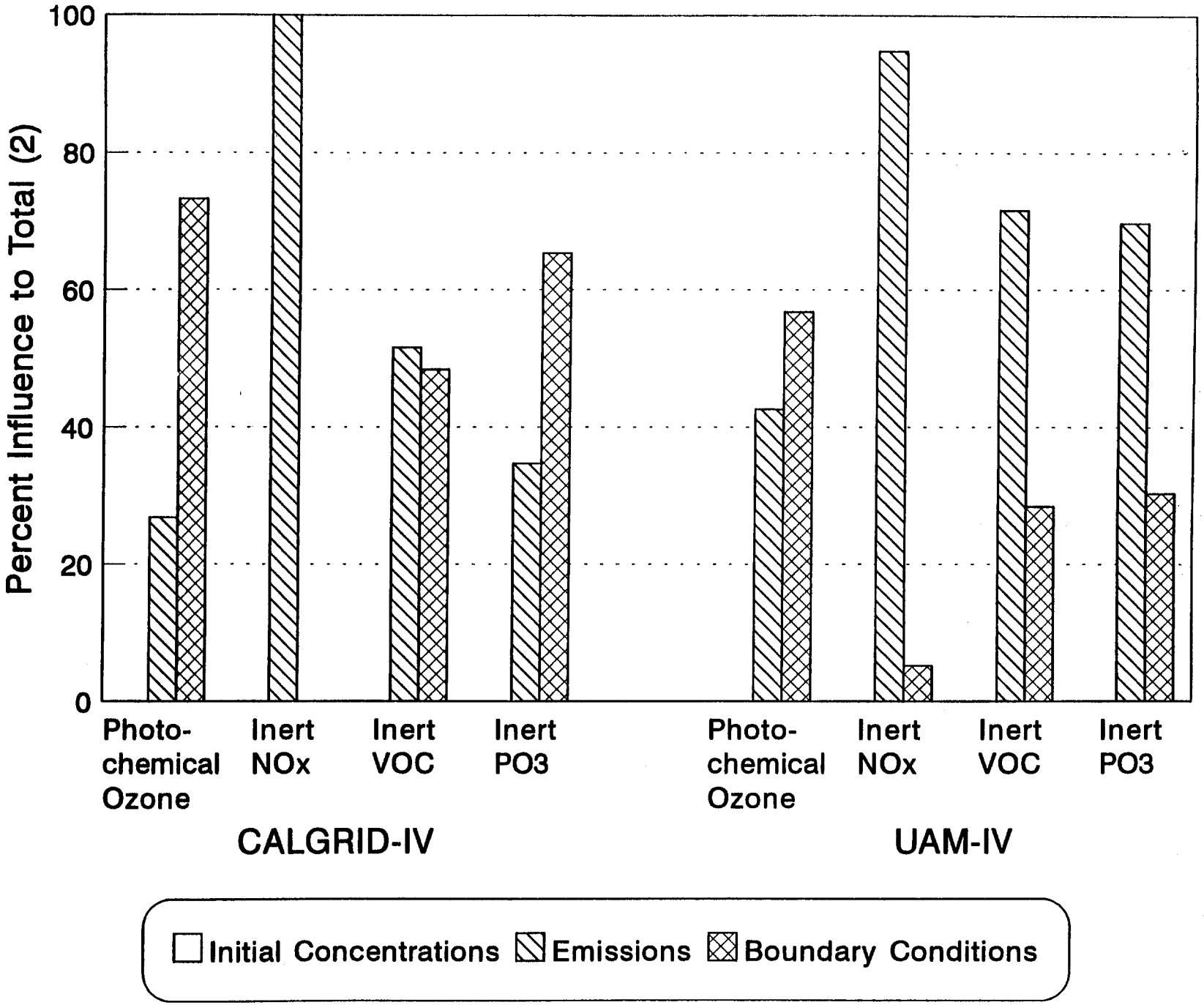

Relative influence of emissions, initial concentrations, and boundary conditions to total for photochemical and inert weight -tracer CALGRID-IV and UAM-IV simulation on September 7, 1984, at Santa Barbara ozone m or.

rem\calgrid

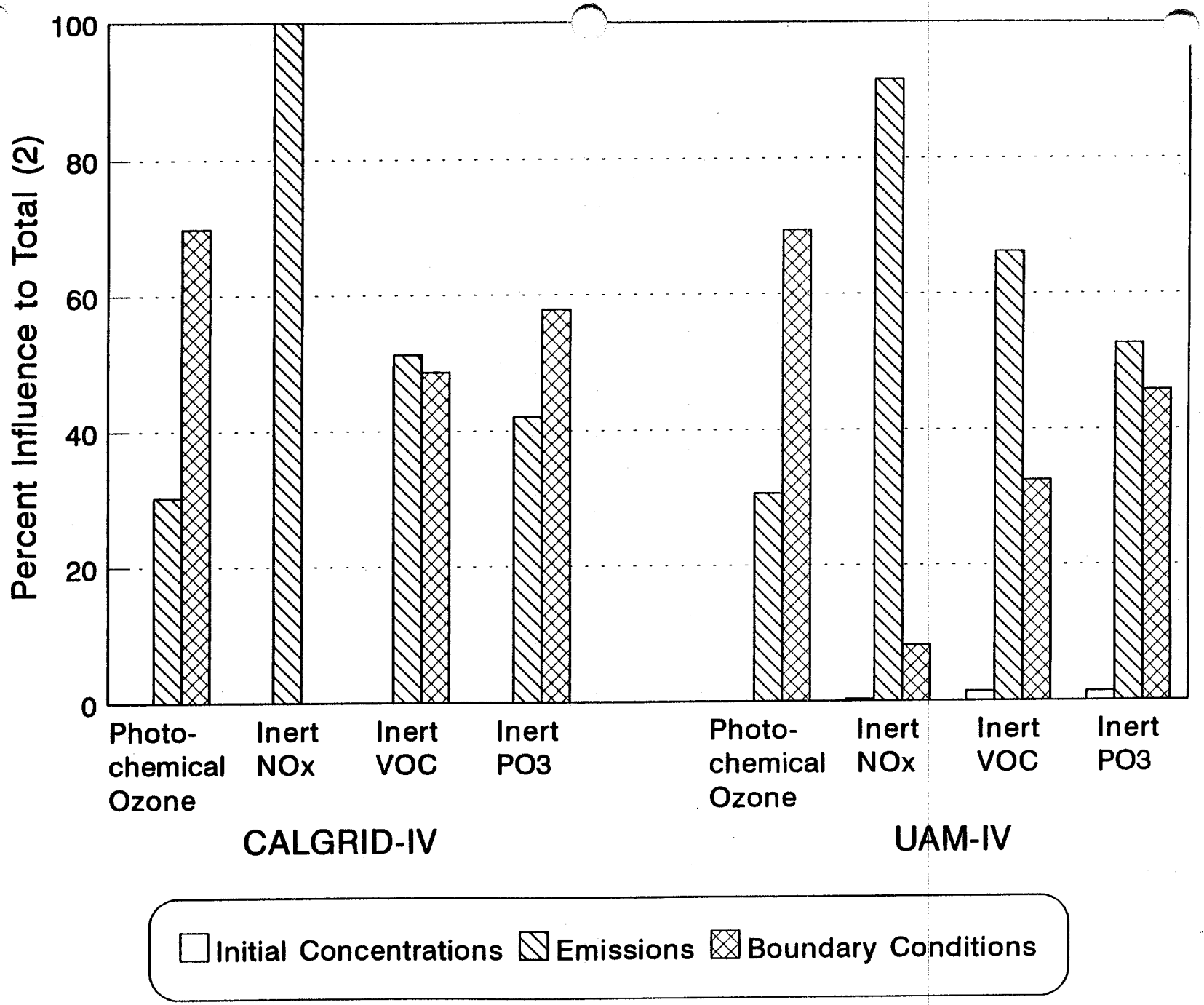

Relative influence of emissions, initial concentrations, and boundary conditions to total for photochemical and inert weighted-tracer CALGRID-IV and UAM-IV simulations on September 17, 1984, at Santa Barbara ozone monitor.

rem\calgrd15

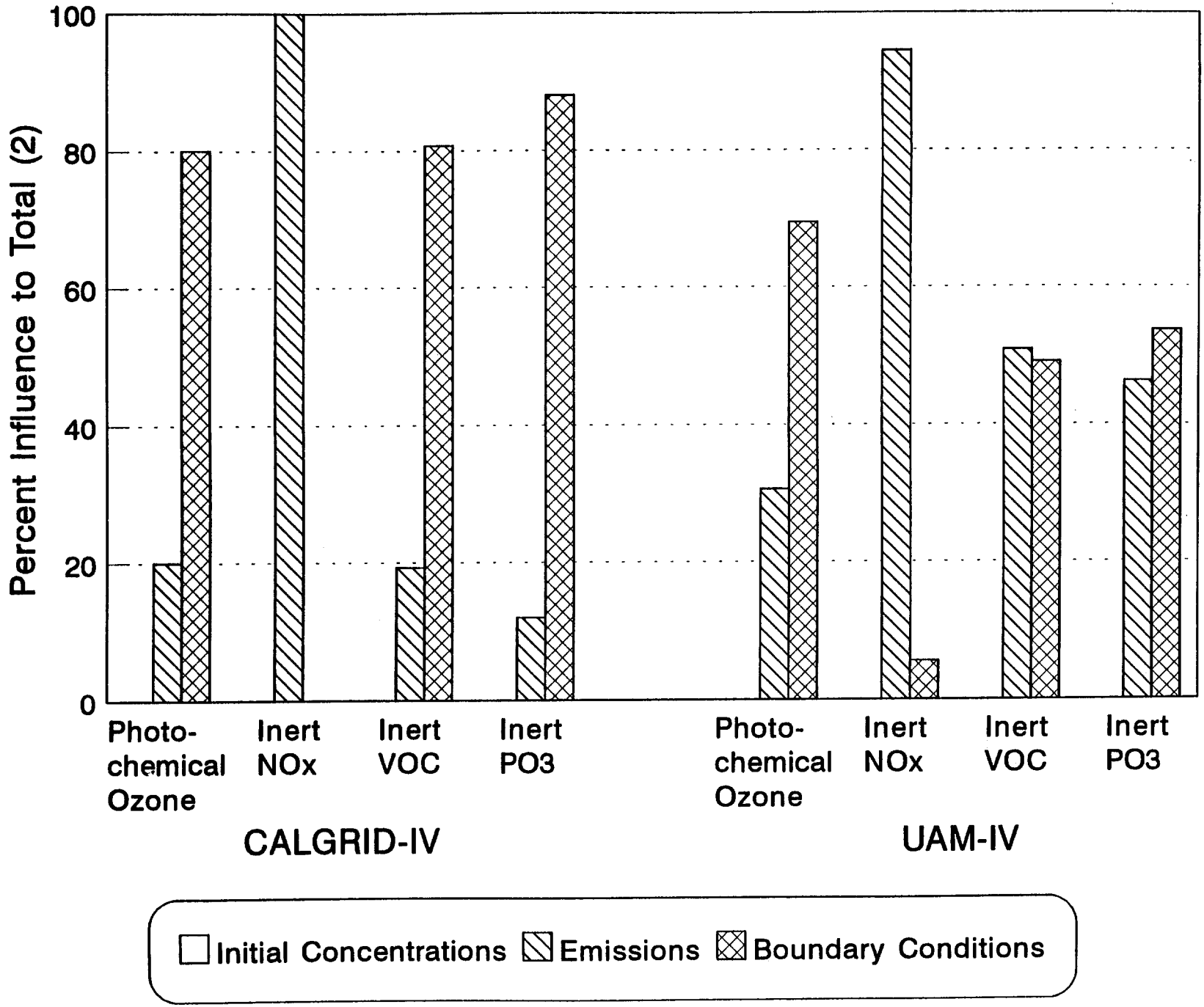

Relative influence of emissions, initial concentrations, and boundary conditions to total for photochemical and inert weight '-tracer CALGRID-IV and UAM-IV simulatio on September 7, 1984, at Casitas ozone monitor.

rem\calgrid1

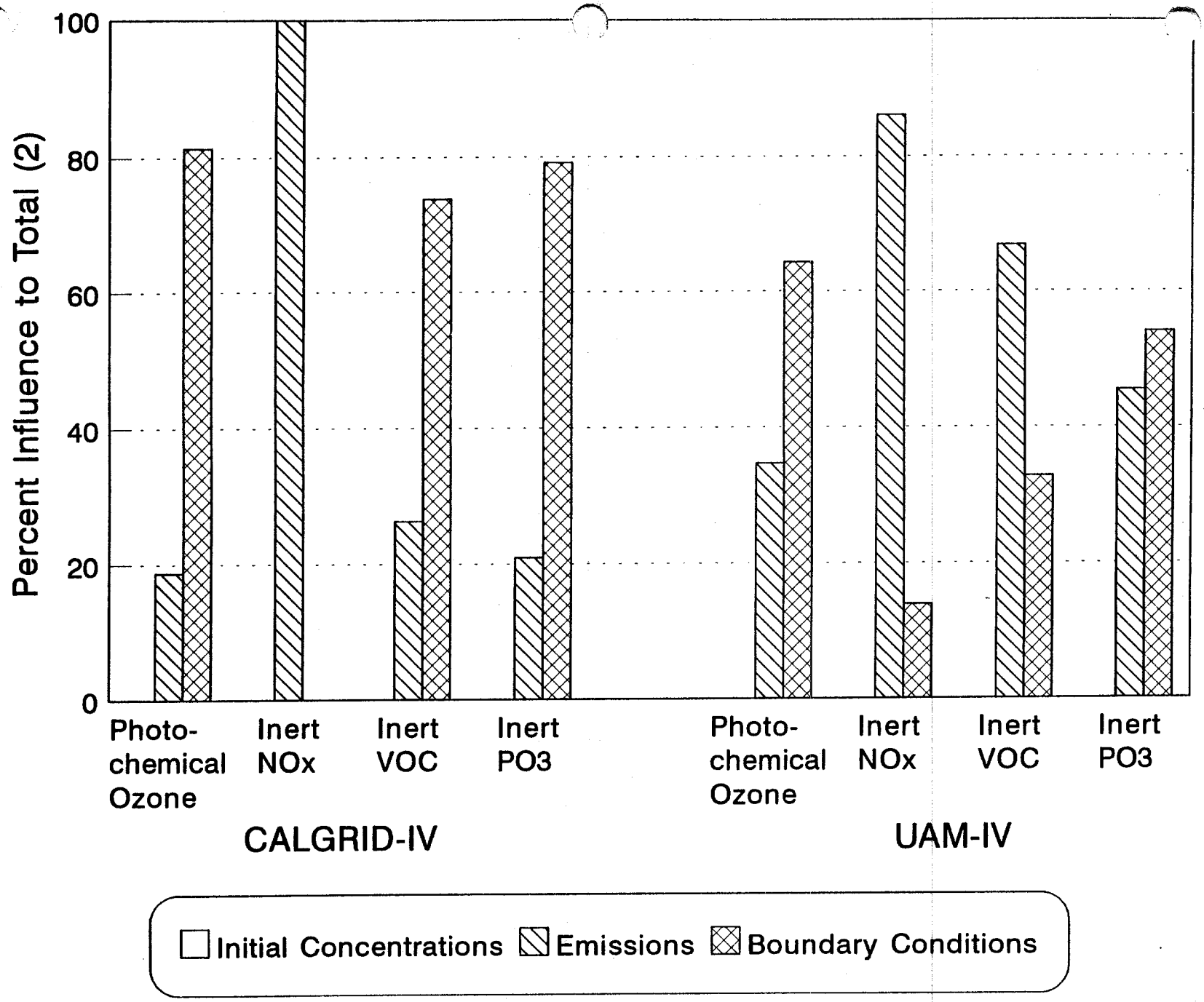

Relative influence of emissions, initial concentrations, and boundary conditions to total for photochemical and inert weighted-tracer CALGRID-IV and UAM-IV simulations on September 17, 1984, at Casitas ozone monitor.

rem\calgrd10

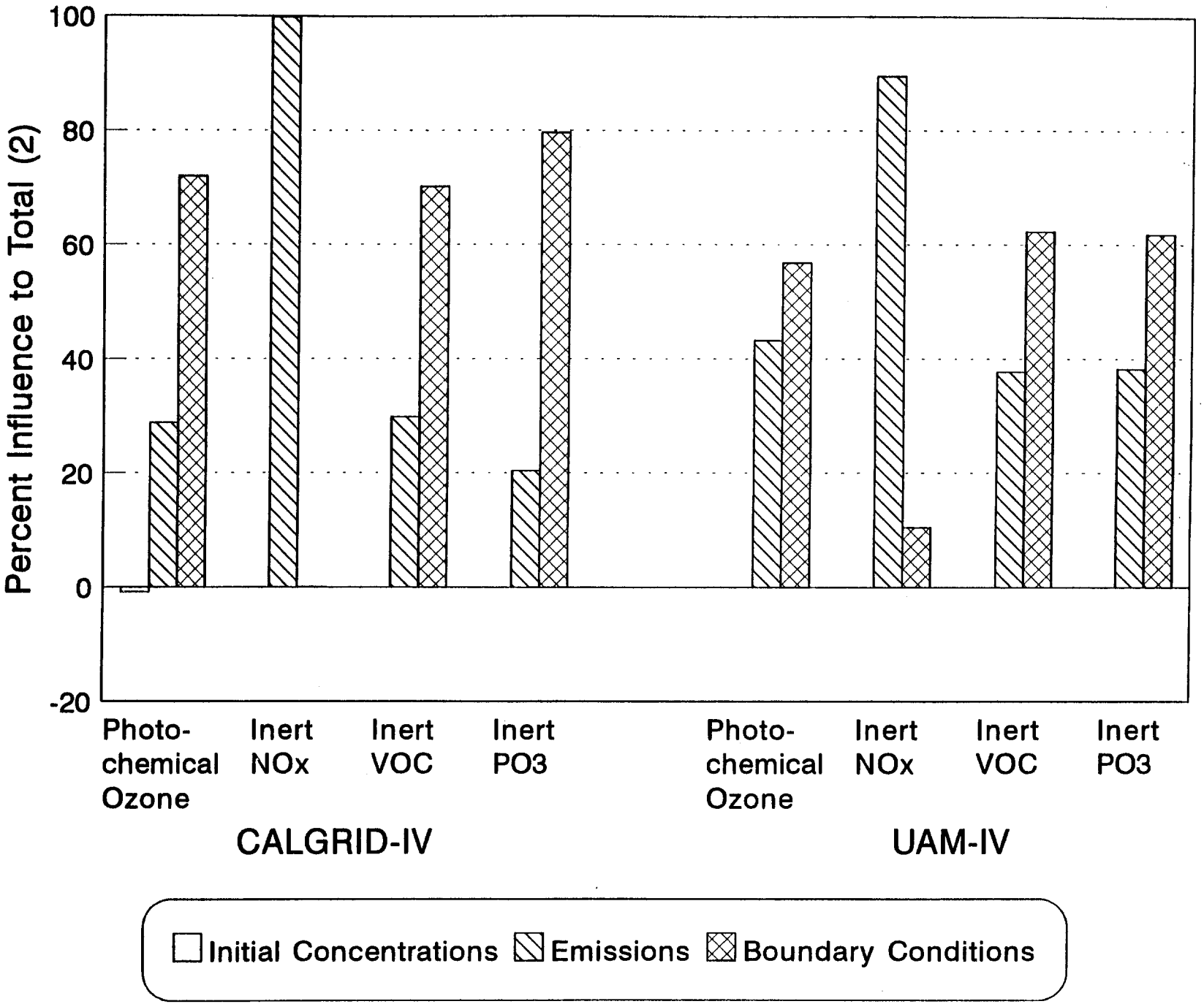

Relative influence of emissions, initial concentrations, and boundary conditions to total for photochemical and inert weight '-tracer CALGRID-IV and UAM-IV simulatio on September 7, 1984, at Ojai ozone monitor.

rem\calgrid4

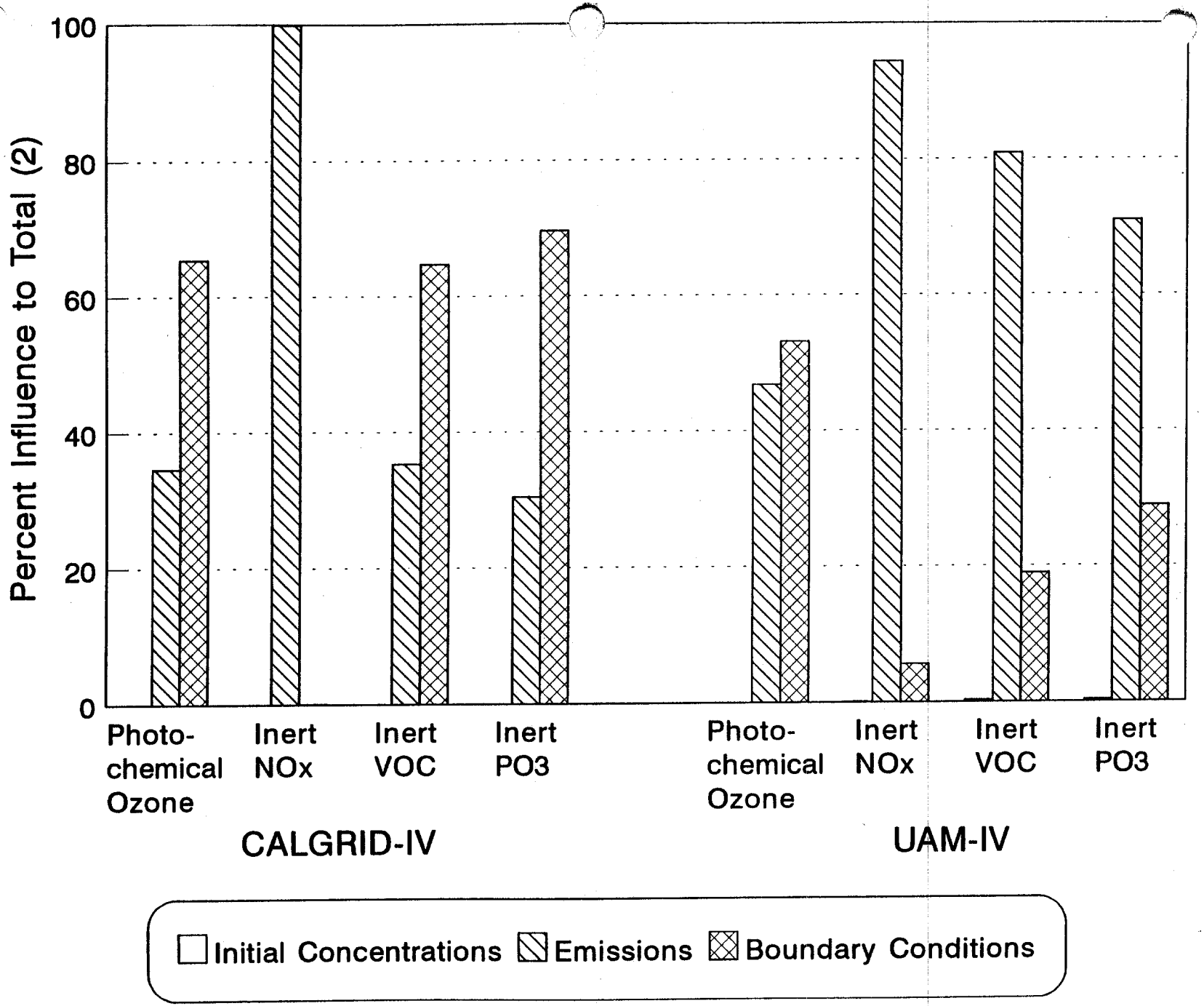

Relative influence of emissions, initial concentrations, and boundary conditions to total for photochemical and inert weighted-tracer CALGRID-IV and UAM-IV simulations on September 17, 1984, at Ojai ozone monitor.

rem\calgrd13

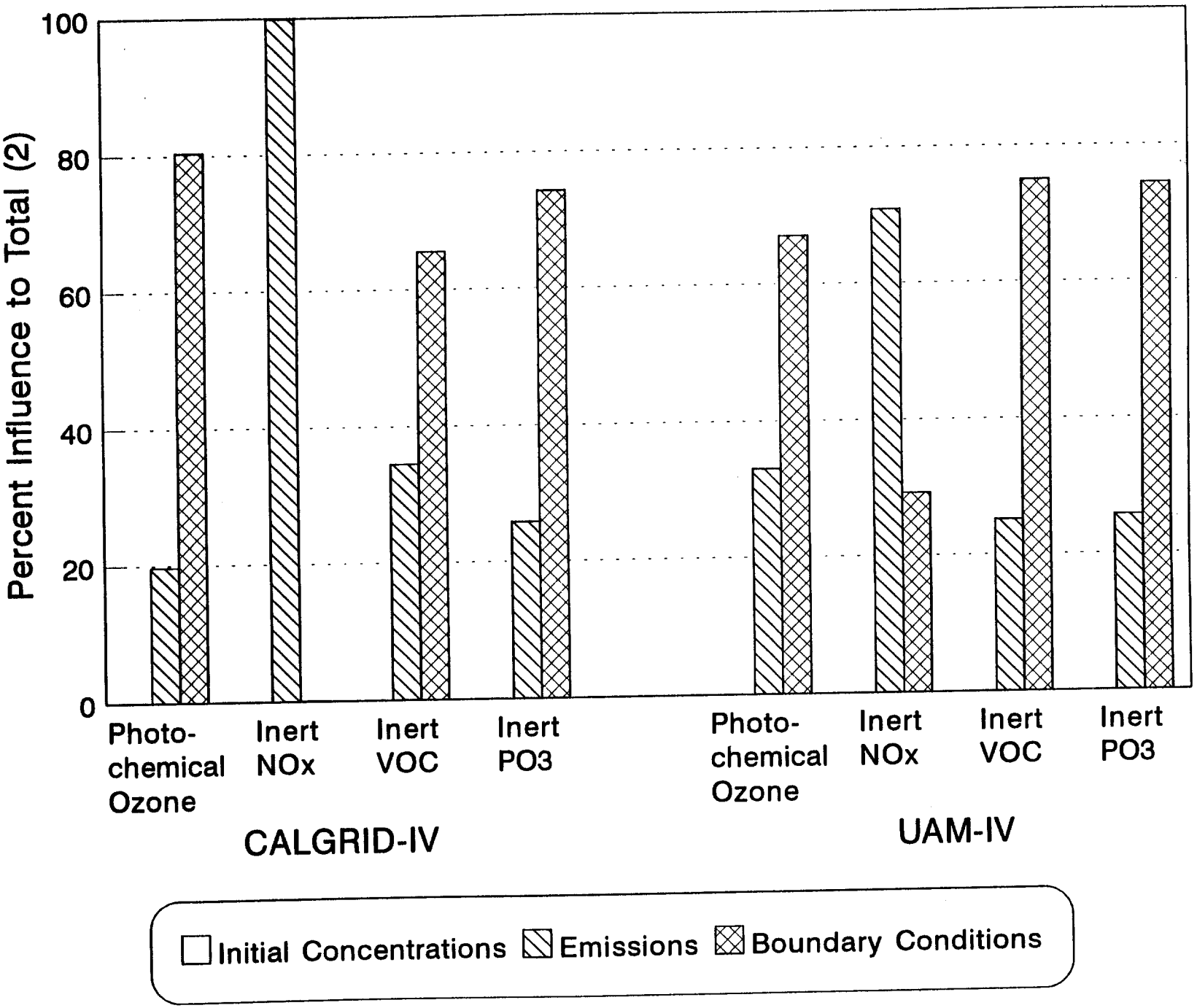

Relative influence of emissions, initial concentrations, and boundary conditions to total for photochemical and inert weigh' d-tracer CALGRID-IV and UAM-IV simulatic s on September 7, 1984, at Ventura ozone monitor.

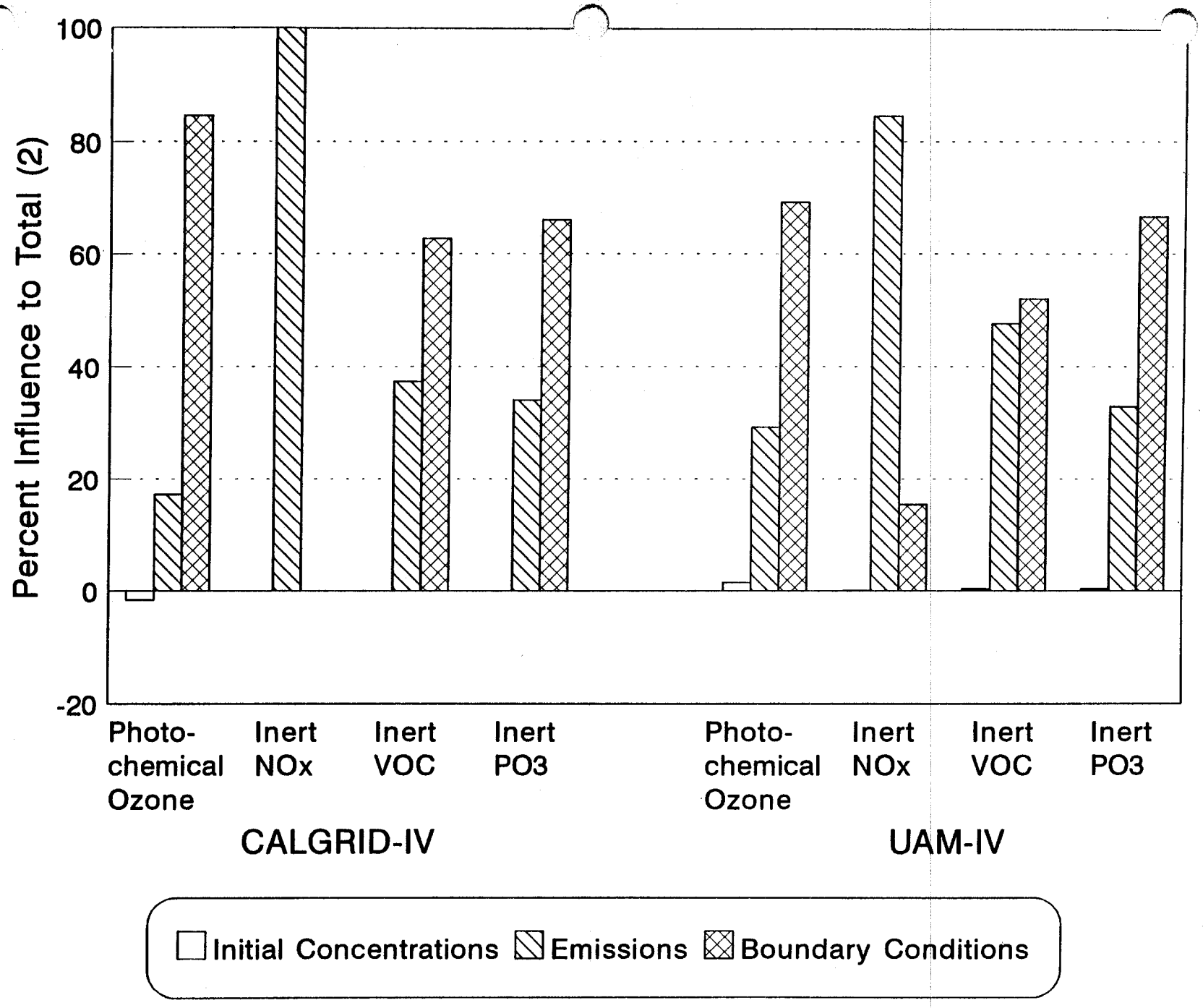

Relative influence of emissions, initial concentrations, and boundary conditions to total for photochemical and inert weighted-tracer CALGRID-IV and UAM-IV simulations on September 17, 1984, at Ventura ozone monitor.

rem\calgrd18

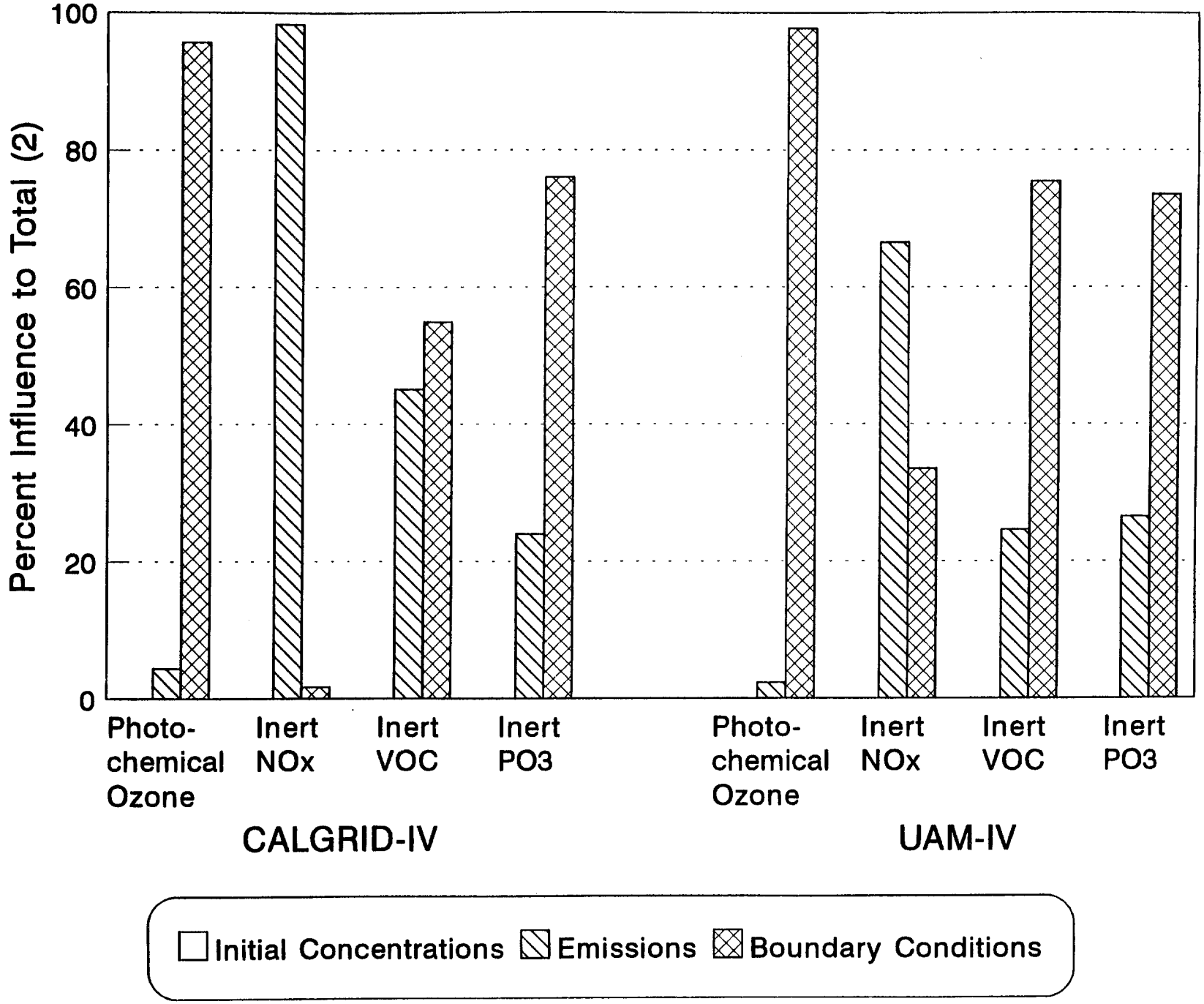

Relative influence of emissions, initial concentrations, and boundary conditions to total for photochemical and inert weighte tracer CALGRID-IV and UAM-IV simulation on September 7, 1984, at Piru ozone monitor.

rem\calgrid5

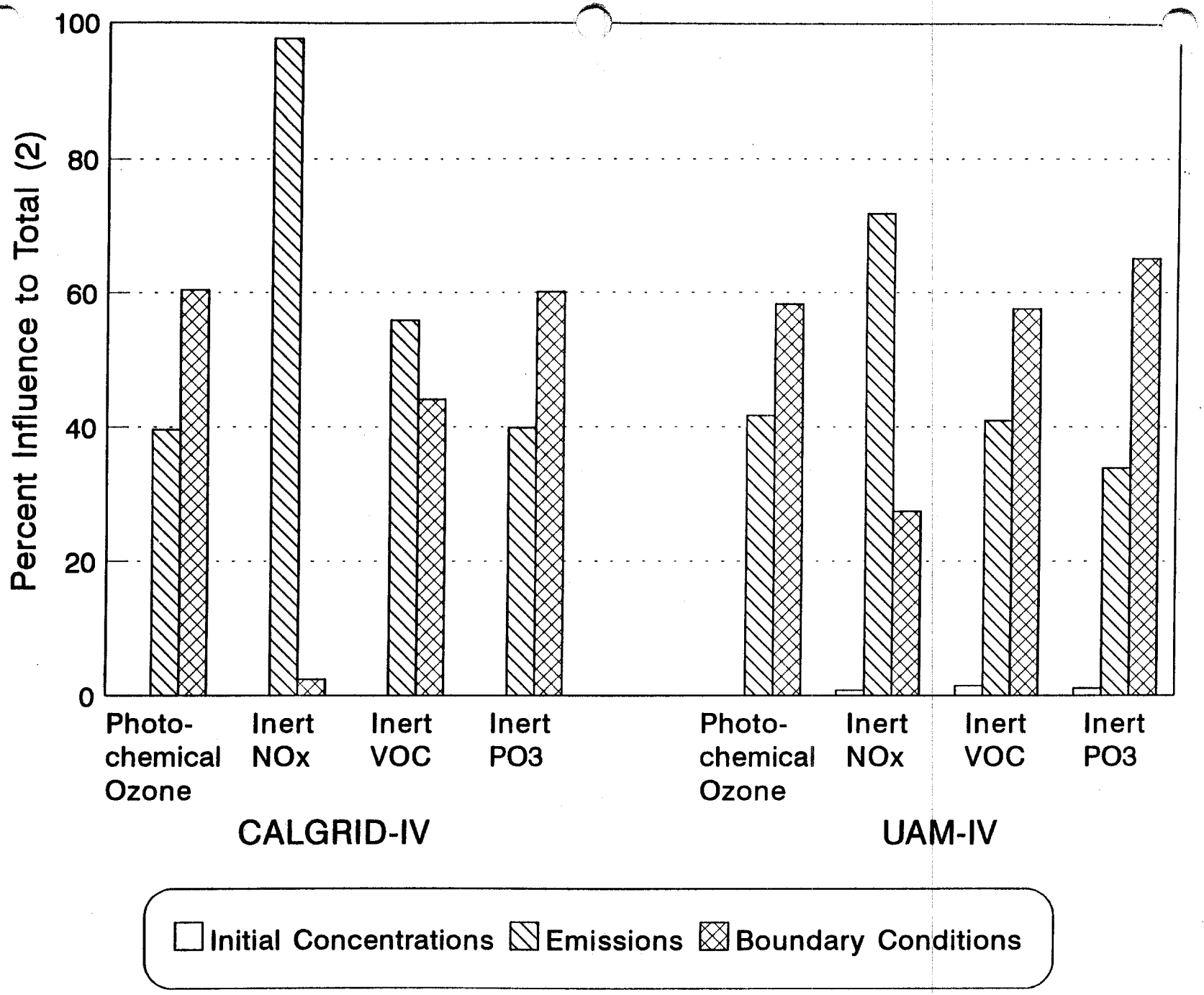

Relative influence of emissions, initial concentrations, and boundary conditions to total for photochemical and inert weighted-tracer CALGRID-IV and UAM-IV simulations on September 17, 1984, at Piru ozone monitor.

rem\calgrd14

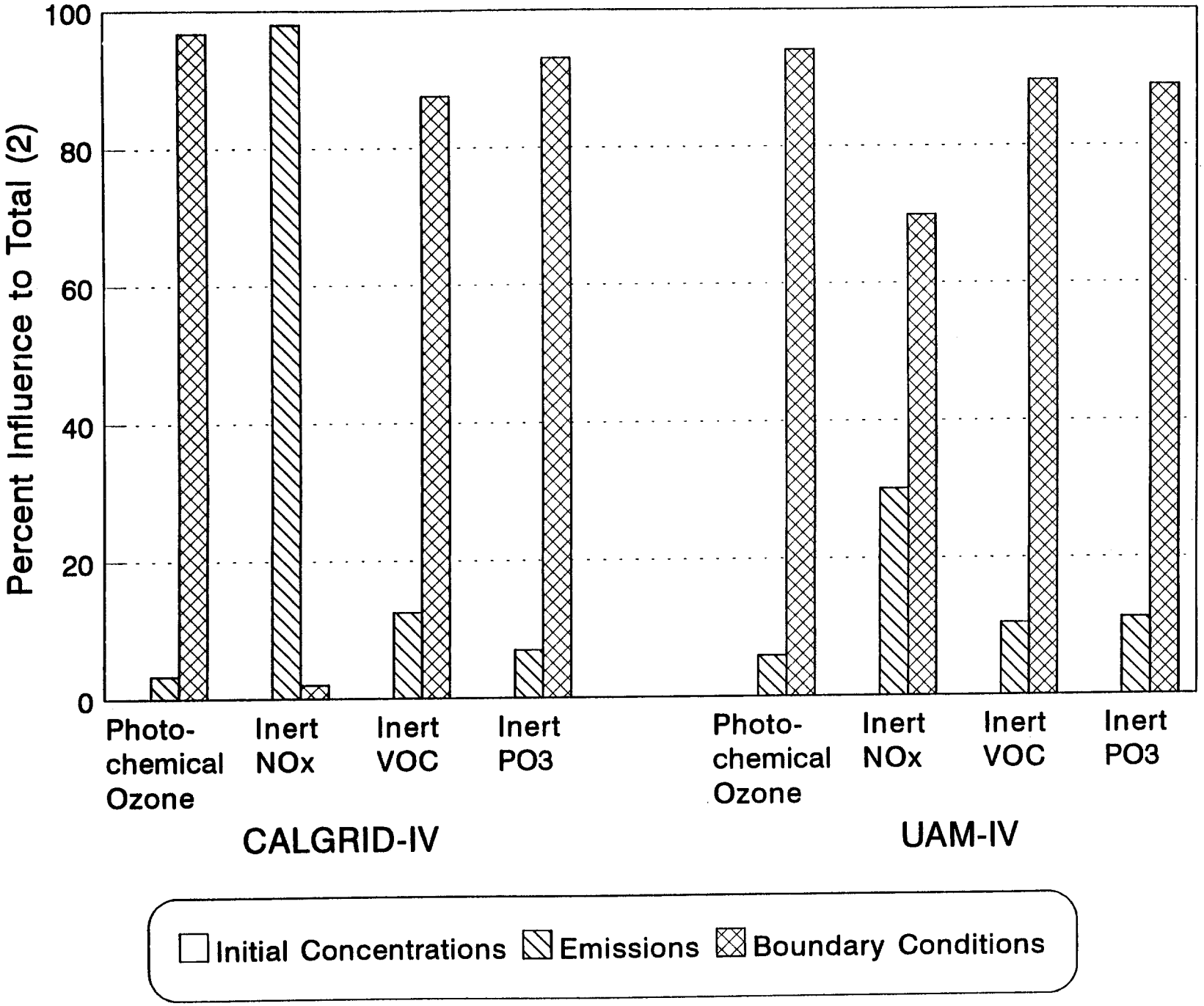

Relative influence of emissions, initial concentrations, and boundary conditions to total for photochemical and inert weighted-tracer CALGRID-IV and UAM-IV simulations on September 7, 1984, at Simi Valley ozone monitor.

rem\calgrid7

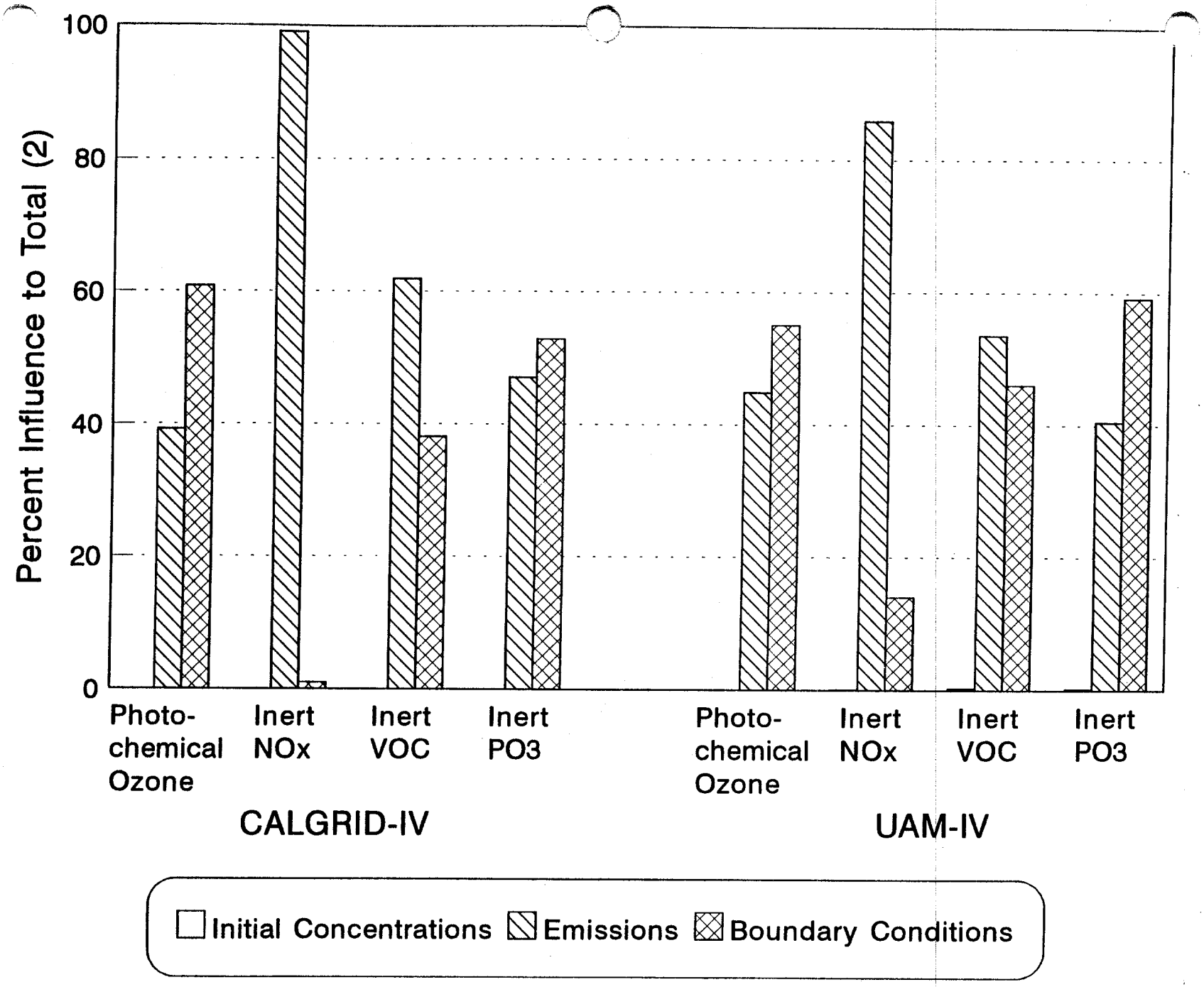

Relative influence of emissions, initial concentrations, and boundary conditions to total for photochemical and inert weighted-tracer CALGRID-IV and UAM-IV simulations on September 17, 1984, at Simi Valley ozone monitor.

rem\calgrd16

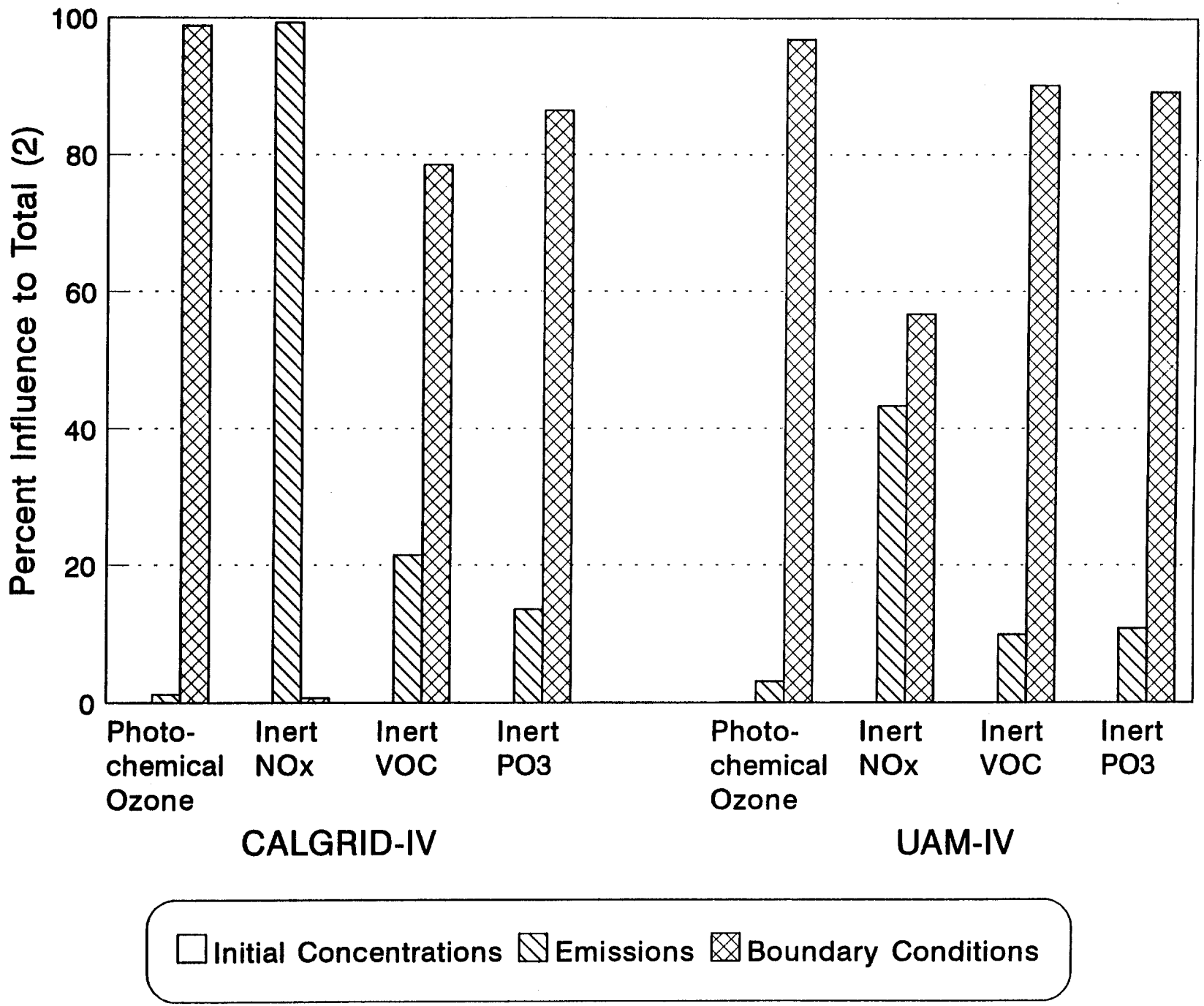

Relative influence of emissions, initial concentrations, and boundary conditions to total for photochemical and inert weighte racer CALGRID-IV and UAM-IV simulation on September 7, 1984, at Thousand Oaks ozon monitor.

rem\calgrid3

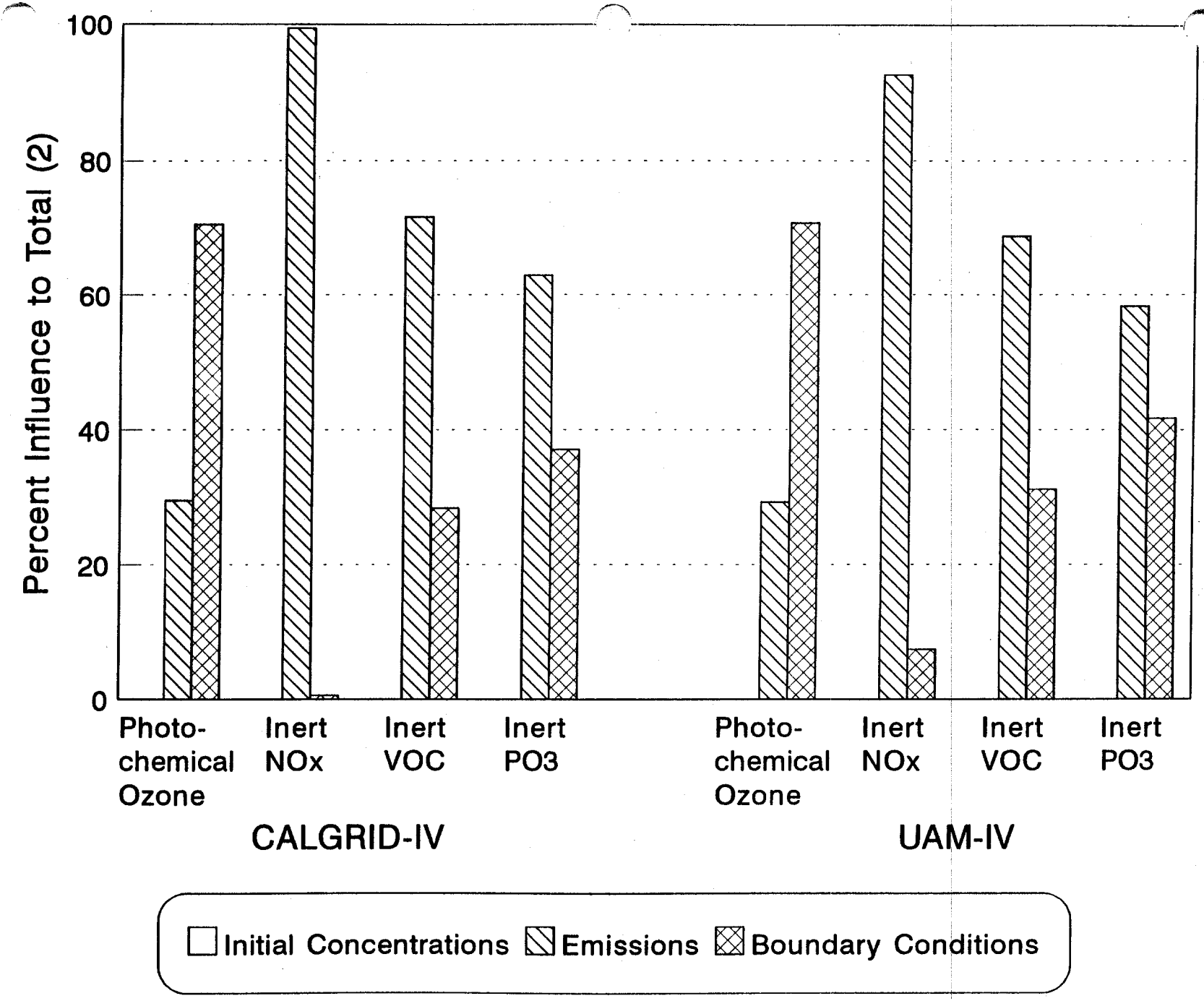

Relative influence of emissions, initial concentrations, and boundary conditions to total for photochemical and inert weighted-tracer CALGRID-IV and UAM-IV simulations on September 17, 1984, at Thousand Oaks ozone monitor.

rem\calgrd12

Appendix E

EMISSION INVENTORIES USED IN THE UAM-IV FOR 5 SEPTEMBER 1984

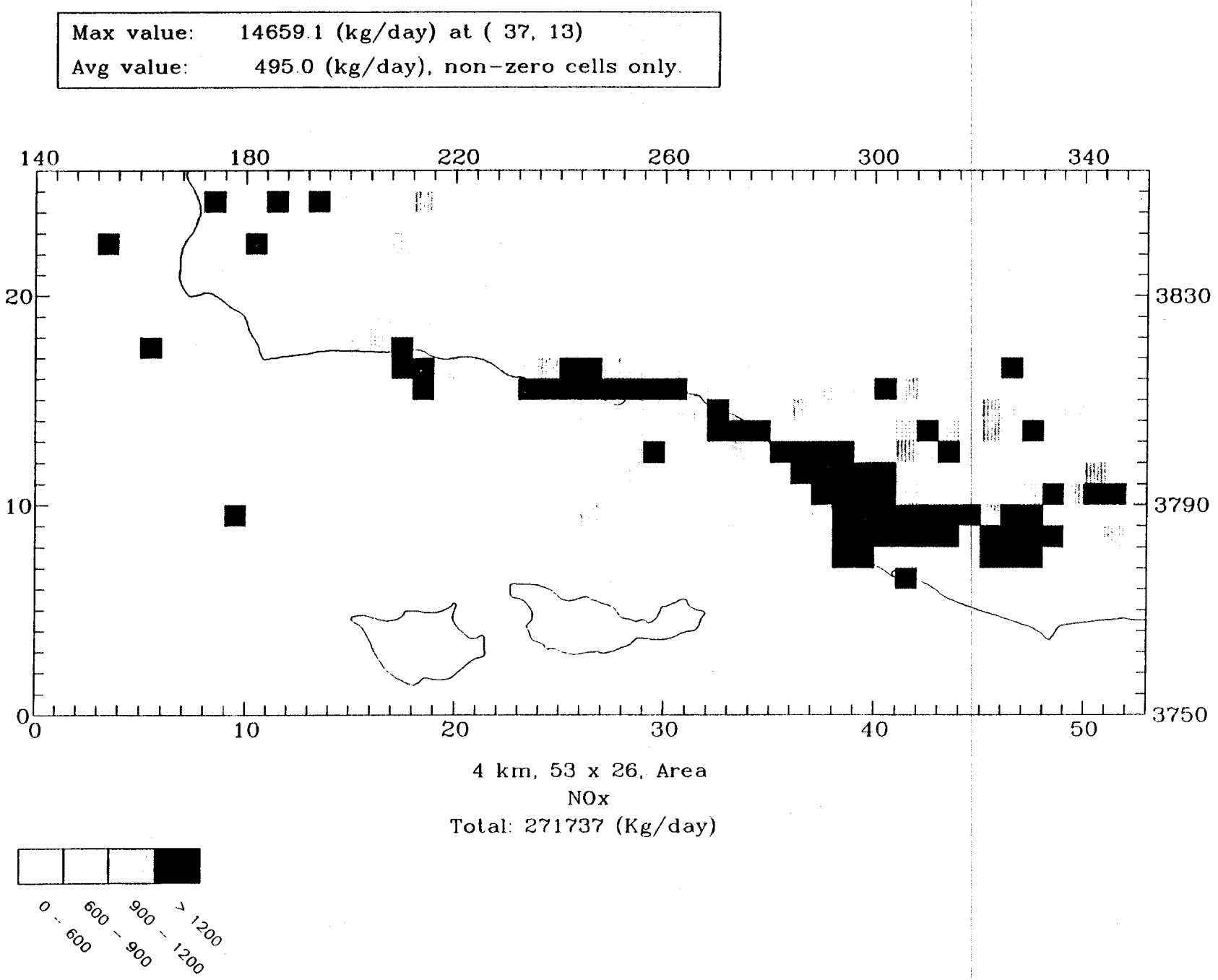
Max value: 14659.1 (kg/day) at (37, 13)
Avg value: 495.0 (kg/day), non-zero cells only.
140
180
220
260
300
340
20
10
0
3830
3790
3750
0
10
20
30
40
50
E-1
4 km, 53 x 26, Area
NOx
Total: 271737 (Kg/day)
0 - 600
600 - 900
900 - 1200
> 1200

Max value:	19901.4 (kg/day) at (24, 15)
Avg value:	665.5 (kg/day), non-zero cells only.

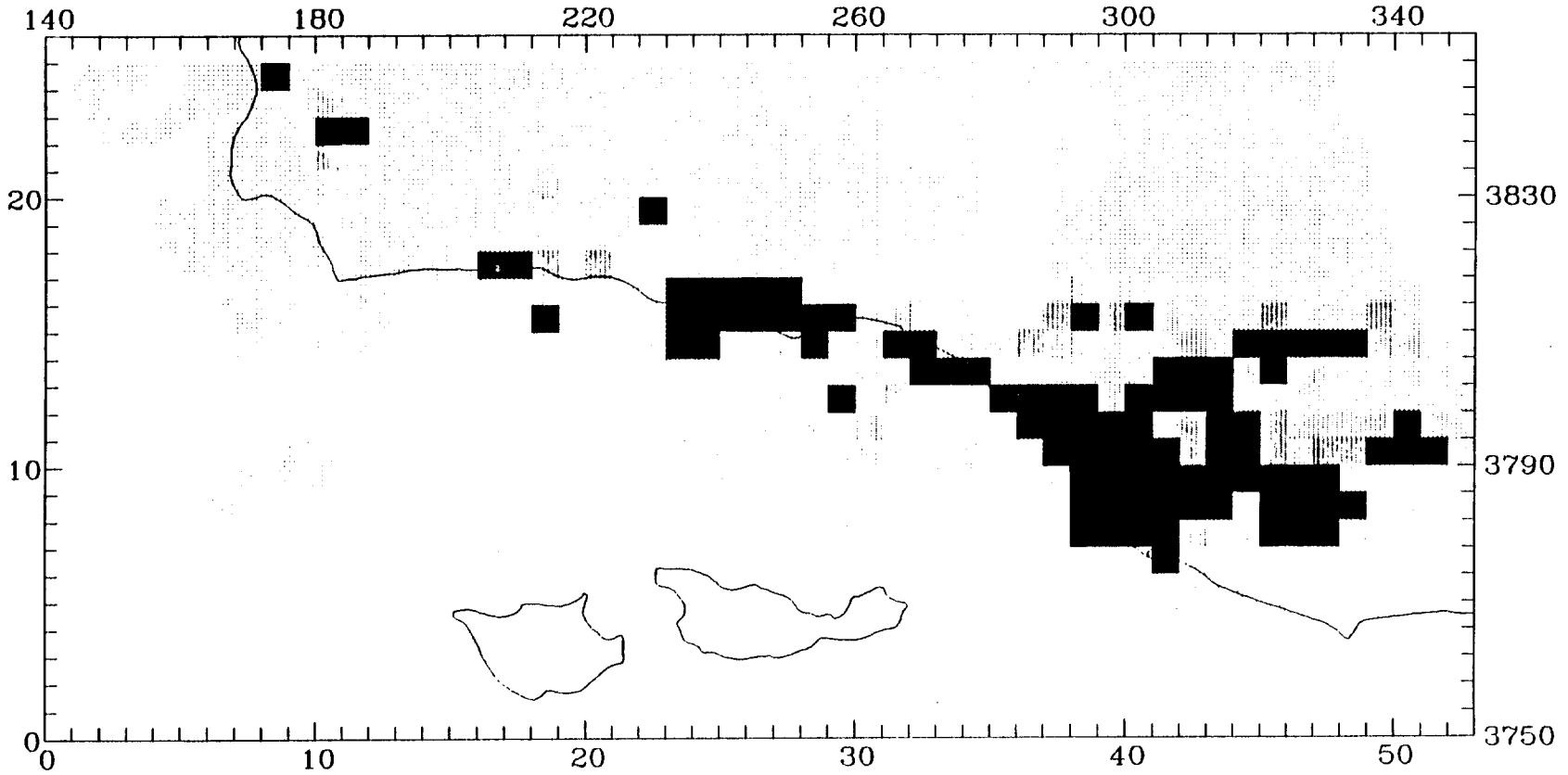

4 km, 53 x 26, Area
RHC
Total: 457881 (Kg/day)

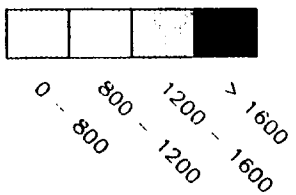

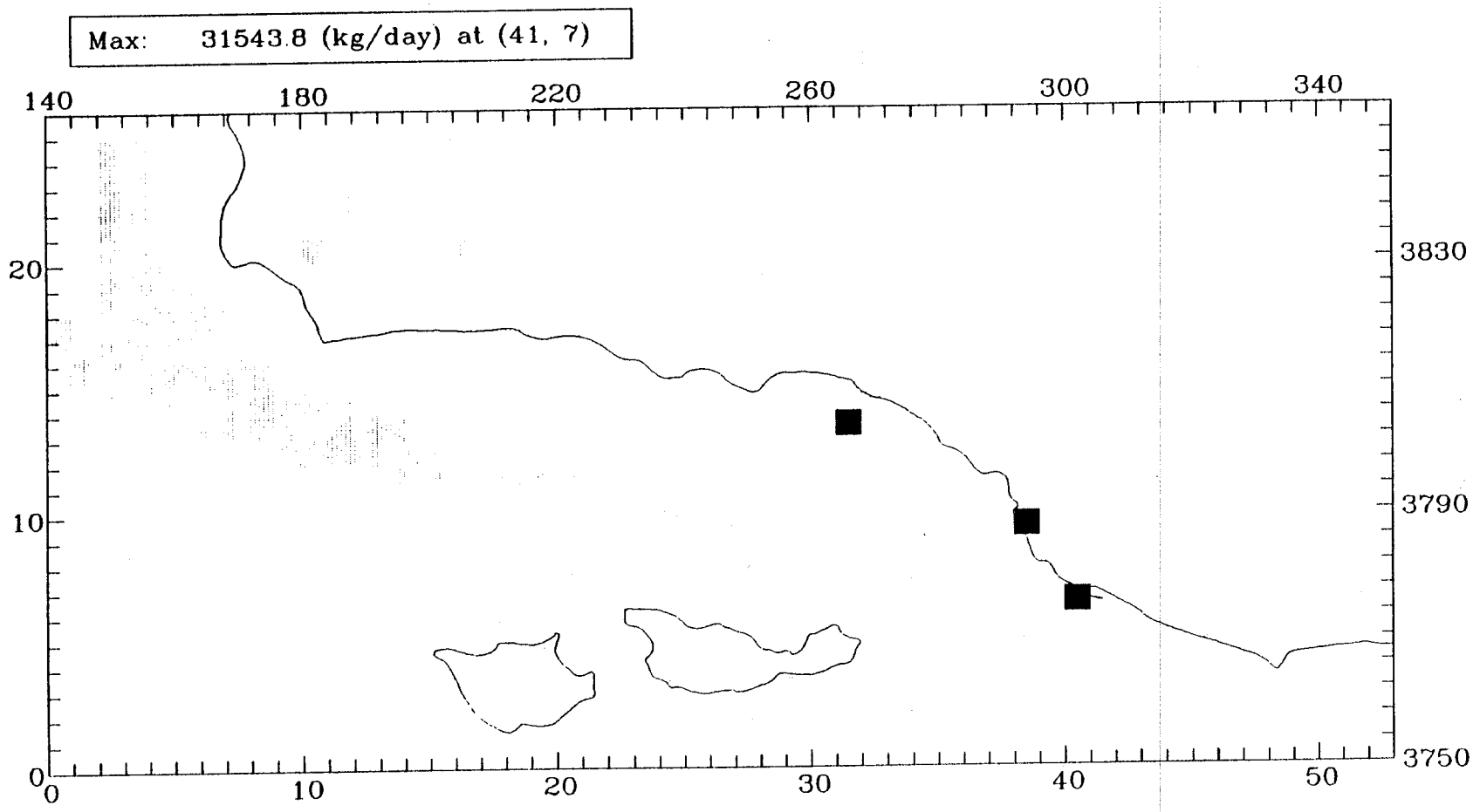

File is ptsrce_567bin.dat 84249
NOx
Total: 75239 (Kg/day)

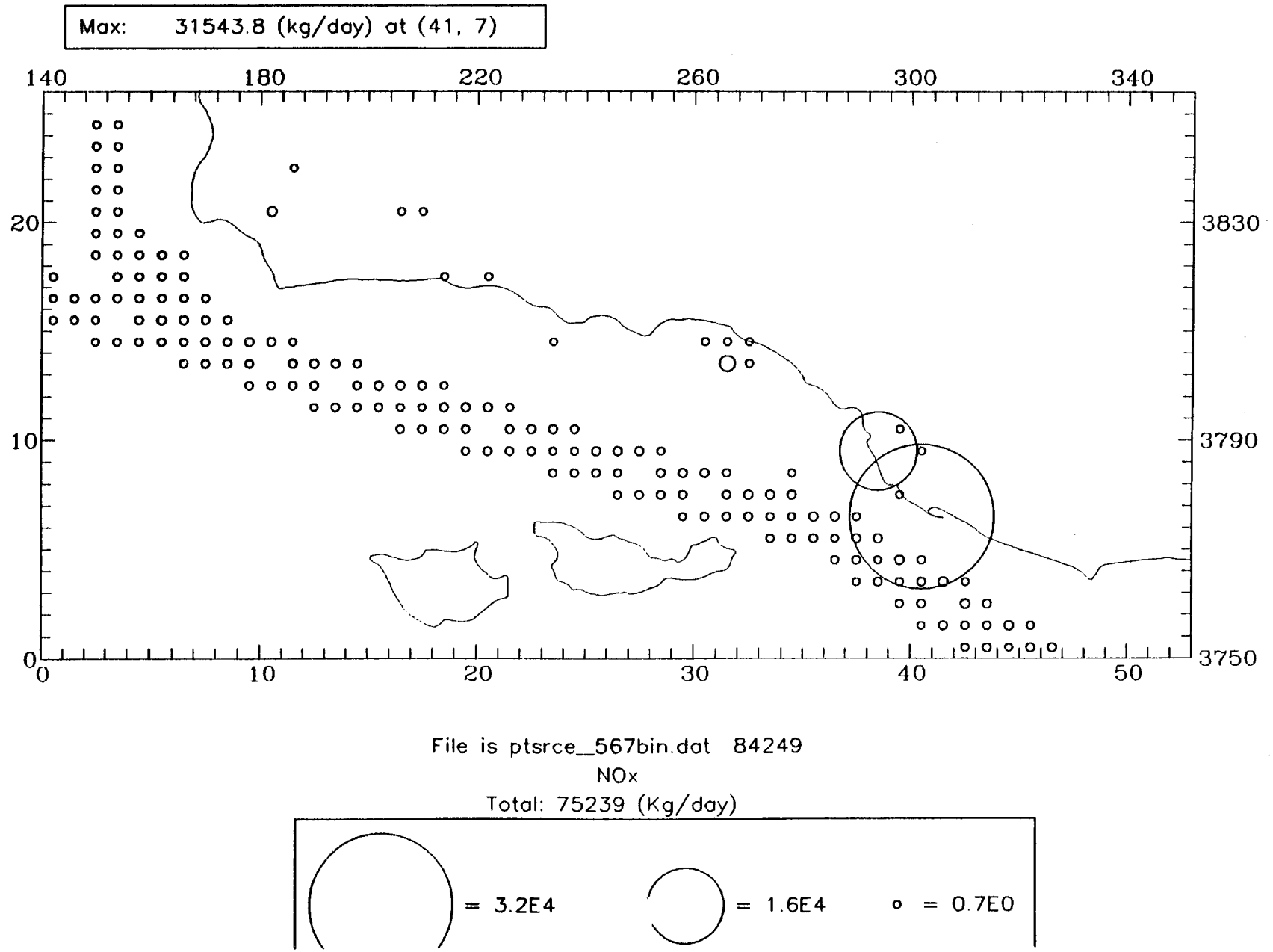
Max: 31543.8 (kg/day) at (41, 7)
140
180
220
260
300
340
20
10
0
0
10
20
30
40
50
3830
3790
3750
File is ptsrce_567bin.dat 84249
NOx
Total: 75239 (Kg/day)
= 3.2E4
= 1.6E4
o = 0.7E0

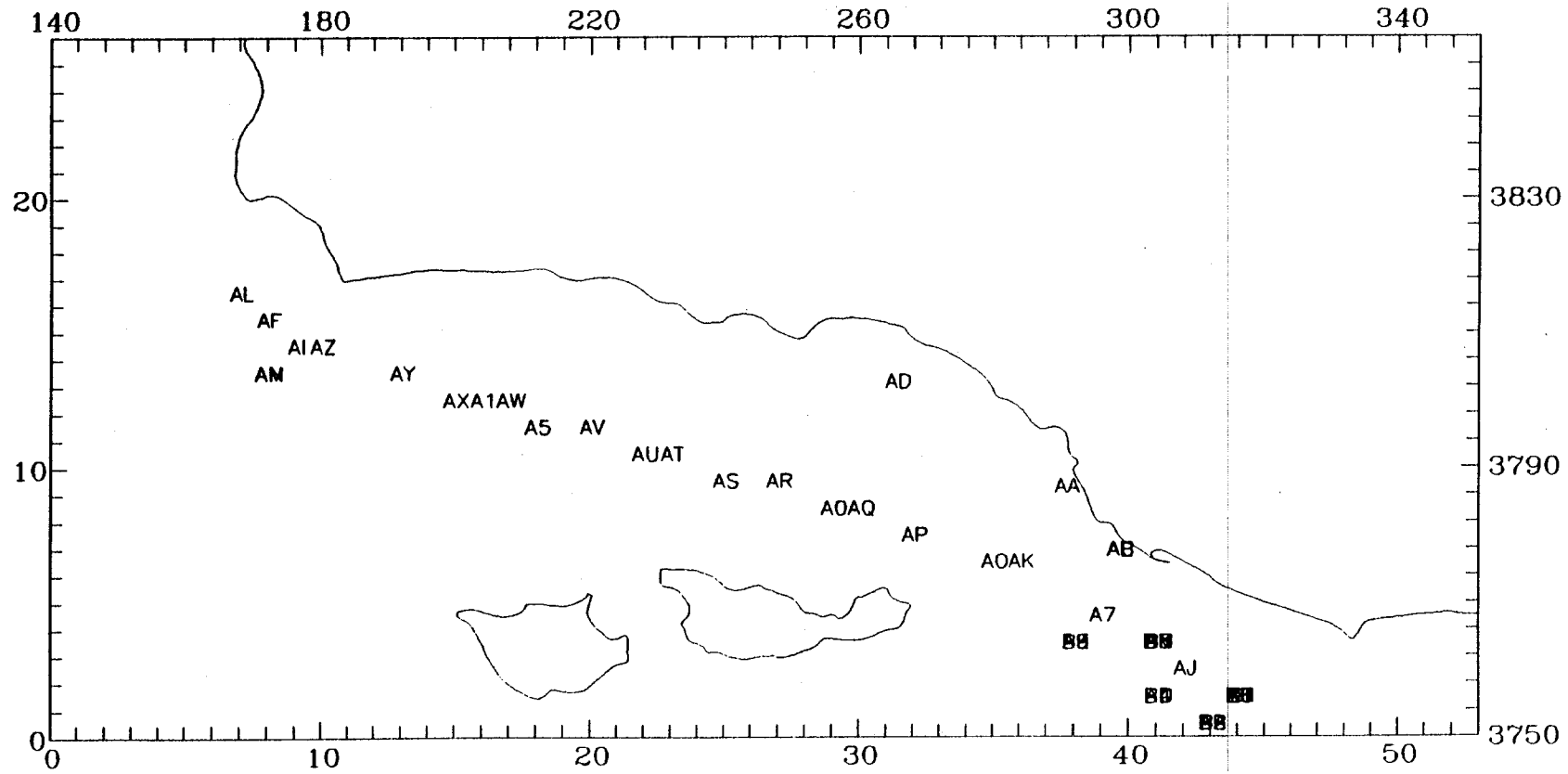

File is ptsrce_567bin.dat 84249

NOx

Top 20 Sources (> 12 Kg/day)

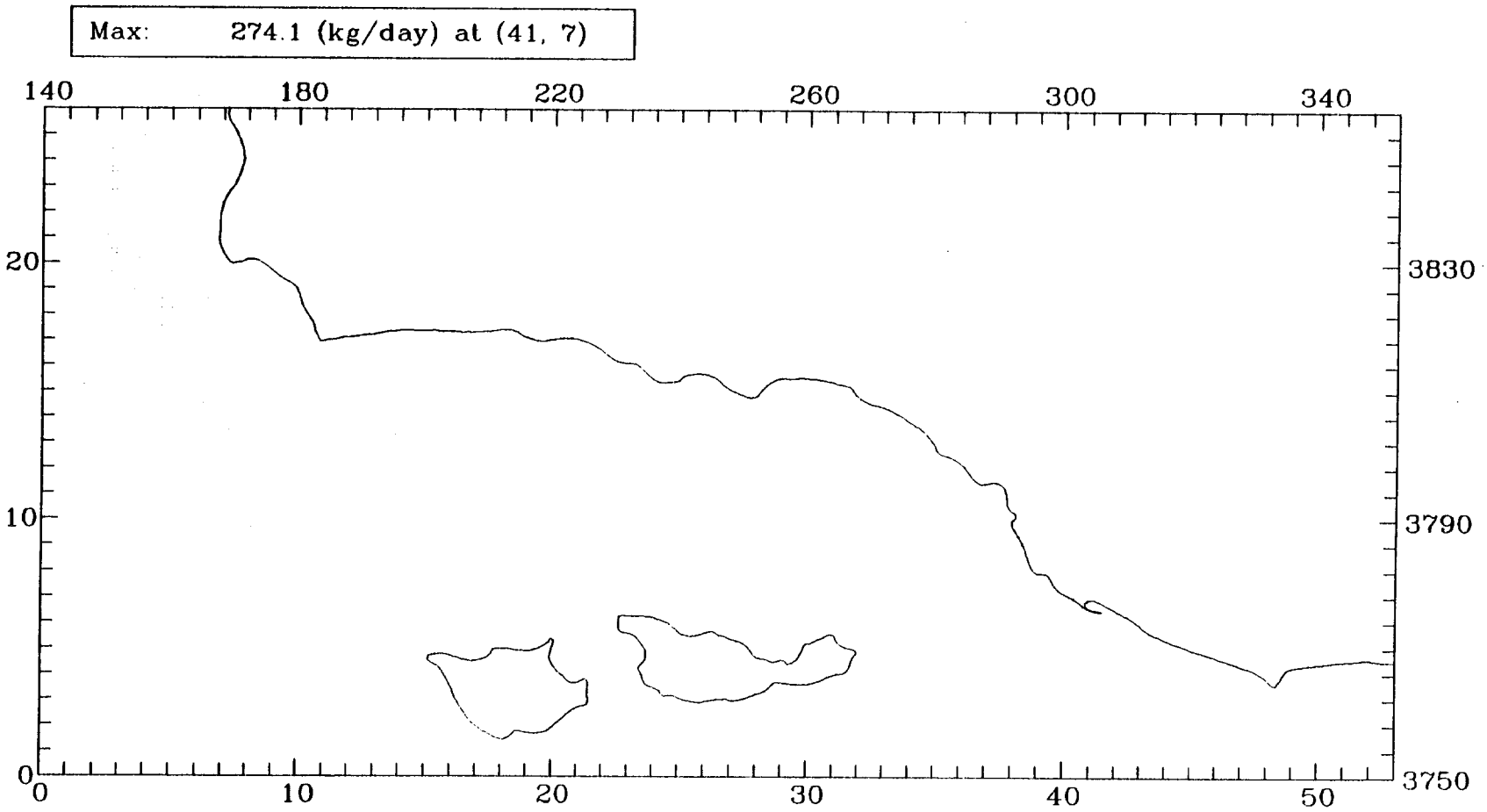

File is ptsrce_567bin.dat 84249
RHC
Total: 5136 (Kg/day)

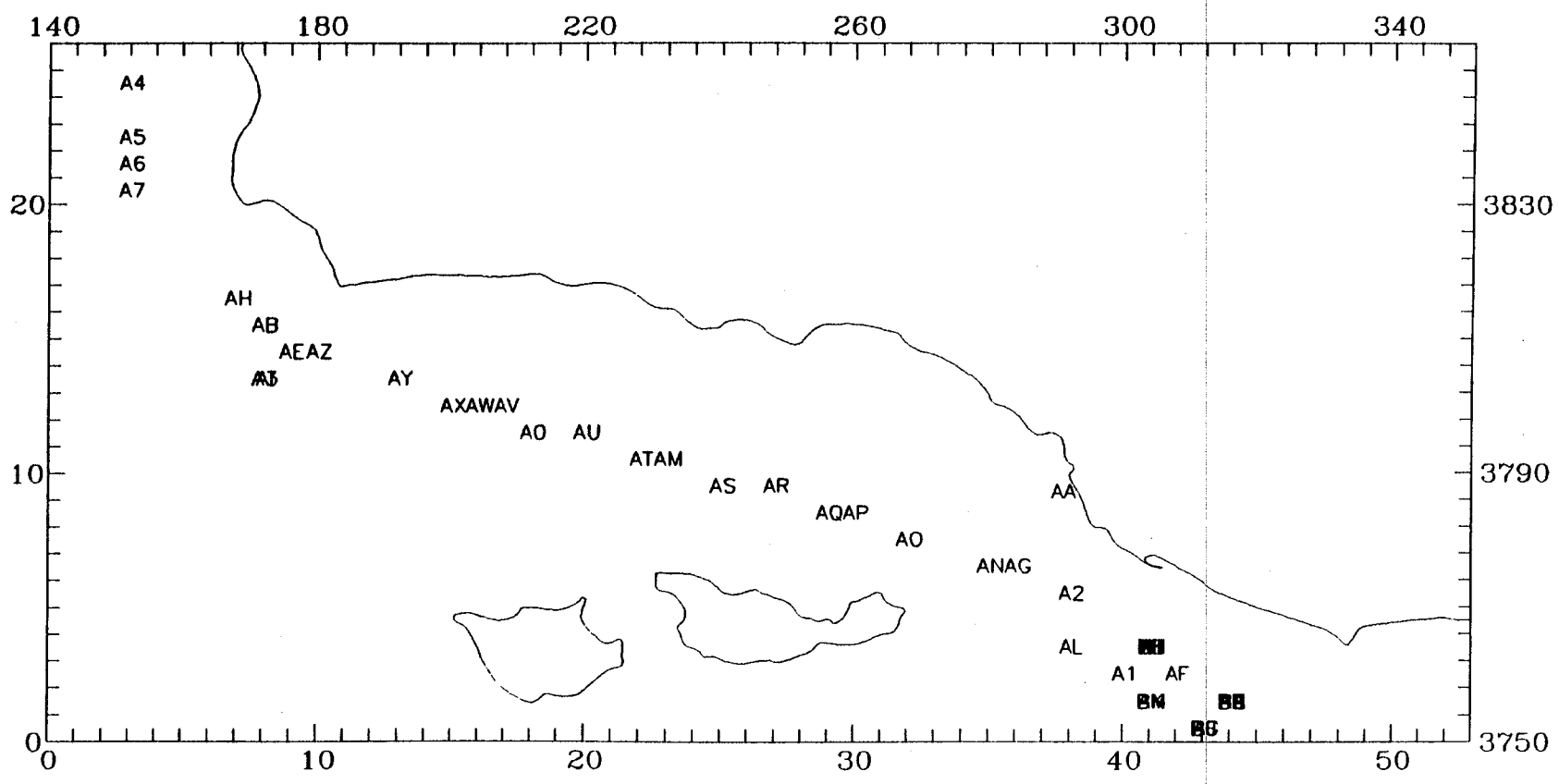

File is ptsrce_567bin.dat 84249
RHC
Top 20 Sources (> 3 Kg/day)

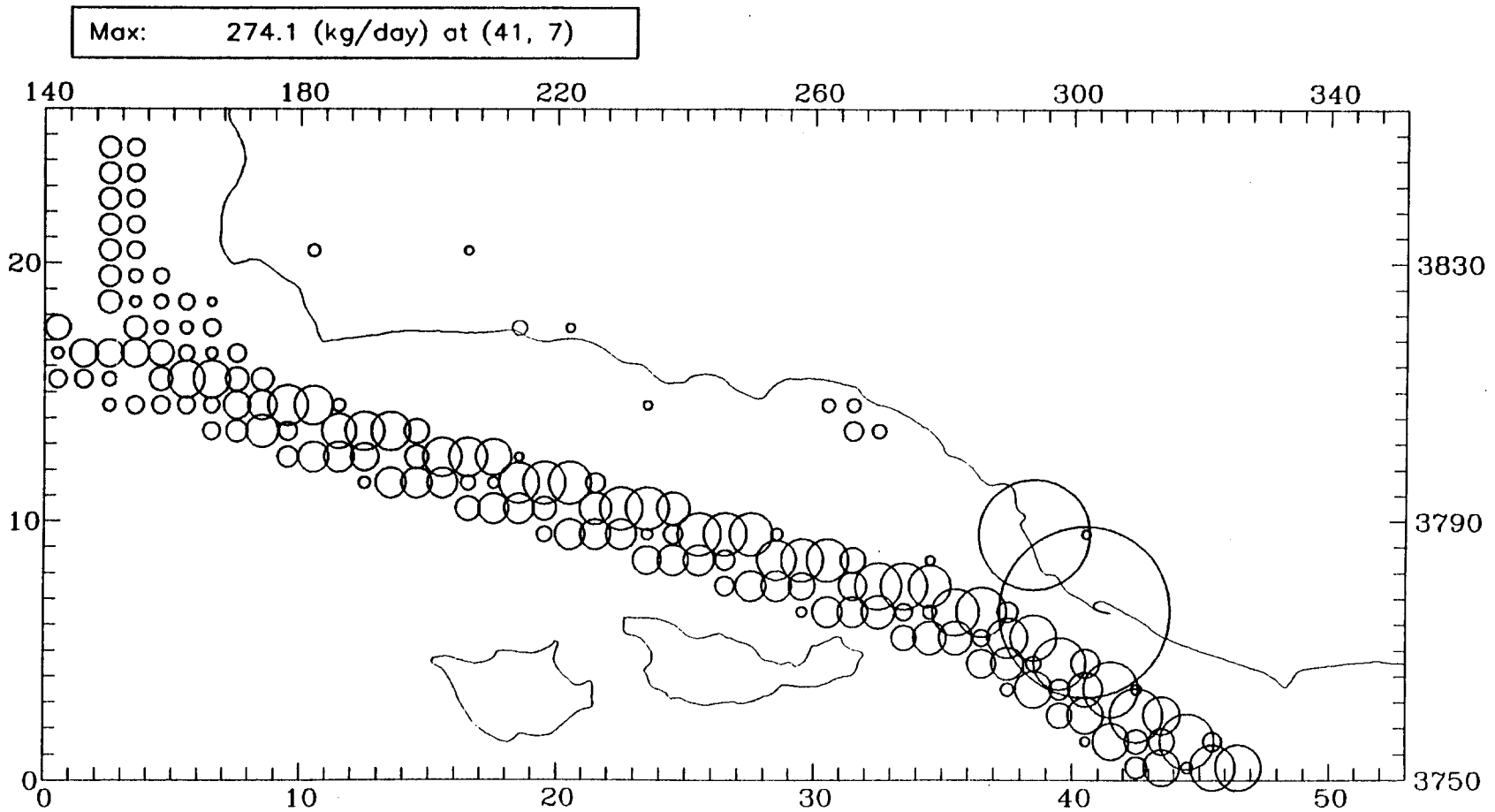

File is ptsrce_567bin.dat 84249
RHC
Total: 5136 (Kg/day)